1 2 9 0

UNIVERSIDADE Ð COIMBRA

José Onésimo Gomes Junyor

BUCKLING RESISTANCE OF MONO-SYMMETRIC STEEL MEMBERS: MONOSYMMETRIC I-SECTIONS AND NON-PRISMATIC BEAMS, AND EQUAL-LEG ANGLES SUBJECTED TO CONCENTRIC AND ECCENTRIC COMPRESSION

December 2023

FEDERAL UNIVERSITY OF MINAS GERAIS
SCHOOL OF ENGINEERING
POSTGRADUATE PROGRAM IN STRUCTURAL ENGINEERING

José Onésimo Gomes Junyor

BUCKLING RESISTANCE OF MONO-SYMMETRIC STEEL MEMBERS:
monosymmetric I-sections and non-prismatic beams, and equal-leg angles subjected to
concentric and eccentric compression

Belo Horizonte
2023

José Onésimo Gomes Junyor

BUCKLING RESISTANCE OF MONO-SYMMETRIC STEEL MEMBERS:

monosymmetric I-sections and non-prismatic beams, and equal-leg angles subjected to

concentric and eccentric compression

Thesis submitted to the Postgraduate Program in Structural Engineering of the School of Engineering at the Federal University of Minas Gerais, in partial fulfillment of the requirements for the degree of "Doctor in Structural Engineering".

Supervisors: Prof. Dr. Hermes Carvalho (UFMG) and Prof. Dr. Luis Alberto Proença Simões da Silva (UC)

Co-supervisor: Prof. Dr. Armando Cesar Campos Lavall (UFMG)

Belo Horizonte
2023

UNIVERSIDADE FEDERAL DE MINAS GERAIS

PROGRAMA DE PÓS-GRADUAÇÃO EM ENGENHARIA DE ESTRUTURAS

ATA DA DEFESA DE TESE DE DOUTORADO EM ENGENHARIA DE ESTRUTURAS Nº: 97 DO ALUNO JOSÉ ONÉSIMO GOMES JUNYOR

Às **10:00** horas do dia **20** do mês de **dezembro** de **2023**, reuniu-se em ambiente virtual da Escola de Engenharia da Universidade Federal de Minas Gerais - UFMG, a Comissão Examinadora indicada pelo Colegiado do Programa em **27 de outubro de 2023**, para julgar a defesa da Tese de Doutorado intitulada **"Buckling Resistance of Mono-Symmetric Steel Members: Monosymmetric I-Sections and Non-Prismatic Beams,and Equal-Leg Angles Subjected to Concentric and Eccentric Compression"**, cuja aprovação é um dos requisitos para a obtenção do Grau de DOUTOR EM ENGENHARIA DE ESTRUTURAS na área de ESTRUTURAS.

Abrindo a sessão, o Presidente da Comissão, **Prof. Dr. Hermes Carvalho**, após dar a conhecer aos presentes o teor das Normas Regulamentares passou a palavra ao candidato para apresentação de seu trabalho. Seguiu-se a arguição pelos examinadores, com a respectiva defesa do candidato. Logo após, a Comissão se reuniu, sem a presença do candidato e do público, para julgamento e expedição do resultado final.

Prof. Dr. Hermes Carvalho - DEES - UFMG (Orientador)
Prof. Dr. Armando Cesar Campos Lavall - DEES - UFMG (Coorientador)
Prof. Dr. Luis Simões da Silva - UC - PT (Orientador)
Prof. Dr. Rodrigo Barreto Caldas - DEES - UFMG
Profa. Dra. Helena Maria dos Santos Gervásio - UC - PT
Profa. Dra. Arlene Maria Cunha Sarmanho - UFOP
Prof. Dr. Luciano Rodrigues Ornelas de Lima - UERJ

Após reunião, a Comissão considerou o candidato APROVADO, conforme pareceres em anexo.

O resultado final foi comunicado publicamente ao candidato pelo Presidente da Comissão.

Nada mais havendo a tratar, o Presidente encerrou a reunião e lavrou a presente ATA, que será assinada por todos os membros participantes da Comissão Examinadora.

Belo Horizonte, 20 de dezembro de 2023.

Observações:

1. A aprovação do candidato na defesa da Tese de Doutorado não significa que a mesma tenha cumprido todos os requisitos necessários para obtenção do Grau de Doutor em Engenharia de

Estruturas;

2. Este documento não terá validade sem a assinatura do Coordenador do Programa de Pós-Graduação.

Documento assinado eletronicamente por **Arlene Maria Cunha Sarmanho**, **Usuário Externo**, em 20/12/2023, às 13:49, conforme horário oficial de Brasília, com fundamento no art. 5º do Decreto nº 10.543, de 13 de novembro de 2020.

Documento assinado eletronicamente por **Rodrigo Barreto Caldas**, **Professor do Magistério Superior**, em 20/12/2023, às 13:50, conforme horário oficial de Brasília, com fundamento no art. 5º do Decreto nº 10.543, de 13 de novembro de 2020.

Documento assinado eletronicamente por **Helena Maria dos Santos Gervásio**, **Usuária Externa**, em 20/12/2023, às 13:56, conforme horário oficial de Brasília, com fundamento no art. 5º do Decreto nº 10.543, de 13 de novembro de 2020.

Documento assinado eletronicamente por **Luciano Rodrigues Ornelas de Lima**, **Usuário Externo**, em 20/12/2023, às 13:56, conforme horário oficial de Brasília, com fundamento no art. 5º do Decreto nº 10.543, de 13 de novembro de 2020.

Documento assinado eletronicamente por **Armando Cesar Campos Lavall**, **Professor do Magistério Superior**, em 20/12/2023, às 13:59, conforme horário oficial de Brasília, com fundamento no art. 5º do Decreto nº 10.543, de 13 de novembro de 2020.

Documento assinado eletronicamente por **Hermes Carvalho**, **Professor do Magistério Superior**, em 20/12/2023, às 14:21, conforme horário oficial de Brasília, com fundamento no art. 5º do Decreto nº 10.543, de 13 de novembro de 2020.

Documento assinado eletronicamente por **Luis Alberto Proença Simões da Silva**, **Usuário Externo**, em 28/12/2023, às 14:09, conforme horário oficial de Brasília, com fundamento no art. 5º do Decreto nº 10.543, de 13 de novembro de 2020.

Documento assinado eletronicamente por **Felicio Bruzzi Barros**, **Coordenador(a) de curso de pós-graduação**, em 29/12/2023, às 10:16, conforme horário oficial de Brasília, com fundamento no art. 5º do Decreto nº 10.543, de 13 de novembro de 2020.

A autenticidade deste documento pode ser conferida no site https://sei.ufmg.br/sei/controlador_externo.php?acao=documento_conferir&id_orgao_acesso_externo=0, informando o código verificador **2849812** e o código CRC **247F9702**.

Referência: Processo nº 23072.273384/2023-34 SEI nº 2849812

ACKNOWLEDGMENTS

In life besides structural engineering, I would like to thank my dear friends Vagner and Marcos, for supporting me unconditionally and giving me well-pondered advice that always helped me put the things into the right perspective.

Finally, I would like to express my deep-felt gratitude to my parents José and Geralda, and sisters Jakeliny and Joyce, who support me in all my decisions, always help me, and with whom I celebrate all my victories. It is to them that I dedicate this thesis. Amo vocês!

"De todos os cilícios, um, apenas,
Me foi grato sofrer:
Cinquenta anos de desassossego
A ver correr,
Serenas,
As águas do Mondego"

Miguel Torga

ABSTRACT

This thesis presents a comprehensive study concerning the buckling behaviour of mono-symmetric I-section beams and angle sections in concentric and eccentric compression. The lateral-torsional resistance of prismatic double-symmetric I-section beams is accurately predicted using a mechanically consistent Ayrton-Perry approach, combined with a calibrated generalized imperfection. The corresponding design formulation was recently adopted in the revised version of Eurocode 3. However, for prismatic mono-symmetric I-section beams, the General Case shall be used while for non-prismatic beams only the General Method is available. Both methods present a very large scatter and, in most cases, highly underestimate the lateral-torsional buckling resistance. This work proposes an extension to the General Formulation for non-prismatic beams with arbitrary boundary conditions, partial lateral restraints, and arbitrary loading for mono-symmetric I-sections. Using an advanced numerical model calibrated with experimental test results, a large parametric study is undertaken, and its results are used to assess the available design methodologies and the proposed method. It is concluded that the General Formulation provides excellent safe-sided estimates of the Lateral Torsional Buckling (LTB) resistance, and it is confirmed the weak performance of the General Case and the General Method. Regarding the angle sections under compression, this work presents an extensive advanced numerical study also calibrated with recent experimental results available in the literature on the buckling behavior of hot-rolled steel angles under concentric and eccentric compression. Conclusions may support the ongoing revision in Europe of the design rules for angles concentrically and eccentrically loaded in compression. The numerical results were used for the assessment of existing design procedures commonly applied in practice (Eurocodes and AISC – American Institute of Steel Construction), as well as new recently proposed recommendations. In general, the current analytical rules do not present good agreement with the experimental and calibrated numerical results, even showing unsafe results for some slenderness ranges. In the case of fixed members in eccentric compression, these design rules are extremely conservative, reaching ratios r_N (ratio between numerical and analytical resistances) more than 2. The new proposals resulting from the project ANGELHY present an improved agreement with the numerical results, showing that they may efficiently replace the current design rules in the Eurocodes. However, for concentric compression, a reliability assessment shows that the required partial factor is $\gamma_{M1}^* = 1.1$. Finally, the General Formulation is adapted to angle sections in compression, where once again good performance of the proposed method is observed.

Keywords: mono-symmetric beams; steel angles in compression; Eurocode 3; stability; General Formulation.

RESUMO

Esta tese apresenta um estudo abrangente sobre o comportamento à flambagem de vigas monossimétricas de seção I e cantoneiras comprimidas concêntrica e excentricamente. A resistência à flambagem lateral com torção de vigas prismáticas de seção I duplamente simétricas é obtida usando-se uma abordagem mecanicamente consistente baseada na Equação de Ayrton-Perry, combinada com uma imperfeição generalizada previamente calibrada. Esta formulação foi adotada nas versões mais recentes do Eurocódigo 3. No entanto, para vigas prismáticas monossimétricas de secção I, deve-se ainda utilizar o Caso Geral, enquanto para vigas não prismáticas o recomendado é o Método Geral. Ambos os métodos apresentam uma dispersão muito grande de resultados e, na maioria dos casos, subestimam fortemente a resistência à flambagem lateral com torção. Este trabalho propõe uma extensão da Formulação Geral para vigas não prismáticas de seção monossimétrica com condições de contorno, restrições laterais parciais e carregamentos arbitrários. Através de um modelo numérico calibrado com resultados de ensaios experimentais, um extenso estudo paramétrico foi realizado e seus resultados foram usados para avaliar as metodologias de dimensionamento disponíveis e o método proposto. Conclui-se que a Formulação Geral fornece excelentes e seguras estimativas para a resistência à flambagem lateral com torção e atesta-se a limitação do uso do Caso Geral e do Método Geral presentes nos Eurocódigos. No que diz respeito às cantoneiras comprimidas, este trabalho apresenta um extenso estudo numérico calibrado com resultados experimentais recentes disponíveis na literatura, sobre o comportamento à flambagem de cantoneiras de aço laminadas a quente sob compressão concêntrica e excêntrica. As conclusões obtidas com esse estudo visam subsidiar a revisão em curso das recomendações de projeto para cantoneiras comprimidas na Europa. Os resultados numéricos foram utilizados para a avaliação dos procedimentos de dimensionamento comumente aplicados na prática (Eurocódigos e AISC – American Institute of Steel Construction), bem como as novas recomendações recentemente propostas na literatura. Em geral, as regras de projeto atuais não apresentaram boa concordância com os resultados numéricos, apresentando resultados fora dos limites admissíveis para algumas faixas de esbeltezes. No caso de barras engastadas nas extremidades e em compressão excêntrica, as recomendações de cálculo são extremamente conservadoras, atingindo relações r_N (razão entre resistências numéricas e analíticas) superiores a 2. As propostas do projeto ANGELHY apresentam a melhor concordância com os resultados numéricos, demonstrando assim que podem substituir de forma eficiente as atuais recomendações de dimensionamento presentes nos Eurocódigos. No entanto, para compressão concêntrica, uma análise de confiabilidade mostra que há necessidade de adoção de um coeficiente parcial de segurança igual a $\gamma_{M1}^{*} = 1{,}1$. Por fim, a Formulação Geral é adaptada para cantoneiras comprimidas, onde mais uma vez observa-se bom desempenho do método proposto.

Palavras-chave: vigas monossiméticas; cantoneiras de aço comprimidas; Eurocódigo 3; estabilidade; Formulação Geral.

LIST OF FIGURES

LIST OF TABLES

ABBREVIATIONS

AISC	American Institute Steel Construction
ASCE	American Society of Civil Engineers
ASD	Allowable Stress Design
BC	Boundary Condition
BF	Bottom Face
C.I.G.R.E	*Conseil International des Grands Réseaux Elétricos*
C.O.V	Coefficient of Variation
CSA	Canadian Standards Association
DL	Distributed Load
EC3	Eurocode 3
ECCS	European Convention for Constructional Steelwork
EN	*Europäische Norm*
FB	Flexural buckling
GC	General Case
GF	General Formulation
GM	General Method
GMNIA	Geometrically and Materially Non-Linear Analysis with Imperfections
KP	Kindem point
LBA	Linear Buckling Analysis
LBM	Linearly Varying Bending Moment
LRFD	Load and Resistance Factor Design
LTB	Lateral-torsional Buckling
MPC	Multipoint Constraint Element
P.L.A	Point Load Application
SSRC	Structural Stability Research Council
TF	Top Face
T-DS	Tapered Doubly Symmetric
TFB	Torsional-flexural Buckling
T-MS	Tapered Mono-symmetric
UC	University of Coimbra

U-DS	Uniform Doubly Symmetric
UFMG	Federal University of Minas Gerais
U-MS	Uniform Mono-symmetric

NOTATIONS

Lowercase Latin Letters

a Buckling curve (Eurocode 3); Geometric parameter for parabolic and anti-parabolic I-section members.

b Buckling curve (Eurocode 3); Flange width.

b_1 Width of the flange with the lowest value of I_z.

b_2 Width of the flange with the largest value of I_z.

c Outstand flange width; Buckling curve (Eurocode 3).

d Buckling curve (Eurocode 3).

d_0 Hole diameter of bolt

$\bar{e}_0$ Maximum amplitude of a member imperfection.

e_1 End distance from the centre of fastener hole to nearest end of any part, measured parallel to the direction of load transfer.

e_u Load application eccentricity about the $u-$ axis.

e_v Load application eccentricity about the $v-$ axis.

e_y Load application eccentricity about the $\mathrm{y}-$ axis.

e_z Load application eccentricity about the $z-$ axis.

f General factor.

f_η Value to determine the generalized imperfection in the General Formulation.

f_χ Value to determine the reduction factor for angle members in eccentric compression in the General Formulation.

f_p Proportionality stress.

f_u Ultimate strength.

f_y Yield strength.

g Drilling template.

h Width or depth of a cross-section.

h' First derivative of h.

h_0 Distance of centerlines of chords of a built-up member.

h_e Effective width.

h_w	Depth of a web.
i_p	Polar radius of gyration.
i_v	Radius of gyration about v-axis.
i_y	Radius of gyration about y-axis.
k_{ij}	Interaction factor.
k_u	Coordinate of the centre of the stability circle in the u-direction.
k_v	Coordinate of the centre of the stability circle in the v-direction.
k_y	Coordinate of the centre of the stability circle in the y-direction.
k_z	Coordinate of the centre of the stability circle in the z-direction.
n	Number of cases.
p_1	Spacing between centres of fasteners measured parallel to the direction of force transfer.
q	Distributed load.
r_e	Ratio between the numerical lateral-torsional buckling resistance and the plastic bending moment resistance of the cross-section.
r_N	Ratio between the numerical and analytical values of the buckling resistance of the member.
r_t	Ratio between the analytical buckling resistance and the cross-sectional plastic bending moment resistance.
s	Parameter to determine the value of residual stress.
t	Thickness of an angle leg.
t_1	Thickness of the flange with the lowest value of I_z.
t_2	Thickness of the flange with the largest value of I_z.
t_w	Web thickness.
u	Major-axis of an angle section; Displacement along the u-axis due the loading application.
u''	Second derivative of u.
u_0	Initial geometric imperfection in the u-direction for angle sections.
u_0''	Second derivative u_0.
$\bar{u}_0$	Amplitude of the initial geometric imperfection in the u-direction for angle sections.
u_{cr}	Displacement component of the mode shape along u-direction for angle sections.
u_{cr}''	Second derivative u_{cr}.
u_D	Coordinate of the torsion centre of the angle section in the u-direction.

u_{tot}	Total displacement ($u_0 + u$) along the u-direction for angle sections.
v	Transverse displacement along the y-axis due the loading application; Minor-axis of an angle section.
$\bar{v}$	Amplitude of the transverse displacement along the y-direction for I-sections, and v-direction for angle sections due the loading application.
v'	First derivative of v.
v''	Second derivative of v.
v_0	Initial geometric imperfection in the y-direction for I-sections, and v-direction for angle sections.
$\bar{v}_0$	Amplitude of the initial geometric imperfection in the y-direction for I-sections, and v-direction for angle sections.
v_{cr}	Transverse displacement component of the mode shape along the y-direction for I-sections, and v-direction for angle sections.
v'_{cr}	First derivative of v_{cr}.
v''_{cr}	Second derivative of v_{cr}.
v_D	Displacement of the torsion centre in the y-direction for I-sections, and v-direction for angle sections.
v''_D	Second derivative of v_D.
v_D^{IV}	Fourth derivative of v_D.
v_{tot}	Total transverse displacement ($v_0 + v$) along the y-direction for I-sections, and v-direction for angle sections.
$\bar{v}_{tot}$	Amplitude of the total transverse displacement ($\bar{v}_0 + \bar{v}$) along the y-direction for I-sections, and v-direction for angle sections.
w	Transverse displacement along the z-axis due the loading application.
$\bar{w}$	Amplitude of the transverse displacement along the z-axis due the loading application.
w'	First derivative of w.
w''	Second derivative of w.
w_0	Initial geometric imperfection in the z-direction.
$\bar{w}_0$	Amplitude of the initial geometric imperfection in the z-direction.
w_D	Displacement of the torsion centre in the z-direction.
w''_D	Second derivative of w_D.
w_D^{IV}	Fourth derivative of w_D.

$\overline{w}_{tot}$	Amplitude of the total transverse displacement ($\overline{w}_0 + \overline{w}$) along the z-axis.
x	Axis along the member.
x_m	Critical location.
y	Principal axis of inertia; Major-axis of an I-section member.
y_0	Distance between the centroid and the torsion centre of the cross-section in the y-direction.
z	Principal axis of inertia; Minor-axis of an I-section member.
z_0	Distance between the centroid and the torsion centre of the cross-section in the z-direction.
z_g	Distance between the point of load application and the torsion centre.
z_G	Position of the cross-section centroid measured from the top face of the flange with the largest value of I_z.

Uppercase Latin Letters

A	Area.
A_{eff}	Effective area of the cross-section.
A_g	Gross area of the cross-section.
B	Bi-moment.
C	Numerical constant.
C_i	Equivalent moment factor.
C_w	Warping constant.
C_φ	Rotational stiffness coefficient.
D	Torsion centre of the cross-section.
E	Modulus of elasticity.
E_r	Reduced modulus of elasticity.
E_t	Tangent modulus of elasticity.
G	Shear modulus; Centroid of the cross-section.
I	Moment of inertia.
I_u	Moment of inertia about u-axis.
I_v	Moment of inertia about v-axis.
I_y	Moment of inertia about y-axis.

I_z	Moment of inertia about z-axis.
I_{zc}	Moment of inertia of the compression flange about the z-axis.
I_{zt}	Moment of inertia of the tension flange about the z-axis.
J	Torsion constant.
K	Effective length factor.
$L_x = K_x L_x$	Effective buckling length of member for torsional buckling.
$L_y = K_y L_y$	Effective buckling length of member for flexural buckling about y-axis.
$L_z = K_z L_z$	Effective buckling length of member for flexural buckling about z-axis.
L	Member Length.
M	Bending moment.
M_{cr}	Elastic critical bending moment.
$M_{cr,anal}$	Analytical value of the elastic critical bending moment.
$M_{cr,num}$	Numerical value of the elastic critical bending moment.
$M_{u,Ed}$	Design bending moment about u-axis.
$M_{v,Ed}$	Design bending moment about v-axis.
M_{pl}	Plastic bending moment resistance about y-axis.
$M_{R,anal}$	Analytical bending moment resistance.
M_{Rk}	Characteristic bending moment resistance.
$M_{R,num}$	Numerical value of the bending moment resistance.
$M_{u,Rk}$	Characteristic bending moment resistance about u-axis.
$M_{v,Rk}$	Characteristic bending moment resistance about v-axis.
$M_{b,u,Rd}$	Design value of the buckling resistance of a member in bending about u-axis.
$M_{b,v,Rd}$	Design value of the buckling resistance of a member in bending about v-axis.
M_y	Bending moment about y-axis.
$M_{y,Ed}$	Design bending moment about y-axis.
M_z	Bending moment about z-axis.
M^{II}	Second-order bending moment.
M_t^{II}	Torsional moment.
M_u^{II}	Second-order bending moment about u-axis.
M_v^{II}	Second-order bending moment about v-axis.
M_w^{II}	Second-order warping moment.
M_y^{II}	Second-order bending moment about y-axis.

M_z^{II}	Second-order bending moment about z-axis.
N	Normal force.
$N_{b,Rk}$	Characteristic member buckling resistance.
$N_{b,u,Rd}$	Design value of the buckling resistance of a member in compression about u-axis.
$N_{b,v,Rd}$	Design value of the buckling resistance of a member in compression about v-axis.
N_{cr}	Elastic critical force.
$N_{cr,TF}$	Elastic critical force for torsional-flexural buckling.
$N_{cr,TF,con}$	Elastic critical force for torsional-flexural buckling of an angle member in concentric compression.
$N_{cr,TF,ecc}$	Elastic critical force for torsional-flexural buckling of an angle member in eccentric compression.
$N_{cr,u}$	Elastic critical axial force for flexural buckling about u-axis.
$N_{cr,v}$	Elastic critical axial force for flexural buckling about v-axis.
$N_{cr,x}$	Elastic critical axial force for torsional buckling.
$N_{cr,y}$	Elastic critical axial force for flexural buckling about y-axis.
$N_{cr,z}$	Elastic critical axial force for flexural buckling about z-axis.
N_{Ed}	Design normal force.
$N_{R,anal}$	Analytical value of the ultimate load capacity for angle members.
$N_{R,exp}$	Experimental value of the ultimate load capacity for angle members.
N_{Rk}	Characteristic resistance of the cross-section.
$N_{R,num}$	Numerical value of the ultimate load capacity for angle members.
P_{ult}	Ultimate load resistance.
R	Radius of the stability circle.
R^2	Coefficient of Determination.
ROT_x	Degree of freedom relative to rotation about x-axis (numerical model).
ROT_y	Degree of freedom relative to rotation about y-axis (numerical model).
ROT_z	Degree of freedom relative to rotation about z-axis (numerical model).
U_x	Degree of freedom relative to translation in the x-direction (numerical model).
U_y	Degree of freedom relative to translation in the y-direction (numerical model).
U_z	Degree of freedom relative to translation in the z-direction (numerical model).

W	Elastic section modulus.
W_w	Elastic warping modulus.
$W_{eff,u}$	Effective section modulus about u-axis.
$W_{eff,v}$	Effective section modulus about v-axis.
W_{el}	Elastic section modulus.
$W_{el,u}$	Elastic section modulus about u-axis.
$W_{el,v}$	Elastic section modulus about v-axis.
$W_{el,y}$	Elastic section modulus about y-axis.
$W_{el,y,c}$	Plastic section modulus about y-axis for the compression part of the cross-section.
$W_{el,z}$	Elastic section modulus about z-axis.
W_{ep}	Elasto-plastic section modulus.
$W_{ep,u}$	Elasto-plastic section modulus about u-axis.
$W_{ep,v}$	Elasto-plastic section modulus about v-axis.
W_{pl}	Plastic section modulus.
$W_{pl,u}$	Plastic section modulus about u-axis.
$W_{pl,v}$	Plastic section modulus about v-axis.
$W_{pl,y}$	Plastic section modulus about y-axis.
W_u	Section modulus about u-axis determined according to cross-section classification in the ANGELHY prescriptions.
$W_{u,i}$	Section modulus about u-axis.
$W_{v,i}$	Section modulus about v-axis.
W_y	Section modulus about y-axis.
W_z	Section modulus about z-axis.

Lowercase Greek Letters

α	Imperfection factor according to EC3-1-1; General factor.
α_{cr}	Load multiplier which leads to the elastic critical resistance.
$\alpha_{cr,op}$	Minimum amplifier for the in-plane design loads to reach the elastic critical resistance with regard to lateral or lateral-torsional buckling.
α_{LT}	Imperfection factor for lateral-torsional buckling.

$\alpha_{ult,k}$	Minimum load amplifier of the design loads to reach the characteristic resistance of the most critical cross-section.
β	General factor.
β_u	Wagner factor for angle section members.
β_z	Wagner factor for I-section members.
γ_{M1}	Partial factor.
γ_{M1}^*	Required partial factor.
$\bar{\delta}_0$	Amplitude of the general displacement of imperfection shape.
$\bar{\delta}_{0,LTB}$	Amplitude of the general displacement of imperfection shape for lateral-torsional buckling.
$\bar{\delta}_{0,TFB}$	Amplitude of the general displacement of imperfection shape for torsional-flexural buckling.
δ^{fl}	General displacement of the critical mode.
ε	Material parameter depending on f_y (Eurocode 3); Strain.
ε_u	Strain corresponding to ultimate strength.
ε_y	Strain corresponding to yielding strength.
ε_M	Utilization ratio regarding the bending moment.
ε_M^I	Utilization ratio regarding the first-order bending moment.
ε_M^{II}	Utilization ratio regarding the second-order bending moment.
ε_N	Utilization ratio regarding the axial force.
ε_N^{II}	Utilization ratio regarding the second-order axial force.
η	Generalized imperfection; Reduction factor for angles according to end connection.
θ	Twist rotation due the loading application.
$\bar{\theta}$	Amplitude of twist rotation due the loading application.
θ'	First derivative of θ.
θ''	Second derivative of θ.
θ'''	Third derivative of θ.
θ^{IV}	Fourth derivative of θ.
θ_0	Initial twist rotation.
$\bar{\theta}_0$	Amplitude of initial twist rotation.
θ_{cr}	Twist rotation component of the mode shape.
$\bar{\theta}_{cr}$	Amplitude of twist rotation component of the mode shape.

θ'_{cr}	First derivative of θ_{cr}.
θ''_{cr}	Second derivative of θ_{cr}.
θ_{tot}	Total twist rotation ($\theta_0 + \theta$).
$\bar{\theta}_{tot}$	Amplitude of total twist rotation ($\bar{\theta}_0 + \bar{\theta}$).
κ_v	Effective slenderness factor about v-axis.
κ_y	Effective slenderness factor about y-axis.
λ	Member slenderness.
$\lambda_{eff,v}$	Effective non-dimensional slenderness for flexural-buckling about the v-axis.
$\lambda_{eff,y}$	Effective non-dimensional slenderness for flexural-buckling about the y-axis.
λ_p	Limiting member slenderness for the limit state of yielding.
λ_r	Limiting member slenderness for the limit state of inelastic lateral-torsional buckling.
$\bar{\lambda}$	Non-dimensional slenderness.
$\bar{\lambda}_{LT}$	Non-dimensional slenderness for lateral-torsional buckling.
$\bar{\lambda}_{op}$	Global non-dimensional slenderness of a structural component for out-of-plane buckling according to the General Method (of clause 6.3.4).
$\bar{\lambda}_\rho$	Relative plate slenderness for plate buckling.
$\bar{\lambda}_{TF}$	Non-dimensional slenderness for torsional-flexural buckling.
$\bar{\lambda}_{TF,con}$	Non-dimensional slenderness for torsional-flexural buckling of an angle member in concentric compression.
$\bar{\lambda}_{TF,ecc}$	Non-dimensional slenderness for torsional-flexural buckling of an angle member in eccentric compression.
$\bar{\lambda}_v$	Non-dimensional slenderness for flexural-buckling about v-axis.
$\bar{\lambda}_y$	Non-dimensional slenderness for flexural-buckling about y-axis.
$\bar{\lambda}_z$	Non-dimensional slenderness for flexural-buckling about z-axis.
ξ	Interaction factor depending on the cross-section classification; General factor.
ρ	Reduction factor for plate buckling.
ρ_u	Reduction factor for plate buckling of an angle section.
σ	Longitudinal stress.
σ_0	Value of residual stress.
σ_{cr}	Elastic critical stress.

σ_{max}	Maximum second-order elastic stress in the most stressed cross-section along the member.
τ	Shear stress.
φ	Gusset plate rotation.
ϕ	Resistance factor.
χ	Reduction factor.
χ_F	Reduction factor due to flexural buckling.
χ_{op}	Reduction factor corresponding to the non-dimensional slenderness $\bar{\lambda}_{op}$.
χ_{LT}	Reduction factor due to lateral-torsional buckling.
χ_T	Reduction factor due to torsional buckling.
χ_{TF}	Reduction factor due to torsional-flexural buckling.
$\chi_{TF,con}$	Reduction factor due to torsional-flexural buckling for angle members in concentric compression.
$\chi_{TF,ecc}$	Reduction factor due to torsional-flexural buckling for angle members in eccentric compression.
χ_u	Reduction factor due to flexural buckling about u-axis.
χ_v	Reduction factor due to flexural buckling about v-axis.
ψ	Ratio between the maximum and minimum bending moments, for a linear bending moment distribution.
ψ_u	Ratio between the maximum and minimum bending moments about u-axis, for a linear bending moment distribution.
ψ_v	Ratio between the maximum and minimum bending moments about v-axis, for a linear bending moment distribution.
ω	Sectorial area.

Uppercase Greek Letters

$\Delta M_{v,Ed}$	Additional bending moment about the minor-axis for class 4 cross-sections due to the shift of the centroidal axis when the cross-section is subjected to compression only.
Φ	Value to determine the reduction factor χ for flexural buckling.
Φ_{LT}	Value to determine the reduction factor χ_{LT} for lateral-torsional buckling.

$\Phi_{TF,ecc}$ Value to determine the reduction factor $\chi_{TF,ecc}$ for torsional-flexural buckling of members in eccentric compression.

TABLE OF CONTENTS

1

INTRODUCTION

1.1 Motivation

Thin-walled welded steel mono-symmetric I-sections provide a cost-efficient solution due to their efficiency in bending and ease of fabrication (Martins et al., 2023). When used in non-prismatic members, mono-symmetric sections allow to adjust the resistance of the section to a variable bending moment along the member, thereby potentially maximizing the efficiency of the design. Tapered steel beams with mono-symmetric I-sections are widely used in crane girders, pitched-roof portal frames and in twin or multiple girder bridge decks, often as part of composite girders.

The lateral-torsional buckling resistance of prismatic mono-symmetric steel beams is tackled in part 1-1 of Eurocode 3, henceforth denoted to as EC3-1-1, using the General Case (GC), that is based on the analogy between N_{cr} and M_{cr} and the assumption that the lateral-torsional buckling behaviour of a beam in bending is similar to a compressed column (Simões da Silva et al., 2016a). This contrasts with the new method for doubly symmetric I- and H-sections (newLTB) that is now included in FprEN 1993-1-1, which is based on a mechanically consistent Ayrton-Perry derivation (Taras and Greiner, 2010; Taras, 2010). It was shown (Simões da Silva et al., 2010) that the GC is too conservative and presents a large scatter of results, while the newLTB presents a good agreement with a large set of experimental and validated numerical results and a low scatter.

Concerning non-prismatic beams, EC3-1-1 proposes the General Method (GM), which is a Merchant-Rankine semi-empirical method that leads to a very wide scatter of results that may even be unsafe (Simões da Silva et al., 2010). In the case of prismatic beams, it was demonstrated that the GM leads to the same results as the GC (Simões da Silva et al., 2010).

Recently, Tankova et al. (2018) proposed a design-oriented method, General Formulation (GF) that can verify the buckling resistance of an arbitrary non-prismatic member, with arbitrary boundary conditions, variable loading and partial lateral restraints for double symmetric I- or H-sections.

Hot-rolled steel angles are widely used in steel construction due to lower manufacturing complexity, high structural efficiency (high strength-to-weight ratio), flexibility of application in connecting systems and easy assembly. They are commonly applied as chord members of plane trusses; bracing systems of latticed towers, trusses, frames; and primary members of electrical transmission and antenna towers. In most practical cases, they are usually subject to axial forces and connected only by one leg. The connection of the angles to the other elements of the structure, for example, gusset plates or other profiles, is carried out by either welding and mainly by bolting, inducing eccentric compression or tension because the line of action of the bolts or welds does not coincide with the longitudinal axis of the angle (Gomes Jr et al., 2023).

The eccentricity of the applied load combined with the mono-symmetric geometry of the cross-sections (associated with the divergence between the principal axes of the angles and the axes of their legs), and the greater susceptibility to torsion are important issues for design (Kettler et al., 2017). Previous studies have shown that the strength of angles under eccentric tensile forces is not much lower than under concentric forces (Woolcock and Kitipornchai, 1986), but the same is not observed in compressed angles, in which the eccentricity can be detrimental to the ultimate load, as evidenced by Stang and Strickenberg (1922), Usami and Galambos (1971), Elgaaly et al. (1991), Bathon et al. (1993). Another complexity in the design of steel angles is the computation of the rigidity of the joints, since the real restrictions applied on their extremities are unknown in most cases (Kettler et al., 2017; Temple and Sakla, 1996; Cheng et al., 2016). Bezas et al. (2022) also pointed out two more issues that differentiate the design of angles from the design of conventional doubly symmetrical members: the resistance to bending and the radius of gyration around the minor-axis of steel angles are significantly lower than those related to the major-axis, and their plastic resistance is substantially larger than their elastic one.

When subjected to concentric compression, steel angles present two main failure modes: flexural or torsional-flexural buckling. However, the exact elastic response of angle sections under eccentric compression is much more complex to obtain. Vlasov (1962) proposed an analytical formulation to study the elastic behavior of thin-walled open cross-section members

in bending and torsion, including angle sections, which leads to a complex solution. EN 1993-1-1, EN 1993-3-1, FprEN 1993-1-1, and AISC 360 present some practical procedures for the design of steel angles under eccentric compression, in which simple formulations are suggested to determine the ultimate load capacity by calculating an equivalent buckling length or an effective slenderness ratio. The interaction equations for bending and axial compression are applicable, but no interaction factors are provided. Flexural buckling around the minor-axis or flexural buckling around the axis parallel to the connected leg is commonly adopted as the main buckling mode and the torsional-flexural buckling mode is not considered in the design.

Several works available in the literature proposed specific design procedures for steel angles. Recent research on the behavior of hot-rolled steel angles under compression was developed at Graz University of Technology, in Austria (Kettler et al., 2017, 2019a, 2019b, 2021, 2022), in which the influence of different boundary conditions of the gusset plate on the behavior of steel angles under eccentric compression was evaluated. Kettler et al. (2017) carried out a numerical study with 126 numerical models of steel angles connected by one and two bolts to a gusset plate with three different boundary conditions: clamped, knife and hinged supports. Kettler et al. (2019a) conducted 27 experimental tests on steel angles connected by one and two bolts with the same boundary conditions considered in Kettler et al. (2017). A design proposal for bolted angle members in compression was then developed, including the consideration of the rigidity of the joints (Kettler et al., 2019b, 2021). Subsequently, the same authors proposed another design model for the compressive strength of angle members that includes also welded end-joints (Kettler et al., 2022).

Another recent work on the behavior of steel angles in compression was the European project ANGELHY. 12 experimental tests on concentric and eccentric compression angles were executed and used to develop an extensive numerical analysis with approximately 225 numerical models. The results led to the development of improved design rules that cover: (i) the classification of cross-sections; (ii) the cross-section resistance in the elastic and elastoplastic ranges; and (iii) the buckling resistance (Bezas et al., 2021, 2022). The proposed methods are already included in Annex F of prEN 1993-3 and are currently being considered for possible inclusion as an amendment in FprEN 1993-1-1.

Finally, it is worth noting the recent works carried out on hot-rolled and cold-formed angle sections at Imperial College London (Behzadi-Sofiani et al., 2021, 2022b, 2023). Behzadi-Sofiani et al. (2021) conducted a parametric study based on 364 calibrated numerical models.

Their results were used as the basis for the development of a design proposal for fixed-ended angle member columns, that contemplates the effects of the interaction between minor-axis flexural and torsional-flexural buckling modes. Based on the same assumptions, the same authors proposed design methods for angle section beams (Behzadi-Sofiani et al., 2022b) and stainless-steel beam-columns (Behzadi-Sofiani et al., 2023).

This thesis presents a consistent study of the behaviour of mono-symmetric I-section steel beams and angle section members in concentric and eccentric compression. As established by the Jointly Supervised PhD Agreement (Cotutelle), it was co-directed between the Federal University of Minas Gerais (UFMG – Brazil) and the University of Coimbra (UC – Portugal), focusing on the behavior of bolted angle members in compression and in the extension of the General Formulation (GF) proposed by Tankova et al. (2018) to generic non-prismatic mono-symmetric cross-section beams.

1.2 Objectives

This thesis aimed to develop a comprehensive study on the behavior of welded mono-symmetric I-section beams and hot-rolled angle sections in concentric and eccentric compression.

Furthermore, the following specific objectives support the purpose of this thesis:

- extend the General Formulation for Class 1 and Class 2 Mono-symmetric I-section beams and angle members under compression;

- evaluate the different design procedures for verification of Mono-symmetric beams and compressed angles by using calibrated numerical models;

- validate the extended General Formulation by using numerical models, and compare its accuracy with other proposals.

1.3 Methodology

Concerning the mono-symmetric beams, an analytical derivation of an extension of the General Formulation that specifically accounts for the mono-symmetric features is firstly presented. Subsequently, an advanced finite element model is validated with experimental results on mono-symmetric beams (Tankova et al., 2021; Lebastard, 2022) and some benchmarks

obtained from the literature (Tankova et al. 2018), followed by an extensive parametric study for class 1 and class 2 cross-sections with prismatic and non-prismatic beams. Finally, the results are compared to the available design methodologies and the proposed extended GF.

Relative to equal leg angle sections in compression, to support the ongoing discussion on the choice and validation of code formulations for inclusion in Eurocode 3, this work assesses the design recommendations of EN 1993-1-1, EN 1993-3-1, FprEN 1993-1-1, and AISC 360 for pinned, fixed and partially restrained steel angle members under concentric and eccentric compression, as well as the methods proposed by the ANGELHY project, Kettler et al. (2017), and Behzadi-Sofiani et al. (2021), (2022b). Thus, an extensive numerical study was defined, in which parameters such as slenderness ratio, cross-sections (small and large angles), and steel grade (conventional and high-strength steel) were investigated. A finite element numerical model was developed and validated against experimental results from Kettler et al. (2019a) and the ANGELHY project. An extensive parametric study was undertaken to enlarge the numerical data available in the literature and the existing analytical rules to determine the ultimate resistance of steel angles under concentric and eccentric compression were critically discussed. Next, a reliability assessment is presented, aimed to establish the partial factor γ_{M1}, in line with the target failure probability recommended in the Eurocodes (Tankova et al., 2014). Finally, the GF is extended to angle sections subjected to concentric and eccentric compression, and a mechanically consistent Ayrton-Perry equation for angles subject to eccentric compression was derived.

1.4 Outline

This thesis is organized into eight chapters, as described below:

- **Chapter 1:** in this chapter, the background that motivates this research is exposed, where information concerning the behavior of mono-symmetric I-section beams and angle members in compression, and the limitations existing in their design are presented. It also gives, the objectives, methodology, motivation, and outline of the thesis;

- **Chapter 2:** this chapter comprises the state of art of this thesis. It is divided into five sections. The first summarizes the outlines of the chapter. The following two sections present the theoretical background concerning the stability of perfect and imperfect

members and its application to mono-symmetric beams and angle sections in compression. Furthermore, in these sections, the Ayrton-Perry equation is presented, as well as its applications in the elaboration of Eurocode prescriptions for members in compression and bending. In the next section, a brief history of the most relevant research related to the behavior of mono-symmetric I-sections subjected to bending and compressed angles is presented. The most relevant works for this thesis are exposed in more detail. In the last section of this chapter, the prescriptions of the codes regarding the buckling resistance of mono-symmetric beams and angle members in compression are detailed;

- **Chapter 3:** this chapter shows the development of the General Formulation: the basic assumptions, and its application to mono-symmetric I-section beams and angle members in concentric and eccentric compression;

- **Chapter 4:** this chapter exhibits the evaluation of the design codes for prismatic mono-symmetric I-section beams, based on validated numerical results;

- **Chapter 5:** this chapter presents the assessment of the prescriptions of the design codes and new proposals for angle members in concentric and eccentric compression. For that, an extensive parametric study based on a validated numerical model is used;

- **Chapter 6:** in this chapter, the General Formulation is further validated for tapered and non-prismatic mono-symmetric beams;

- **Chapter 7:** this chapter presents the validation of General Formulation for angle section members in concentric and eccentric compression;

- **Chapter 8:** this chapter presents the final remarks regarding the research carried out. It also gives recommendations for future works.

2

STATE OF ART

2.1 Introduction

This chapter aims to summarize the state of the art and the theoretical background necessary to achieve the objectives mentioned in Chapter 1, being organized into four sections, as described below:

- **Section 2.2:** this section covers all the theoretical background related to the stability of perfect members, starting with a brief history of the buckling problem. Next, the development of Vlasov's Theory on the phenomenon of torsional-flexural buckling is described in detail, where important concepts related to the torsion center, bi-moment, stability circle, among others, are presented. This section ends with the application of Vlasov's Theory to mono-symmetric I-beams and angles in compression.

- **Section 2.3:** this section presents the theoretical background concerning the buckling problem of imperfect members. Thus, the development of the Ayrton-Perry Equation and its use in the construction of the Eurocode 3 approach for buckling design is presented.

- **Section 2.4:** this section presents a brief survey involving the evolution of research related to the study of mono-symmetric I-sections and non-prismatic beams, and angle members in compression. The most relevant works for this work are described in detail.

- **Section 2.5:** this section summarizes the prescriptions of the main codes related to the design of mono-symmetric I-section beams and compressed angles.

2.2 Stability of Perfect Members

2.2.1 A Brief History Concerning the Stability of Perfect Members

According to Ballio and Mazzolani (1983), theoretical studies on the stability of perfect members date back to the year 75 BC with Erone d'Alexandria (see Figure 2.1). Similar studies were found in descriptions by Leonardo da Vinci (1452-1519), P. Van Musschenbroek (1693-1761) and Bernoulli (1700-1782). These studies served as the inspiration for the Swiss mathematician Leonard Euler (1707-1783) to propose, in 1744, and publish, in 1759, the formula for the elastic critical force (N_{cr}) of a member compressed axially in the elastic range, according to the equation:

$$N_{cr} = \frac{\pi^2 EI}{L^2} \qquad (2.1)$$

where E is the modulus of elasticity, I is the moment of inertia and L is the length of the compressed member. Euler considered a perfectly straight member, with no eccentricity of application of force and with both ends attached without restriction to rotation (pinned). However, Euler's theory failed to describe members with small slenderness (stocky). In other words, for stocky members, Equation (2.1) provided very high values for the buckling resistance of the members and, in many cases, higher than the yield strength of the entire cross-section.

The study of the stability of compressed members was extended from the works of Euler, being the focus of interest of many researchers and extending to the present day. Since the appearance of Equation (2.1) in the literature, theoretical and experimental developments on compressed members have never stopped.

Figure 2.1 – History of the studies carried out on the stability of members in compression. Source: Ballio and Mazzolani (1983) – Modified.

In practice, most compressed members have geometric and material imperfections and suffer localized plasticization and, therefore, the ultimate resistance obtained experimentally is lower than the force predicted by Equation (2.1). Engesser (1889) found that Euler's formula gave unreliable values for the ultimate resistance of axially compressed members and developed a theory of buckling based on the concept of the tangent modulus of elasticity. Engesser (1889) proposed that the modulus of elasticity (E) be replaced by the tangent modulus of elasticity (E_t) in Equation (2.1). On the other hand, Considéré (1890) suggested using the reduced modulus of elasticity (E_r) in the same equation. Jasinsky (1895) pointed out that the Theory of the Tangent Modulus of Elasticity was incorrect from the perspective of the classical stability theory. The author also highlighted that the reduced modulus of elasticity did not depend only on E and E_t, but also on the cross-sectional shape.

Based on the considerations of Considère (1890) and Jasinsky (1895), Engesser (1899) then presented the Theory of the Reduced Modulus of Elasticity or Double Modulus. In the elaboration of the theory, the author assumed the premise that inelastic buckling occurred without significant increments of force.

The Theory of Reduced Modulus of Elasticity was later perfected by von Karman (1910). This author derived expressions for calculating the reduced modulus of elasticity specifically for H-sections and members with rectangular cross-sections. Thus, to calculate the elastic critical force of these members, the author suggested the use of Equation (2.1) with the replacement of E by a function of two variables: E and E_t.

Nevertheless, both theories, Tangent and Reduced Modulus of Elasticity, were accepted to describe the phenomenon of inelastic buckling. However, engineers at the time were confused by the fact that the Theory of Reduced Modulus of Elasticity was correct, but the experimental results were closer to the Theory of Tangent Modulus of Elasticity (Bashar, 2012). Shanley (1947) solved this problem by conducting a detailed experiment on stocky aluminum members subjected to compression. The author observed that buckling started with loading values very close to those of the theoretical force obtained through the Theory of Tangent Modulus of Elasticity and that the value of this loading increased with the increase in displacements resulting from the buckling phenomenon. It was also observed that the ultimate resistance of the member never reached the value of the force calculated through the Theory of the Reduced Modulus of Elasticity. Given these results, the author presented a mathematical model for the determination of the critical force in the inelastic regime, thus showing that the tangent modulus model represented the real member behaviour well from the point of view of the value of the critical force.

In 1952, Friedrich Bleich published his famous book "Buckling Strength of Metal Structures", one of the most important and influential references on the buckling behavior of compressed metallic sections. The book was sponsored by the Department of the Maritime of the United States and was written to assist architects and engineers in the US Navy, thus being one of the first essential practical references on the stability of steel members to be published. In the book, different theories on the subject are presented, and several basic premises are examined. Bleich (1952) proposed a parabolic expression for calculating the elastic critical stress (σ_{cr}) of compressed steel members, given by:

$$\sigma_{cr} = f_y - \left(\frac{f_p}{\pi^2 E}\right)(f_y - f_p)\left(\frac{KL}{i_v}\right)^2 \tag{2.2}$$

where f_y is the yield strength, f_p is the proportionality stress, K is the effective length factor, and i_v is the radius of gyration about the minor-axis. In the 1950s, Equation (2.2) was used as the basis for the construction of the first curve of CRC (Column Research Council – former name of the Structural Stability Research Council - SSRC) that came to be widely known and adopted by the codes of several countries. Following this trend, in the 1960s studies began on the multiple resistance curves currently available at Lehigh University, in the United States, and at the European Convention for Constructional Steelwork (ECCS), in Europe.

As seen, the first research related to the behavior of compressed members was directed almost exclusively to understanding flexural buckling. Concepts related to the torsion center (also called shear center) were left out of the scope of the first studies on stability. And, obviously, torsional-flexural buckling was also not covered.

Torsional-flexural buckling began to be ostensibly investigated from the 1930s onwards and intensified from the second half of the 20th century, driven largely by the demands of a rational design of aircraft structures, naval constructions, and applied commonly in metallic structures, in the calculation of prefabricated elements of reinforced concrete and the calculation of cores in tall buildings (Mori, 2003). However, the first important work related to the subject was carried out by Saint-Venant (1855) on uniform torsion, which provided important descriptions of the torsional behavior of members. Michel (1899) and Prandtl (1899) later explored lateral-torsional buckling of beams with rectangular cross-sections. Warping of members subjected to torsion was firstly considered by Timoshenko (1905). Wagner and Pretschner (1936) were the first to investigate the torsional buckling of thin-walled open sections. However, the authors arbitrarily made assumptions about the torsion center that were later shown not to be entirely true (Shani, 1998). The first exact solution to the torsional-flexural problem of angle members was proposed by Ostenfeld (1931). Kappus (1937), Lundquist and Fligg (1937), Goodier (1942), Bleich (1952) and Timoshenko and Gere (1961) were the first researchers to study the torsional-flexural problem of members subjected to compression.

The torsional-flexural problem in the elastic regime of thin-walled open cross-section members was systematized by Vlasov (1962). The studies concerning stability, from the 1960s, received a considerable advance with the Torsional-flexural Theory proposed by Vlasov (1962).

However, the differential equations obtained from Vlasov´s Theory are difficult to solve when considering loads and general boundary conditions, requiring, for their resolution, Bessel functions or power series, or even numerical processes of integration (Rachid, 1975).

2.2.2 Basic Assumptions of Vlasov's Theory

The members of this subsection are referred to as a system of axes x y z, being y and z the principal axes of inertia of the cross-section and x the longitudinal axis that passes through the centroids of the sections. Consider, then, a generic, open, thin-walled cross-sectional member subject to an axial force (N) and bending moments (M_y and M_z) applied at the ends, as shown in Figure 2.2. In this figure, G represents the centroid of the cross-section, D is the torsion center, z_0 and y_0 are the coordinates of the torsion center (D) in the direction of the principal axes of inertia, dA is an infinitesimal element of area of the cross-section, G' and D' are, respectively, the centroid and the torsion center of the deformed shape, w_D and v_D are the displacements of the torsion center (D) in the z and y-direction, respectively, and θ is the twist rotation of the cross-section, with D' as reference.
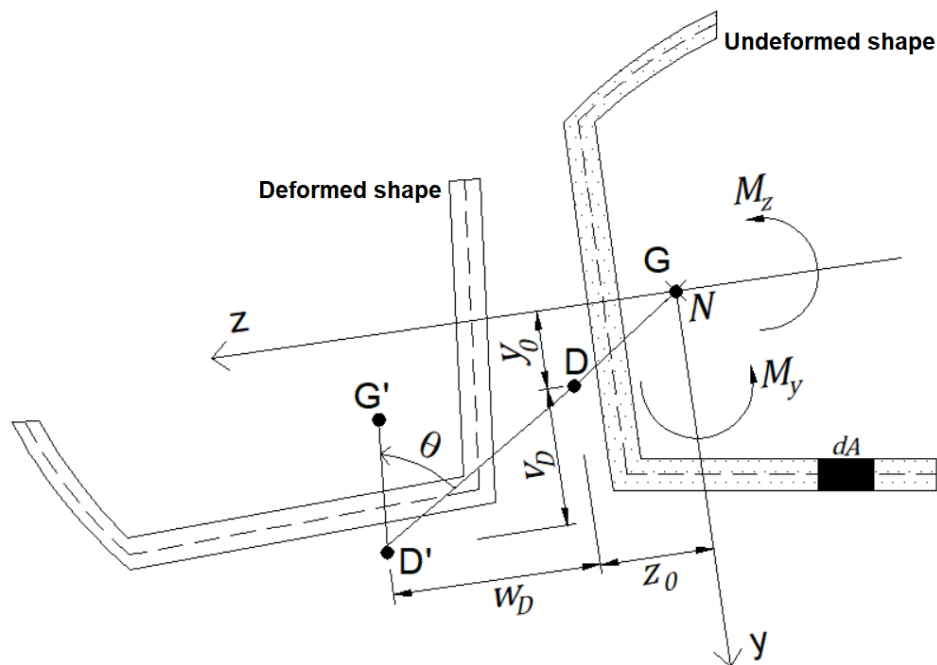
Figure 2.2 – Generic thin-walled open cross-section subjected to axial force and bending moments about the principal axes of inertia and its deformed shape.

According to Vlasov (1962), when this member is subjected to a load capable of causing its instability (critical load), it will occupy a new equilibrium position (deformed shape).

In the development of the Vlasov´s Theory, the following hypotheses are initially adopted:

- The thickness of the section is much smaller than the other dimensions of the cross-section, and these are much smaller than the length of the member;

- The cross-section is undeformable in its plane, and its dimensions is constant along the member length;

- The members are initially straight, without any initial geometric imperfection;

- The effects of residual stresses are negligible;

- Axial and shear strains are negligible;

- The material law is linear elastic.

The second hypothesis allows the problem to be treated as a rigid body movement in the plane yz, and thus, the new equilibrium position of the members can be characterized by three functions in x: angle of twist rotation ($\theta(x)$) and displacements ($w_D(x)$ and $v_D(x)$) of the torsion center in the directions of the principal axes of inertia (z and y, respectively), as shown in Figure 2.2. From these functions, differential equations are obtained. In Subsection 2.2.3, the differential equations for the cross-section shown in Figure 2.2 are derived, using the Equilibrium Method in the deformed shape and Second-Order Theory with small displacements.

2.2.3   Stability of a Generic Cross-section

As shown in Figure 2.2, the displacement of the cross-section in its plane can be considered as the superposition of displacements related to translation and twist rotation. Thus, using Second-Order Theory with small displacements, the following equations can be obtained:

$$v = v_D + (z - z_0)\theta \tag{2.3}$$

$$w = w_D - (y - y_0)\theta \tag{2.4}$$

, which express the displacements of the cross-section, v and w, in the directions y and z, respectively. v and w are functions of $v_D(x)$, $w_D(x)$ and $\theta(x)$, and the conditions that must satisfy these functions are expressed by three dependent differential equations. To deduce these equations, the basic equations of bending moment (of the Stability Theory) – Equations (2.5) and (2.6) - and torsional moment (proposed by Vlasov (1962)) – Equation (2.7) - are considered. From now on, the following sign conventions for the loading are adopted: compressive force or stress has a negative sign, and tension has a positive sign. The Second-order bending moments, M_y^{II} and M_z^{II}, have positive signs if they tension the part of the cross-section where z and y, respectively, are positive (see Figure 2.2) and negative signs otherwise. The Second-order torsional moment (M_t^{II}) has a positive sign if the cross-section rotates clockwise (see Figure 2.3-d), and a negative sign if rotation occurs in a counterclockwise direction.

$$EI_z v_D'' = M_z^{II} \tag{2.5}$$

$$EI_y w_D'' = M_y^{II} \tag{2.6}$$

$$EC_w \theta''' - GJ\theta' = -M_t^{II} \tag{2.7}$$

where:

I_z and I_y are the moments of inertia about to z and y, respectively;

M_t^{II} is the Second-order torsion moment;

J is the torsion constant;

G is the shear modulus;

C_w is the warping constant, obtained through the equation:

$$C_w = \int_A \omega^2 dA \tag{2.8}$$

In Equation (2.8), ω is the principal sectorial area and A, the cross-sectional area.

Differentiating Equations (2.5), (2.6) and (2.7) with respect to x, the following expressions are obtained:

$$EI_z v_D^{IV} = \frac{dQ_y}{dx} \tag{2.9}$$

$$EI_y w_D^{IV} = \frac{dQ_z}{dx} \tag{2.10}$$

$$EC_w \theta^{IV} - GJ\theta'' = -\frac{dM_t^{II}}{dx} \tag{2.11}$$

Equations (2.9), (2.10), and (2.11), in this form, only have first-order effects and are valid for the small displacements considered in this work. The derivatives of the right sides of these equations correspond to the distributed loads (forces and moments) along the length, being Q_y and Q_z the shear forces in the y- and z-directions, respectively. As only axial forces and bending moments applied at the ends are being considered (without distributed or concentrated loads along the member length), the normal stress (σ) is constant in x and the shear stress (τ) is zero. Consider an infinitesimal area element (dA) of a thin-walled generic open cross-section in its deformed shape, as shown in Figure 2.3-a and Figure 2.3-b:
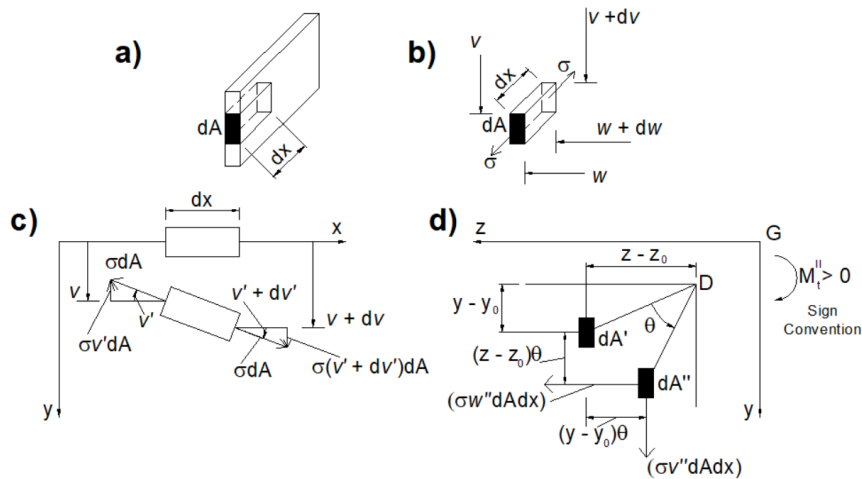
Figure 2.3 – Loading diagram on an infinitesimal element of area of a thin-walled generic open cross-section in its deformed shape.

Based on the loading diagram shown in Figure 2.3-c, the following equation is obtained:

$$dQ_y = \int_A[-\sigma dAv' + \sigma dA(v' + dv')] \tag{2.12}$$

Dividing Equation (2.12) by dx, the expression for the distributed load in the y-direction is obtained:

$$\frac{dQ_y}{dx} = \int_A\left(\sigma dA\frac{dv'}{dx}\right) \tag{2.13}$$

Analogously, the expression for the force distributed in the z-direction can be achieved:

$$\frac{dQ_z}{dx} = \int_A\left(\sigma dA\frac{dw'}{dx}\right) \tag{2.14}$$

In Figure 2.3-d, dA' corresponds to the translation of dA, and dA'' is its final deformed position (translation and rotation). From Figure 2.3-d the following equation is obtained:

$$dM_t^{II} = \int_A\{\sigma w''dAdx[(y - y_0) + (z - z_0)\theta] - \sigma v''dAdx[(z - z_0) + (y - y_0)\theta]\} \tag{2.15}$$

Dividing Equation (2.15) by dx gives the distributed torsion moment, given by:

$$\frac{dM_t^{II}}{dx} = \int_A\{\sigma w''dA[(y - y_0) + (z - z_0)\theta] - \sigma v''dA[(z - z_0) + (y - y_0)\theta]\} \tag{2.16}$$

Substituting Equations (2.13), (2.14) and (2.16) in Equations (2.9), (2.10) and (2.11), respectively, the following equation system is obtained:

$$EI_z v_D^{IV} = \int_A\sigma v''dA \tag{2.17}$$

$$EI_y w_D^{IV} = \int_A\sigma w''dA \tag{2.18}$$

$$EC_w\theta^{IV} - GJ\theta'' = \int_A\{\sigma v''[(z - z_0) - (y - y_0)\theta]\}dA - \int_A\{\sigma w''[(y - y_0) + (z - z_0)\theta]\}dA \tag{2.19}$$

According to Vlasov (1962), the normal stresses acting on the member receive the contribution of the bi-moment (B), according to the equation:

$$\sigma = \frac{N}{A} + \frac{M_y}{I_y}z + \frac{M_z}{I_z}y + \frac{B}{C_w}\omega \qquad (2.20)$$

Combining Equations (2.3), (2.4), and (2.20) with Equations (2.17), (2.18) and (2.19), the following equations can be achieved:

$$EI_z v_D^{IV} = \int_A \left[\frac{N}{A} + \frac{M_y}{I_y}z + \frac{M_z}{I_z}y + \frac{B}{C_w}\omega\right][v_D'' + (z - z_0)\theta'']dA \qquad (2.21)$$

$$EI_y w_D^{IV} = \int_A \left[\frac{N}{A} + \frac{M_y}{I_y}z + \frac{M_z}{I_z}y + \frac{B}{C_w}\omega\right][w_D'' + (y - y_0)\theta'']dA \qquad (2.22)$$

$$EC_w\theta^{IV} - GJ\theta'' = \int_A \left\{\left[\frac{N}{A} + \frac{M_y}{I_y}z + \frac{M_z}{I_z}y + \frac{B}{C_w}\omega\right][v_D'' + (z - z_0)\theta''][(z - z_0) - \right.$$
$$(y - y_0)\theta]\right\}dA - \int_A \left\{\left[\frac{N}{A} + \frac{M_y}{I_y}z + \frac{M_z}{I_z}y + \frac{B}{C_w}\omega\right][w_D'' + (y - y_0)\theta''][(y - y_0) + \qquad (2.23)$$
$$(z - z_0)\theta]\right\}dA$$

In Equations (2.21), (2.22), and (2.23), the following integrals are zero:

$$\int_A(yz)dA = \int_A(y)dA = \int_A(z)dA = \int_A(\omega)dA = \int_A(z\omega)dA = \int_A(y\omega)dA = 0 \qquad (2.24)$$

And so, after several algebraic manipulations, Equations (2.21), (2.22), and (2.23) then assume the best-known forms of differential stability equations for a thin-walled generic open cross-section member:

$$EI_z v_D^{IV} - Nv_D'' + (Nz_0 - M_y)\theta'' = 0 \qquad (2.25)$$

$$EI_y w_D^{IV} - Nw_D'' - (Ny_0 - M_z)\theta'' = 0 \qquad (2.26)$$

$$EC_w\theta^{IV} - [Ni_p^2 + 2M_y(k_z - z_0) + 2M_z(k_y - y_0) + GJ]\theta'' - (M_y - Nz_0)v_D''$$
$$+ (M_z - Ny_0)w_D'' = 0 \qquad (2.27)$$

where i_p is the polar radius of gyration, given by:

$$i_p^2 = \frac{I_z + I_y}{A} + z_0^2 + y_0^2 \tag{2.28}$$

and k_y and k_z are the coordinates of the center of the stability circle (Kindem point coordinates), calculated through Equations (2.29) and (2.30), respectively.

$$k_y = \frac{1}{2I_z}\int_A y(z^2 + y^2)dA \tag{2.29}$$

$$k_z = \frac{1}{2I_y}\int_A z(z^2 + y^2)dA \tag{2.30}$$

The fork boundary condition is very common in practical cases of metallic connections, where the ends of the member have free rotation about the principal axes of inertia, free warping, and restricted torsion. By imposing fork boundary conditions (see Table 2.1) on the ends of a member and subjecting it to a compressive force (by making $N = -N$), the solutions of Vlasov's differential equations, when the loading reaches its critical value, are:

$$v_D(x) = \bar{v}sen\frac{\pi}{L}x \tag{2.31}$$

$$w_D(x) = \bar{w}sen\frac{\pi}{L}x \tag{2.32}$$

$$\theta(x) = \bar{\theta}sen\frac{\pi}{L}x \tag{2.33}$$

where $\bar{v}$, $\bar{w}$, and $\bar{\theta}$ are the amplitudes of the displacements and rotations and L is the member length.

Table 2.1 – Fork boundary conditions.

Displacements and rotations	Bending moments and bi-moment
$v_D(0) = v_D(L) = 0$	$v_D''(0) = v_D''(L) = 0$
$w_D(0) = w_D(L) = 0$	$w_D''(0) = w_D''(L) = 0$
$\theta(0) = \theta(L) = 0$	$\theta''(0) = \theta''(L) = 0$

Combining Equations (2.31), (2.32) and (2.33) in the system of differential equations (Equations (2.25), (2.26) and (2.27)), the following matrix equation can be obtained:

$$\begin{bmatrix} \left(\frac{\pi^2 EI_z}{L_z^2} - N\right) & 0 & \left(Nz_0 + M_y\right) \\ 0 & \left(\frac{\pi^2 EI_y}{L_y^2} - N\right) & -(Ny_0 + M_z) \\ \left(Nz_0 + M_y\right) & -(Ny_0 + M_z) & \left[\begin{array}{c} \frac{\pi^2 EC_w}{L_x^2} - Ni_p^2 + 2M_y(k_z - z_0) + \\ 2M_z(k_y - y_0) + GJ \end{array}\right] \end{bmatrix} \begin{Bmatrix} \bar{v} \\ \bar{w} \\ \bar{\theta} \end{Bmatrix} = \begin{Bmatrix} 0 \\ 0 \\ 0 \end{Bmatrix} \qquad (2.34)$$

where L_x, L_y and L_z are the effective buckling lengths about x-, y- and z-axis, respectively.

Equation (2.34) can be generalized to several cases of boundary conditions by properly using effective buckling factors (K). Thus, the elastic critical axial force for flexural buckling about z- and y-axis, $N_{cr,z}$ and $N_{cr,y}$, respectively, and the elastic critical axial force for torsional buckling, $N_{cr,x}$, can be defined as:

$$N_{cr,z} = \frac{\pi^2 EI_z}{(K_z L_z)^2} \qquad (2.35)$$

$$N_{cr,y} = \frac{\pi^2 EI_y}{\left(K_y L_y\right)^2} \qquad (2.36)$$

$$N_{cr,x} = \frac{1}{i_p^2}\left[\frac{\pi^2 EC_w}{(K_x L_x)^2} + GJ\right] \qquad (2.37)$$

where

$K_z L_z$ and $K_y L_y$ are the effective buckling lengths about z- and y-axis;

$K_x L_x$ is the effective buckling length for torsional buckling.

Substituting the expressions given by Equations (2.35), (2.36), and (2.37) in Equation (2.34), and looking for a solution to the linear system other than the trivial one, the following is obtained:

$$\begin{vmatrix} (N_{cr,z} - N) & 0 & (Nz_0 + M_y) \\ 0 & (N_{cr,y} - N) & -(Ny_0 + M_z) \\ (Nz_0 + M_y) & -(Ny_0 + M_z) & \begin{bmatrix} i_p^2(N_{cr,x} - N) + 2M_y(k_z - z_0) \\ +2M_z(k_y - y_0) \end{bmatrix} \end{vmatrix} = 0 \qquad (2.38)$$

This equation can be rewritten in the following form:

$$(N_{cr,z} - N)(N_{cr,y} - N)\{N_{cr,x}i_p^2 + [-Ni_p^2 + 2M_y(k_z - z_0) + 2M_z(k_y - y_0)]\}$$
$$- (Nz_0 + M_y)^2(N_{cr,y} - N) - (Ny_0 + M_z)^2(N_{cr,z} - N) = 0 \qquad (2.39)$$

Equation (2.39) is a general equation, from which it is possible to determine the critical values of axial compressive forces and bending moments applied to the ends of a member.

Considering the more general case of torsional-flexural buckling, with longitudinal loads applied eccentrically to the extreme sections, as shown in Figure 2.4, with e_z and e_y being the coordinates of the point of application of the compressive load (N), the following is obtained:

$$M_z = -Ne_y \qquad (2.40)$$

$$M_y = -Ne_z \qquad (2.41)$$

The part of the cross-section where $z > 0$ and $y > 0$ (see Figure 2.4) is in compression, therefore the bending moments have negative values. Substituting Equations (2.40) and (2.41) in Equation (2.39), the following expression is obtained:

$$(N_{cr,z} - N)(N_{cr,y} - N)\{N_{cr,x}i_p^2 + [-Ni_p^2 - 2Ne_z(k_z - z_0) - 2Ne_y(k_y - y_0)]\}$$
$$- (Nz_0 - 2Ne_z)^2(N_{cr,y} - N) - (Ny_0 - 2Ne_y)^2(N_{cr,z} - N) = 0 \qquad (2.42)$$
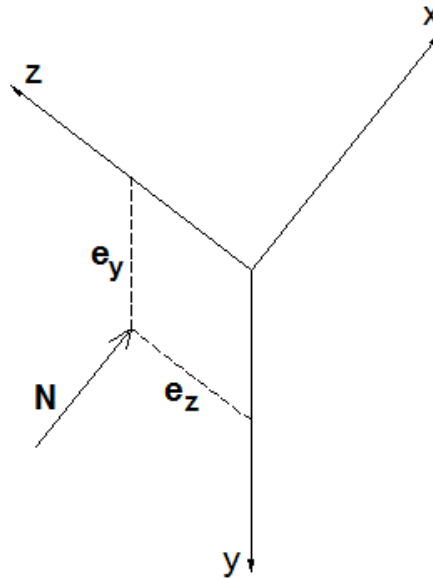
Figure 2.4 – Application of longitudinal eccentric load at the ends of a member.

Equation (2.42) gives three possible roots, where the elastic critical force (N_{cr}) is the smallest of the positive roots. In some cases, this equation may have negative roots and, therefore, there is the mathematical possibility of instability due to torsional flexural buckling when applying an eccentric longitudinal tension load. Setting a value for N, Equation (2.42) becomes a function with variables e_z and e_y, that is, an equation of a curve $f(e_z, e_y) = 0$. Establishing e_z and e_y as coordinates of points in the plane yz, the equation $f(e_z, e_y) = 0$ determines the region where, applying the force, one of the roots will be the given value N.

Thus, the instability of a member due to the action of an eccentric tension force is mathematically expressed by the fact that the curve defined by Equation (2.42) can be obtained with $N < 0$. Physically, this instability is explained by the possibility that there are normal compressive stresses, in part of the cross-section, generated by eccentric tensile forces. It is intuitive to think that a compression force has at least one critical value. The same does not happen with a tension force. If a tension force is applied in the central core of the section, there are tensile stresses and these do not cause instability of the member, and it is concluded that, for the occurrence of instability, the tensile force must be applied outside the central core.

Therefore, it is of interest to know if there is (and which is) the region of the cross-section where it is possible to apply a tension force, without provoking, with certainty, the instability of the member, that is, a region of stability.

Dividing Equation (2.42) by $\left(- N^2\left(N_{cr,y} - N\right)\left(N_{cr,z} - N\right)\left(N_{cr,x} - N\right) \neq 0\right)$, the following is obtained:

$$-\frac{i_p^2}{N^2} + \frac{2e_z(k_z - z_0)}{N\left(N_{cr,x} - N\right)} + \frac{2e_y\left(k_y - y_0\right)}{N\left(N_{cr,x} - N\right)} + \frac{(e_z - z_0)^2}{\left(N_{cr,z} - N\right)\left(N_{cr,x} - N\right)} + \frac{\left(e_y - y_0\right)^2}{\left(N_{cr,y} - N\right)\left(N_{cr,x} - N\right)} = 0 \qquad (2.43)$$

Dividing the denominator by N^2, and rearranging the expression, the following is achieved:

$$\frac{(e_z - z_0)^2}{\left(\frac{N_{cr,z}}{N} - 1\right)\left(\frac{N_{cr,x}}{N} - 1\right)} + \frac{\left(e_y - y_0\right)^2}{\left(\frac{N_{cr,y}}{N} - 1\right)\left(\frac{N_{cr,x}}{N} - 1\right)} + \frac{2e_z(k_z - z_0)}{\left(\frac{N_{cr,x}}{N} - 1\right)} + \frac{2e_y\left(k_y - y_0\right)}{\left(\frac{N_{cr,x}}{N} - 1\right)} - i_p^2 = 0 \qquad (2.44)$$

A force applied in the stability region (see Figure 2.5) leads to a cubic equation with three positive solutions (compression N). A force applied outside the region leads to a cubic equation with at least one negative solution (tension N). As in the limit of the region (see Figure 2.5) a root changes sign, it follows that the sign change cannot occur by the null value. Therefore, this change must occur through an infinite value. Thus, using $N \rightarrow \infty$ in Equation (2.44), the equation of the curve that limits the stability region is defined as:

$$(e_z - z_0)^2 + \left(e_y - y_0\right)^2 - 2e_z(k_z - z_0) - 2e_y\left(k_y - y_0\right) - i_p^2 = 0 \qquad (2.45)$$

Substituting Equation (2.28) in Equation (2.45), the following is found:

$$e_z{}^2 + e_y{}^2 - 2e_zk_z - 2e_yk_y = \frac{I_z + I_y}{A} \qquad (2.46)$$

Adding the expression $(k_z{}^2 + k_y{}^2)$ to both sides of Equation (2.46), the following is finally obtained:

$$(e_z - k_z)^2 + \left(e_y - k_y\right)^2 = k_z{}^2 + k_y{}^2 + \frac{I_z + I_y}{A} \qquad (2.47)$$
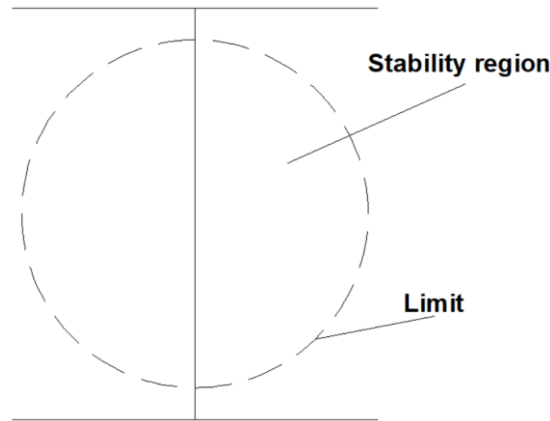
Figure 2.5 – Stability region of an I-section and its limits.

Equation (2.47) expresses the equation of a circle where k_x and k_y are the coordinates of its center about the principal axes of inertia (Kinden Point – KP – coordinates) and the expression $\left(k_z{}^2 + k_y{}^2 + \frac{I_z + I_y}{A}\right)$ is the square of its radius (R). The stability region is bounded by the stability circle, regardless of the cross-sectional shape, value of N and boundary condition of the member.

In summary, under the action of an eccentric longitudinal force, the instability of a member can occur in cases of compression or tension forces. In the case of compressive force, it can occur regardless of the loading point application. In the case of tension force, there is only the possibility of the occurrence of instability if the force is applied outside the stability circle. From a purely mathematical point of view, it is possible the occurrence of instability with an eccentric longitudinal tension force applied within the cross-section. From a practical point of view, however, the tensile stresses that appear are very high, surpassing the yielding strength of the materials used in the manufacture of the members. Thus, the failure of the member must occur because the ultimate strength of the material is exceeded rather than instability occurrence.

2.2.4 Stability of Mono-Symmetric I-Section Beams

Figure 2.6 shows a typical mono-symmetric I-section studied in this work. This section is symmetric with respect to the minor axis, z, and asymmetric around the major axis, y. The members are subjected to bending moment around y-axis. In this figure, h is the height of the section, h_0 is the distance between the centerlines of the flanges, h_w is the height of the web

and t_w is its thickness; b_1 and t_1 are the dimensions of the flange with the smallest value of I_z (moment of inertia about the z-axis), and b_2 and t_2 are the dimensions of the largest flange; z_G is the position of the cross-section centroid measured from the top face of the flange with the largest value of I_z.
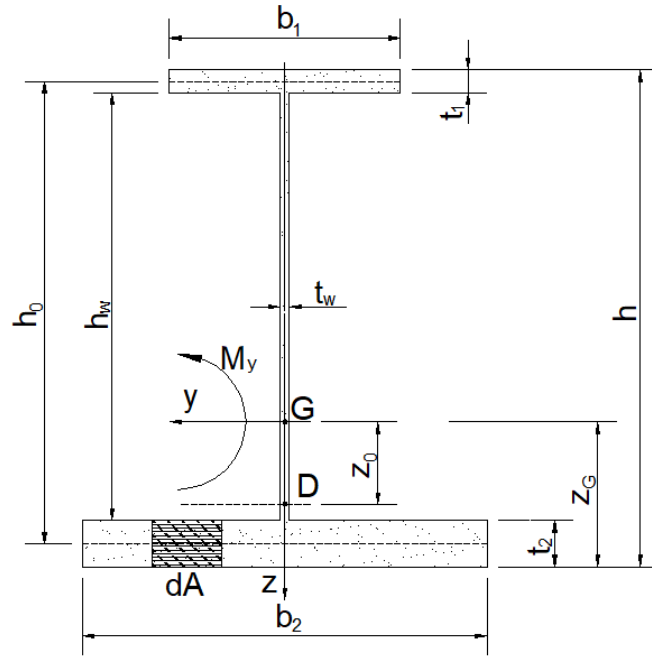
Figure 2.6 – Typical mono-symmetric I-section beam.

For a mono-symmetric I profile subjected to constant bending moment ($\pm M_y$) around the axis of greatest inertia (Figure 2.6), the stability equations (see Equations (2.25), (2.26) and (2.27)) become (considering $k_y = y_0 = 0$):

$$EI_z v_D^{IV} \pm M_y \theta'' = 0 \tag{2.48}$$

$$EC_w \theta^{IV} - \left[\pm 2M_y(k_z - z_0) + GJ\right]\theta'' - \left(\pm M_y - Nz_0\right)v_D'' = 0 \tag{2.49}$$

Through the same rearrangement made to obtain Equation (2.39), the following expression can be obtained:

$$N_{cr,z}\left[N_{cr,x}i_p^2 \pm 2M_y(k_z - z_0)\right] - M_y{}^2 = 0 \rightarrow$$

$$M_y{}^2 \pm 2M_y N_{cr,z}(k_z - z_0) - N_{cr,x}N_{cr,z}i_p^2 = 0 \tag{2.50}$$

, whose solution $M_y = M_{cr}$ is given by:

$$M_{cr} = \frac{\pi^2 EI_z}{(K_z L_z)^2} \left\{ \sqrt{\left(\frac{K_z}{K_x}\right)^2 \frac{C_w}{I_z} + \frac{(K_z L_z)^2 GJ}{\pi^2 EI_z} + \beta_z{}^2} \pm \beta_z \right\} \tag{2.51}$$

Considering $K_x = K_z = 1.0$, the value obtained by Equation (2.51) is the elastic critical bending moment for lateral-torsional buckling for a mono-symmetric I-section with constant bending moment diagram and fork boundary conditions (see Table 2.1). β_z is a factor that incorporates the Wagner effect (Wagner, 1936) due to the mono-symmetry, given by:

$$\beta_z = z_0 - k_z = z_0 - \frac{1}{2I_y} \int_A [z(z^2 + y^2)] dA \tag{2.52}$$

Conventionally, β_z is positive when the flange with the larger value of I_z is in compression at the point of the largest bending moment.

For uniform members with variable boundary conditions and arbitrary loading, Equation (2.51) becomes:

$$M_{cr} = C_1 \frac{\pi^2 EI_z}{(K_z L)^2} \left\{ \sqrt{\left(\frac{K_z}{K_x}\right)^2 \frac{C_w}{I_z} + \frac{(K_z L)^2 GJ}{\pi^2 EI_z} + (\pm C_2 z_g \pm C_3 \beta_z)^2} - (\pm C_2 z_g \pm C_3 \beta_z) \right\} \tag{2.53}$$

C_1, C_2 and C_3 are factors depending on the loading and end restraint conditions, and z_g is the distance between the point of load application and the torsion center, being positive for loads acting towards the torsion center from their point of application.

Table 2.2 summarizes some equations for determining the geometric properties of a mono-symmetric I-section: the centroid position (z_G - see Figure 2.6), the torsion center coordinate (z_0 - see Figure 2.6), the Wagner factor (β_z), and the warping constant (C_w).

Table 2.2 – Geometric properties for mono-symmetric I-section.

$$z_G = \frac{b_2 \frac{t_2^2}{2} + h_w t_w \left[\frac{h_w}{3} + t_2\right] + b_1 t_1 \left(h - \frac{t_1}{2}\right)}{(b_1 t_1 - b_2 t_2) + h_w t_w} \tag{2.54}$$

$$z_0 = \frac{\left(z_G - \frac{t_2}{2}\right) t_2 b_2^3 - \left(h - z_G - \frac{t_1}{2}\right) t_1 b_1^3}{t_1 b_1^3 + t_2 b_2^3} \tag{2.55}$$

$$\beta_z = z_0 - \frac{1}{2I_y} \left\{ \begin{array}{l} b_2 \frac{t_2}{4} (2z_G - t_2)\left(\frac{b_2^2}{6} + 2z_G^2 - 2z_G t_2 + t_2^2\right) + \\[2mm] \frac{t_w}{4} h_w (2z_G + t_2 - h - t_1)\left[\frac{t_w^2}{6} + (t_1 - z_G)^2 + (h - z_G - t_2)^2\right] + \\[2mm] b_1 \frac{t_1}{4} [t_1 - 2(h - z_G)]\left[\frac{b_1^2}{6} + (h - z_G - t_1)^2 + (h - z_G)^2\right] \end{array} \right\} \tag{2.56}$$

$$C_w = \frac{h_0^2}{12}\left(\frac{t_1 b_1^3 t_2 b_2^3}{t_1 b_1^3 + t_2 b_2^3}\right) \tag{2.57}$$

2.2.5 Stability of Angle Members in Compression

The geometric and principal axes of inertia of angle sections do not coincide, therefore, unlike the mono-symmetric I-section, the cross-section properties and elastic critical loads of this section are referred to as the principal axes of inertia: u and v – the major- and minor-axis, respectively. The analysis of the stability of angle members in compression begins with the most general case: eccentric compression. In this work, the eccentricity of load application (e_u and e_v) is related to the use of bolts in only one leg (connection configuration most typically used in angle members), as shown in Figure 2.7. In this figure, h is the width of the leg, and t is its thickness, g is the drilling template, dh is an infinitesimal length element along the flange, y and z are the geometric axes parallel to the legs, with y being the axis parallel to the connected leg.
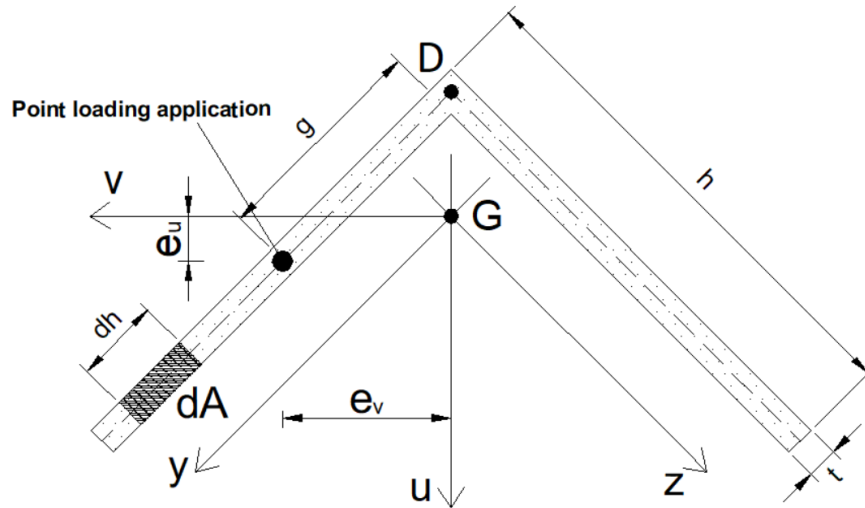
Figure 2.7 – Typical angle section in eccentric compression.

Angle sections, as well as the cruciform section and the T-section, belong to a group of sections in which their elements coincide at one point, which gives them certain peculiarities. The torsion center (D) (see Figure 2.7) of the angle section is located where the legs meet, therefore, the warping constant, C_w, is zero (see Equation (2.8)). This fact makes the angle member more susceptible to torsional-flexural buckling. Furthermore, due to the symmetry of the cross-section around the major-axis, the values of the coordinate of the torsion center in the v-direction and k_v (the coordinate of the Kindem Point in the v-direction) are also zero. The coordinate of the Kindem point (KP) of the angle section about the major axis, k_u, is obtained through Equation (2.29), making $dA = tdh$. From Figure 2.7, it is known that:

$$dh = \sqrt{(dv)^2 + (du)^2}$$ (2.58)

and therefore, the following is obtained:

$$dA = t\left(\sqrt{1 + \left(\frac{du}{dv}\right)^2}\right)dz$$ (2.59)

It is possible to parameterize u in terms of v, where the following expression is obtained:

$$u = \begin{cases} v - u_D, & for\ v \geq 0 \\ -v - u_D, & for\ v < 0 \end{cases}, \ u_D < 0 \tag{2.60}$$

where u_D is the coordinate of the torsion center in the u-direction. Thus, the Equation (2.59) reduces to:

$$dA = \sqrt{2}tdv \tag{2.61}$$

Thus, the value of k_u can be calculated using the equation:

$$k_u = \frac{1}{2I_v} \int_{-\sqrt{2}h/2}^{\sqrt{2}h/2} \sqrt{2}u(v^2 + u^2)\, tdv \tag{2.62}$$

Substituting the parameterized value of u (given by Equation (2.60)) in Equation (2.62), the following expression is achieved:

$$k_u = \frac{\sqrt{2}t}{2I_v} \left\{ \int_{-\sqrt{2}h/2}^{0} (-v - u_D)[v^2 + (-v - u_D)^2]\, dv + \int_{0}^{\sqrt{2}h/2} (v - u_D)[v^2 + (v - u_D)^2]\, dv \right\} \tag{2.63}$$

Finally, after an algebraic manipulation of Equation (2.63), the following is found:

$$k_u = \frac{\sqrt{2}t}{I_v} \left(0.125h^4 + \frac{\sqrt{2}}{3} u_D h^3 + 0.75 u_D^2 h^2 + \frac{\sqrt{2}}{2} u_D^3 h \right),\ \text{with}\ u_D < 0 \tag{2.64}$$

It is interesting to note in Equation (2.64) that the Kindem point coordinate of the angle section, k_u, depends only on the cross-section properties. From Equation (2.47), the equation of the stability circle for an angle section is obtained:

$$v^2 + (u^2 - k_u)^2 = k_u^2 + \frac{I_v + I_u}{A} = R^2 \tag{2.65}$$

Figure 2.8 presents the stability circle for an equal-leg angle section. It can be seen in this figure that the regions located at the half-width of the legs are inside the stability region, while the corner and the tips are outside. Combining Equations (2.60) and (2.65), it is possible to define

exactly the portion of the cross-section of the angle section that lies within the stability circle, delimited by the following expressions:

$$\begin{cases} -0.5\left[k_u + u_D + \sqrt{2R^2 - (k_u + u_D)^2}\right] \le e_v \le -0.5\left[k_u + u_D - \sqrt{2R^2 - (k_u + u_D)^2}\right] \\ 0.5\left[k_u + u_D - \sqrt{2R^2 - (k_u + u_D)^2}\right] - u_D \le e_u \le 0.5\left[k_u + u_D + \sqrt{2R^2 - (k_u + u_D)^2}\right] - u_D \\ -\frac{\sqrt{2}}{2}\left[k_u + u_D + \sqrt{2R^2 - (k_u + u_D)^2}\right] \le g \le -\frac{\sqrt{2}}{2}\left[k_u + u_D - \sqrt{2R^2 - (k_u + u_D)^2}\right] \end{cases} \quad (2.66)$$

These expressions delimit the region of the legs that is inside the stability circle (see Figure 2.8). As seen in Subsection 2.2.3, when a compressive force is applied in this region, only positive roots of Equation (2.42) are obtained.
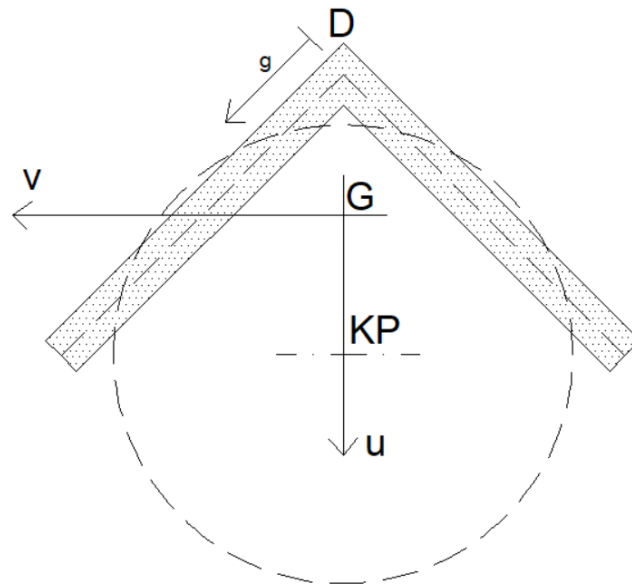
Figure 2.8 – Stability Circle for an equal-leg angle section.

Inserting the cross-section properties of an angle section in Equation (2.38), Equation (2.67) is obtained. This equation describes the problem of instability of angles in eccentric compression:

$$\begin{vmatrix} (N_{cr,v} - N) & 0 & -Ne_v \\ 0 & (N_{cr,u} - N) & N(e_u + u_D) \\ -Ne_v & N(e_u + u_D) & i_p^2(N_{cr,x} - N) - 2N(k_u - u_D)e_u \end{vmatrix} = 0 \quad (2.67)$$

Equation (2.67) can be rewritten in the form of the equation:

$$\begin{aligned}&(N_{cr,v} - N)(N_{cr,u} - N)\{N_{cr,x}i_p^2 - N[i_p^2 + 2e_u(k_u - u_D)]\} - N^2 e_v^2 (N_{cr,u} - N) \\ &- N^2 (e_u - u_D)^2 (N_{cr,v} - N) = 0\end{aligned} \qquad (2.68)$$

where $N_{cr,v}$ and $N_{cr,u}$ are calculated through Equations (2.35) and (2.36), respectively (replacing z by v and y by u). As the warping constant of an angle is zero, the first part of Equation (2.37) disappears, and elastic critical axial force for torsional buckling, $N_{cr,x}$, is given by:

$$N_{cr,x} = \frac{GJ}{i_p^{\,2}} \qquad (2.69)$$

Equation (2.68) gives three possible roots, where the elastic critical force (N_{cr}) is the smallest of the positive roots.

If N is applied at the centroid (G), the angle section is in concentric compression ($e_v = e_u = 0$), and Equation (2.25) becomes decoupled from the others. With that, Equation (2.67) takes the following form:

$$\begin{vmatrix} (N_{cr,v} - N) & 0 & 0 \\ 0 & (N_{cr,u} - N) & Nu_D \\ 0 & Nu_D & i_p^2 (N_{cr,x} - N) \end{vmatrix} = 0 \qquad (2.70)$$

Equation (2.70) has three positive solutions: two of them relative to elastic critical axial forces for torsional-flexural buckling and one to elastic critical axial force for flexural buckling about the minor axis. However, one of the solutions, relative to one of the axial forces for torsional-flexural buckling, is always greater than the other roots. Therefore, the concentrically compressed angle members present flexural buckling about the minor axis ($N_{cr,v}$) or torsional-flexural buckling ($N_{cr,TF}$). The value of N_{cr} is the smallest value between $N_{cr,v}$ and $N_{cr,TF}$, being $N_{cr,TF}$ obtained through the equation:

$$N_{cr,TF} = \frac{N_{cr,u} + N_{cr,x}}{2\left[1 - \left(\frac{u_D}{i_p}\right)^2\right]} \left[1 - \sqrt{1 - \frac{4 N_{cr,u} N_{cr,x}\left[1 - \left(\frac{u_D}{i_p}\right)^2\right]}{(N_{cr,u} + N_{cr,x})^2}}\right] \qquad (2.71)$$

where $N_{cr,u}$ and $N_{cr,x}$ are given by Equations (2.36) and (2.69), respectively. These formulations are considered in most prescriptions related to the design of mono-symmetric members subjected to concentric compression.

If the compressive force is applied at the torsion center (at D, where $e_v = 0$ and $e_u = u_0$), Equations (2.25), (2.26), and (2.27) become decoupled from each other, and Equation (2.67) can be rewritten as follows:

$$\begin{vmatrix} (N_{cr,v} - N) & 0 & 0 \\ 0 & (N_{cr,u} - N) & 0 \\ 0 & 0 & i_p^2(N_{cr,x} - N) - 2N(k_u - u_D)u_D \end{vmatrix} = 0 \qquad (2.72)$$

Since the force is applied at a point outside the stability circle, Equation (2.72) has two positive roots and one negative root. Concerning the positive roots, one of them is relative to flexural buckling about the v-axis (see Equation (2.35)) and the other is relative to the flexural buckling about the u-axis (see Equation (2.36)). As the first is always smaller than the second, the angle member always suffers flexural buckling about the minor axis when the compressive force acts on the torsion center. Concerning the negative root, the following result is obtained:

$$N_{cr,x} = \frac{GJ}{i_p^2 + 2u_0(k_u - u_D)}, \text{ with } u_D < 0 \qquad (2.73)$$

That is, theoretically, if a tension force is applied at the center of torsion, the angle will suffer instability associated with torsional buckling. In practice, the value of this force is very high, and therefore, the angle will fail for reasons related to overcoming the yield strength of the steel before suffering instability.

2.3 Stability of Imperfect Members

2.3.1 General Description of Members with Initial Geometric Imperfections

In Section 2.2, the problem of elastic buckling of perfectly straight members is exposed. It was seen that this study was initiated with the publication of Euler's theory of stability (1759) for compressed members, and continued successively by Engesser (1889), Consideré (1890), von Karman (1910), Shanley (1947), among others. However, in practice, a structure is not perfectly

straight, and the analysis of this structure must be carried out as realistically as possible, considering small deviations that exist in the directions of the principal axes of inertia. At the same time as the first studies on the buckling of straight members, the study of the behavior of imperfect elements became of interest to many researchers, starting with Young (1807), who evaluated the elastic behavior of elements with initial geometric imperfections. The classic work in this direction was carried out by Ayrton and Perry (1886), who were the first to propose compressive strength curves based on yielding strength (f_y). These authors, by using the Second-order theory, defined the resistance of compressed members as being when the yielding of the most compressed fiber of the cross-section occurs. The studies of these authors provided the well-known Ayrton-Perry Equation. Robertson (1925) experimentally validated the model proposed by Ayrton and Perry (1886) and provided an important advance in the study of imperfect members by presenting a relationship between the generalized imperfection factor (η) and the slenderness of the members (λ).

Given the existence of initial geometric imperfections, it is not possible to consider the hypothesis of perfectly straight structural elements. In other words, the equilibrium bifurcation problem becomes a problem where small variations in the force application cause large changes in the displacements. To verify this phenomenon, consider the diagram of amplitudes of imperfections in the elastic regime, at the mid-span of the member, shown in Figure 2.9. In this figure, w_0 and v_0 are the initial geometric imperfection of translation about the principal axes of inertia, z and y, respectively; and θ_0 is the initial geometric imperfection of twist rotation.
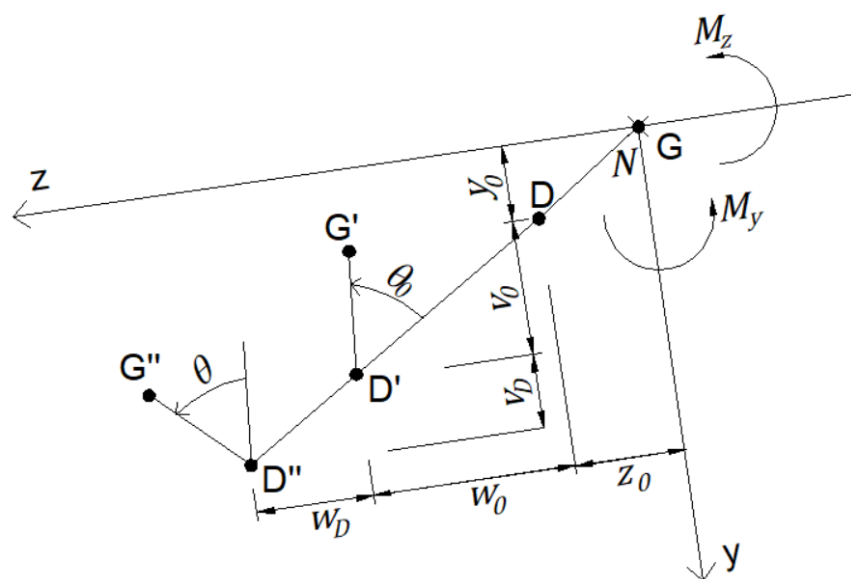
Figure 2.9 – Initial geometric imperfections diagram.

Based on the diagram shown in Figure 2.9, Equations (2.25), (2.26) and (2.27) become:

$$EI_z v_D^{IV} - N(v_D'' + v_0'') + (Nz_0 - M_y)(\theta'' + \theta_0'') = 0 \tag{2.74}$$

$$EI_y w_D^{IV} - N(w_D'' + w_0'') - (Ny_0 - M_z)(\theta'' + \theta_0'') = 0 \tag{2.75}$$

$$\begin{aligned} EC_w \theta^{IV} - GJ\theta'' &- \left[Ni_p^2 + 2M_y(k_z - z_0) + 2M_z(k_y - y_0)\right](\theta'' + \theta_0'') - (M_y \\ &- Nz_0)(v_D'' + v_0'') + (M_z - Ny_0)(w_D'' + w_0'') = 0 \end{aligned} \tag{2.76}$$

Analogously to the displacements and rotations caused by loads (Equations (2.31), (2.32) and (2.33)), the initial geometric imperfections can be equated by:

$$v_0(x) = \bar{v}_0 sen\frac{\pi}{L}x \tag{2.77}$$

$$w_0(x) = \bar{w}_0 sen\frac{\pi}{L}x \tag{2.78}$$

$$\theta_0(x) = \bar{\theta}_0 sen\frac{\pi}{L}x \tag{2.79}$$

Combining the solutions represented by Equations (2.31) to (2.33) and Equations (2.77) to (2.79) in the system of Equations (2.74) to (2.76), the amplitudes of the total displacements at mid-span of an imperfect member can be obtained:

$$\begin{bmatrix} \bar{v}_{tot} \\ \bar{w}_{tot} \\ \bar{\theta}_{tot} \end{bmatrix} = \begin{bmatrix} \bar{v} \\ \bar{w} \\ \bar{\theta} \end{bmatrix} + \begin{bmatrix} \bar{v}_0 \\ \bar{w}_0 \\ \bar{\theta}_0 \end{bmatrix} \tag{2.80}$$

$$=$$

$$\frac{1}{C}\begin{bmatrix}\begin{bmatrix}-N_{cr,z}(N-N_{cr,y})\\ \begin{bmatrix} Ni_p^2 - 2M_y(k_z-z_0)\\ -2M_z(k_y-y_0)-i_p^2N_{cr,x}\end{bmatrix}\\ +(M_z+Ny_0)N\\ -(Ny_0+M_z)^2(N-N_{cr,z})\end{bmatrix} & \begin{bmatrix}N_{cr,y}M_yM_z+N_{cr,y}M_yNy_0\\ +N_{cr,y}M_zNz_0+N_{cr,y}N^2z_0y_0\end{bmatrix} & [-i_p^2N_{cr,x}(N-N_{cr,y})(Nz_0+M_y)]\\[20pt] \begin{bmatrix}N_{cr,z}M_yM_z+N_{cr,z}M_zNz_0\\ +N_{cr,z}M_yNy_0+N_{cr,z}N^2z_0y_0\end{bmatrix} & \begin{bmatrix}-N_{cr,y}(N-N_{cr,z})\\ \begin{bmatrix} Ni_p^2 - 2M_y(k_z-z_0)\\ -2M_z(k_y-y_0)-i_p^2N_{cr,x}\end{bmatrix}\\ +(M_y+Nz_0)N\\ -(Nz_0+M_y)^2(N-N_{cr,y})\end{bmatrix} & [i_p^2N_{cr,x}(N-N_{cr,z})(Ny_0+M_z)]\\[20pt] \begin{bmatrix}-NN_{cr,z}M_y-N_{cr,z}N^2z_0\\ +N_{cr,z}N_{cr,y}M_y+N_{cr,z}N_{cr,y}Nz_0\end{bmatrix} & \begin{bmatrix}NN_{cr,y}M_z+N_{cr,y}N^2y_0\\ -N_{cr,z}N_{cr,y}M_z-N_{cr,z}N_{cr,y}Ny_0\end{bmatrix} & [-i_p^2N_{cr,x}(N-N_{cr,z})(N-N_{cr,y})]\end{bmatrix}$$

$$\text{x}\begin{bmatrix}\bar{v}_0\\ \bar{w}_0\\ \bar{\theta}_0\end{bmatrix}$$

where C is given by:

$$C = (N-N_{cr,z})(N-N_{cr,y})[Ni_p^2 - 2M_y(k_z-z_0) - 2M_z(k_y-y_0) - i_p^2N_{cr,x}] - \\ (Nz_0+M_y)^2(N-N_{cr,y}) - (Ny_0+M_z)^2(N-N_{cr,z}) \tag{2.81}$$

Considering the bi-dimensional model proposed by Young (1807) - Figure 2.10 -, Equation (2.80) becomes the Equation of Young (Slazai, 2017):

$$\bar{v}_{tot} = \left(\frac{1}{1-\frac{N}{N_{cr}}}\right)\bar{v}_0 \tag{2.82}$$

Considering the equilibrium of the member in the deformed shape (see Figure 2.10), the second-order bending moment is obtained:

$$M^{II} = N\bar{v}_{tot} = N\left(\frac{1}{1-\frac{N}{N_{cr}}}\right)\bar{v}_0 \tag{2.83}$$
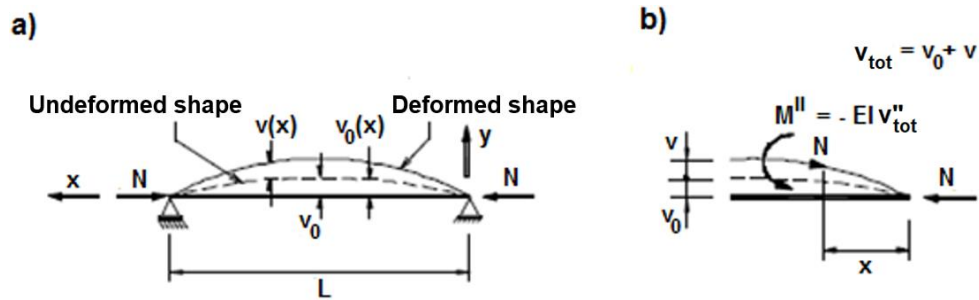
Figure 2.10 – Member with initial geometric imperfection.

Equation (2.83) became important for determining the parameters that govern the compressive strength curves. From the publication of the work of Young (1807) the study of imperfect members and design curves began. The most prominent work developed on the subject was carried out by Ayrton and Perry (1886).

The following subsection brings more details about the Ayrton-Perry Equation and its application in the construction of design curves.

2.3.2 Ayrton-Perry Equation

Assuming that the maximum stress in a member in compression (see Figure 2.10 - Subsection 2.3.1) is equal to the yielding strength (f_y), the following expression can be defined:

$$\frac{N}{A} + \frac{M^{II}}{W} = f_y \tag{2.84}$$

where W is the elastic section modulus. Substituting Equation (2.83) in Equation (2.84), and multiplying the second term on the right side of the resulting equation by (A/A), the following is obtained:

$$\frac{N}{A} + \frac{N}{W} \left(\frac{A}{A}\right) \bar{v}_0 \left(\frac{1}{1 - \frac{N}{N_{cr}}}\right) = f_y \tag{2.85}$$

Manipulating algebraically the Equation (2.85), the following expression is found:

$$\frac{N}{A} + \frac{N}{A}\eta\left(\frac{1}{1 - \frac{N}{N_{cr}}}\right) = f_y \tag{2.86}$$

where η is the generalized imperfection factor, obtained by the equation:

$$\eta = \frac{A\bar{v}_0}{W} \tag{2.87}$$

Rewriting the terms of Equation (2.86), the following expression is obtained:

$$\eta\left(\frac{N}{A}\right) = \left(f_y - \frac{N}{A_g}\right)\left(1 - \frac{N}{N_{cr}}\right) \tag{2.88}$$

Dividing both sides of Equation (2.88) by f_y and rearranging the terms, the following equation is achieved:

$$\eta\chi = (1 - \chi)\left(1 - \chi\bar{\lambda}^2\right) \tag{2.89}$$

where χ is the reduction factor associated with the compressive strength, and $\bar{\lambda}$ is the non-dimensional slenderness, given by, respectively:

$$\chi = \frac{N}{Af_y} \tag{2.90}$$

$$\bar{\lambda} = \sqrt{\frac{Af_y}{N_{cr}}} \tag{2.91}$$

Equation (2.89) is known as the dimensionless Ayrton-Perry equation. The generalized imperfection factor, η, mathematically represents the influence of initial geometric imperfections and the effects of residual stresses. This parameter also provides information regarding the cross-section shape. Robertson (1925), based on experimental results, presented a relationship between this factor and the member slenderness, according to the equation:

$$\eta = 0.003\,\lambda \tag{2.92}$$

The combination of Equations (2.89) and (2.92) is known as the Perry-Robertson Equation. According to Tankova et al. (2018), this model is at the origin of the European buckling curves that were established in the 1970s, based on an extensive experimental program conducted by the ECCS, and developed through theoretical analyses of the experimental results and reliability analyzes through Monte Carlo simulations. Thus, the buckling curves of the European codes were elaborated according to the member geometry and their imperfections, also considering the material properties and residual stresses.

Maquoi and Rondal (1978), (1979) showed a significative influence on the development of the curves of Eurocode 3. Maquoi and Rondal (1978) presented a formulation for new buckling curves for the ECCS based on the dimensionless Ayrton-Perry equation (Equation (2.89)), where the factor η represented the generalized imperfections and the curves were characterized by a yielding plateau when $\bar{\lambda} \leq 0.2$. Maquoi and Rondal (1979) showed that the way to represent the generalized imperfection depended on the type of material used and that this representation must be different for steel and aluminum. The dimensionless Ayrton-Perry equation continued to be used to determine the new European buckling curves, but with the generalized imperfection factor given by the equation:

$$\eta = \alpha\big(\bar{\lambda} - 0.2\big) \tag{2.93}$$

Equation (2.93) is adopted by EN 1993-1-1, where α is the imperfection factor, given according to the buckling curve. As can be seen from Equation (2.93), the buckling curves of the European code are based on the calibration of imperfection factors to determine the ultimate resistance of the members, which gives the flexibility to adjust these factors according to the type of cross-section, steel grade, and other relevant parameters. This feature allows the adoption of the Ayrton-Perry Equation for more general applications.

Recently, Taras and Greiner (2010) proposed new design curves for lateral-torsional buckling based on the Ayrton-Perry Equation, providing more accurate results than those of the current expression (Equation (2.93)). Considering a prismatic doubly symmetric I-section beam subjected to constant bending moment about the y-axis, and the coupling relationship proposed by Chen and Astuta (1977):

$$\bar{v}_0 = \frac{M_{cr}}{N_{cr,z}}\bar{\theta}_0 = i_p\sqrt{\frac{N_{cr,x}}{N_{cr,z}}}\bar{\theta}_0 \tag{2.94}$$

Equation (2.80) provides the following relationships:

$$\bar{v}_{tot} = \bar{\theta}_0\frac{M_{cr}^2}{N_{cr,z}}\frac{1}{M_{cr} - M_y} \tag{2.95}$$

$$\bar{\theta}_{tot} = \bar{\theta}_0\frac{M_{cr}}{M_{cr} - M_y} \tag{2.96}$$

By using Equations (2.95) and (2.96) in the expressions for the second-order out-of-plane (M_z^{II}) and warping (M_w^{II}) bending moment, respectively, the following is obtained:

$$M_z^{II} = M_y\bar{\theta}_{tot} = \frac{M_y}{1 - \frac{M_y}{M_{cr}}}\bar{\theta}_0 \tag{2.97}$$

$$
\begin{aligned}
M_w^{II} &= M_y\bar{v}_{tot} - GJ\bar{\theta} = M_y\bar{\theta}_0\frac{M_{cr}^2}{N_{cr,z}}\frac{1}{M_{cr} - M_y} - GJ\left[\bar{\theta}_0\frac{M_{cr}}{M_{cr} - M_y} - \bar{\theta}_0\right]\\
&= \bar{\theta}_0\frac{M_y}{M_{cr} - M_y}\left(\frac{M_{cr}^2}{N_{cr,z}} - GJ\right) = \bar{\theta}_0\frac{M_y}{M_{cr} - M_y}\frac{EC_w\pi^2}{L^2}\\
&= \frac{N_{cr,z}}{M_{cr}}\frac{C_w}{I_z}\frac{M_y}{1 - \frac{M_y}{M_{cr}}}\bar{\theta}_0
\end{aligned}
\tag{2.98}
$$

Equation (2.84) can be expanded for beams, assuming the following form:

$$\frac{M_y}{W_yf_y} + \frac{M_z^{II}}{W_zf_y} + \frac{M_w^{II}}{W_wf_y} \leq 1.0 \tag{2.99}$$

where W_y and W_z are the section moduli relative to the y- and z-axes, respectively, and $W_w = C_w/\omega_{max}$ is the elastic warping modulus, with $\omega_{max} = hb/4$ for doubly symmetric I-sections. By using the geometric relationship between the lateral displacement and the section rotation, defined by:

$$\bar{\theta}_0 = \frac{\bar{e}_0}{\frac{M_{cr}}{N_{cr,z}} + \frac{h}{2}} \tag{2.100}$$

, in Equations (2.97) and (2.98), Equation (2.99) becomes:

$$\frac{M_y}{W_y f_y} + \frac{M_y}{1 - \frac{M_y}{M_{cr}}\left(\frac{M_{cr}}{N_{cr,z}} + \frac{h}{2}\right)} \frac{\bar{e}_0}{} \left[\frac{1}{W_z} + \frac{N_{cr,z}}{M_{cr}} \frac{C_w}{I_z} \frac{1}{W_w}\right]\frac{1}{f_y} \leq 1.0 \tag{2.101}$$

Considering $W_z = I_z/(b/2)$, and expanding the second term on the left side with W_y/W_y and A/A, Equation (2.101) is reduced to:

$$\frac{M_y}{W_y f_y} + \frac{M_y}{W_y f_y} \frac{1}{1 - \frac{M_y}{M_{cr}}} \frac{A\bar{e}_0}{W_z} \frac{W_y}{A\left(\frac{M_{cr}}{N_{cr,z}} + \frac{h}{2}\right)} \left[1 + \frac{N_{cr,z}}{M_{cr}} \frac{h}{2}\right] \leq 1.0 \tag{2.102}$$

The reduction factor due to lateral-torsional buckling (χ_{LT}) and the non-dimensional slenderness for lateral-torsional buckling ($\bar{\lambda}_{LT}$) and buckling about the z-axis ($\bar{\lambda}_z$) are now defined:

$$\chi_{LT} = \frac{M_y}{W_y f_y} \tag{2.103}$$

$$\bar{\lambda}_{LT} = \sqrt{\frac{W_y f_y}{M_{cr}}} \tag{2.104}$$

$$\bar{\lambda}_z = \sqrt{\frac{A f_y}{N_{cr,z}}} \tag{2.105}$$

Using Equations (2.103) to (2.105) in Equation (2.102), and rearranging the resulting terms, the following expression is finally obtained:

$$\chi_{LT} + \frac{\chi_{LT}}{1 - \chi_{LT}\bar{\lambda}_{LT}^2}\eta = 1.0 \tag{2.106}$$

where η is given by:

$$\eta = \frac{\bar{\lambda}_{LT}^2}{\bar{\lambda}_z^2} \frac{A\bar{e}_0}{W_z} \tag{2.107}$$

This formulation was included in Clause 8.3.2.3(3) of FprEN 1993-1-1.

2.4 Research on the Buckling Behavior of Mono-symmetric Sections

2.4.1 Mono-symmetric I-sections and Non-prismatic Beams

The effect of mono-symmetry on the critical buckling moment of singly symmetric I-section beams was investigated by Kitpornchai and Trahair (1980) at the beginning of the 1980s. The authors derived approximations for the section properties important to calculate the elastic critical loads, proposed new rules for design, and compared them to results from different codes. In 1985, Roberts and Burt (1985) studied the lateral-torsional buckling of mono-symmetric I-beams and cantilevers under uniform moment, distributed, and concentrated loads using a general energy method derived by Roberts and Azizian (1983). The method is based on vanishing the second variation of the total potential energy and it guarantees that the influence of pre-buckling displacements is included in the analysis by incorporating strains, which stemmed from nonlinear expressions developed by Roberts (1981). The authors derived closed-form solutions for defining elastic critical loads of simply supported beams, which were proven valid for a wide range of cross-sections but overestimating certain cases. Wang and Kitpornchai (1986) continued the work by extending the formulation for different load scenarios. Furthermore, the influence of intermediate restraints was studied by Wang et al. (1987).

Earlier, Vlasov (1962) and Goodier (1942) obtained solutions for simply supported I-beams with mono-symmetric cross-sections, but only subjected to uniform moment, and Anderson and Trahair (1972) discussed the shortage of information available in the literature until the 1960s, including previous solutions and differences of opinion on the effects of the mono-symmetry. They developed numerical solutions for mono-symmetric I-beams and cantilevers using differential equations, considering central concentrated loads for beams, end concentrated loads for cantilevers, and uniformly distributed loads, which were applied at several distances from the shear center. In the end, the authors concluded that the influence of the mono-symmetry and the distance from the point of application of the load to the shear center are beneficial for the critical loads of simply supported beams and detrimental for cantilevers.

Several tables, charts, and approximate expressions concerning the critical buckling of mono-symmetric I-section members were proposed by the studies (Vlasov, 1962; Kitipornchai and Trahair, 1980; Roberts and Burt, 1985; Roberts and Azizian, 1983; Roberts, 1981; Wang and Kitipornchai, 1986; Wang et al., (1987); Goodier, 1942; Anderson and Trahair, 1972), until the beginning of 2000s. The 3-factor formula developed by Clark and Hill (1960), which was one

of the most common general formulations to predict the elastic critical moment hitherto, was included in the ENV version of Eurocode 3. However, two aspects were missing: the influence of the warping restraint condition on the elastic lateral-torsional buckling of mono-symmetric I-section members and the extension of the domain of application of the 3-factor formula to cantilever members. In 2007, Andrade et al. (2007) proposed expressions for each factor of Equation (2.53) for cantilevers with equal or unequal flanges, fully built-in or free to warp at the ends and submitted to uniformly distributed or concentrated loads. In 2012, Camotim et al. (2012) explained the interesting fact that the lowest critical bending moment is not necessarily related to the case of uniform bending for mono-symmetric I-section beams. From numerous numerical examples performed using the software LTBeam, it was proven that beams submitted to bending moment diagrams from transverse loads benefit the least from the cross-section asymmetry, which may lead to critical moments below the ones associated with the uniform bending.

Non-linear phenomena associated with the stability of beams with mono-symmetric I-section were investigated (Nethercot, 1973; Mohri et al., 2010; Trahair, 2012; Surla et al., 2015). Mohri et al. (2010) extended the available solutions developed for non-linear stability, studying the lateral buckling of beams in case of moment gradient applied at the extremities of the beam, considering large displacements and pre-buckling deflections. Trahair (2012) investigated uniform and non-uniform bending and compared them with available design recommendations, observing divergences between the numerical and analytical results. By these investigations, it was proven that the lateral buckling resistance depends not only on pre-buckling deformation, but also on section shape, load distribution, and if the largest flange is under compression or tension.

Recently, experimental tests and numerical simulations (Tankova et al., 2021; Yang et al., 2017; Kang et al., 2018; Zhao et al., 2023) have also been dedicated to studying the ultimate resistance of mono-symmetric I-section beams made with high-strength steels, evaluating the influence of initial geometric imperfections and residual stresses, aiming to improve the current design rules.

Tapered beams with thin-walled I-sections are commonly applied due to their efficiency under bending and easy fabrication, and the use of mono-symmetric cross-sections can be advantageous for the buckling resistance, mainly when the area of the flange under compression is increased. Bradford and Kuk (1988) and Andrade and Camotim (2005) addressed the elastic critical buckling moment of tapered mono-symmetric I-beams. Andrade et al. (2007) discussed

the use of beam or shell elements in the modeling of tapered mono-symmetric beams and Cockalingam et al. (2021) proposed an improved Timoshenko beam formulation for the in-plane behavior of tapered mono-symmetric beams.

As tapered beams are used to be assumed with similar behavior as uniform beams, which can lead to inaccurate shear stress distributions, Trahair and Ansourian (2016) studied the distributions of normal and shear stresses to mono-symmetric tapered I-beams considering inclined stress trajectories along the member instead of the methods commonly applied so far, in which plane sections are supposed to continue plane, shear strains are not considered when analyzing the bending deflections and stress concentrations are neglected. Comparing to finite element analysis, the authors concluded that their method could predict more accurate solutions to the transverse shear stresses. Trahair (2014) and Trahair (2017) proposed a method to analyze tapered mono-symmetric I-section beams related to the elastic in-plane bending and out-of-plane flexural-torsional buckling based on numerical integration (Trahair, 2014) and the elastic lateral buckling using the energy method (Trahair, 2017) instead of closed forms commonly applied for uniform elements. An arbitrary axis system associated with the web mid-line was considered to avoid problems related to the variations of the centroid and shear center axes along the members. A computer program was written and validated to investigate the behavior of uniform beams, tapered doubly and mono-symmetric beams, beam-columns, and tapered cantilevers under different load and boundary conditions. The method developed showed to be efficient with rapid convergence and good approximated solutions since there is no need to consider many elements to obtain an accurate solution, as it is required when replacing tapered elements by many uniform elements.

Recently, Abdelrahman et al. (2022) proposed generalized line-element formulations for geometrically nonlinear analysis of nonsymmetric tapered steel members. The element stiffness matrix was derived through the total potential energy, where elastic strains, as well as the warping deformations and the Wagner effects, were considered. Consequently, appropriate equations for the geometric parameters reflecting the variable geometry along the member were developed. In summary, average values of the area, torsional rigidity, shear center coordinates, and Wagner coefficients are utilized in the element formulation, considering a certain number of interval points along the length of the member. Although the method is validated for various cases, the validation included only tapered members. Furthermore, the element formulation involves incremental-iterative procedures, which may not be currently practical in the design offices in the face of other more simplified methods that already exist.

Marques et al. (2013) highlighted that the stability verification of tapered beams presents several inconsistencies and difficulties. Based on the new method for double symmetric prismatic I-sections developed by Taras and Greiner (2010) – see Subsection 2.3.2 -, Marques et al. (2013) derived a second-order analytical model using an Airton-Perry approach for web-tapered doubly symmetric beams and a generalized imperfection, which provided excellent agreement with experimental tests and was further validated by a large parametric study. Marques et al. (2013) proposal is based on a linear interaction between the first- and second-order bending moment utilization, leading to a maximum utilization at a certain location, denoted as the second-order failure location (x_c^{II}), and can be given by:

$$
\chi_{LT}(x_c^{II})
$$
$$
+ \frac{\chi_{LT}(x_c^{II})}{1 - \bar{\lambda}_{LT}^2(x_c^{II})\chi_{LT}(x_c^{II})} \left[\alpha_{LT}\left(\bar{\lambda}_z(x_c^{II})\right. \right.
$$
$$
\left. - 0.2\right) \left] \left(\frac{\bar{\lambda}_{LT}^2(x_c^{II})}{\bar{\lambda}_z^2(x_c^{II})} \right) \frac{\xi\left(-\delta_{cr,h_{min}}^{"}(x_c^{II})\right) EI_z(x_c^{II})}{N_{cr,z,Tap}} \left[\frac{1 + \frac{N_{cr,z,Tap}}{M_{cr,Tap}}\frac{h(x_c^{II})}{2}}{1 + \frac{N_{cr,z,Tap}}{M_{cr,Tap}}\frac{h_{min}}{2}} \right] = 1.0 \tag{2.108}
$$

where $N_{cr,z,Tap}$ and $M_{cr,Tap}$ are the elastic critical force of the tapered column about the minor axis and the elastic critical bending moment of the tapered beam, respectively; h_{min} is the minimum cross-section height; ξ is the weighing factor for the imperfection; and $\delta_{cr,h_{min}}^{"}$ is the second derivative of the lateral displacement of the critical mode at $h = h_{min}$. The imperfection factor for lateral-torsional buckling (α_{LT}) is given by:

$$
\alpha_{LT} = 0.21 \sqrt{\frac{W_{el,y}(x_c^{II})}{W_{el,z}(x_c^{II})}} \leq 0.64 \tag{2.109}
$$

in which $W_{el,z}$ and $W_{el,y}$ are the values of the elastic section moduli about the minor and the major axes, respectively, at x_c^{II} - location.

Finally, Tankova et al. (2018) developed a General Formulation for the stability design of steel columns, beams, and beam-columns with variable geometry, loads, and different support conditions. However, the proposed approach was not extended for mono-symmetric I-section members, but it will serve as the basis for the proposed methodology in this thesis.

2.4.2 Angle Members in Compression

One of the first documented works in the literature on the behavior of hot-rolled angle members in compression was published by Stang and Strickenberg (1922). The authors published the test results of angle members in concentric and eccentric compression. The objective of the tests was to determine the final compressive strength of angle members with boundary conditions that simulate the connections found in a transmission tower, where a wide variety of connections and slenderness ratios were evaluated. According to Adluri and Madugula (1996a), the elaboration of the first version of the American Society of Civil Engineers (ASCE) prescriptions for transmission tower design, "Guide for Design of Steel Transmission Towers, Manual of Practice Nº 52" (1971), was based largely on the experimental results of Stang and Strickenberg (1922).

The main works on angle members in compression began to be published in the 1960s, with works of Wakabayashi and Nonaka (1965), Usami and Galambos (1971), and Kennedy and Madugula (1972). Wakabayashi and Nonaka (1965), through their experimental results, highlighted that the torsion phenomenon has a great role in the buckling of angle members with slenderness about the minor axis smaller than 70 and that in slender members, the flexural buckling about the minor axis rules. Usami and Galambos (1971) promoted one of the first studies dedicated exclusively to angle members in eccentric compression. They observed that the initial geometric imperfections had a reasonable effect on the ultimate resistance of the members. Kennedy and Madugula (1972) presented an extensive buckling analysis to overcome the limitations of the specifications of the AISC and Canadian Standards Association (CSA). Based on their studies, the authors proposed a design of compressed angles where torsional-flexural buckling is considered for members with slender legs.

In 1974, an experimental program with 153 hot-rolled angle sections was carried out in laboratories in England, Spain, and Germany, and conducted by the *Conseil International des Grands Réseaux Elétricos* (C.I.G.R.E). The tests aimed to evaluate the ultimate resistance of compressed angles present in the bracings of transmission towers. The test configuration was chosen to simulate the boundary conditions of a transmission tower as realistically as possible. The results obtained by C.I.G.R.E served as the basis for the elaboration of the ECCS recommendations relative to transmission tower design (Kettler et al., 2017), published in 1985. It is worth noting that the current procedure for transmission tower design from Eurocode 3 (EN 1993-3-1) originated from the ECCS (1985) recommendations.

During the 1980s the professor at the University of Queensland, Australia, Sritawat Kitipornchai, and his associates published many works dedicated to the study of the behavior of hot-rolled angles in compression: Kitipornchai (1983), Kitipornchai et al. (1990) and Woolcock and Kitipornchai (1986). Kitipornchai (1983) presented a parametric study on torsional-flexural buckling of angle sections with equal and unequal legs. The author presented a solution for the equation obtained from Vlasov's Theory (Equation (2.39)) parameterized as a function of the leg width, the h/t ratio, and the slenderness about the minor axis. Kitipornchai et al. (1990) compared two types of numerical models to evaluate the influence of the nonlinearity of the material on the behavior of eccentrically compressed angles. The comparison between numerical and experimental results showed that the two numerical models were reasonably consistent with the experimental results for the ultimate resistance of the angle members. Woolcock and Kitipornchai (1986) proposed a design for eccentrically compressed angles present in trusses, where an interaction equation was recommended to calculate the ultimate resistance of eccentrically compressed angles. The proposed design showed a good correlation with numerical and experimental results.

Also noteworthy is the work developed by Al-Sayed and Bjorhovde (1989) during the 1980s. These authors presented an investigation of the ultimate resistance and behavior of angle members subjected to concentric compression, with emphasis on the inelastic response of the members. Their results showed that torsional-flexural buckling always governs the failure mode of unequal-leg angle members, and in equal-leg angle sections with low h/t ratio, this bucking mode is not relevant.

In the 1990s, relevant works on the behavior of compressed angle members were carried out by researchers from the University of Windsor, Canada: Adluri and Madugula (1992), Adluri and Madugula (1996b), Adluri and Madugula (1996a), Haidar (1997), Temple and Sakla (1998) and Shani (1998). Adluri and Madugula (1992), based on experimental results, proposed adaptations to the interaction equations adopted by AISC – Load and Resistance Factor Design (LRFD) (1986) and AISC – Allowable Stress Design (ASD) (1989) for I-section members, making them more applicable to eccentrically compressed angles members. The new formulation showed good agreement with the experimental results. Adluri and Madugula (1996b) presented the results of an experimental investigation of hot-rolled angle sections subjected to concentric compression. The authors found values for the measured geometric imperfection lower than that found in the experimental investigations of Bjorhovde (1972) and used by the AISC prescriptions: $L/1,500$. Adluri and Madugula (1996a), continuing their

previous work, evaluated the prescriptions of AISC-LRFD (1993). Adluri and Madugula (1996a) suggested adopting the intermediate curve to the SSRC 1P and 2P curves to design concentrically compressed angles. Haidar (1997) carried out an extensive experimental program to investigate the effects of the connection on member behavior. The authors did not observe a significative difference in the strength of angle sections connected by tight and pretensioned bolts. Temple and Sakla (1998), based on their experimental results, showed a strong influence of the thickness and width of the gusset plate on the compressive strength of the angle members compressed eccentrically, but a low influence of their unconnected length. Shani (1998) investigated through experimental tests the behavior of angle members in eccentric compression by one bolt. The author concluded that the distance between the angle corner and the bolt location significantly affects the ultimate resistance of the member.

In addition to the works carried out at the University of Windsor, two other research developed in the 1990s are relevant: Elgaaly et al. (1991) and Bathon et al. (1993). Elgaaly et al. (1991) conducted an experimental program to evaluate the behavior of angle members subjected to eccentric compression in three-dimensional trusses. The results showed that the behavior of the members varied according to their boundary conditions, slenderness and h/t ratio. Bathon et al. (1993) investigated the ultimate resistance of angle sections subjected to eccentric compression, performing an experimental program. Connections with one, two, three, and five bolts were used in the tests. The authors verified that the increase in the number of bolts increased the compressive strength of the members until the number of bolts was equal to 2. Adding one or more bolts did not significantly increase the resistance capacity of the members.

Recent research was published by Professor Markus Kettler and his associates and conducted at the Institute of Steel Structures at Graz University of Technology, in Austria (Kettler et al., 2017, 2019a, 2019b, 2021, 2022), whose objective is to investigate the influence of different boundary conditions of the gusset plate on the buckling resistance of eccentrically compressed angles. Kettler et al. (2017) carried out a numerical study with about 126 numerical models of angles connected by one and two bolts to a gusset plate subject to three different boundary conditions (see Figure 2.11): clamped support (BC1 – with all degrees of freedom of rotation restricted at both ends of the gusset), knife edge (BC2 – only the rotation around the axis parallel to the connected leg is not restricted) and fully hinged (BC3 – only the rotation around the longitudinal axis of the gusset is restricted). As shown in Figure 2.11, the boundary conditions were applied to the gusset plate, at the opposite end to the bolt position.
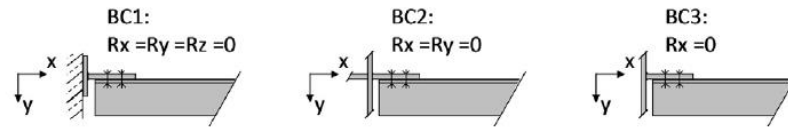
Figure 2.11 – Boundary condition adopted in the numerical model of Kettler et al. (2017). Source: Kettler et al. (2017) - Modified.

Kettler et al. (2019a), continuing their previous study (Kettler et al. (2017)), carried out an extensive experimental study on the compression of angle members connected by one leg, where the boundary conditions BC1, BC2, and BC3 were evaluated (see Figure 2.11). In addition to the compression tests, measurements of the initial geometric imperfections and evaluation of the mechanical properties of the material were carried out. Kettler et al. (2019b) developed numerical models to estimate the stiffness of the connections similar to those in Figure 2.11. The authors focused their investigations on connections with two bolts. Thus, three types of situations were analyzed: angle member bolted to a clamped gusset plate (BC1 – Figure 2.12-a), angle member bolted to the flange of an I-section member (BC2 - Figure 2.12-b), and angle member bolted to a gusset plate welded perpendicularly to the web of an I-section member (BC3 - Figure 2.12-c). In the numerical analysis, a certain bending moment was applied to the connection, and then the rotational stiffness was calculated, dividing the value of this bending moment by the rotation resulting from the loading.
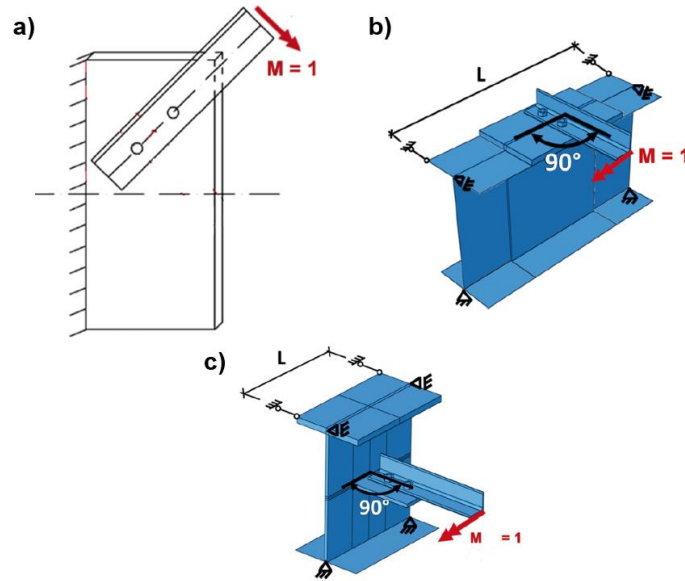
Figure 2.12 – Numerical models used to estimate the rotational stiffness for a) BC1, b) BC2 and c) BC3 boundary conditions. Source: Kettler et al. (2019b) - Modified.

As the first situation is the most recurrent in practical cases and it influenced most the resistance capacity of the angles section (the other two situations provided results very close to each other and up to three times lower than the first situation – Kettler et al., 2019b), only this type of connection (see Figure 2.12) was evaluated within the scope of this work.

For this type of connection (see Figure 2.13), Kettler et al. (2019b) proposed rotational stiffness coefficients that represent the effects of the gusset plate. These coefficients can be calculated by:

$$C_{\varphi,in\ plane} = \infty \tag{2.110}$$

$$C_{\varphi,out\ of\ plane} = \frac{Eh_{eff}t_p}{4(3x + e_1)} \tag{2.111}$$

where t_p is the gusset plate thickness, and h_{eff} is given by:

$$h_{eff} = min.\begin{cases} H \\ 4(x + e_1) \end{cases} \tag{2.112}$$

The values of the rotational stiffness coefficients were determined considering the application of a bending moment (M – see Figure 2.13) with unitary value and disregarding the deformations of the angle and the gusset plate. Also, these values were calibrated through numerical and experimental models (Kettler et al., 2019; Kettler et al., 2021). For the

application of Equations (2.110) and (2.111) it is required that $H \geq 1.5h$, $x \leq 60\ mm$, $e_1 \geq 2.5d_0$, $p_1 \geq 3.0d_0$ and $t_p \geq max.\begin{cases} t \\ 10\ mm \end{cases}$, where d_0 is the bolt diameter.

Equations (2.110) and (2.111), show that the connection has infinite stiffness in the plane of the connection ($C_{\varphi,in\ plane}$); henceforth, when there are references to "stiffness coefficient", "connection spring" or "C_{φ}" this refers to the out-of-plane stiffness of the connection ($C_{\varphi,out\ plane}$).
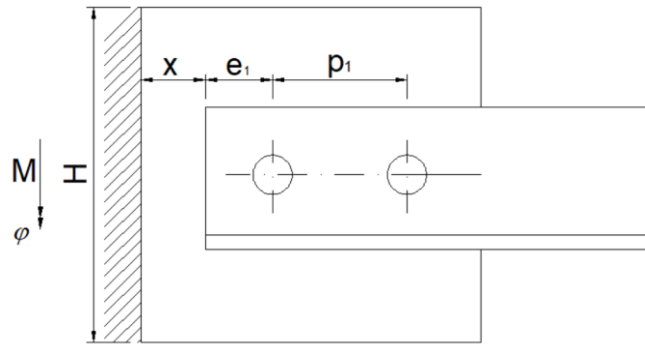
Figure 2.13 – Diagram of the connection of an angle member with a *gusset plate* fitted.

Kettler et al. (2021), based on previous research, proposed a design method for hot-rolled angle sections compressed eccentrically by one and two bolts and which consider the boundary conditions of the gusset plate (Figure 2.11) through the use of the proposed stiffness coefficients by Kettler et al. (2019b). Thus, according to this proposal, the verification of the angle members is completed when the following equation – shown here without safety factors – is satisfied:

$$|\sigma_{max.}| \leq f_y f_{D1} \tag{2.113}$$

where $\sigma_{max.}$ is the maximum second-order elastic stress in the most stressed cross-section along the member, considering the eccentricities of load application and the rotational stiffnesses shown by Equations (2.110) and (2.111) at both ends of the member. Furthermore, an equivalent bow imperfection, with an amplitude about the weak axis equal to $e_{0,u} = L/300$, must be considered. As an alternative to a numerical 2nd order calculation, $\sigma_{max.}$ can be estimated with an analytical expression by:

$$\sigma_{max} = \begin{cases} \dfrac{N_{Ed}}{A_g} + \dfrac{N_{Ed}.e_{0,u}\dfrac{1}{1-\frac{N_{Ed}}{N_{cr,v}}}}{W_{el,v,tip}} + \dfrac{N_{Ed}e_v\dfrac{1}{1-\frac{N_{Ed}}{N_{cr,u}}}}{W_{el,u,tip}} & \text{(at the angle tip)} \\[4mm] \dfrac{N_{Ed}}{A_g} + \dfrac{N_{Ed}.e_{0,u}\dfrac{1}{1-\frac{N_{Ed}}{N_{cr,v}}}}{W_{el,v,corner}} & \text{(at the angle corner)} \end{cases}$$

(2.114)

In this equation:

- the term N_{Ed}/A_g is related to pure compressive stress due to the action of the normal force, N_{Ed};

- the term containing $N_{Ed}e_{0,u}$ is related to the maximum second-order stresses resulting from the amplification of the first-order bending moment (where $e_{0,u}$ is an out-of-plane equivalent imperfection equal to $L/300$);

- the term containing $N_{Ed}e_v$ is related to the second-order stresses resulting from the amplification of the first-order bending moment (where e_v is the in-plane eccentricity of load application);

- $N_{cr,v}$ and $N_{cr,u}$ are the elastic buckling loads around the minor- and major-axis, respectively, obtained numerically;

- $W_{el,v,tip}$ and $W_{el,v,corner}$ are the values of the elastic section moduli for bending about the minor-axis relative to the angle tip and the angle corner, respectively;

- $W_{el,u,tip}$ is the elastic section modulus for bending about the major-axis relative to the angle tip.

f_{D1} is a correction factor that considers the precise behavior of the member with the final connections considered. This factor considers the effects that were simplified in the determination of the rotational stiffness coefficient (C_φ) – Equations (2.110) and (2.111) -, such as the effects of the variation of rotational stiffness and stiffness reduction due to local yielding in the region of the connections. For the connection shown in Figure 2.13, f_{D1} is calculated by:

$$f_{D1} = 0.96 - 0.036\overline{\lambda_v} \le 0.93$$

(2.115)

Kettler et al. (2019a) results showed that angles compressed eccentrically through one bolt tend to behave like pinned members. Thus, for this situation, Kettler et al. (2021) suggest using

Equation (2.113) without the effects of springs (i.e., $C_\varphi = 0$) but considering the effects of eccentricities of load application.

After Kettler et al. (2021), the same authors proposed another design model for the compressive strength of angle members with welded joints, considering the stiffness of the welded connection (Kettler et al., 2022). As angle members with welded ends are not covered by this work, this approach is not addressed here.

Another recent and highly relevant work on the behavior of compressed angle members is the European project ANGELHY. 12 experimental tests on concentrically and eccentrically compressed angle members were performed and used for the development of an extensive numerical study with approximately 225 numerical models. The results of this work led to the development of improved design rules that cover:

(i)   the cross-section classification;

(ii)   the cross-section resistance in the elastic and elastoplastic ranges (Bezas et al., 2021); and

(iii)   the buckling resistance (Bezas et al., 2022).

The proposed methods (see Subsection 2.5.3) are already included in Annex F of prEN 1993-3 and are being considered for possible inclusion as an amendment in FprEN 1993-1-1.

Adopting the Eurocode format as the basis, Behzadi-Sofiani et al. (2021) proposed an improved design methodology for fixed-ended steel equal-leg angle section (hot-rolled and cold-formed) columns, based mainly on flexural and torsional-flexural buckling interactions. According to this method, the buckling resistance, $N_{b,Rk}$, depends on the $N_{cr,\mathrm{TF}}/N_{cr,\mathrm{v}}$ ratio (where $N_{cr,\mathrm{TF}}$ is the torsional-flexural buckling load), and the factor, β, that modifies the imperfection factor (see Equation (2.123)). Table 2.3 summarizes the application of the procedure (without safety factors) for hot-rolled steel angle sections.

Table 2.3 – Application of the proposal of Behzadi-Sofiani et al. (2021) for hot-rolled steel angles.

For the cases where $N_{cr,\text{TF}}/N_{cr,v} \leq 1.0$

$$N_{b,Rk} = \chi_{TF} A_g f_y \tag{2.116}$$

$$\chi_{TF} = \chi_F + \Delta_F(\chi_T - \chi_F) \tag{2.117}$$

$$\chi_T = \frac{\bar{\lambda}_{TF} - 0.188}{\bar{\lambda}_{TF}^2} \leq 1.0 \tag{2.118}$$

$$\chi_F = \frac{1}{\Phi + \sqrt{\Phi^2 - \bar{\lambda}_{TF}^2}} \leq 1.0 \tag{2.119}$$

$$\Delta_F = \left(1 - \frac{N_{cr,\text{TF}}}{N_{cr,v}}\right)^p \tag{2.120}$$

$$p = \begin{cases} 2.0\bar{\lambda}_{TF} \text{ for } \bar{\lambda}_{TF} \leq 2.0 \\ 2.93\bar{\lambda}_{TF}^{0.45} \text{ for } \bar{\lambda}_{TF} > 2.0 \end{cases} \tag{2.121}$$

$$\overline{\lambda_{TF}} = \sqrt{\frac{A_g f_y}{N_{cr,\text{TF}}}} \tag{2.122}$$

$$\Phi = 0.5\left[1 + \alpha\beta(\bar{\lambda}_{TF} - 0.2)^\beta + \bar{\lambda}_{TF}^2\right], \text{ with } \beta = 1.75 \tag{2.123}$$

For the cases where $N_{cr,\text{TF}}/N_{cr,v} > 1.0$

$$N_{b,Rk} = \begin{cases} \chi_F A_g f_y & \text{for class 1, 2 or 3 cross} - \text{sections} \\ \chi_F A_{eff} f_y & \text{for class 4 cross} - \text{sections} \end{cases} \tag{2.124}$$

$$\chi_F = \frac{1}{\Phi + \sqrt{\Phi^2 - \bar{\lambda}_v^2}} \leq 1.0 \tag{2.125}$$

$$\overline{\lambda_v} = \begin{cases} \sqrt{\dfrac{A_g f_y}{N_{cr,v}}}, \text{for class 1, 2 or 3 cross} - \text{sections} \\ \\ \sqrt{\dfrac{A_{eff} f_y}{N_{cr,v}}}, \text{for class 4 cross} - \text{sections} \end{cases} \tag{2.126}$$

$$\Phi = 0.5\left[1 + \alpha\beta(\bar{\lambda}_v - 0.2)^\beta + \bar{\lambda}_v^2\right],$$
$$\text{with } \beta = 2.5 - 0.75\frac{N_{cr,\text{TF}}}{N_{cr,v}} \text{ but } 1.0 \leq \beta \leq 1.75 \tag{2.127}$$

χ_F, χ_T and χ_{TF} are the reduction factors for flexural buckling, torsional buckling, and torsional-flexural buckling, respectively; $\bar{\lambda}_{TF}$ is the relative slenderness for torsional-flexural buckling. The imperfection α is 0.34, following the EN 1993-1-1 recommendations.

Behzadi-Sofiani et al. (2022b) proposed a design model for equal-leg angle section beams, considering the same assumptions of Behzadi-Sofiani et al. (2021) relative to the interactions between flexural and torsional-flexural buckling. As this paper only addresses angles subjected to eccentric compression about the major axis, only the method of Behzadi-Sofiani et al. (2022b) for bending about the major axis is reproduced here. According to these authors, the proposed reduction factor (χ) for steel equal-leg angle section beams in bending about the major axis may capture the influence of both local and lateral-torsional buckling. Table 2.4 summarizes how χ may be obtained:

Table 2.4 – Reduction factor for buckling resistance of angle members subjected to bending about the major-axis according to Behzadi-Sofiani et al. (2022b).

$$\chi = \chi_{LT} + \Delta(\chi_1 - \chi_{LT}) \tag{2.128}$$

$$\chi_1 = \frac{\bar{\lambda}_{max,u} - 0.188}{\bar{\lambda}_{max,u}^2} \leq 1.0 \tag{2.129}$$

$$\chi_{LT} = \frac{1}{\Phi_{LT} + \sqrt{\Phi_{LT}^2 - \bar{\lambda}_{max,u}^2}} \leq 1.0 \tag{2.130}$$

$$\Delta = \begin{cases} \left(1 - \dfrac{M_{cr,1,u}}{M_{cr}}\right)^{3.5} \text{ for } \dfrac{M_{cr,1,u}}{M_{cr}} \leq 1.0 \\ \qquad 0 \text{ for } \dfrac{M_{cr,1,u}}{M_{cr}} > 1.0 \end{cases} \tag{2.131}$$

$$\bar{\lambda}_{max,u} = \sqrt{\frac{W_{\text{pl,u}} f_y}{\min(M_{cr}; M_{cr,1,u})}} \tag{2.132}$$

$$\Phi_{LT} = 0.5 \left[1 + \alpha_{LT}(\bar{\lambda}_{max,u} - 0.2) + \bar{\lambda}_{max,u}^2\right] \tag{2.133}$$

χ_1 is the local buckling reduction factor; $\bar{\lambda}_{max,u}$ is the maximum relative slenderness; and $M_{cr,1,u}$ is the elastic local buckling bending moment.

2.5 Design Codes for Buckling Resistance of Mono-Symmetric Sections

2.5.1 General Aspects

In this section, the main design rules for the buckling resistance of mono-symmetric and non-prismatic I-welded sections subjected to bending and hot-rolled steel angle members in concentric and eccentric compression are exposed. This section does not cover resistance or safety factors, as only the characteristic values of the resistances are of interest to this work.

2.5.2 Mono-symmetric I-section Beams

2.5.2.1 EN 1993-1-1

In EN 1993-1-1, the General Case (Clause 6.3.2.2) must be applied for uniform mono-symmetric beams. For non-prismatic, including tapered mono-symmetric beams, the General Method (Clause 6.3.4) must be applied.

According to the General Case, the reduction factor for lateral-torsional buckling (χ_{LT}), is given by:

$$\chi_{LT} = \frac{1}{\varPhi_{LT} + \sqrt{\varPhi_{LT}{}^2 - \bar{\lambda}_{LT}{}^2}}$$
(2.134)

where $\varPhi_{LT}$ is obtained by:

$$\varPhi_{LT} = 0.5\left[1 + \alpha_{LT}\left(\bar{\lambda}_{LT} - 0.2\right) + \bar{\lambda}_{LT}{}^2\right]$$
(2.135)

and the relative slenderness for lateral-torsional buckling, $\bar{\lambda}_{LT}$, should be determined from Equation (2.104), in which W_y is obtained according to the classification of the cross-section. For welded I-sections, EC3-1-1 recommends curve c (imperfection factor $- \alpha_{LT} = 0.49$) for sections with $h/min(b_1; b_2) \leq 2$, and curve d ($\alpha_{LT} = 0.76$) in the cases where $h/min(b_1; b_2) > 2$.

According to the General Method, the reduction factor for lateral and lateral-torsional buckling (χ_{op}) can be obtained by Equation (2.134), by adopting curve c for α_{LT} and replacing $\bar{\lambda}_{LT}$ in Equations (2.134) and (2.135) by:

$$\bar{\lambda}_{op} = \sqrt{\frac{\alpha_{ult,k}}{\alpha_{cr,op}}} \tag{2.136}$$

where $\alpha_{ult,k}$ is the minimum amplifier of the design load reaching the characteristic resistance of the most critical cross-section of the beam, without taking lateral or lateral-torsional buckling into account, and $\alpha_{cr,op}$ is the minimum amplifier of the design loads to reach the elastic lateral-torsional buckling of the beam.

2.5.2.2 AISC 360

The bending moment resistance of mono-symmetric I-section beams is given in Chapter F of AISC 360, where the buckling curve is divided into three ranges: plastic, elastoplastic, and purely elastic. Thus, the lateral-torsional buckling resistance is given (without partial factors), $M_{R,anal.}$, by:

$$M_{R,anal.} = \begin{cases} M_{pl}, \text{for } \lambda \leq \lambda_p \\ C_b \left[M_{pl} - \left(M_{pl} - 0.7 f_y W_{el,y,c} \right) \frac{\lambda - \lambda_p}{\lambda_r - \lambda_p} \right] \leq M_{pl}, \text{for } \lambda_p < \lambda \leq \lambda_r \\ M_{cr} \leq M_{pl}, \text{for } \lambda > \lambda_r \end{cases} \tag{2.137}$$

where λ is the ratio between the unbraced length and radius of gyration of the "T" section formed by the compressed flange and the compressed part of the adjacent web, in the elastic range, about the z-axis; λ_p is the limiting parameter for the limit state of yielding; λ_r is the limiting parameter for the limit state of inelastic lateral-torsional buckling; C_b is a factor depending on the bending moment diagram and cross-section geometry; M_{pl} is the plastic bending moment; and $W_{el,y,c}$ is the elastic modulus about the y-axis of the compressed part of the section.

For determining the buckling resistance of tapered members, the American code recommends the guide "Frame Design Using Web-Tapered Members, Steel Design Guide 25". The method consists basically of determining an equivalent uniform beam with the same first-order resistance and the same elastic critical load as the tapered beam, and then, following the guidance for uniform beams (Equation (2.137)) and applying it to the equivalent beam.

2.5.3   Angle Members in Compression

2.5.3.1   EN 1993-1-1

The design of an equal leg steel angle, typically illustrated in Figure 2.14, is dealt with by EN 1993-1-1 by establishing (Simões da Silva et al., 2016a):

(i)   the classification of the cross-section reflecting its capacity to behave as a plastic hinge, reach its plastic resistance, and the susceptibility to local buckling;

(ii)   the cross-section resistance under combined loads; and

(iii)   the proposal of buckling reduction factors related to all relevant buckling modes that quantify the reduction of the cross-section resistance due to buckling;
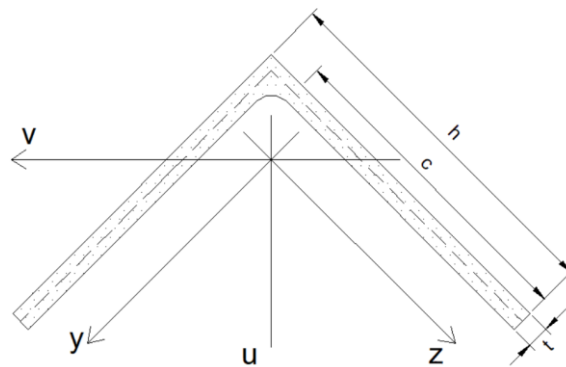
Figure 2.14 – Notations for geometric properties and axes.

EN 1993-1-1 classifies hot-rolled steel angles according to the equation:

$$class = \begin{cases} 1 \text{ for } c/t \le 9\varepsilon \\ 2 \text{ for } 9\varepsilon < c/t \le 10\varepsilon \\ 3 \text{ for } 10\varepsilon < c/t \le 11.5\varepsilon \\ 4 \text{ for } c/t > 11.5\varepsilon \end{cases} \tag{2.138}$$

where $\varepsilon = \sqrt{235/f_y}$, with f_y given in Mpa.

The cross-section resistance of steel angles follows the general expressions given for all cross-section shapes and is not reproduced here (EN 1993-1-1). For class 4 sections, an effective area

A_{eff} is adopted to account for the effects of local buckling on the overall behavior of the member A_{eff} is given by:

$$A_{eff} = A_g - 2ct(1 - \rho)$$

(2.139)

The reduction factor (ρ) due to local buckling of the angle legs is given in EN 1993-1-5 and is calculated by:

$$\rho = \begin{cases} 1.0, & \text{for } \bar{\lambda}_p \leq 0.748 \\ \dfrac{\bar{\lambda}_p - 0.188}{\bar{\lambda}_p^{\,2}}, & \text{for } \bar{\lambda}_p > 0.748 \end{cases}$$

(2.140)

where the non-dimensional plate slenderness of the leg, $\bar{\lambda}_p$, is given by:

$$\bar{\lambda}_p = \frac{\frac{c}{t}}{18.6\varepsilon}$$

(2.141)

The buckling resistance of compressed angles is obtained by establishing first the normalized slenderness of the member and then calculating the buckling reduction factor χ. This procedure is summarized in Table 2.5:

Table 2.5 – Expressions for obtaining the buckling resistance according to EN 1993-1-1.

$$N_{b,Rk} = \begin{cases} \chi A_g f_y & \text{for class 1, 2 or 3 cross} - \text{sections} \\ \chi A_{eff} f_y & \text{for class 4 cross} - \text{sections} \end{cases}$$

(2.142)

$$\chi = \frac{1}{\Phi + \sqrt{\Phi^2 - \bar{\lambda}^2}} \leq 1$$

(2.143)

$$\bar{\lambda} = \begin{cases} \sqrt{\dfrac{A_g f_y}{N_{cr}}}, & \text{for class 1, 2 or 3 cross} - \text{sections} \\ \sqrt{\dfrac{A_{eff} f_y}{N_{cr}}}, & \text{for class 4 cross} - \text{sections} \end{cases}$$

(2.144)

$$\Phi = 0.5\left[1 + \alpha(\bar{\lambda} - 0.2) + \bar{\lambda}^2\right]$$

(2.145)

where A_g is the gross area, χ is the reduction factor, $\bar{\lambda}$ is the normalized slenderness, N_{cr} is the smallest relevant critical buckling force (flexural buckling around the weak axis or torsional-flexural buckling), Φ is a dimensionless coefficient and α is the imperfection factor corresponding to buckling curve b, $\alpha = 0.34$.

EN 1993-1-1 does not provide specific prescriptions for buckling resistance of steel angles subject to bending and axial force (eccentric compression). However, Annex BB.1 (EN 1993-1-1) provides rules to check the buckling resistance of angles under eccentric compression due to the eccentricity of the load application, provided that at least two bolts are used in the connection. The buckling resistance is obtained by substituting $\bar{\lambda}$ in Equations (2.143) and (2.145) by the highest effective slenderness ratio: with respect to the weak axis ($\bar{\lambda}_{eff,v}$) and with respect to the y-axis ($\bar{\lambda}_{eff,y}$), see Figure 2.14. $\bar{\lambda}_{eff,v}$ and $\bar{\lambda}_{eff,y}$ are given by Equations (2.146) and (2.147), respectively:

$$\bar{\lambda}_{eff,v} = 0.35 + 0.7\bar{\lambda}_v \tag{2.146}$$

$$\bar{\lambda}_{eff,y} = 0.50 + 0.7\bar{\lambda}_y \tag{2.147}$$

where $\bar{\lambda}_v$ and $\bar{\lambda}_y$ are the relative slenderness ratios with respect to the $v-$ and $y-$ axes, respectively.

If only one bolt is used at each end of an angle in eccentric compression, the eccentricity of load application must be considered in the verification of the member resistance using an interaction equation, where the system length L should be used in the calculation of the buckling resistance:

$$\frac{N_{Ed}}{N_{b,u,Rd}} + k_{uu}\frac{M_{u,Ed}}{M_{b,u,Rd}} + k_{uv}\frac{M_{v,Ed} + \Delta M_{v,Ed}}{M_{b,v,Rd}} \leq 1.0 \tag{2.148}$$

$$\frac{N_{Ed}}{N_{b,v,Rd}} + k_{vu}\frac{M_{u,Ed}}{M_{b,u,Rd}} + k_{vv}\frac{M_{v,Ed} + \Delta M_{v,Ed}}{M_{b,v,Rd}} \leq 1.0 \tag{2.149}$$

where N_{Ed}, $M_{u,Ed}$ and $M_{v,Ed}$ are the design values of the compression force and the maximum moments about the $u-u$ and $v-v$ axis along the member, respectively; $\Delta M_{v,Ed}$ is the

additional bending moment about the weak axis for class 4 cross-sections due to the shift of the centroidal axis when the cross-section is subjected to compression only; $N_{b,u,Rd}$ and $N_{b,v,Rd}$ are the design values of the buckling resistance about the $u - u$ and $v - v$ axis, respectively, of a member in compression; $M_{b,u,Rd}$ and $M_{b,v,Rd}$ are the design values of the resistance to bending moment about the $u - u$ and $v - v$ axis, respectively; and k_{uu}, k_{uv}, k_{vu} and k_{vv} are the interaction factors. The method proposed by Equations (2.148) and (2.149) is not analyzed in this work.

2.5.3.2   FprEN 1993-1-1

FprEN 1993-1-1 presents a small difference when compared to EN 1993-1-1 regarding the design of angles. EN 1993-1-1 recommends the use of the buckling curve b whatever the steel grade (clause 6.3.1), while in FprEN 1993-1-1 (clause 8.3.1), this buckling curve must be used only for steel grades up to S460, while for steel grade equal to or greater than S460, curve a ($\alpha = 0.21$) may be used.

2.5.3.3   EN 1993-3-1

EN 1993-3-1 is the part of Eurocode 3 that provides prescriptions relative to the design of transmission towers, masts, and chimneys. The design of transmission tower structures proposed by this code complies with the criteria established by EN 1993-1-1. However, the latter establishes general procedures for steel structures, which may lead to conservative results for specific types of structures. EN 1993-3-1 proposes a more specific and detailed procedure for truss structures of transmission towers, taking advantage of the specific features of these structures. In the following, only the differences with respect to EN 1993-1-1 are presented.

EN 1993-3-1 classifies the structural elements of a transmission tower as follows: support members (legs), diagonal bracing members, and horizontal bracing members. In the case of bracing members, their classification is carried out according to their arrangement in the structure, the other members to which they are connected, and their geometry. The buckling resistance of angles in compression is given by:

$$N_{b,Rk} = \begin{cases} \chi A_g f_y \eta & \text{for class 1, 2 or 3 cross} - \text{sections} \\ \chi A_{eff} f_y \eta & \text{for class 4 cross} - \text{sections} \end{cases} \tag{2.150}$$

where η is a reduction factor for angles that is equal to 0.8 for connections with one bolt at each end and 0.9 whenever one of the ends is rigid (two bolts or more) and the other end is connected by one bolt. The reduction factor, χ, and the dimensionless coefficient, Φ, are obtained from Equations (2.143) and (2.145), respectively, where $\bar{\lambda}$ is replaced by an effective slenderness ratio that considers the effects of the eccentricity of the load application and end fixities typically present in a transmission tower. The effective slenderness ratio is taken as the largest of Equations (2.151) and (2.152):

$$\bar{\lambda}_{eff,v} = \kappa_v \bar{\lambda}_v \tag{2.151}$$

$$\bar{\lambda}_{eff,y} = \kappa_y \bar{\lambda}_y \tag{2.152}$$

where κ_v and κ_y are effective slenderness factors relative to $v-$ and y-axes (see Figure 2.14), respectively. κ_v and κ_y are obtained from Tables G1 and G2 of Annex G (EN 1993-3-1) and are determined according to the function and connections of the angle member in the transmission tower.

As only isolated angles are studied in this work (without the influence of intermediate restraints along the length), it was decided to evaluate only the cases related to bracing, i.e., the cases from Table G2 (Annex G), where κ_v and κ_y are calculated as follows:

- for eccentric compression angles with one bolt at each end:

$$\kappa_v = 0.7 + \frac{0.35}{\bar{\lambda}_v} \tag{2.153}$$

$$\kappa_y = 0.7 + \frac{0.58}{\bar{\lambda}_y} \tag{2.154}$$

- for eccentric compression angles with two bolts at each end:

$$\kappa_v = 0.7 + \frac{0.35}{\bar{\lambda}_v} \tag{2.155}$$
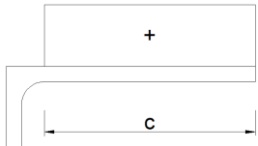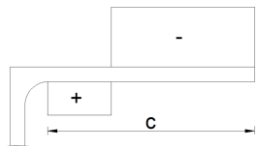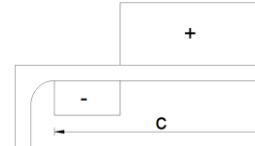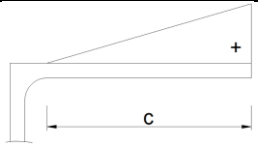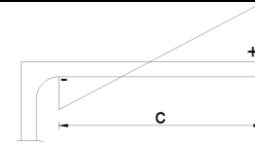
$$\kappa_y = 0.7 + \frac{0.40}{\bar{\lambda}_y} \tag{2.156}$$

It is finally noted that, according to EN 1993-3-1, the length measured between the transmission tower work points (structural nodes) must be adopted as the buckling length for the calculation of $\bar{\lambda}_{\mathrm{v}}$ and $\bar{\lambda}_y$.

2.5.3.4 ANGELHY / prEN 1993-3

The ANGELHY project aimed to reassess the design of steel angles with a specific focus on masts and towers. Concerning cross-section classification, Table 2.6 details the proposed new classification:

Table 2.6 – Maximum width-to-thickness ratios for angle sections according to the ANGELHY project.

	Section under compression	Section under strong axis bending	Section under weak axis bending	
			Tip in tension	Tip in compression
Class 1	-	-	-	-
Class 2	-	$\dfrac{c}{t} \leq 16\varepsilon$	$\dfrac{c}{t} \leq 30\varepsilon$	$\dfrac{c}{t} \leq 14\varepsilon$
Class 3	$\dfrac{c}{t} \leq 14\varepsilon$	$\dfrac{c}{t} \leq 26\varepsilon$	-	$\dfrac{c}{t} \leq 27\varepsilon$

According to the results of the project, the characteristic buckling resistance of angle members is given by Equation (2.142), where the smallest reduction factor associated with the buckling modes around the principal axes ($\chi_{min} = \{\chi_{\mathrm{v}}; \chi_{\mathrm{u}}\}$) is adopted.

The reduction factors must be determined from the buckling curve b for steel grades S235-S460, or from the curve a for higher steel grades ($\geq$ S460) – following the FprEN 1993-1-1 recommendations.

Concerning local buckling, ANGELHY determines that the equation that provides the non-dimensional plate slenderness (see Eq. (2.141)) must be multiplied by $\sqrt{\chi_{min}}$, to contemplate the interaction between the local and global buckling modes in an empirical way (Bezas, 2021).

According to Bezas et al. (2022), "*weak axis flexural buckling always prevails at failure even for angles exhibiting a flexural-torsional elastic critical instability mode*". This is why the ANGELHY proposal (unlike the design proposed by Behzadi-Sofiani et al. (2021)) disregards torsional-flexural buckling in the design of angles in concentric compression, in contrast to the EN 1993-1-1 recommendations. Therefore, the compressive strength of hot-rolled steel angles is calculated by using the relative slenderness ratio with respect to flexural buckling only, disregarding the buckling modes with torsional effects (in contrast to EN 1993-1-1 and FprEN1993-1-1).

It is noted that there is no specific guidance in the ANGELHY project to account for the effects of boundary conditions. Instead, their influence is considered in the calculation of N_{cr}.

The ANGELHY project proposes a new interaction formulation to evaluate the buckling resistance in eccentric compression, whereby the bending moment is caused by the eccentricity of load application. Similarly to the resistance of I-section members subject to bending and axial compression, the design verification consists of two equations for buckling around one or the other principal axes. Torsional buckling is not checked separately but is included in the local buckling check. These conditions (without safety factors) are given by:

- strong axis check:

$$\left(\frac{N_{Ed}}{\chi_u N_{Rk}} + k_{uu}\frac{M_{u,Ed}}{\chi_{LT}M_{u,Rk}}\right)^{\xi} + k_{uv}\frac{M_{v,Ed} + \Delta M_{v,Ed}}{M_{v,Rk}} \leq 1.0 \qquad (2.157)$$

- weak axis check:

$$\left(\frac{N_{Ed}}{\chi_v N_{Rk}} + k_{vu}\frac{M_{u,Ed}}{\chi_{LT}M_{u,Rk}}\right)^{\xi} + k_{vv}\frac{M_{v,Ed} + \Delta M_{v,Ed}}{M_{v,Rk}} \leq 1.0 \qquad (2.158)$$

where N_{Rk} is the characteristic value of the compressive resistance; $M_{u,Rk}$ and $M_{v,Rk}$ are the characteristic values of the maximum bending moment resistance along the member about the u-u axis and v-v axis, respectively, given by equations:

$$M_{u,Rk} = W_{u,i}f_y \tag{2.159}$$

$$M_{v,Rk} = W_{v,i}f_y \tag{2.160}$$

where $W_{u,i}$ and $W_{v,i}$ are the section moduli given according to cross-section classification, as shown in Table 2.7. In this table, $W_{pl,u}$ and $W_{pl,v}$ are the plastic section moduli for bending about the u-u axis and v-v axis, respectively; $W_{ep,u}$ and $W_{ep,v}$ are the elastoplastic section moduli for Class 3 section for bending about $u - u$ axis and $v - v$ axis, respectively; and $W_{eff,u}$ and $W_{eff,v}$ are the effective section moduli for bending about $u - u$ axis and $v - v$ axis, respectively. $W_{ep,u}$ and $W_{ep,v}$ are determined from an interpolation between the plastic section modulus W_{pl} and the elastic section modulus W_{el} about one principal axis of a cross-section as follows:

$$W_{ep,u} = W_{pl,u} - \left(W_{pl,u} - W_{el,u}\right)\left(\frac{\frac{c}{t}-16\varepsilon}{10\varepsilon}\right) \tag{2.161}$$

$$W_{ep,v} = W_{pl,v} - \left(W_{pl,v} - W_{el,v}\right)\left(\frac{\frac{c}{t}-14\varepsilon}{13\varepsilon}\right) \tag{2.162}$$

Table 2.7 – Section modulus for angle sections.

Class	1	2	3	4
$W_{u,i}$	$W_{pl,u}$	$W_{pl,u}$	$W_{ep,u}$	$W_{ef,u}$
$W_{v,i}$	$W_{pl,v}$	$W_{pl,v}$	$W_{ep,v}$	$W_{ef,v}$

ξ is a factor that expresses a plastic, intermediate of elastic interaction and may be determined by Equation (2.163), and k_{ij} are the interaction factors that are provided in Table 2.8.

$$\xi = \begin{cases} 2 \text{ for } c/t \leq 16\varepsilon \\ \left[1 + 0.5\left(\frac{26.3\varepsilon - c/t}{26.3\varepsilon - 16\varepsilon}\right)\right] \text{ for } 16\varepsilon < c/t < 26.3\varepsilon \\ 1 \text{ for } c/t > 26.3\varepsilon \end{cases} \tag{2.163}$$

χ_{LT} is the reduction factor for lateral-torsional buckling, given by Equation (2.134) but considering $\chi_{LT} \leq 1.0$ and $\chi_{LT} \leq 1/\bar{\lambda}_{LT}^2$. In this case, the dimensionless coefficient (Φ_{LT}), is obtained by:

$$\Phi_{LT} = 0.5 \left[1 + \alpha_{LT} (\bar{\lambda}_{LT} - 0.4) + \bar{\lambda}_{LT}^2 \right] \tag{2.164}$$

where α_{LT} is equal to 0.21 (buckling curve a), and $\bar{\lambda}_{LT}$ is given by:

$$\bar{\lambda}_{LT} = \sqrt{\frac{W_u f_y}{M_{cr}}} \tag{2.165}$$

M_{cr} is the elastic critical moment for lateral-torsional buckling, given by Equation (2.53), and W_u is the section modulus, given by:

$$W_u = \begin{cases} 1.5 W_{el,u}, \text{for class 1 or 2 cross} - \text{sections} \\ \left[1 + 0.5 \left(\frac{26.3\varepsilon - c/t}{26.3\varepsilon - 16\varepsilon} \right) \right] W_{el,u}, \text{for class 3 cross} - \text{section} \\ \rho_u^2, \text{for class 4 cross} - \text{section} \end{cases} \tag{2.166}$$

in which $W_{el,u}$ is the elastic section modulus for bending about the strong axis. ρ_u is given by Equation (2.140) but in this case $\bar{\lambda}_p$ is calculated by:

$$\overline{\lambda_\rho} = \sqrt{\chi_{LT}} \frac{\frac{c}{t}}{35.58\varepsilon} \tag{2.167}$$

Table 2.8 – Interaction factors k_{ij}.

$k_{uu} = \dfrac{C_u}{1 - \dfrac{N_{Ed}}{N_{cr,u}}}$	$k_{uv} = C_v$
$k_{vu} = C_u$	$k_{vv} = \dfrac{C_v}{1 - \dfrac{N_{Ed}}{N_{cr,v}}}$
$C_u = 0.6 + 0.4\psi_u$	$C_v = 0.6 + 0.4\psi_v$
$-1 \leq \psi_u = \dfrac{M_{2u}}{M_{1u}} \leq 1$	$-1 \leq \psi_v = \dfrac{M_{2v}}{M_{1v}} \leq 1$

* M_{iv} and M_{iu} are the bending moments about weak and strong axes, respectively, at the ends of the member.

This formulation was included in Annex F of prEN 1993-3.

The reduction factor proposed by Behzadi-Sofiani et al. (2022b) – Equation (2.128) – has many differences when compared to the reduction factor in the ANGELHY proposal – Equation (2.134), as follows:

(i)   the adopted imperfection factor – the ANGELHY proposal follows the FprEN 1993-1-1 recommendations and adopts $\alpha_{LT} = 0.21$ (buckling curve a), while Behzadi-Sofiani et al. (2022b) adopts $\alpha_{LT} = 0.34$ (buckling curve b), following the EN 1993-1-1 recommendations;

(ii)   the plateau length of the lateral-torsional buckling curve, $\bar{\lambda}_{LT,0}$ – equal to 0.4 in the ANGELHY proposal, and equal to 0.2 in Behzadi-Sofiani et al. (2022b);

(iii)   the section modulus used in the relative slenderness calculation – in the ANGELHY proposal, the section modulus is determined according to the cross-section class (see Equation (2.166)), while in Behzadi-Sofiani et al. (2022b), the plastic section modulus is used for all classes of cross-sections (see Equation (2.132));

(iv)   the interaction between global and local buckling modes – in the ANGELHY proposal, this is guaranteed by multiplying the non-dimensional plate slenderness by $\sqrt{\chi_{LT}}$ (see Equation (2.167)), in Behzadi-Sofiani et al. (2022b), this interaction is given by the interaction factor Δ (see Equations (2.128) and (2.131)).

In Chapter 4, to assess the local-buckling interaction proposed by Behzadi-Sofiani et al. (2022b), the reduction factor for lateral-torsional buckling, χ_{LT}, present in Equations (2.157) and (2.158) – ANGELHY proposal – is replaced by the reduction factor given by Equation (2.128). The resulting method is referenced as "ANGELHY_MOD".

2.5.3.5   AISC 360

AISC 360 determines that the design buckling resistance (without safety factors) of the angle in compression (concentric or eccentric) is calculated by:

$$N_{b,Rk} = \begin{cases} \chi A_g f_y & \text{for members without slender elements} \\ \chi A_{eff} f_y & \text{for members with slender elements} \end{cases} \tag{2.168}$$

where χ is the reduction factor obtained from the 2P curve of the Structural Stability Research Council – SSRC. The values of χ can be determined by Equation (2.169). It is noted that in the American code prescriptions, an initial sinusoidal geometric imperfection with a magnitude equal to $L/1,500$ and a modulus of elasticity equal to 200,000 Mpa are adopted.

$$\chi = \begin{cases} 0.658^{\overline{\lambda}^2}, for \ \overline{\lambda} \leq 1.5 \\ \frac{0.877}{\overline{\lambda}^2}, for \ \overline{\lambda} > 1.5 \end{cases} \tag{2.169}$$

For eccentric compression, AISC 360 allows to neglect the effects of eccentricity when adopting an equivalent buckling length ($K_y L_y$). Thus, the axial elastic buckling force is calculated considering flexural buckling around the axis parallel to the connected leg. It is also required that the following requirements are met:

- members are loaded at the ends in compression through the same leg;

- members are attached by welding or by connections with a minimum of two bolts;

- there are no intermediate transverse loads.

For equal-leg angles that are individual members or web members of planar trusses with adjacent web members attached to the same side of the gusset plate or chord, $K_y L_y$ is calculated by:

$$K_y L_y = \begin{cases} 72i_y + 0.75L_y, \text{for } \frac{L_y}{i_y} \leq 80 \\ 32i_y + 1.25L_y, \text{for } \frac{L_y}{i_y} > 80 \end{cases} \tag{2.170}$$

where L_y is the length of the member between work points at truss chord centerlines, and i_y is the radius of gyration about the geometric axis parallel to the connected leg.

According to AISC 360, angles with connections other than the configuration described above must be treated as members subjected to a combination of axial force and bending moments and then be designed according to Chapter H of the referred code.

For the consideration of local buckling, the angle legs are classified as slender or non-slender elements according to their local slenderness (h/t ratio):

$$\frac{h}{t} \leq 0.45 \sqrt{\frac{E}{f_y}} \rightarrow \text{non} - \text{slender elements} \tag{2.171}$$

$$\frac{h}{t} > 0.45 \sqrt{\frac{E}{f_y}} \rightarrow \text{slender elements} \tag{2.172}$$

For angles with slender elements, an effective area, A_{eff}, must be used. A_{eff} is calculated by:

$$A_{eff} = A_g - 2(h - h_e)t \tag{2.173}$$

where h_e is the effective width, given by:

$$h_e = \begin{cases} h \text{ for } \dfrac{h}{t} \leq 0.45 \sqrt{\dfrac{E}{\chi f_y}} \\ 0.67 \sqrt{\dfrac{E}{\chi f_y}} \left[1 - \dfrac{0.15}{\left(\dfrac{h}{t}\right)} \sqrt{\dfrac{E}{\chi f_y}} \right] t \text{ for } \dfrac{h}{t} < 0.45 \sqrt{\dfrac{E}{\chi f_y}} \end{cases} \tag{2.174}$$

Finally, AISC 360, unlike EN 1993-1-1, considers that local and torsional instabilities modes are coincident, therefore, only flexural buckling is considered in the calculation of $\bar{\lambda}$.

2.5.3.6 Summary

Table 2.9 summarizes the application of all design procedures mentioned previously, as well as the proposals of Ketter et al. (2021), Behzadi-Sofiani et al. (2021), and "ANGELHY_MOD".

Table 2.9 – Design procedures application for angle members in compression.

Design procedures	Concentric compression		Eccentric compression	
	one bolt	two bolts	one bolt	two bolts
EN 1993-1-1	✓	✓	X	✓**
FprEN 1993-1-1	✓	✓	X	✓**
EN 1993-3-1*	X	X	✓**	✓**
ANGELHY/prEN 1993-3 (Annex F)	✓	✓	✓	✓
ANGELHY_MOD	X	X	✓	✓
AISC 360	✓	✓	X	✓**
Kettler et al. (2021)	X	X	✓	✓
Behzadi-Sofiani et al. (2021)	✓	✓	X	X

* Considering angle members only as bracing members.
** An equivalent buckling length or effective slenderness ratio is adopted.

3

GENERAL FORMULATION

3.1 Introduction

As seen previously, the Eurocode 3 prescriptions for column and beam design are based on the use of generalized imperfection factors (see Equations (2.93) and (2.107) – Subsection 2.3.2, Chapter 2). In this chapter, a new formulation for checking the buckling resistance of mono-symmetric section members is presented. This proposal adopts the philosophy of the Ayrton-Perry Equation, however in its most direct form, and not in its reduced form (as shown by Equation (2.89)).

Given a single member, the following assumptions must be considered in the General Formulation application:

- the eigenvalues and eigenvectors obtained from the Linear Buckling Analysis are used to calculate the second-order moments;

- the law material of the member is linearly elastic until the yielding strength of the material is reached (f_y);

- Second-order, and Small Displacements Theory and Bernoulli's hypotheses must be considered in the stress determination;

- the amplitudes of imperfection are adopted for each Second-order stress and according to their corresponding buckling mode.

In the next sections, based on the stability concepts presented in Sections 2.2 and 2.3, the General Formulation is further detailed for mono-symmetric I-section beams and angle members in compression.

3.2 General Formulation for Mono-symmetric Beams

The utilization ratio of a generic single member may be expressed by equating the total longitudinal stress, σ, due to first- and second-order forces, to the yield stress, f_y:

$$\frac{\sigma(x)}{f_y} = \frac{N(x)}{A(x)f_y} + \frac{M_y(x)}{W_y(x)f_y} + \frac{M_z(x)}{W_z(x)f_y} + \frac{M_y^{II}(x)}{W_y(x)f_y} + \frac{M_z^{II}(x)}{W_z(x)f_y} + \frac{M_w^{II}(x)}{W_w(x)f_y} \tag{3.1}$$

where $W_w(x)$ is calculated for the compressed part of the section. For mono-symmetric sections, ω_{max} is given by:

$$\omega_{max} = \left(h(x) - z_G(x) \pm z_0(x)\right)\frac{b_{comp}(x)}{2} \tag{3.2}$$

where $z_G(x)$ is the position of the cross-section centroid measured from the top face of the largest flange (see Figure 2.6); $z_0(x)$ is the distance between the centroid and the torsion center of the cross-section (see Figure 2.6); and b_{comp} is the width of the compressed flange. It is noted that for section classes 1 and 2 the plastic section moduli should be used. Then, provided the second-order contributions can be determined, the buckling resistance may be verified for an appropriate number of locations along the member, as follows:

$$\frac{N(x)}{A(x)f_y} + \frac{M_y(x)}{W_y(x)f_y} + \frac{M_z(x)}{W_z(x)f_y} + \frac{M_y^{II}(x)}{W_y(x)f_y} + \frac{M_z^{II}(x)}{W_z(x)f_y} + \frac{M_w^{II}(x)}{W_w(x)f_y} \leq 1.0 \tag{3.3}$$

The verification of a single member with variable geometry, and boundary conditions, subject to arbitrary loading, is done by verifying Equation (3.3) at enough locations (n) along the member, akin to the verification of the cross-section resistance. At each position, the respective values of the first-order axial force, $N(x)$, bending moments $M_y(x)$, $M_z(x)$, second-order contributions obtained from the relevant buckling mode and cross-section properties, $A(x)$, $I_z(x)$, etc. are to be used.

For prismatic members, all these buckling cases are covered by the Eurocode 3 design rules. The only condition is that the designer needs to choose the relevant buckling mode and the corresponding verification format (see Table 3.1).

Table 3.1 – Buckling mode for I-section beams.

Buckling mode	Applied loads	Critical loads	Critical mode shape component
LTB	M_y	$M_{cr,N} + N_{cr,NM}$	$v_{cr}(x) + \theta_{cr}(x)$

For lateral-torsional buckling (LTB) of mono-symmetric beams, considering Table 3.1, the general interaction (Equation (3.1)) becomes:

$$\frac{\sigma(x)}{f_y} = \frac{M_y(x)}{W_y(x)f_y} + \frac{M_z^{II}(x)}{W_z(x)f_y} + \frac{M_w^{II}(x)}{W_w(x)f_y} \tag{3.4}$$

where there are two second-order contributions, the out-of-plane bending moment depending on the lateral displacement:

$$M_z^{II}(x) = -EI_z(x)v''(x) \tag{3.5}$$

and the bi-moment depending on the twist rotation:

$$M_w^{II}(x) = -EC_w(x)\left[\theta''(x) + \frac{W_w(x)}{W_z(x)}\frac{I_z(x)}{C_w(x)}\theta'(x)h'\right] \tag{3.6}$$

Hence, when considering the amplitude of the initial imperfection, both components (lateral displacement and twist rotation) must be considered. For simply supported mono-symmetric beams it is possible to obtain the amplitude by the coupling of the lateral displacement and twist rotation (Chen and Astuta, 1977), given by:

$$\frac{\bar{v}_0}{\bar{\theta}_0} = \frac{M_{cr}}{N_{cr,z}} = \left(\sqrt{i_p^2\frac{N_{cr,x}}{N_{cr,z}} + \beta_z^2} + \beta_z\right) \tag{3.7}$$

In a more general configuration (variation of the geometry along the member, different boundary and loading conditions, etc.), this relationship may not hold. For that reason, it was chosen to use both components of the mode shape as initial imperfection, assuming that they are multiplied by the same amplitude:

$$v_0(x) = v_{cr}(x)\bar{\delta}_{0,LTB} \tag{3.8}$$

and

$$\theta_0(x) = \theta_{cr}(x)\bar{\delta}_{0,LTB} \tag{3.9}$$

where v_{cr} is the out-of-plane component and θ_{cr} is the twist rotation.

The resulting amplification relationship for the displacement and rotation is given by:

$$v(x) = \frac{1}{\alpha_{cr} - 1} v_0(x) \tag{3.10}$$

and

$$\theta(x) = \frac{1}{\alpha_{cr} - 1} \theta_0(x) \tag{3.11}$$

It is assumed that the real beam should have the same resistance as an equivalent beam with fork supports and constant bending moment. This equivalent beam has the same geometry as the real beam at the critical cross-section and the same elastic critical moment. Hence, it is possible to obtain the required generalized imperfection by setting equal the second-order utilization for the equivalent and real beams. The second-order moments for a simply supported beam at mid-span are given by:

$$M_z^{II}(x_m) = M_{y,Ed}\theta_{tot} = M_{y,Ed}\theta_0 \frac{1}{1 - 1/\alpha_{cr}} = \frac{\alpha_{cr}M_{y,Ed}(x_m)\bar{e}_0\theta_{cr}(x_m)}{\alpha_{cr} - 1} \tag{3.12}$$

$$M_w^{II}(x_m) = M_{y,Ed}v_{tot} - GJ\theta - 2M_{y,Ed}\beta_z\theta_{tot} =$$

$$M_{y,Ed}v_0 \frac{1}{1 - 1/\alpha_{cr}} - GJ\left(\theta_0 \frac{1}{1 - 1/\alpha_{cr}} - \theta_0\right) - 2M_{y,Ed}\beta_z\theta_0 \frac{1}{1 - 1/\alpha_{cr}} =$$

$$\frac{\alpha_{cr}M_{y,Ed}(x_m)\bar{e}_0\theta_{cr}(x_m)}{\alpha_{cr} - 1}\left(\frac{v_0(x_m)}{\theta_0(x_m)} - \frac{GJ(x_m)}{M_{cr}} - 2\beta_z(x_m)\right) \tag{3.13}$$

The second-order utilization ratio for the equivalent member is given by:

$$\varepsilon_M^{II}(x_m) = \frac{M_z^{II}(x_m)}{W_z(x_m)f_y} + \frac{M_w^{II}(x_m)}{W_w(x_m)f_y} =$$

$$\frac{\alpha_{cr}M_{y,Ed}(x_m)\bar{e}_0\theta_{cr}(x_m)}{W_z(x_m)f_y(\alpha_{cr}-1)}\left(1 + \frac{v_{cr}(x_m)}{\theta_{cr}(x_m)}\frac{W_z(x_m)}{W_w(x_m)} + \frac{GJ(x_m)}{M_{cr}}\frac{W_z(x_m)}{W_w(x_m)}\right.$$

$$\left. + 2\beta_z(x_m)\frac{W_z(x_m)}{W_w(x_m)}\right) = \frac{N_{cr,TF}\bar{e}_0}{W_z(x_m)f_y(\alpha_{cr}-1)} \quad (3.14)$$

with

$$N_{cr,TF} = \alpha_{cr}M_{y,Ed}(x_m)\theta_{cr}(x_m)\frac{W_z(x_m)}{W_w(x_m)}\left(\frac{W_w(x_m)}{W_z(x_m)} + \frac{v_{cr}(x_m)}{\theta_{cr}(x_m)} + \frac{GJ(x_m)}{M_{cr}} + 2\beta_z(x_m)\right) \quad (3.15)$$

The second-order utilization of the real beam at the location x_m is given by:

$$\varepsilon_M^{II}(x_m) = \frac{M_z^{II}(x_m)}{W_z(x_m)f_y} + \frac{M_w^{II}(x_m)}{W_{w,comp}(x_m)f_y} =$$

$$\frac{EI_z(x_m)}{W_z(x_m)f_y(\alpha_{cr}-1)}$$

$$x\left[v''_{cr}(x_m) + \frac{W_z(x_m)}{W_{w,comp}(x_m)}\frac{C_w(x_m)}{I_z(x_m)}\left(\theta''_{cr}(x_m)\right.\right.$$

$$\left.\left. + \frac{W_{w,comp}(x_m)}{W_z(x_m)}\frac{I_z(x_m)}{C_w(x_m)}\theta'_{cr}(x_m)h'\right)\right]\bar{\delta}_0 \quad (3.16)$$

Equaling the second-order utilization ratio for the equivalent beam and the real beam at the location x_m leads to the following expression for the amplitude of the imperfection:

$$\bar{\delta}_{0,LTB} = \frac{N_{cr,TF}\bar{e}_0}{EI_z(x_m)\left[v''_{cr}(x_m) + \frac{W_z(x_m)}{W_w(x_m)}\frac{C_w(x_m)}{I_z(x_m)}\left(\theta''_{cr}(x_m) + \frac{W_w(x_m)}{W_z(x_m)}\frac{I_z(x_m)}{C_w(x_m)}\theta'_{cr}(x_m)h'\right)\right]} =$$

$$f_\eta\bar{e}_0 \quad (3.17)$$

This amplitude is used with the proposed generalization. It contains the equivalent geometrical imperfection $\bar{e}_0$ but also additional terms ensuring consistency with the Eurocode 3 design rules. Ideally, x_m should be chosen as the correct critical location. To avoid an iterative procedure, the location x_m is adopted where $|v''_{cr}(x)|$ reaches a maximum. The amplitude of the generalized imperfection is given by:

$$\eta^*(x) = \alpha\big(\bar\lambda(x) - 0.2\big)f_\eta\big|\delta^{fl}(x)\big|\frac{W_z(x)}{A(x)} \qquad (3.18)$$

where α is calculated according to FprEN 1993-1-1 prescriptions for lateral-torsional buckling of welded prismatic members (α_{LT}), and

$$f_\eta = \frac{N_{cr,TF}}{EI_z(x_m)\left[v''_{cr}(x_m) + \frac{W_z(x_m)}{W_w(x_m)}\frac{C_w(x_m)}{I_z(x_m)}\left(\theta''_{cr}(x_m) + \frac{W_w(x_m)}{W_z(x_m)}\frac{I_z(x_m)}{C_w(x_m)}\theta'_{cr}(x_m)h'\right)\right]} \qquad (3.19)$$

For mono-symmetric I-sections, the general displacement of the critical mode, $\delta^{fl}(x)$, is given by a geometric relationship between the lateral displacement and the section rotation, as defined by Equation (3.20) and Figure 3.1:

$$\delta^{fl}(x) = v_{cr}(x) + \big(h(x) - z_G(x) \pm z_0(x)\big)\theta_{cr}(x) \qquad (3.20)$$
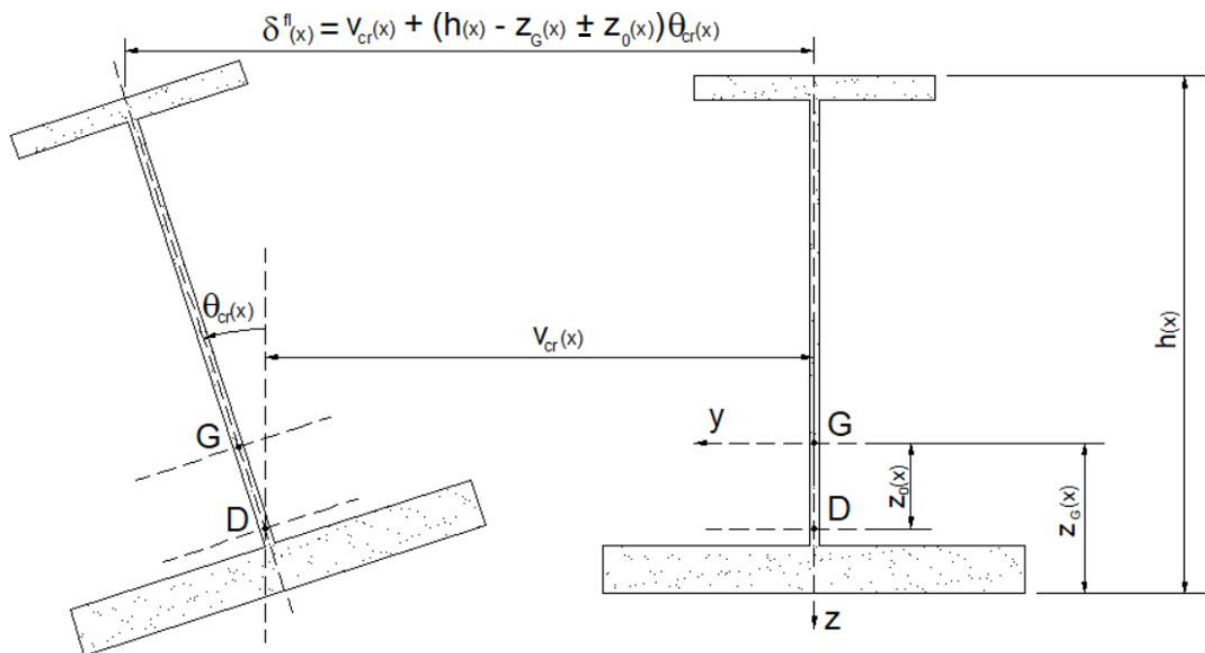
Figure 3.1 – General displacement of the critical mode for mono-symmetric I-section beams.

Thus, the final verification equation is given by:

$$\varepsilon_M(x)$$

$$= \frac{M_{y,Ed}(x)}{W_y(x)f_y} + \frac{EI_z(x)\left[v''_{cr}(x) + \frac{W_z(x)}{W_w(x)}\frac{C_w(x)}{I_z(x)}\left(\theta''_{cr}(x) + \frac{W_w(x)}{W_z(x)}\frac{I_z(x)}{C_w(x)}\theta'_{cr}(x)h'\right)\right]}{A(x)f_y(\alpha_{cr} - 1)}\eta(x) \tag{3.21}$$

$$\leq 1.0$$

with

$$\eta(x) = \alpha\big(\bar{\lambda}(x) - 0.2\big)f_\eta\big|\delta^{fl}(x)\big| \tag{3.22}$$

An equivalent elastic critical force $N_{cr,TF,eq}$ is "retrieved" from the buckling mode using the differential equation for flexural buckling:

$$EI_z(x)v''_{cr}(x) - N_{cr,TF}v_{cr}(x) - z_0 N_{cr,TF}\theta_{cr}(x) = 0. \tag{3.23}$$

Then, the equivalent force becomes:

$$N_{cr,TF,eq} = \frac{EI_z(x_m)|v''_{cr}(x_m)|}{|v_{cr}(x_m) + z_0\theta_{cr}(x_m)|} \tag{3.24}$$

It is this force that is used for the calculation of the normalized slenderness:

$$\bar{\lambda}(x) = \sqrt{\frac{A(x)f_y}{N_{cr,TF,eq}}}. \tag{3.25}$$

3.3 General Formulation for Angle Members in Compression

Similarly to beams, the proposed extension of General Formulation for angle members in compression is applied only for Class 1 and Class 2 cross-sections, and therefore, the gross area of the cross-sections and the plastic section moduli should be used. Furthermore, the imperfection factor for compressed angle members presents in the current form of Eurocode 3 ($\alpha = 0.34$ - curve b) should be considered in the proposed method.

Considering an angle section with its principal axis in the u- and v-directions (see Figure 2.7), its relevant buckling modes and the corresponding verification format are given in Table 3.2.

Table 3.2 – Buckling mode for angle sections in compression.

Buckling mode	Applied loads	Critical loads	Critical mode shape component
FB v-v	N (concentric)	$N_{cr,v}$	$u_{cr}(x)$
TFB	N (concentric)	$N_{cr,TF,con}$	$v_{cr}(x) + \theta_{cr}(x)$
TFB	N (eccentric)	$N_{cr,TF,ecc}$	$v_{cr}(x) + u_{cr}(x) + \theta_{cr}(x)$

In the next subsections, both loading types (concentric and eccentric compression) are treated separately.

3.3.1   Concentric Compression

For angle sections in concentric compression ($e_u = e_v = 0$ – see Figure 2.7), considering Table 3.2, there are two critical buckling modes to be verified: flexural buckling about the minor-axis (FB v-v) and torsional-flexural buckling (TFB).

3.3.1.1   Flexural Buckling about the Minor-axis (FB v-v)

For angle members subjected to flexural buckling about the minor-axis (FB v-v), Equation (3.1) becomes:

$$\frac{\sigma(x)}{f_y} = \frac{N(x)}{A(x)f_y} + \frac{M_v^{II}(x)}{W_v(x)f_y} \tag{3.26}$$

where the second-order contribution, the out-of-plane bending moment depending on out-of-plane displacement, is given by:

$$M_v^{II}(x) = -EI_v(x)u''(x) \tag{3.27}$$

At each cross-section, the curvature can be calculated from the amplification relationship:

$$u''(x) = \frac{u_0''(x)}{\alpha_{cr} - 1} \tag{3.28}$$

The resulting amplification relationship for the displacement is given by:

$$u_0(x) = u_{cr}(x)\bar{u}_0 \rightarrow u_0^{''}(x) = u_{cr}^{''}(x)\bar{u}_0 \tag{3.29}$$

where u_0 is the initial geometric imperfection in the u-direction.

Similarly to beams (see Section 3.2), It is assumed that the real column should have the same resistance as an equivalent column with fork supports. This equivalent column has the same geometry as the real column at the critical cross-section. Hence, it is possible to obtain the required generalized imperfection by setting equal the second-order utilization for the equivalent and real columns. The second-order moments for a simply supported column at mid-span are given by:

$$M_v^{II}(x_m) = N_{Ed}(x_m)u_{tot} = N_{Ed}(x_m)u_0\frac{1}{1 - 1/\alpha_{cr}} = \frac{\alpha_{cr}N_{Ed}(x_m)\bar{e}_0}{\alpha_{cr} - 1} \tag{3.30}$$

Thus, the second-order bending moment for the real column at the maximum of the deformed shape is given by:

$$M_v^{II}(x_m) = \frac{-EI_v(x_m)u_{cr}^{''}(x_m)\bar{u}_0}{\alpha_{cr} - 1} \tag{3.31}$$

Equaling the second-order moment for the equivalent column and the real column at the critical location (x_m) leads to the following expression for the amplitude of the imperfection:

$$\bar{u}_0 = \frac{\alpha_{cr}N_{Ed}\bar{e}_0}{EI_v(x_m)u_{cr}^{''}(x_m)} = f_\eta\bar{e}_0 \tag{3.32}$$

Similarly to beams (see Section 3.2), the location x_m is adopted where $u''_{cr}(x)$ reaches a maximum, and then, the amplitude of the generalized imperfection is given by:

$$\eta^*(x) = \alpha(\bar{\lambda}(x) - 0.2)f_\eta|u_{cr}(x)|\frac{W_v(x)}{A(x)} \tag{3.33}$$

where $\bar{\lambda}(x)$ is given by:

$$\bar{\lambda}(x) = \sqrt{\frac{A(x)f_y}{\alpha_{cr}N(x)}} \tag{3.34}$$

Thus, the final verification equation for flexural buckling about the minor-axis of angle members in compression is obtained by:

$$\varepsilon_N(x) = \frac{N_{Ed}(x)}{A(x)f_y} + \frac{EI_v(x)u_{cr}''(x)}{A(x)f_y(\alpha_{cr}-1)}\,\eta(x) \leq 1.0 \tag{3.35}$$

with

$$\eta(x) = \alpha\big(\bar{\lambda}(x) - 0.2\big)f_\eta|u_{cr}(x)| \tag{3.36}$$

and

$$f_\eta = \frac{\alpha_{cr}N_{Ed}}{EI_v(x_m)u_{cr}''(x_m)} \tag{3.37}$$

For members with uniform cross-sections, the shape of the buckling mode is given by:

$$u_{cr}(x) = sin\left(\frac{\pi x}{L}\right) \tag{3.38}$$

and then, the verification leads to:

$$\frac{N_{Ed}(x_m)}{A(x_m)f_y} + \frac{EI_v(x_m)u_{cr}''(x_m)}{A(x_m)f_y(\alpha_{cr}-1)}\,\alpha\big(\bar{\lambda}(x_m) - 0.2\big)\frac{\alpha_{cr}N_{Ed}}{EI_v(x_m)u_{cr}''(x_m)}|u_{cr}(x_m)|$$

$$= 1.0 \leftrightarrow$$

$$\frac{N_{Ed}}{Af_y} + \frac{\alpha\big(\bar{\lambda} - 0.2\big)}{Af_y\frac{N_{cr,v}}{N_{Ed}}\left(1 - \frac{N_{Ed}}{N_{cr,v}}\right)}\,N_{cr,v} = 1.0 \leftrightarrow \tag{3.39}$$

$$\frac{N_{Ed}}{Af_y} + \frac{N_{Ed}}{Af_y}\frac{\alpha\big(\bar{\lambda} - 0.2\big)}{1 - \frac{N_{Ed}}{N_{cr,v}}} = 1.0 \leftrightarrow$$

$$\chi_v + \frac{\chi_v}{1 - \chi_v \bar{\lambda}_v^2} \alpha(\bar{\lambda}_v - 0.2) = 1.0$$

which is the equation for the flexural buckling of prismatic columns of the current version of Eurocode 3 (see Equation (2.143)).

3.3.1.2 Torsional-flexural Buckling (TFB)

For the verification of torsional-flexural buckling (TFB) of angle members in compression, the general interaction (Equation (3.1)) becomes:

$$\frac{\sigma(x)}{f_y} = \frac{N(x)}{A(x)f_y} + \frac{M_u^{II}(x)}{W_u(x)f_y} + \frac{M_w^{II}(x)}{W_w(x)f_y} \tag{3.40}$$

where there are two second-order contributions, the in-plane bending moment depending on the in-plane displacement:

$$M_u^{II}(x) = -EI_u(x)v''(x) \tag{3.41}$$

and the bi-moment depending on the twist rotation given by Equation (3.6) but considering the second term on the right side of this equation (the additional warping component due to the inclination of the flanges) equal to zero.

Unlike the concentric compression case, the lateral displacement and twist rotation must now be considered for the computation of the initial imperfection. Considering the torsional-flexural buckling of an angle section member, Equation (2.80) (see Section 2.3.1 – Chapter 2) gives:

$$\bar{v}_{tot} = \frac{\left[-N_{cr,u}(N-N_{cr,x})i_p^2\right]\bar{v}_0 + \left(i_p^2 N_{cr,x}Nu_D\right)\bar{\theta}_0}{(N-N_{cr,u})(N-N_{cr,x})i_p^2 - N^2 u_D^2} \tag{3.42}$$

and

$$\bar{\theta}_{tot} = \frac{N_{cr,u}Nu_D\bar{v}_0 - i_p^2 N_{cr,x}(N-N_{cr,u})\bar{\theta}_0}{(N-N_{cr,u})(N-N_{cr,x})i_p^2 - N^2 u_D^2} \tag{3.43}$$

Combining Equations (3.42) and (3.43), the following relationship is obtained:

$$\frac{\bar{v}_{tot}}{\bar{\theta}_{tot}} = \frac{N_{cr,u}(N_{cr,x} - N)i_p^2\left(\frac{\bar{v}_0}{\bar{\theta}_0}\right) + i_p^2 N_{cr,x} N u_D}{N_{cr,u} N u_D\left(\frac{\bar{v}_0}{\bar{\theta}_0}\right) + i_p^2 N_{cr,x}(N_{cr,u} - N)}$$

$$= \frac{N_{cr,u}\left(\frac{N_{cr,x}}{N} - 1\right)\left(\frac{\bar{v}_0}{\bar{\theta}_0}\right) + N_{cr,x} u_D}{N_{cr,u} u_D\left(\frac{\bar{v}_0}{\bar{\theta}_0}\right)\frac{1}{i_p^2} + N_{cr,x}\left(\frac{N_{cr,u}}{N} - 1\right)} \tag{3.44}$$

$$= \frac{1}{\left(\frac{N_{cr,u}}{N} - 1\right)} u_D$$

Simply, similarly to beams (see Section 3.2), it is assumed that lateral displacement and twist rotation are multiplied by the same amplitude:

$$v_0(x) = v_{cr}(x)\bar{\delta}_{0,TFB} \qquad \theta_0(x) = \theta_{cr}(x)\bar{\delta}_{0,TFB} \tag{3.45}$$

And then, the resulting amplification relationship for both components is given by Equations (3.10) and (3.11). As the amplitude of the imperfection of the equivalent member and the real member should be the same, the second-order moments for a simply supported angle column at mid-span are given by:

$$M_u^{II}(x_m) = N_{Ed}(x_m)(v_{tot} + u_D\theta_{tot}) =$$

$$N_{Ed}(x_m)\frac{1}{1 - 1/\alpha_{cr}}\left(v_0(x_m) + u_D\theta_0(x_m)\right) = \tag{3.46}$$

$$\frac{\alpha_{cr} N_{Ed}(x_m)\bar{e}_0\theta_{cr}(x_m)}{\alpha_{cr} - 1}\left(\frac{v_{cr}(x_m)}{\theta_{cr}(x_m)} + u_D\right)$$

$$M_w^{II}(x_m) = N_{Ed}u_D v_{tot} - GJ\theta + N_{Ed}i_p^2\theta_{tot} =$$

$$N_{Ed}u_D v_0(x_m)\frac{1}{1 - 1/\alpha_{cr}} - GJ\left(\theta_0\frac{1}{1 - 1/\alpha_{cr}} - \theta_0\right) + N_{Ed}i_p^2\theta_0\frac{1}{1 - 1/\alpha_{cr}} = \tag{3.47}$$

$$= \frac{\alpha_{cr} N_{Ed}(x_m)\bar{e}_0\theta_{cr}(x_m)}{\alpha_{cr} - 1}\left(\frac{v_{cr}(x_m)}{\theta_{cr}(x_m)}u_D - \frac{GJ(x_m)}{N_{cr,TF,con}} + i_p^2\right)$$

The second-order utilization ratio for the equivalent member is given by:

$$\varepsilon_N^{II}(x_m) = \frac{M_u^{II}(x_m)}{W_u(x_m)f_y} + \frac{M_w^{II}(x_m)}{W_w(x_m)f_y} =$$

$$\frac{\alpha_{cr}N_{Ed}(x_m)\bar{e}_0\theta_{cr}(x_m)}{W_u(x_m)f_y(\alpha_{cr}-1)}\left(\frac{v_{cr}(x_m)}{\theta_{cr}(x_m)} + u_D + \frac{v_{cr}(x_m)}{\theta_{cr}(x_m)}\frac{W_u(x_m)}{W_w(x_m)}u_D\right.$$

$$\left. + \frac{GJ(x_m)}{N_{cr,TF,con}}\frac{W_u(x_m)}{W_w(x_m)} + i_p^2\frac{W_u(x_m)}{W_w(x_m)}\right) =$$

$$= \frac{N_{cr,TF,con}\bar{e}_0}{W_u(x_m)f_y(\alpha_{cr}-1)}$$

(3.48)

with

$$N_{cr,TF,con} = \alpha_{cr}N_{Ed}(x_m)\theta_{cr}(x_m)\frac{W_u(x_m)}{W_w(x_m)}\left(\frac{W_w(x_m)}{W_u(x_m)}\frac{v_{cr}(x_m)}{\theta_{cr}(x_m)} + \frac{W_w(x_m)}{W_u(x_m)}u_D\right.$$

$$\left. + \frac{v_{cr}(x_m)}{\theta_{cr}(x_m)}u_D + \frac{GJ(x_m)}{N_{cr,TF,con}} + i_p^2\right)$$

(3.49)

The second-order utilization of the real column at the location x_m is given by:

$$\varepsilon_N^{II}(x_m) = \frac{M_u^{II}(x_m)}{W_u(x_m)f_y} + \frac{M_w^{II}(x_m)}{W_w(x_m)f_y} =$$

$$= \frac{EI_u(x_m)}{W_u(x_m)f_y(\alpha_{cr}-1)}\left[v''_{cr}(x_m) + \frac{W_u(x_m)}{W_w(x_m)}\frac{C_w(x_m)}{I_u(x_m)}\theta''_{cr}(x_m)\right]\bar{\delta}_{0,TFB}$$

(3.50)

As angle members have very low torsion resistance, the second term on the right-hand side can be disregarded, and then, Equation (3.50) becomes:

$$\varepsilon_N^{II}(x_m) = \frac{EI_u(x_m)}{W_u(x_m)f_y(\alpha_{cr}-1)}v''_{cr}(x_m)\bar{\delta}_{0,TFB}$$

(3.51)

Equaling the second-order utilization ratio for the equivalent angle column and the real column at the location x_m leads to the following:

$$\bar{\delta}_{0,TFB} = \frac{N_{cr,TF,con}\bar{e}_0}{EI_u(x_m)v''_{cr}(x_m)} = f_\eta \bar{e}_0 \tag{3.52}$$

Similarly to the previous case, the location x_m is adopted where $v''_{cr}(x)$ reaches a maximum and then the amplitude of the generalized imperfection is given by:

$$\eta^{**}(x) = \alpha(\bar{\lambda}(x) - 0.2)f_\eta|\delta^{fl}(x)|\frac{W_u(x)}{A(x)} \tag{3.53}$$

where

$$f_\eta = \frac{N_{cr,TF,con}}{EI_u(x_m)|v''_{cr}(x_m)|} \tag{3.54}$$

and

$$\bar{\lambda}(x) = \sqrt{\frac{A(x)f_y}{N_{cr,TF,con}}}. \tag{3.55}$$

For angle sections subjected to torsional-flexural buckling, the general displacement of the critical mode, $\delta^{fl}(x)$, is given by a geometric relationship between the in-plane displacements and the section twist rotation, as defined by Equation (3.56) and Figure 3.2:

$$\delta^{fl}(x) = v_{cr}(x) + u_D\theta_{cr}(x) \tag{3.56}$$
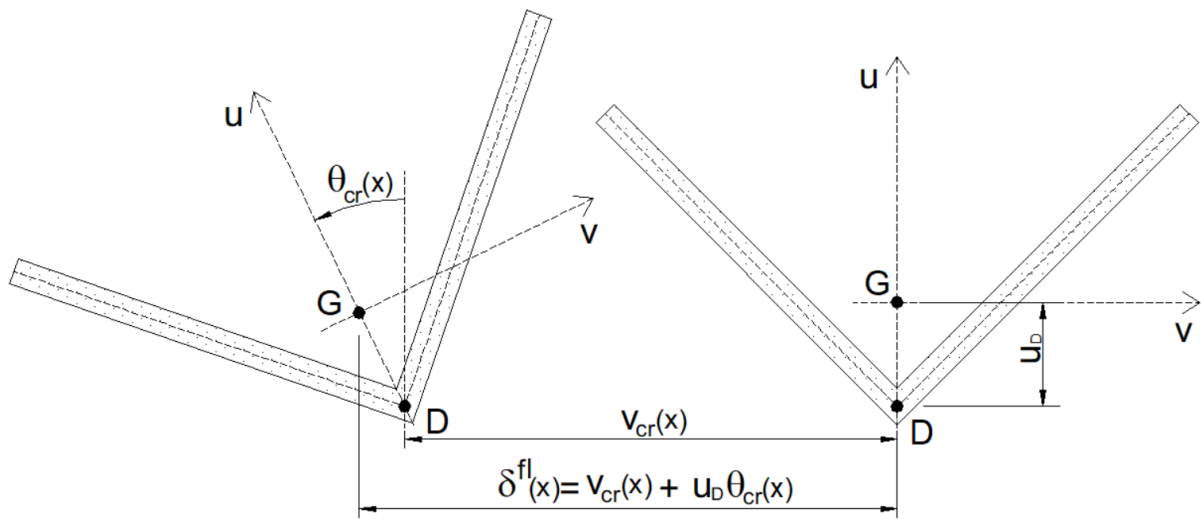
Figure 3.2 – General displacement for the torsional-flexural buckling of an angle section in concentric compression.

Finally, the verification equation becomes:

$$\varepsilon_N(x) = \frac{N_{Ed}(x)}{A(x)f_y} + \frac{EI_u(x)v''_{cr}(x)}{A(x)f_y(\alpha_{cr} - 1)}\, \eta^{**}(x) \le 1.0 \tag{3.57}$$

Thus, the verification of an angle column compressed concentrically subjected to torsional-flexural buckling leads to:

$$\frac{N_{Ed}(x_m)}{A(x_m)f_y} + \frac{-EI_u(x_m)v''_{cr}(x_m)}{A(x_m)f_y(\alpha_{cr} - 1)}\, \alpha\big(\bar{\lambda}(x_m) - 0.2\big)\frac{N_{cr,TF,con}}{EI_u(x_m)|v''_{cr}(x_m)|}|v_{cr}(x_m)$$
$$+ u_D\theta_{cr}(x_m)| = 1.0 \leftrightarrow$$

$$\frac{N_{Ed}}{Af_y} + \frac{\alpha\big(\bar{\lambda} - 0.2\big)}{Af_y(\alpha_{cr} - 1)}\, N_{cr,TF,con}|v_{cr}(x_m) + u_D\theta_{cr}(x_m)| = 1.0 \leftrightarrow$$

$$\frac{N_{Ed}}{Af_y} + \frac{\alpha\big(\bar{\lambda} - 0.2\big)}{Af_y \frac{N_{cr,TF,con}}{N_{Ed}}\left(1 - \frac{N_{Ed}}{N_{cr,TF,con}}\right)}\, N_{cr,TF,con} = 1.0 \leftrightarrow \tag{3.58}$$

$$\frac{N_{Ed}}{Af_y} + \frac{N_{Ed}}{Af_y}\frac{\alpha\big(\bar{\lambda} - 0.2\big)}{\left(1 - \frac{N_{Ed}}{N_{cr,TF,con}}\right)} = 1.0 \leftrightarrow$$

$$\chi_{TF,con} + \frac{\chi_{TF,con}}{\left(1 - \chi_{TF,con}\bar{\lambda}^2_{TF,con}\right)} \alpha\left(\bar{\lambda}_{TF,con} - 0.2\right) = 1.0$$

which is the formulation of Eurocode 3 for verification of torsional-flexural buckling.

3.3.2 Eccentric Compression

According to Table 3.2, for angle members in eccentric compression, the only critical buckling mode to be verified is the torsional-flexural buckling. Because of the effects associated with eccentricity load application, the analyses to be carried out, in this case, are more complex than in the concentric compression case. Furthermore, the elastic response for angle members in eccentric compression cannot be directly obtained as the torsional-flexural buckling observed in members compressed concentrically (see Equation (2.71)). The elastic critical force for torsional-flexural buckling of angle members in eccentric compression, referred now as $N_{cr,TF,ecc}$, is obtained by solving Equation (2.68) or conducting a Linear Buckling Analysis (LBA). Hence, new terms appear in Equation (3.26), that becomes:

$$\frac{\sigma(x)}{f_y} = \frac{N(x)}{A(x)f_y} + \frac{M_u(x)}{W_u(x)f_y} + \frac{M_v(x)}{W_v(x)f_y} + \frac{M_u^{II}(x)}{W_u(x)f_y} + \frac{M_v^{II}(x)}{W_v(x)f_y} + \frac{M_w^{II}(x)}{W_w(x)f_y} \qquad (3.59)$$

where the first-order bending moments, M_u and M_v, are caused by the eccentricity load application (e_u and e_v) and given by:

$$M_u = -Ne_v \qquad (3.60)$$

$$M_v = -Ne_u \qquad (3.61)$$

and where there are three second-order contributions: the out-of-plane bending moment depending on out-of-plane displacement (given by Equation (3.27)), the in-plane bending moment depending on the in-plane displacement (given by Equation (3.41)), and the bi-moment depending on the twist rotation (given by Equation (3.6) but disregarding the additional warping component due to the inclination of the flanges).

It was chosen to use all components (displacements and twist rotation) of the mode shape as initial imperfection, and assuming the resulting amplification relationship for the displacement

and rotation is given by Equations (3.28), (3.29), (3.45), (3.10), and (3.11) (adopting $\bar{u}_0 = \bar{\delta}_{0,TFB}$ in Equation (3.29)). Hence, the second-order bending moments for a simply supported angle member in eccentric compression at mid-span are given by:

$$M_u^{II}(x_m) = N_{Ed}(x_m)[v_{tot} + (u_D - e_u)\theta_{tot}] =$$

$$N_{Ed}(x_m)\frac{1}{1 - 1/\alpha_{cr}}[v_0(x_m) + (u_D - e_u)\theta_0(x_m)] =$$

$$\frac{\alpha_{cr}N_{Ed}(x_m)\bar{e}_0\theta_{cr}(x_m)}{\alpha_{cr} - 1}\left(\frac{v_{cr}(x_m)}{\theta_{cr}(x_m)} + u_D - e_u\right)$$

<div align="right">(3.62)</div>

$$M_v^{II}(x_m) = N_{Ed}(x_m)(u_{tot} + e_v\theta_{tot}) =$$

$$N_{Ed}(x_m)\frac{1}{1 - 1/\alpha_{cr}}\left(u_0(x_m) + e_v\theta_0(x_m)\right) =$$

$$\frac{\alpha_{cr}N_{Ed}(x_m)\bar{e}_0\theta_{cr}(x_m)}{\alpha_{cr} - 1}\left(\frac{u_{cr}(x_m)}{\theta_{cr}(x_m)} + e_v\right)$$

<div align="right">(3.63)</div>

$$M_w^{II}(x_m) = N_{Ed}(x_m)[(u_D - e_u)v_{tot} + e_v u_{tot}] - GJ\theta + N_{Ed}(i_p^2 + 2\beta_u e_v)\theta_{tot}$$

$$= N_{Ed}\frac{1}{1 - 1/\alpha_{cr}}[(u_D - e_u)v_0(x_m) + e_v u_0(x_m)]$$

$$- GJ\left(\theta_0(x_m)\frac{1}{1 - 1/\alpha_{cr}} - \theta_0(x_m)\right)$$

<div align="right">(3.64)</div>

$$+ N_{Ed}\theta_0(x_m)\frac{1}{1 - 1/\alpha_{cr}}\left(i_p^2 + 2\beta_u e_u\right) =$$

$$\frac{\alpha_{cr}N_{Ed}(x_m)\bar{e}_0\theta_{cr}(x_m)}{\alpha_{cr} - 1}\left[(u_D - e_u)\frac{v_{cr}(x_m)}{\theta_{cr}(x_m)} + e_v\frac{u_{cr}(x_m)}{\theta_{cr}(x_m)} - \frac{GJ(x_m)}{N_{cr,TF,ecc}} + i_p^2\right.$$

$$\left. + 2\beta_u(x_m)e_u\right]$$

where β_u is the Wagner factor for angle sections, equal to $\beta_u = u_D - k_u$.

The second-order utilization ratio for the equivalent angle member in eccentric compression is given by:

$$\varepsilon_N^{II}(x_m) = \frac{M_u^{II}(x)}{W_u(x)f_y} + \frac{M_v^{II}(x)}{W_v(x)f_y} + \frac{M_w^{II}(x)}{W_w(x)f_y} =$$

$$= \frac{\alpha_{cr}N_{Ed}(x_m)\bar{e}_0\theta_{cr}(x_m)}{W_u(x_m)f_y(\alpha_{cr}-1)}\left[\frac{v_{cr}(x_m)}{\theta_{cr}(x_m)} + u_D + e_u + \left(\frac{u_{cr}(x_m)}{\theta_{cr}(x_m)} + e_v\right)\frac{W_u(x_m)}{W_v(x_m)}\right.$$

$$+ \left((u_D - e_u)\frac{v_{cr}(x_m)}{\theta_{cr}(x_m)} + e_v\frac{u_{cr}(x_m)}{\theta_{cr}(x_m)} + \frac{GJ(x_m)}{N_{cr,TF,ecc}} + i_p^2\right.$$

$$\left.\left. + 2\beta_u(x_m)e_u\right)\frac{W_u(x_m)}{W_w(x_m)}\right] = \frac{N_{cr,TF,ecc}\bar{e}_0}{W_u(x_m)f_y(\alpha_{cr}-1)} \tag{3.65}$$

with

$$N_{cr,TF,ecc} = \alpha_{cr}N_{Ed}(x_m)\theta_{cr}(x_m)\frac{W_u(x_m)}{W_w(x_m)}\left[\left(\frac{v_{cr}(x_m)}{\theta_{cr}(x_m)} + u_D + e_u\right)\frac{W_w(x_m)}{W_u(x_m)}\right.$$

$$+ \left(\frac{u_{cr}(x_m)}{\theta_{cr}(x_m)} + e_v\right)\frac{W_w(x_m)}{W_v(x_m)}$$

$$+ \left((u_D - e_u)\frac{v_{cr}(x_m)}{\theta_{cr}(x_m)} + e_v\frac{u_{cr}(x_m)}{\theta_{cr}(x_m)} + \frac{GJ(x_m)}{N_{cr,TF}} + i_p^2\right. \tag{3.66}$$

$$\left.\left. + 2\beta_u(x_m)e_u\right)\right]$$

The second-order utilization or the real member at the location x_m is given by:

$$\varepsilon_N^{II}(x_m) = \frac{M_u^{II}(x_m)}{W_u(x_m)f_y} + \frac{M_v^{II}(x_m)}{W_v(x_m)f_y} + \frac{M_w^{II}(x_m)}{W_w(x_m)f_y}$$

$$= \frac{EI_u(x_m)}{W_u(x_m)f_y(\alpha_{cr}-1)}\left[v_{cr}''(x_m) + \frac{W_u(x_m)}{W_v(x_m)}\frac{I_v(x_m)}{I_u(x_m)}u_{cr}''(x_m)\right. \tag{3.67}$$

$$\left. + \frac{W_u(x_m)}{W_w(x_m)}\frac{C_w(x_m)}{I_u(x_m)}\theta''_{cr}(x_m)\right]\bar{\delta}_{0,TFB}$$

Due to the same reasons already stated in the case of angles in concentric compression subjected to torsional-flexural buckling (Section 3.3.1), the second term on the right-hand side is ignored, and then, the second-order utilization of the real angle member in eccentric compression becomes:

$$\varepsilon_N^{II}(x_m) = \frac{EI_u(x_m)}{W_u(x_m)f_y(\alpha_{cr} - 1)}\left[v_{cr}"(x_m) + \frac{W_u(x_m)}{W_v(x_m)}\frac{I_v(x_m)}{I_u(x_m)}u_{cr}"(x_m)\right]\bar{\delta}_{0,TFB} \tag{3.68}$$

Equaling Equations (3.65) and (3.68) leads to the following expression for the amplitude of the imperfection:

$$\bar{\delta}_{0,TFB} = \frac{N_{cr,TF,ecc}\bar{e}_0}{EI_u(x_m)\left[v_{cr}"(x_m) + \frac{W_u(x_m)}{W_v(x_m)}\frac{I_v(x_m)}{I_u(x_m)}u_{cr}"(x_m)\right]} = f_\eta\bar{e}_0 \tag{3.69}$$

Similarly to the other cases, the location x_m is adopted where $max\ (v''_{cr}(x); u''_{cr}(x))$ reaches a maximum and then the amplitude of the generalized imperfection is given by Equation (3.53) where:

$$f_\eta = \frac{N_{cr,TF,ecc}}{EI_u(x_m)\left[v_{cr}"(x_m) + \frac{W_u(x_m)}{W_v(x_m)}\frac{I_v(x_m)}{I_u(x_m)}u_{cr}"(x_m)\right]} \tag{3.70}$$

For angle members in eccentric compression, the general displacement of the critical mode, $\delta^{fl}(x)$, is given by a geometric relationship between the in-plane and out-of-plane displacements and the section rotation, as defined by Equation (3.71) and Figure 3.3, where the rotation contribution in the u-direction was disregarded.

$$\delta^{fl}(x) = \sqrt{\left(v_{cr}(x) + u_D\theta_{cr}(x)\right)^2 + \left(u_{cr}(x)\right)^2} \tag{3.71}$$
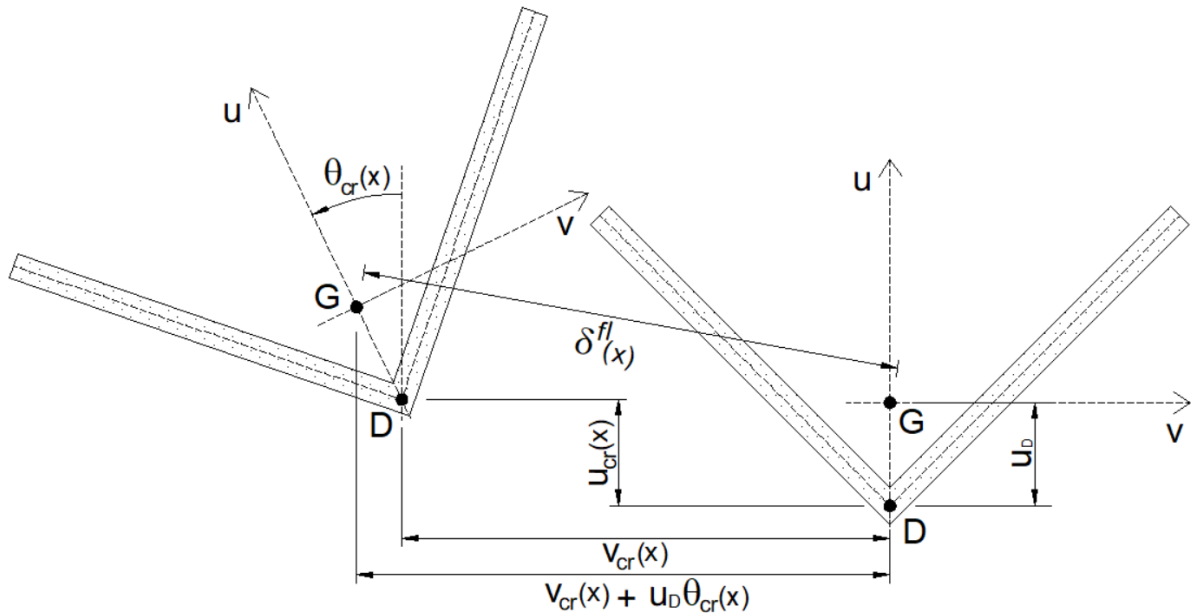
Figure 3.3 – General displacement for the torsional-flexural buckling of an angle section in eccentric compression.

Thus, the final verification equation is given by:

$$\varepsilon_N(x) = \frac{N_{Ed}(x)}{A(x)f_y} + \frac{N_{Ed}(x)e_v}{W_u(x)f_y} + \frac{N_{Ed}(x)e_u}{W_v(x)f_y}$$
$$+ \frac{EI_u(x)\left[v_{cr}''(x) + \frac{W_u(x)}{W_v(x)}\frac{I_v(x)}{I_u(x)}u_{cr}''(x)\right]}{A(x)f_y(\alpha_{cr}-1)}\eta(x) \le 1.0 \tag{3.72}$$

The generalized imperfection is given by Equation (3.53), adjusted to the appropriate values of general displacement of the critical mode (Equation (3.71)) and f_η (Equation (3.70)). Furthermore, $\bar{\lambda}(x)$ is given by:

$$\bar{\lambda}(x) = \sqrt{\frac{A(x)f_y}{N_{cr,TF,ecc}}} \tag{3.73}$$

Equation (3.72) can be expressed in a more simplified form given by:

$$\frac{N_{Ed}(x_m)}{A(x_m)f_y} + \frac{N_{Ed}(x_m)e_v}{W_u(x_m)f_y} + \frac{N_{Ed}(x_m)e_u}{W_v(x_m)f_y}$$

$$+ \frac{EI_u(x_m)\left[v_{cr}"(x_m) + \frac{W_u(x_m)}{W_v(x_m)}\frac{I_v(x_m)}{I_u(x_m)}u_{cr}"(x)\right]}{A(x_m)f_y(\alpha_{cr}-1)}\alpha(\bar{\lambda}(x)$$

$$-0.2)\frac{N_{cr,TF,ecc}}{EI_u(x_m)\left[v_{cr}"(x_m) + \frac{W_u(x_m)}{W_v(x_m)}\frac{I_v(x_m)}{I_u(x_m)}u_{cr}"(x_m)\right]}$$

$$\cdot\left|\sqrt{\left(v_{cr}(x_m) + u_D\theta_{cr}(x_m)\right)^2 + \left(u_{cr}(x_m)\right)^2}\right| \leq 1.0 \leftrightarrow$$

$$\frac{N_{Ed}}{Af_y} + \frac{N_{Ed}e_v}{W_uf_y} + \frac{N_{Ed}e_u}{W_vf_y} + \frac{\alpha(\bar{\lambda}-0.2)}{Af_y\frac{N_{cr,TF,ecc}}{N_{Ed}}\left(1-\frac{N_{Ed}}{N_{cr,TF,ecc}}\right)}N_{cr,TF,ecc} \leq 1.0 \leftrightarrow \qquad (3.74)$$

$$\frac{N_{Ed}}{Af_y} + \frac{N_{Ed}e_v}{W_uf_y} + \frac{N_{Ed}e_u}{W_vf_y} + \frac{\alpha(\bar{\lambda}-0.2)}{Af_y\frac{N_{cr,TF,ecc}}{N_{Ed}}\left(1-\frac{N_{Ed}}{N_{cr,TF,ecc}}\right)}N_{cr,TF,ecc} \leq 1.0 \leftrightarrow$$

$$\frac{N_{Ed}}{Af_y}\left(1 + \frac{Ae_v}{W_u} + \frac{Ae_u}{W_v}\right) + \frac{N_{Ed}}{Af_y}\frac{\alpha(\bar{\lambda}-0.2)}{\left(1-\frac{N_{Ed}}{N_{cr,TF,ecc}}\right)} \leq 1.0 \leftrightarrow$$

$$\chi_{TF,ecc}\left(1 + \frac{Ae_v}{W_u} + \frac{Ae_u}{W_v}\right) + \frac{\chi_{TF,ecc}}{\left(1-\chi_{TF,ecc}\bar{\lambda}^2_{TF,ecc}\right)}\alpha(\bar{\lambda}_{TF,ecc}-0.2) \leq 1.0$$

Finally, an expression for a reduction factor for torsional-flexural buckling of angles in eccentric compression ($\chi_{TF,ecc}$), in the Eurocode 3 format, can be obtained:

$$\chi_{TF,ecc} = \frac{1}{\Phi_{TF,ecc} + \sqrt{\Phi_{TF,ecc}^2 - f_\chi\bar{\lambda}_{TF,ecc}^2}} \qquad (3.75)$$

with

$$\Phi_{TF,ecc} = 0.5\left[f_\chi + \alpha(\bar{\lambda}_{TF,ecc}-0.2) + \bar{\lambda}_{TF,ecc}^2\right] \qquad (3.76)$$

and

$$f_\chi = 1 + \frac{Ae_v}{W_u} + \frac{Ae_u}{W_v} \qquad (3.77)$$

3.4 Summary

In this chapter, a General Formulation is proposed for the verification of mono-symmetric beams and angle sections in compression. This proposal consists basically of equating the longitudinal stresses referring to first- and second-order loadings for each cross-section along the member length.

The proposed method keeps the buckling mode verification, using their deformed shape as the initial geometric imperfection. Additionally, the load multiplier α_{cr} adopted in General Formulation is consistent with that used in Eurocode 3, however, the new proposal avoids the calibration of additional factors and the use of reduction factors for buckling resistance.

It can be noted that the calculation of the resistance of the cross-section located at the member ends is automatically included in the analysis, therefore eliminating the use of effective buckling factors. The General Formulation is easily applicable to members with variable geometry, loading, and boundary conditions. In Chapters 6 and 7 the proposed approach is further validated for mono-symmetric I-section beams and angles in compression, respectively.

Finally, Table 3.3 summarizes the stress utilization expressions demonstrated in this chapter. Notably, Equations (3.79) and (3.80) are coincident with methods of EN-1993-1-1 for flexural and torsional-flexural buckling, respectively. Equation (3.81) leads to a simplified expression, in the Eurocode 3 format, for verification of angle members in eccentric compression.

Table 3.3 – Stress utilization ratios according to each case.

Mono-symmetric I-section beams	$\dfrac{M_{y,Ed}(x)}{W_y(x)f_y}$ $+\dfrac{EI_z(x)\left[v''_{cr}(x)+\frac{W_z(x)}{W_w(x)}\frac{C_w(x)}{I_z(x)}\left(\theta''_{cr}(x)+\frac{W_w(x)}{W_z(x)}\frac{I_z(x)}{C_w(x)}\theta'_{cr}h'\right)\right]}{A(x)f_y(\alpha_{cr}-1)}\,\eta(x)$ ≤ 1.0	(3.78)
Angles in concentric compression (Flexural Buckling)	$\dfrac{N_{Ed}(x)}{A(x)f_y}+\dfrac{EI_v(x)u''_{cr}(x_m)}{A(x)f_y(\alpha_{cr}-1)}\,\eta(x)\leq 1.0$	(3.79)
Angles in concentric compression (Torsional-Flexural Buckling)	$\dfrac{N_{Ed}(x)}{A(x)f_y}+\dfrac{EI_u(x)v''_{cr}(x)}{A(x)f_y(\alpha_{cr}-1)}\,\eta(x)\leq 1.0$	(3.80)
Angles in eccentric compression	$\dfrac{N_{Ed}(x)}{A(x)f_y}+\dfrac{N_{Ed}(x)e_v}{W_u(x)f_y}+\dfrac{N_{Ed}(x)e_u}{W_v(x)f_y}$ $+\dfrac{EI_u(x)\left[v_{cr}''(x)+\frac{W_u(x)}{W_v(x)}\frac{I_v(x)}{I_u(x)}u_{cr}''(x)\right]}{A(x)f_y(\alpha_{cr}-1)}\eta(x)\leq 1.0$	(3.81)

4

ASSESSMENT OF DESIGN PROCEDURES FOR PRISMATIC MONO-SYMMETRIC I-SECTION STEEL BEAMS

4.1 General Remarks

The main objective of this chapter is to evaluate the recommendations of EN 1993-1-1 (General Case) and AISC 360 relative to the design of prismatic mono-symmetric beams (see Subsection 2.5.2 -Chapter 2).

For that, first, the description of the numerical model (meshing, boundary conditions, material law, etc.) is presented. Next, the numerical model is validated against the experimental results of Tankova et al. (2021) and Lebastard (2022) and compared with numerical benchmarks from Tankova et al. (2018). The numerical model is tested with many parameters: steel grade, cross-section class, residual stress pattern, bending moment diagram, prismatic and tapered geometry, etc. Thus, an extensive parametric study is proposed, and its results are used to obtain statistical parameters for the ratio between the numerical lateral-torsional buckling resistance and the analytical lateral-torsional buckling resistance. Relevant conclusions are pointed out based on these results.

4.2 Numerical Modelling

4.2.1   Description of the Numerical Model

The numerical analyses were performed using the finite element software ANSYS (version 22.0). The geometry of the models was defined using the nominal dimensions of the cross-sections. The SHELL181 element, which is composed of 4 nodes with 6 degrees of freedom

per node, was chosen to discretize the mesh. After a mesh-sensitive study, 16 elements were defined across the flange´s width and 16 across the web´s depth (see Figure 4.1), in agreement with previous studies (Ferreira Filho et al., 2022). The same size of the elements across the width and depth was used along the length of the member, generating only quadratic elements (see Figure 4.1).
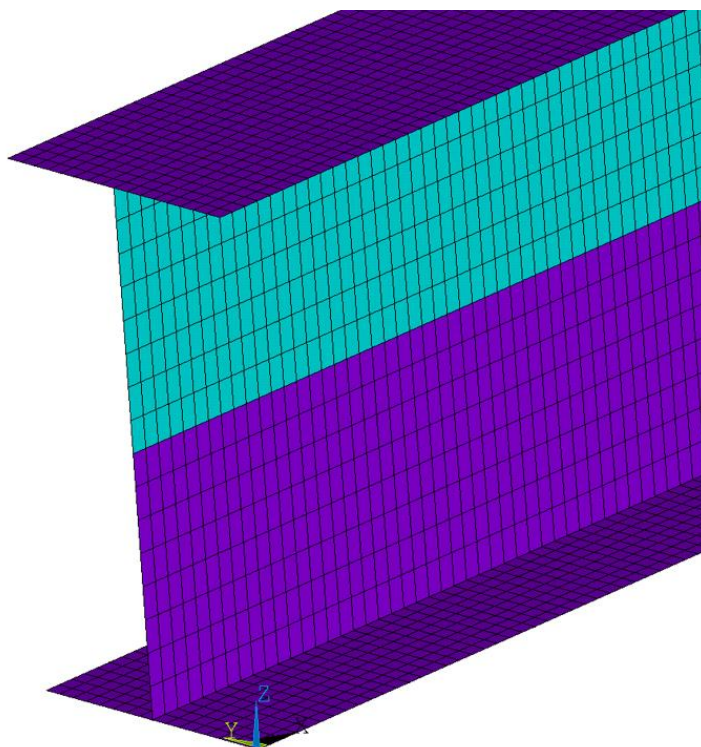
Figure 4.1 – Representation of the mesh for an I-section member.

Geometrically and materially nonlinear analyses with imperfections (GMNIA) were executed to obtain the ultimate resistance of the numerical models by using the arc-length method and the von Mises failure criterion. Initial geometric imperfections were introduced with a shape corresponding to the first buckling mode obtained from previous linear buckling analyses (LBA). The validation models were run considering the measured material stress-strains curves, residual stress diagrams, and amplitude of the initial geometrical imperfections obtained from experimental works found in the literature. In the parametric study, following ECCS (1976) recommendations, an amplitude of imperfection equal to $L/1,000$ and the ECCS pattern of residual stresses for welded I-sections (see Figure 4.2-b) were implemented in the numerical models. The constitutive law was adopted according to Yun and Gardner (2017) as the true stress-strain curve for the parametric study,

which is representative of hot-rolled steels with a yield plateau and strain hardening and was recently included in prEN 1993-1-14.
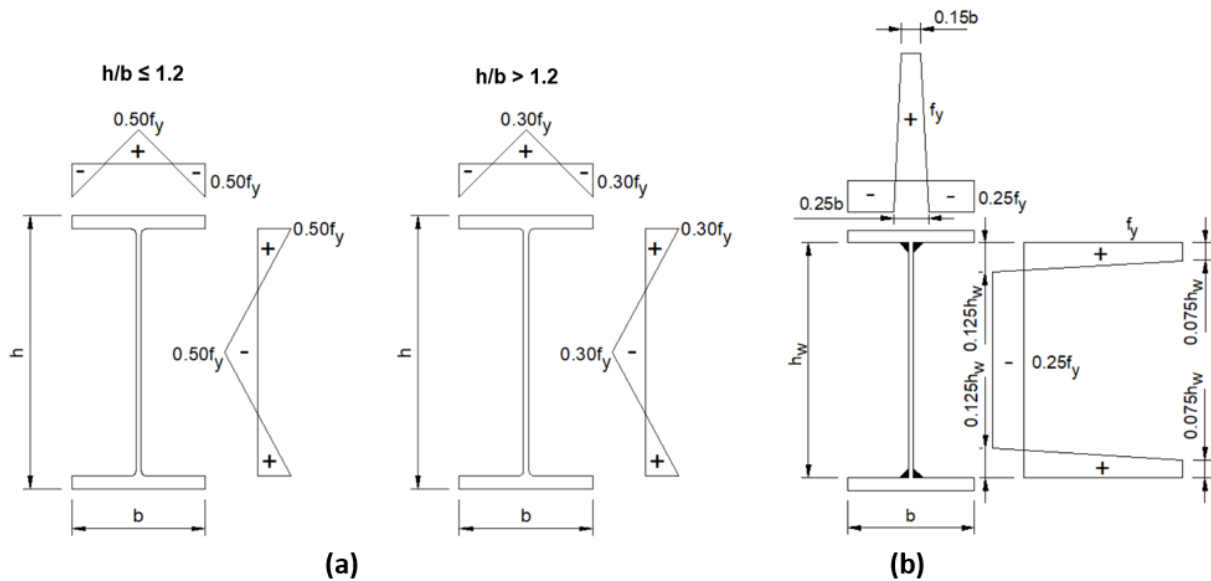
Figure 4.2 – Pattern of residual stresses for (a) hot-rolled and (b) welded I-sections, recommended by ECCS (1976).

To simulate fork boundary conditions, the validated boundary conditions adopted by Snijder et al. (2018) (see Figure 4.3) are utilized. On both end extremities of the beam, all nodes of top flanges (namely slave nodes - see Figure 4.3) are coupled for all their displacements (Ux, Uy, and Uz) and rotation (ROTx, ROTy, and ROTz) to the node located at the middle of this flange (indicated node – namely master node) by using kinematic coupling constraints, and the same is applied to the bottom flange. This makes the flange infinitely rigid. For the web, all nodes (namely slave nodes - see Figure 4.3) are coupled for all their displacements (Ux, Uy, and Uz) and rotations about x and y (ROTx and ROTy – see Figure 4.3) to the node located in the middle of the web (indicated node – namely master node). As a result of these constraints, the sections at extremities are infinitely rigid and can warp. Secondly, for fixing the numerical model, boundary conditions are applied at the node located in the middle of the web. In one of the ends of extremities, the displacements Ux, Uy, Uz and the rotation ROTx of this node are restricted, and in the other one, only Uy, Uz, and ROTx are zero. The end bending moments are applied at the same node where the boundary conditions are implemented.
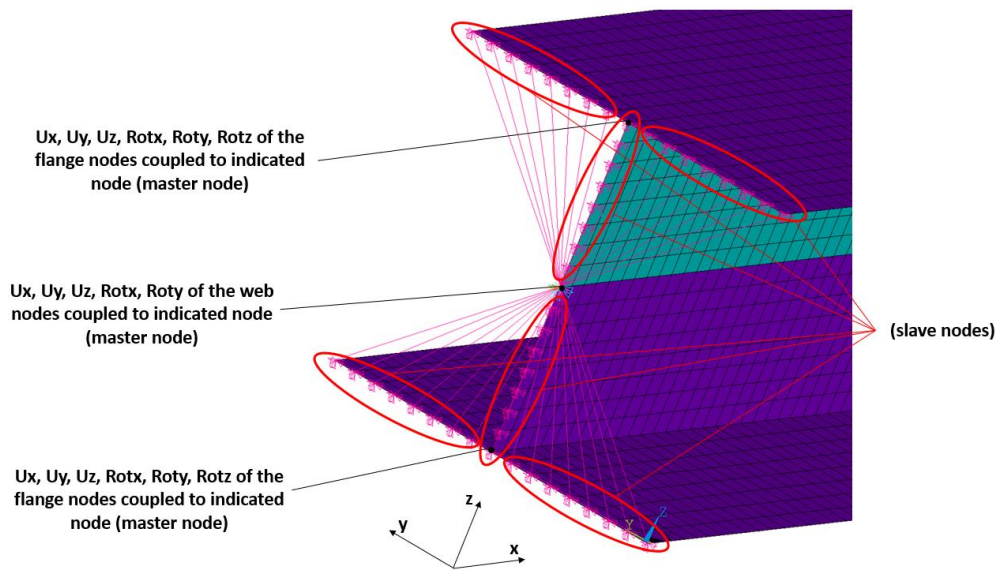
Figure 4.3 – Kinematic coupling constraints for the cross-sections of the end extremities of the numerical beam model.

4.2.2   Numerical Methodology Validation

The numerical model was validated using the experimental test results from Tankova et al. (2021) and Lebastard (2022). Additionally, available numerical benchmarks by Tankova et al. (2018) for uniformly distributed loads (DL) and linearly varying bending moments (LBM) were used to cover loading cases that were not covered by the experimental tests that were both implemented with concentrated loads.

4.2.2.1   Experimental Results by Tankova et al. (2021)

The experimental model of Tankova et al. (2021) is a four-point bending model where the vertical forces are applied at two locations, as shown in Figure 4.4. 16 mm-thickness stiffeners are considered at extremities and at the locations where the vertical forces were applied. Fork-support conditions are considered at the extremities, with additional lateral restraints at the location of the vertical forces (see Figure 4.4). All prototypes are 6 m long, with an unbraced distance between the vertical forces equal to 4 meters. The main parameters of the mono-symmetric I-section beams are shown in Table 4.1. All prototypes have identical cross-section

but are fabricated from different steel grades: S460, S690, and hybrid. The geometrical imperfections exhibited in Table 4.1 were measured using an optical 3D scan system.

Figure 4.4 – Numerical models based on experimental tests by Tankova et al. (2021).

Table 4.1 – Experimental parameter from Tankova et al. (2021) used in the numerical model validation.

Prototype	Member	$\bar{\lambda}_{LT}$	Fab.	Steel grade		Section classification	Amplitudes of Geometrical Imperfections (mm)*	
				Flanges	Web		In-plane	Out-of-plane
B11	700 X 200(400) X 8 X 16	1.01	Welded	S690	S690	4	0.96	0.34
B12		1.00		S690	S355		0.07	4.48
B13		0.84		S460	S460		1.31	0.90
B14		0.83		S460	S355		1.93	1.29

* Measurements at mid-span.

Table 4.2 presents the measured material properties from the plates that make up each section shown in Table 4.1 that were included in the numerical models according to the constitutive law shown in Figure 4.5, which was also adopted in the numerical analyses of Tankova et al. (2021).

Table 4.2 – Material properties measured by Tankova et al. (2021) and used in the numerical model validation.

Plate/Thickness	Steel grade	E (GPa)	f_y (MPa)	f_u (MPa)	ε_u (%)
8 mm	S355	202.6	425.5	634.7	12.2
8 mm	S690	200.4	755.3	813.0	6.2
16 mm	S690	204.0	798.4	854.8	5.9
8 mm	S460	212.5	528.8	639.2	11.0
16 mm	S460	201.1	498.9	656.2	9.4
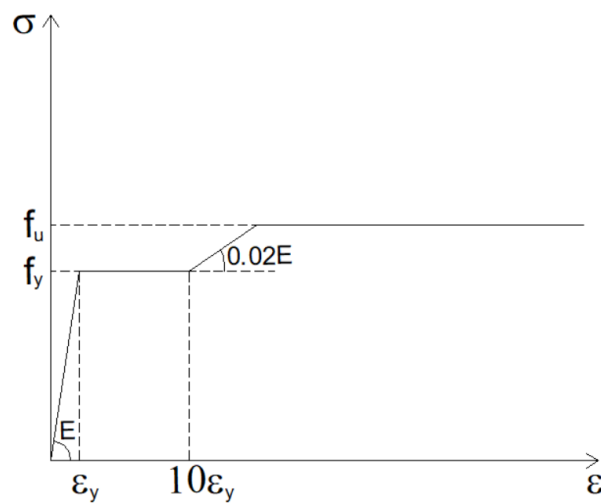
Figure 4.5 – Constitutive material law adopted in the numerical model validation.

Figure 4.6 shows the measured residual stresses obtained from prototype B11 (see Table 4.1) and implemented in the numerical models. The diagrams shown in this figure were applied in all the numerical model validation.
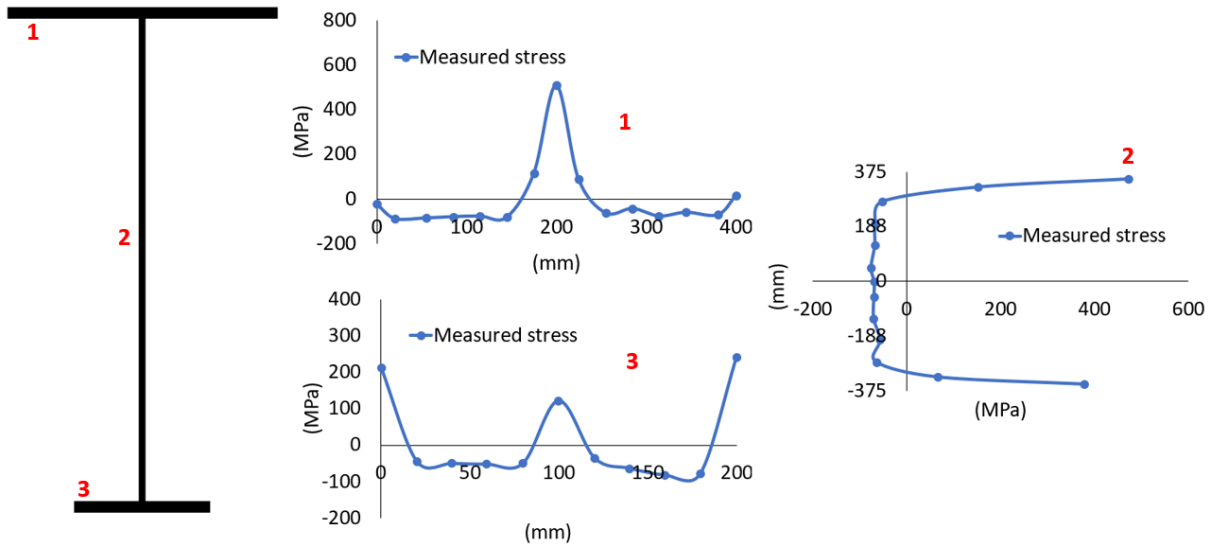
Figure 4.6 – Residual stress measured by Tankova et al. (2021) for prototype B11 and adopted in the numerical model validation.

Table 4.3 and Figure 4.7 to Figure 4.9 compare the experimental and numerical results. There is excellent agreement between numerical and experimental results, both in terms of stiffness and ultimate resistance. It is noted that the larger differences for the B14 test may be attributed to the fact that there was no measurement of residual stresses for this cross-section. All numerical models failed by lateral-torsional buckling, in line with the experimental results, as depicted in Figure 4.10.

Table 4.3 – Experimental and numerical results for P_{ult}, considering experimental results from Tankova et al. (2021).

Prototype	P_{ult} (kN)		Num./Exp.
	Experimental	Numerical	
B11	1731.8	1732.0	1.00
B12	1601.0	1610.9	1.01
B13	1307.2	1301.1	1.00
B14	1133.3	1210.0	1.07
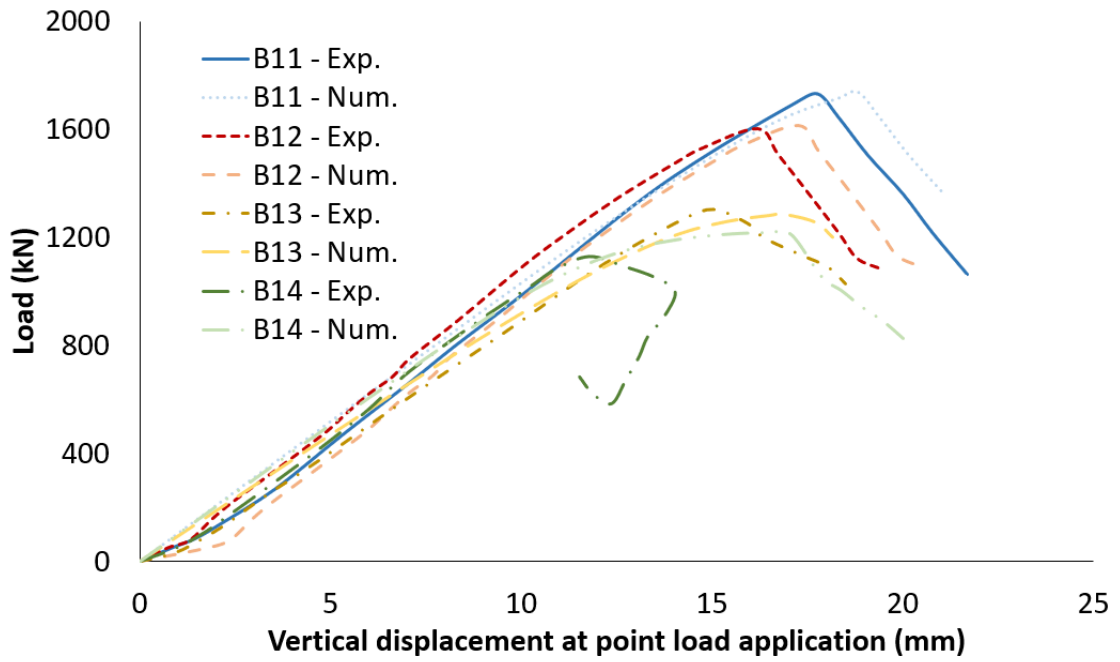
Figure 4.7 – Load-vertical displacement curves – displacements measured at point load application.
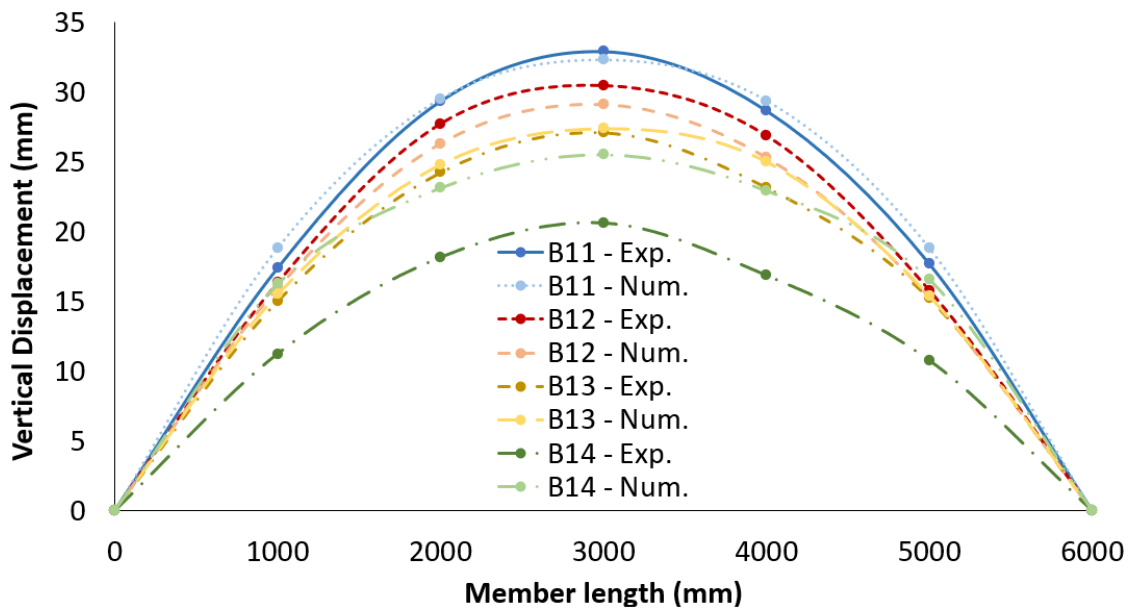
Figure 4.8 – Vertical displacement at maximum load – displacements measured at bottom flange.
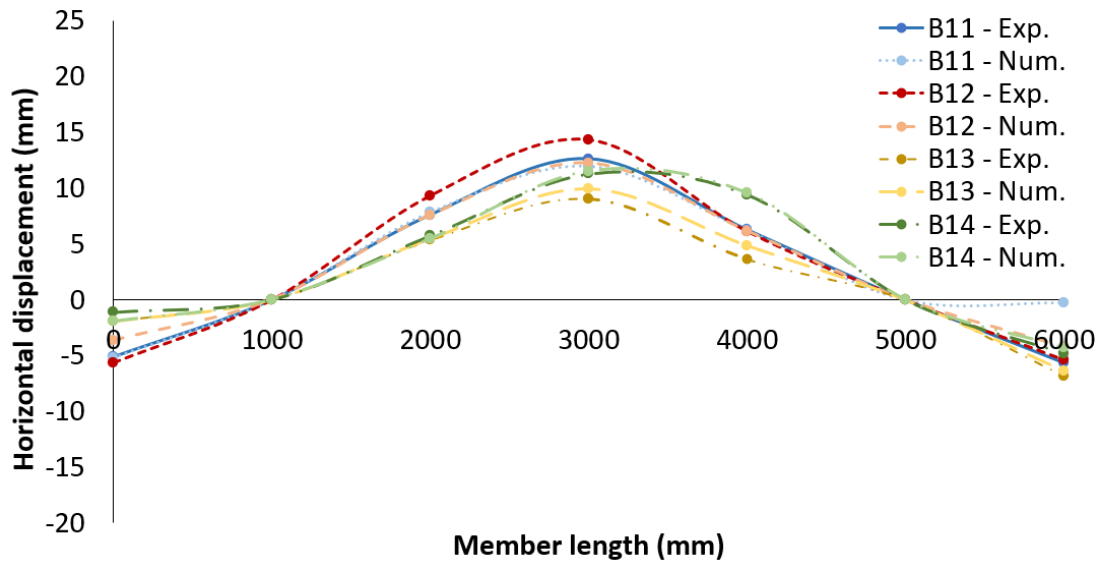
Figure 4.9 – Horizontal displacements at maximum load – displacements measured at the middle of the web.
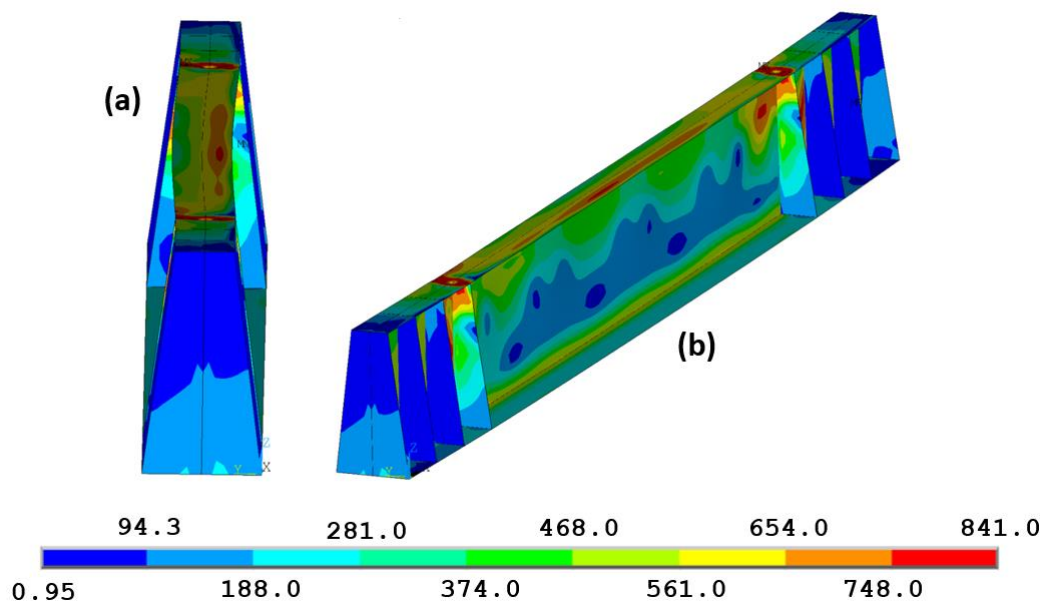
Figure 4.10 – von Mises stress distribution (in MPa) relative to the ultimate load capacity of the numerical model B11 – (a) longitudinal view; (b) perspective view.

4.2.2.2 Experimental Results by Lebastard (2022)

The experimental work by Lebastard (2022) included lateral-torsional buckling tests on two uniform and two tapered members, one having a mono-symmetric cross-section while the other is doubly symmetrical within each of the groups. The test setup of the four 8.43 m long beams was similar. The load was applied at the top flange of a laterally restrained cross-section located

at 2.18 m from one of the extremities of the member (see Figure 4.11). Fork support conditions were imposed at both end extremities. On both sides of the web, 30 mm-thick transverse stiffeners were placed at the three laterally restrained cross-sections. Besides, a 20 mm-thick longitudinal stiffener was positioned on both sides of the web along the 2.18 m-long segment (see Figure 4.11), and thus, the unbraced length was 6.25 m. The nominal dimensions and material of the tested members, as well as the measured amplitudes of the geometrical imperfections, are given in Table 4.4. Note that, unlike the prototypes from Tankova et al. (2021), where the sections have flanges with different widths and equal thicknesses (see Table 4.1), the mono-symmetry of the sections shown in Table 4.4 is due only to the difference in thickness of the flanges, which have the same width. Furthermore, it is noteworthy that the bending moment diagrams of these two experimental works are different: a constant bending moment in Tankova et al. (2021) and a triangular-diagram in Lebastard (2022) within the unbraced lengths.
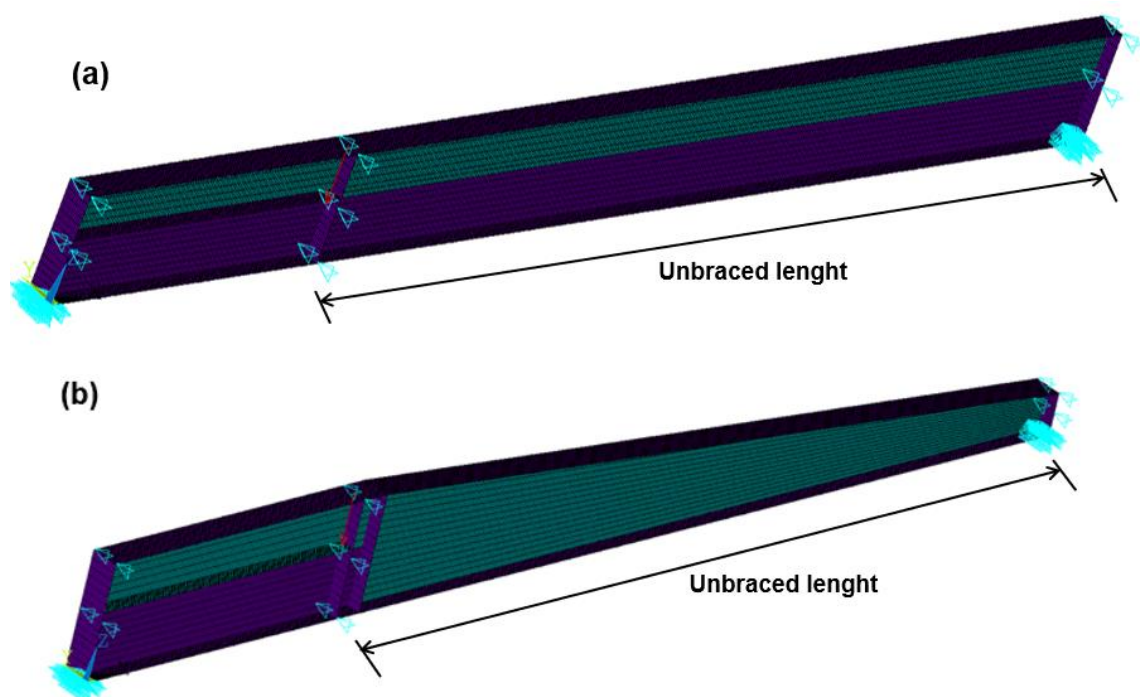
Figure 4.11 – Numerical models based on experimental prototypes geometry of (a) uniform and (b) tapered members from Lebastard (2022).

Table 4.4 – Experimental parameters from Lebastard (2022) used in the numerical model validation.

Prototype	Member	$\bar{\lambda}_{LT}$	Fab.	Steel grade	Section classification	Out–of-plane imperfections (mm)*
U-DS	804 X 200 X 8 X 20					3.4
U-MS	804 X 200 X 8 X 20(15)					4.0
T-DS	(836 to 286) X 200 X 8 X 20	0.74	Welded	S355	3	3.3
T-MS	(836 to 286) X 200 X 8 X 20(15)					5.0

* Amplitude of imperfection measured at the flange in compression.
Note: U-DS = Uniform Doubly Symmetric; U-MS = Uniform Mono-symmetric; T-DS = Tapered Doubly Symmetric; T-MS = Tapered Mono-symmetric.

Figure 4.12 presents the material laws for each plate thickness that were implemented in the numerical model. Each material law corresponds to the true stress-strain behavior relative to the results of coupon tests performed by Lebastard (2022). Figure 4.13 presents the residual stress diagram measured by Lebastard (2022) for each prototype shown in Table 4.4 and adopted in the numerical simulations.
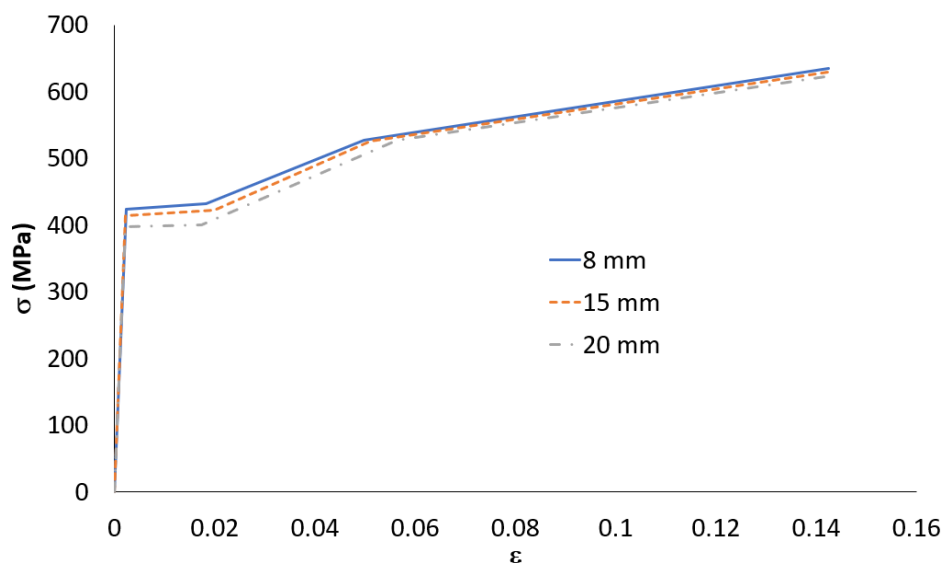
Figure 4.12 – Material law obtained by Lebastard (2022) and implemented in the numerical model validation.
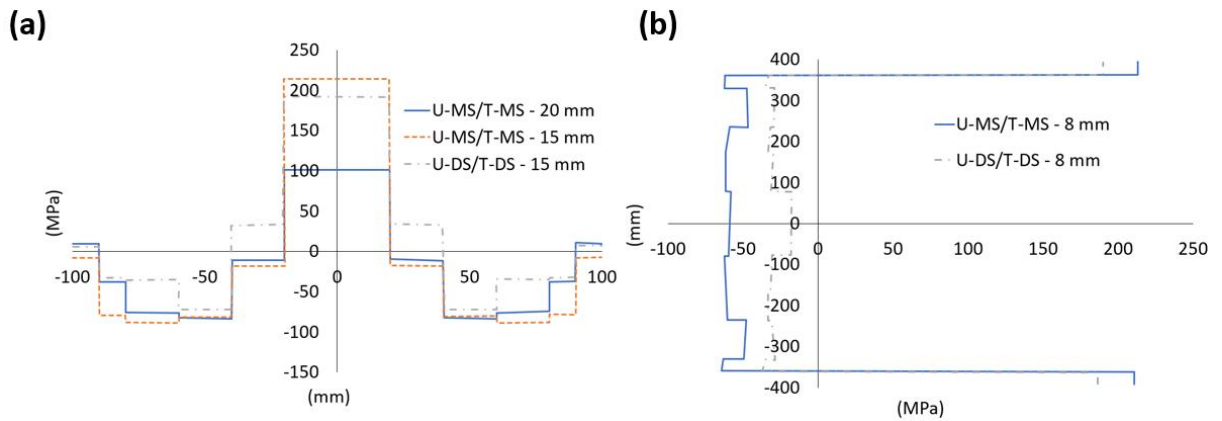
Figure 4.13 – Residual stress measured by Lebastard (2022) and adopted in the numerical model validation – (a) flanges and (b) web.

Table 4.5 and Figure 4.14 to Figure 4.16 compare the experimental and the numerical results. These comparisons show that the stiffness of the numerical models as well as their ultimate resistance are in good agreement with the experimental results. Similarly to the experimental prototypes, all numerical models failed by lateral-torsional buckling, as can be seen in Figure 4.17, further evidencing the validity of the numerical model of this work.

Table 4.5 – Experimental and numerical results for P_{ult}, considering experimental results from Lebastard (2022).

Prototype	P_{ult} (kN)		Num./Exp.
	Experimental	Numerical	
U-DS	747.6	733.6	0.98
U-MS	903.6	887.3	0.98
T-DS	720.6	684.6	0.95
T-MS	775.8	726.3	0.94
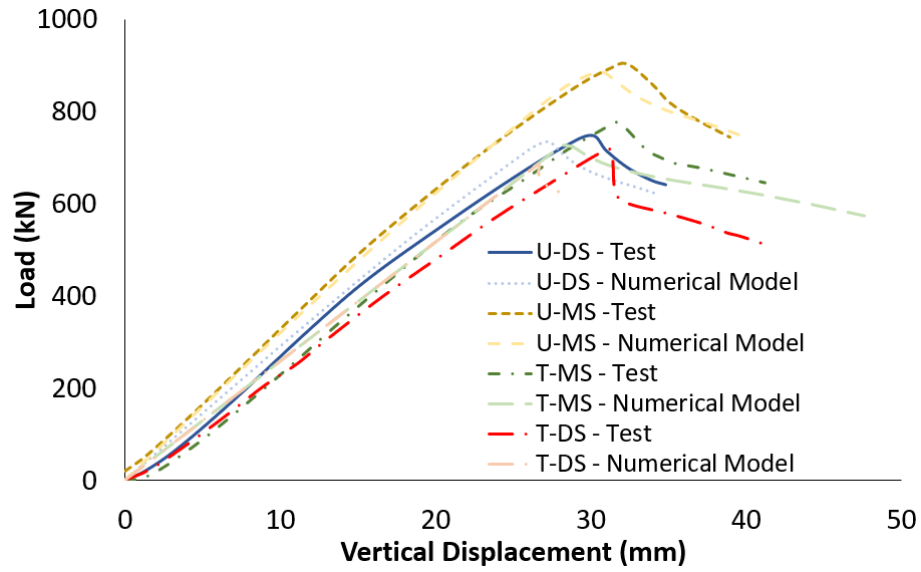
Figure 4.14 – Load-vertical displacement curves – displacements measured at top flange at 1.042 m from point load application (within buckling length).
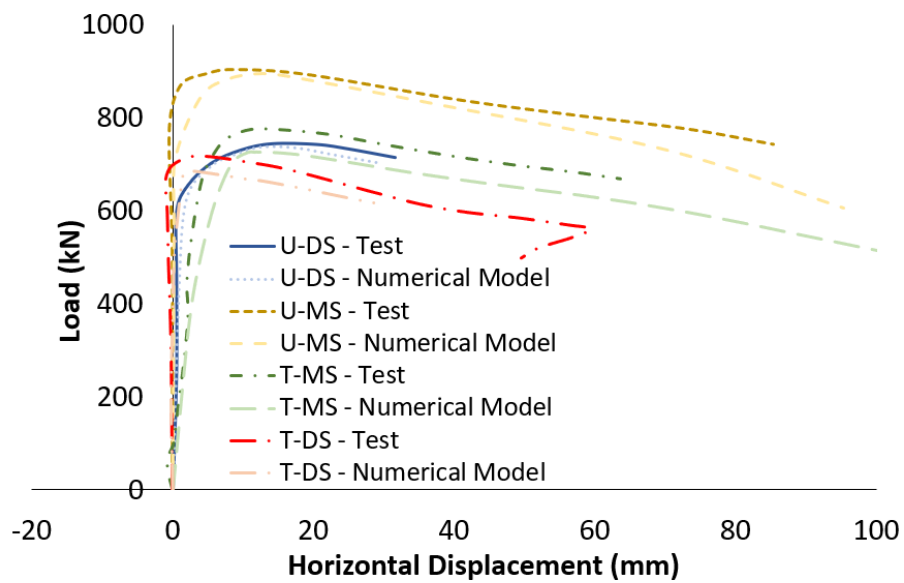
Figure 4.15 – Load-horizontal displacement curves – displacements measured at the middle of the web at 1.042 m from point load application (within buckling length).
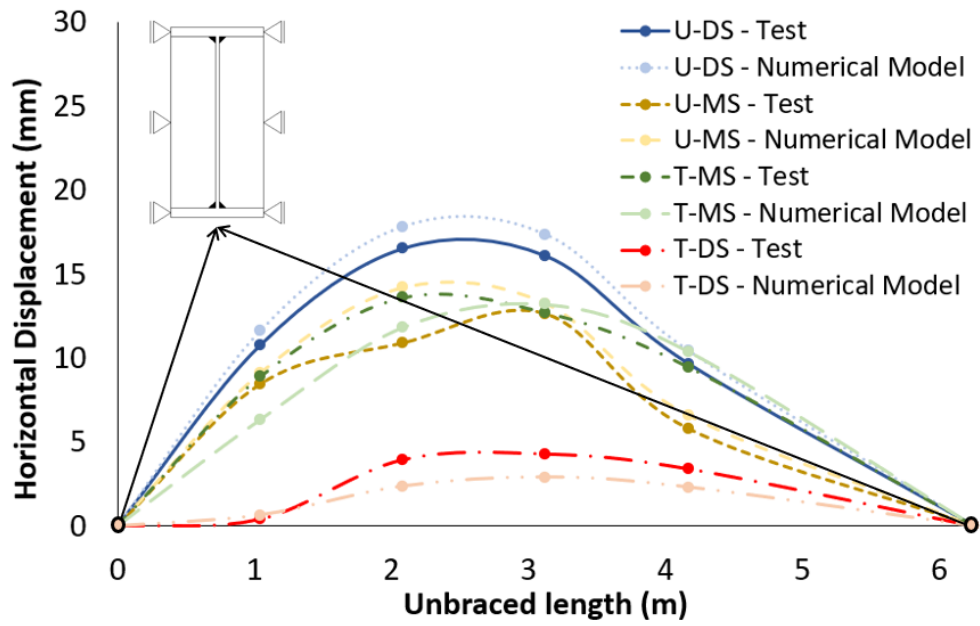
Figure 4.16 – Horizontal displacements at maximum load – displacements measured at the middle of the web along the member.
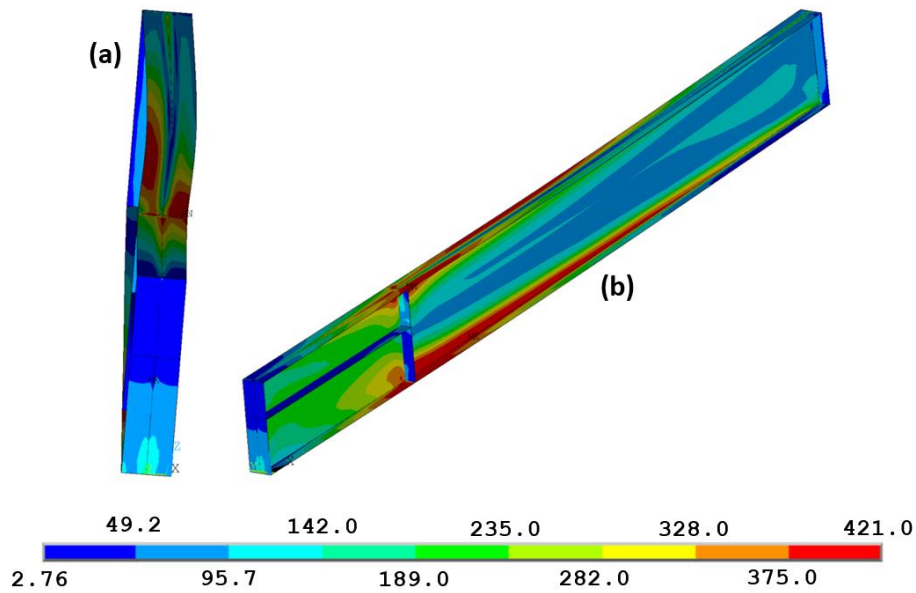
Figure 4.17 – von Mises stress distribution (in MPa) relative to the ultimate load capacity of the numerical model U-MS – (a) longitudinal view; (b) perspective view.

4.2.2.3 Numerical Benchmarks

The calibrated numerical models conducted by Tankova et al. (2018) present the following features:

(i)   hot-rolled double symmetric sections, steel grade S235 and Class 1;

(ii)   fork boundary conditions at the end extremities;

(iii)   uniformly distributed loads in the z-direction or linearly varying end bending moments;

(iv)   no transverse or longitudinal stiffeners;

(v)   initial geometric imperfections with an amplitude equal to $L/1,000$ and with the hot-rolled residual stress pattern shown in Figure 4.2-a, as recommended by ECCS (1976).

Table 4.6 shows that both numerical models are practically coincident, presenting excellent agreement.

Table 4.6 – Numerical parameters from Tankova et al. (2018) used in the numerical model validation and comparison between both numerical results.

#	Section	L (m)	$\bar{\lambda}_z$	$\bar{\lambda}_{LT}$	Load	$\chi^*_{Tankova\ et\ al.\ (2018)}$	$\chi^*_{Num.Mod.}$	$\dfrac{\chi_{Num.Mod}}{\chi_{Tankova\ et\ al.\ (2018)}}$
1		9.68	2	0.77	LBM ($\psi = 0$)	0.999	1.000	1.00
2	HBE200	14.52	3	0.96	LBM ($\psi = 0$)	0.945	0.926	0.98
3		7.26	1.5	0.82	DL	0.874	0.864	0.99
4		6.40	2	0.84	LBM ($\psi = -1$)	0.936	0.943	1.01
5	IPE300	9.60	3	1.08	LBM ($\psi = -1$)	0.724	0.709	0.98
6		4.80	1.5	1.05	DL	0.640	0.633	0.99

* Ratio between ultimate numerical bending moment and plastic bending moment.

4.3 Assessment of Design Procedures

In the following subsections, the bending moment resistance of prismatic I-section beams obtained by the numerical model ($M_{R,num}$) are compared to the analytical values ($M_{R,anal}$) calculated by using prescriptions of EN 1993-1-1 (General Case – GC) and AISC 360 – see Subsection 2.5.2 – Chapter 2. The results are displayed in terms of r_N for the different loading types covered in this work, where r_N is the ratio given by:

$$r_N = M_{R,num}/M_{R,anal} \tag{4.1}$$

and assessed by analyzing the mean values and the Coefficient of Variation (C.O.V) of r_N for appropriate sub-sets.

Firstly, the parametric study is defined in a comprehensive way, followed by the assessment of the design proposals mentioned previously.

4.3.1   Parametric Study

Using the validated numerical model, a large parametric study on mono-symmetric welded I-beams is defined and performed. The results of this parametric study are used to assess the design procedures presented in Subsection 2.5.2 (Chapter 2) for prismatic mono-symmetric I-sections. The proposed parametric study comprises prismatic beams, subjected to linear bending moment, uniformly distributed load, and concentrated loads, with fork boundary conditions - see Table 4.7 –, totaling 1,296 numerical models. The boundary conditions of the numerical models of the parametric study are modeled as shown in Figure 4.3.

Table 4.7 – Parametric study for prismatic mono- and doubly symmetric cross-sections.

Section $h \; x \; b_2(b_1) \; x \; t_w \; x \; t_2(t_1)$	$\bar{\lambda}_z$	Steel grade	Bending Moment diagram	Stress on the largest flange[**]
300 x 150(150) x 8 x 20(15) 300 x 150(150) x 8 x 30(20) 400 x 180(180) x 10 x 30(20) 400 x 180(180) x 10 x 40(25) 500 x 200(150) x 12 x 50(30) 400 x 180(180) x 10 x 30(30) [*]			Linear (ψ = 1.0, 0.0 and -1.0)	Tension Compression
400 x 180(180) x 10 x 40(25) 500 x 200(150) x 12 x 50(30) 430 x 350(200) x 8 x 40(20) 400 x 180(180) x 10 x 30(30) [*]			Distributed load (applied at the top face -TF, the centroid - G, the torsion center - D[***], and the bottom face - BF)	
			Point load (applied at the top face -TF, the centroid - G, the torsion center - D[***], and the bottom face - BF)	
	0.50 to 5.0	S235 S355 S460	Linear (ψ = 1.0)	
600 x 476(476) x 100 x 140(140) [*] 1138 x 410(410) x 31 x 55(55) [*] 600 x 476(350) x 100 x 140(140) 1138 x 410(410) x 31 x 70(55)			Distributed load (applied at the top face -TF, the centroid - G, the torsion center - D[***], and the bottom face - BF)	Tension
			Point load (applied at the top face -TF, the centroid - G, the torsion center - D[***], and the bottom face - BF)	
			Linear (ψ = 1.0)	
2320 x 900(950) x 35 x 130(80) 2440 x 800(950) x 40 x 80(60)			Distributed load (applied at the top face -TF, the centroid - G, the torsion center - D, and the bottom face - BF)	
			Point load (applied at the top face -TF, the centroid - G, the torsion center – D, and the bottom face - BF)	

[*]   Doubly symmetric cross-sections.
[**]   Only applicable to mono-symmetric cross-sections / Not applicable to cases where $\psi = -1.0$.
[***] Only applicable to mono-symmetric cross-sections.

Table 4.8 summarizes the range of some parameters covered by the parametric study shown in Table 4.7. For the mono-symmetric beams, sections with flanges with the largest value of I_z in tension or compression are analyzed separately. In this table, the ratios $z_G/(h/2)$ and $W_{el,y,min}/W_{el,y,max}$ show the level of asymmetry of the cross-section with respect to the y-axis, where $W_{el,y,min}$ and $W_{el,y,max}$ are respectively the minimum and maximum values of the elastic section moduli about the major axis. When the values of both ratios are equal to 1.0, the cross-section is doubly symmetric.

Table 4.8 – Parameters range covered by the parametric study for prismatic beams.

h/b_{min}	b_2/b_1	t_2/t_1	$z_G{}^*/(h/2)$	$W_{el,y,min}/W_{el,y,max}$	Class
1.26 to 3.33	0.84 to 1.75	1.00 to 2.00	0.58 to 1.00	0.41 to 1.00	1 and 2

* See Figure 2.6.

4.3.2 Prismatic Mono-symmetric Beams

Firstly, for the analyzed mono-symmetric beams, it is interesting to note that the numerically calculated elastic critical moments (M_{cr}) are very similar to those obtained using the analytical 3-factor formula for the elastic critical bending moment (ENV 1993-1-1) as shown in Table 4.9.

Table 4.9 – Comparison between numerical and analytical (ENV 1993-1-1) values for the elastic critical bending moment for lateral-torsional buckling.

Subset	n	$M_{cr,num}/M_{cr,anal}$	
		Average	C.O.V (%)
All	1,296	0.97	6.91
Linear Bending Moment	408	0.96	6.71
Distributed Load	444	0.97	8.22
Point Load	444	0.99	5.07

The statistical evaluation of GC (EN 1993-1-1) and AISC are shown in Table 4.10 to Table 4.12. Globally, the following values were obtained: an average $r_N = 1.42$ and a C.O.V of 8.33% for GC and an average $r_N = 0.90$ and a C.O.V of 7.34% for AISC. In general, AISC exhibits a large scatter and unsafe results, while GC leads to safe-sided values. However, GC rules are too conservative for all cases studied.

Furthermore, the comparison of the results for double- and mono-symmetric cross-sections shows that the results are approximately 1% to 4% worse for mono-symmetric beams for AISC, while for GC this difference increases to 4% to 6% (see Table 4.10 to Table 4.12).

Table 4.10 – Statistical parameters for linear bending moment distribution.

		Linear Bending Moment							
Subset	n	$r_{N,AISC}$				$r_{N,GC}$			
		Average	C.O.V (%)	Min	Max	Average	C.O.V (%)	Min	Max
All	408	**0.93**	7.34	0.81	1.08	**1.41**	8.33	1.20	1.58
S235	136	**0.89**	10.09	0.73	1.05	**1.32**	7.93	1.13	1.47
S355	136	**0.93**	7.41	0.82	1.08	**1.43**	8.42	1.21	1.59
S460	136	**0.96**	7.21	0.88	1.11	**1.48**	8.73	1.27	1.67
$\psi = 1.0$	204	**0.90**	8.83	0.81	1.08	**1.39**	8.03	1.20	1.58
$\psi = 0.0$	132	**0.93**	1.08	0.92	0.94	**1.54**	5.55	1.43	1.60
$\psi = -1.0$	72	**0.99**	2.17	0.96	1.02	**1.46**	5.20	1.34	1.52
Stress on Fl. $> I_z =$ Ten., $\psi = 0; \psi = 1$	192	**0.89**	8.23	0.81	1.08	**1.43**	8.37	1.20	1.62
Stress on Fl. $> I_z =$ Comp., $\psi = 0; \psi = 1$	120	**0.93**	1.36	0.91	0.95	**1.50**	6.05	1.38	1.57
Mono-symmetric cross-section	348	**0.92**	7.81	0.81	1.08	**1.42**	7.88	1.20	1.58
Doubly symmetric cross-section	60	**0.94**	6.91	0.90	1.02	**1.38**	11.17	1.21	1.51

Table 4.11 – Statistical parameters for distributed load.

Subset	n	$r_{N,AISC}$				$r_{N,GC}$			
		Average	C.O.V (%)	Min	Max	Average	C.O.V (%)	Min	Max
All	444	**0.87**	9.23	0.78	1.00	**1.42**	8.55	1.20	1.59
S235	148	**0.84**	11.52	0.70	1.00	**1.34**	9.32	1.13	1.56
S355	148	**0.87**	9.76	0.77	1.00	**1.44**	8.71	1.21	1.60
S460	148	**0.89**	10.08	0.77	1.01	**1.48**	8.43	1.26	1.69
Point load application = TF	120	**0.78**	16.25	0.78	1.00	**1.44**	10.67	1.21	1.75
Point load application = BF	120	**0.94**	8.41	0.85	1.09	**1.41**	8.26	1.19	1.58
Point load application = G	120	**0.88**	8.23	0.80	1.00	**1.41**	8.19	1.20	1.59
Point load application = D	84	**0.87**	7.82	0.80	1.00	**1.30**	25.81	0.59	1.59
Mono-symmetric cross-section	336	**0.86**	9.02	0.78	1.00	**1.43**	8.90	1.20	1.59
Doubly symmetric cross-section	108	**0.90**	10.80	0.81	1.00	**1.38**	8.59	1.24	1.47

The header "Distributed Load" spans the entire table.

Table 4.12 – Statistical parameters for point load.

Subset	n	$r_{N,AISC}$				$r_{N,GC}$			
		Average	C.O.V (%)	Min	Max	Average	C.O.V (%)	Min	Max
All	444	**0.90**	7.89	0.82	1.01	**1.44**	10.03	1.18	1.65
S235	148	**0.88**	11.43	0.75	1.00	**1.36**	10.93	1.11	1.60
S355	148	**0.91**	8.21	0.83	1.02	**1.45**	10.15	1.19	1.67
S460	148	**0.93**	7.38	0.84	1.01	**1.49**	9.54	1.23	1.67
Point load application = TF	120	**0.80**	17.46	0.64	1.00	**1.44**	10.75	1.19	1.65
Point load application = BF	120	**0.99**	6.29	0.93	1.14	**1.43**	10.49	1.16	1.64
Point load application = G	120	**0.92**	7.15	0.83	1.01	**1.44**	10.24	1.18	1.66
Point load application = D	84	**0.91**	8.05	0.83	1.01	**1.45**	10.18	1.19	1.67
Mono-symmetric cross-section	336	**0.90**	8.07	0.82	1.01	**1.45**	9.86	1.18	1.65
Doubly symmetric cross-section	108	**0.91**	9.22	0.84	1.00	**1.39**	11.90	1.20	1.51

5

ASSESSMENT OF DESIGN PROCEDURES FOR THE BUCKLING RESISTANCE OF HOT-ROLLED STEEL EQUAL LEG ANGLES UNDER CONCENTRIC AND ECCENTRIC COMPRESSION

5.1 General Remarks

As seen in Subsection 2.5.3 (Chapter 2), the design proposal of the ANGELHY project has already been included in the last version of prEN 1993-3. Thus, to support the ongoing discussion on the choice and validation of formulation to be included in future versions of Eurocode 3, this Chapter aims to evaluate the recommendation of EN 1993-1-1, FprEN 1993-1-1, EN 1993-3-1 and AISC 360, concerning the design of angle members in concentric and eccentric compression. The recent proposals of the ANGELHY project, Kettler et al. (2021), and Behzadi-Sofiani et al. (2021), (2022b) are also evaluated.

Therefore, in this chapter, firstly, the characteristics of the numerical model (meshing, boundary conditions, material law, residual stresses, geometric imperfection) are presented. Then, the numerical model is validated and, hence, an extensive parametric study is described. The results of this study are used to carefully assess the design prescriptions previously mentioned. After the evaluation of each proposal, a deeper discussion of the physical behavior of angle members in compression is accomplished and, finally, a reliability assessment of the design procedure of the ANGELHY project for angle section in concentric compression is performed.

5.2 Numerical Methodology

5.2.1 Numerical Model Description

The numerical analyses were performed using the finite element software ANSYS (version 22.0). The geometry of the models was elaborated using nominal dimensions and the angles were simulated with straight corners without any curvature, since it showed no significative influence on the capacity of the members, as also observed by Liu and Hui (2010), Hussain et al. (2018), and Jiang et al. (2023). The SHELL181 element, which is composed of 4 nodes with 6 degrees of freedom per node, was chosen to discretize the mesh since it is suitable enough for executing non-linear analysis of members with small thickness and subjected to large deformations and rotations and has been also successfully applied in previous studies reported in the literature (Kettler et al., 2017; Liu and Hui, 2010; Ananthi et al., 2021; Abdelrahman et al., 2019; Sirqueira et al., 2020). After a mesh sensitivity study, a quadratic mesh was defined for almost the entire model (Figure 5.1-a and -b) with a global size equal to $h/8$ (where h is the width of the leg), except in the region of the connections, where a circumferential mesh was established around the holes (Figure 5.1-c). These divisions led to adequate precision without affecting the computational efficiency.
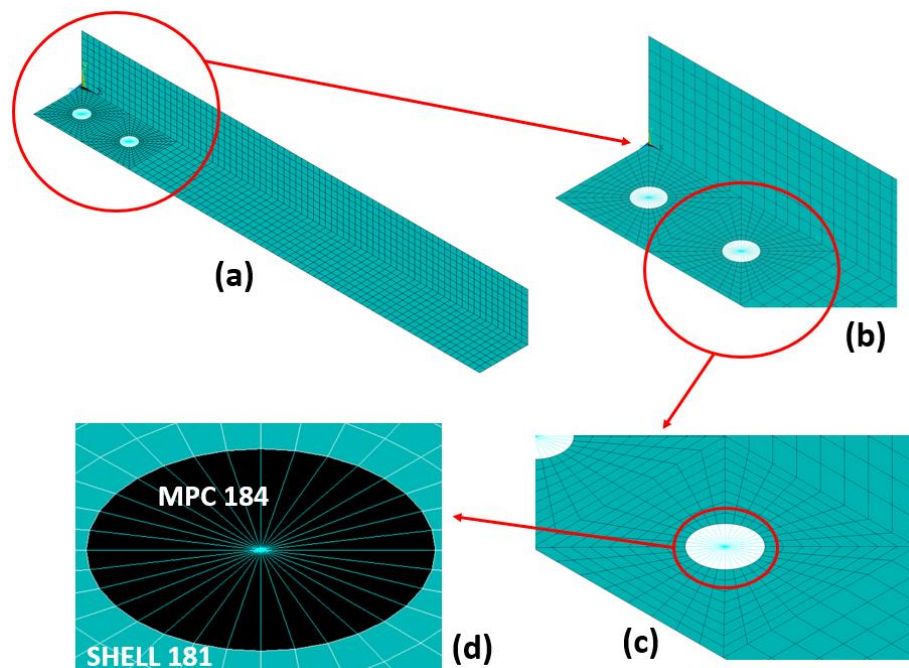
Figure 5.1 – Finite element mesh adopted in the numerical model.

The bolts were not explicitly modeled and holes with diameters equal to $0.30h$ were created to represent the connections. All the nodes of the circumference of the holes were coupled to their central node by using MPC184 (Multipoint Constraint Element) rigid elements (Figure 5.1-d), which allowed for the compatibility of forces and displacements. The restrictions to simulate the fork boundary condition, as well as the application of the load, were applied at the central nodes, see Figure 5.2-a and -b and Table 5.1. In this table, Uy and Uz are the degrees of freedom relative to translation in the y- and z-directions (see Figure 5.2), and ROTx is the degree of freedom relative to rotation about the x-axis (see Figure 5.2). Furthermore, to optimize the time spent on computational processing, symmetry boundary conditions were used for all models analyzed, in which only half of the original length of the angle was modeled (Figure 5.2-c). No difference was found when comparing the analyzes performed with the actual length of the members.
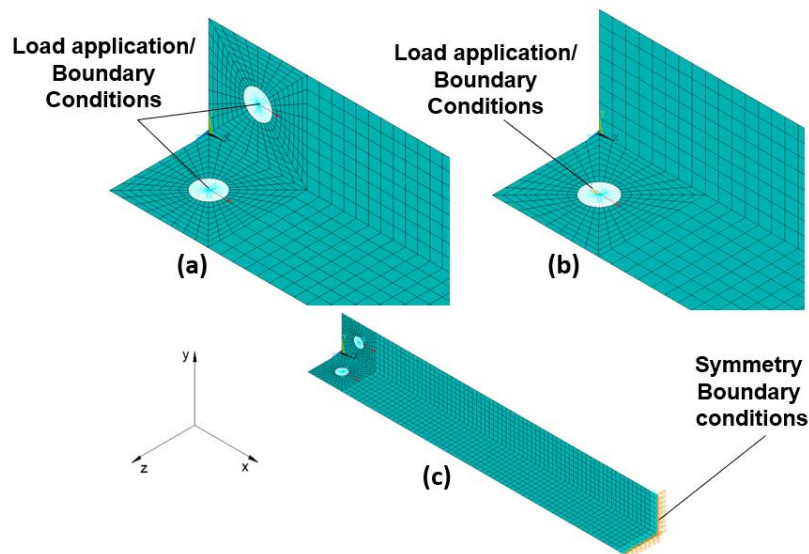
Figure 5.2 – Boundary conditions and load application.

Table 5.1 – Restrictions adopted in the central nodes of the holes.

Loading type	Degrees of freedom restricted
concentric	Uy, Uz
eccentric	Uy, Uz, ROTx

The elastic-perfectly plastic model described in Annex C of EN 1993-1-5 was assumed as the constitutive law to reproduce the behavior of the steel material. The yield plateau was applied without any slope and the steel properties were represented by a bilinear stress-strain curve without strain hardening, as exhibited in Figure 5.3.
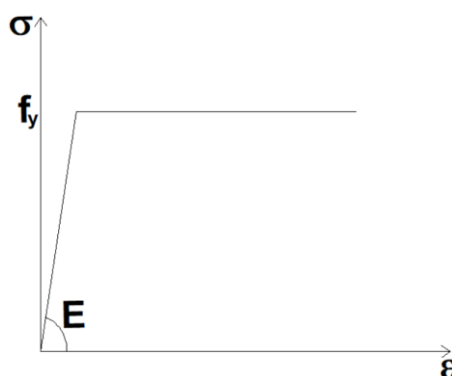
Figure 5.3 – Elastic-perfectly plastic model implemented in the numerical simulations.

Geometrically and materially non-linear analyses with imperfections (GMNIA) were executed to obtain the ultimate load of the models by using the arc-length method. Initial geometric imperfections were introduced with the shape corresponding to the first buckling mode obtained from a previous linear buckling analysis (LBA). For the validation of the numerical model, the amplitude of the imperfections followed the measurements from Kettler et al. (2019) and the ANGELHY project, which is specified hereafter, and was defined as equal to $L/1,000$ to conduct the parametric analysis, following (EN 1993-1-1). The residual stresses were implemented following the linear three-point residual stress model shown in Figure 5.4, the same model adopted in the numerical models of the ANGELHY project. This model is considered suitable enough for small and large angle sections according to Behzadi-Sofiani et al. (2022a), Zhang and Jaspart (2013), and Moze et al. (2014). A fixed value of 70 MPa is assumed for the amplitude of the residual stresses (see Figure 5.4).
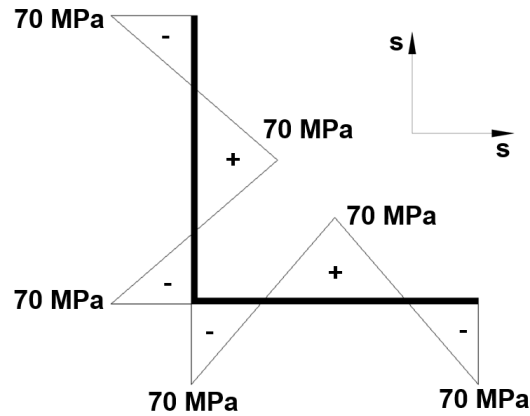
Figure 5.4 – Residual stress model adopted in the numerical model.

The residual stresses were simulated as initial longitudinal stresses (Figure 5.5), in which discrete values were obtained from the function σ_0, for each node of the member, according to Equation (5.1):

$$\sigma_0 = \begin{cases} \left(\frac{1.20s}{h} - 0.30\right) f_y, & \text{for } 0 \leq s \leq \frac{h}{2} \\ \left(-\frac{1.20s}{h} + 0.90\right) f_y, & \text{for } \frac{h}{2} < s \leq h \end{cases} \tag{5.1}$$

where s is a coordinate, as shown in Figure 5.4.
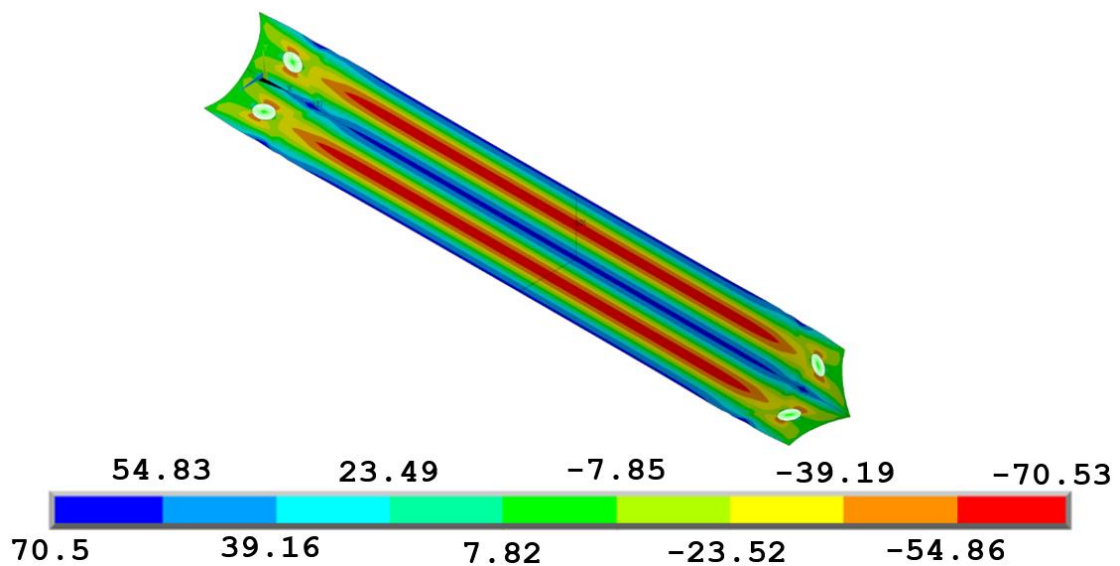
Figure 5.5 – Residual stress implemented in the numerical simulations (in MPa).

The implementation of the residual stresses is in agreement with the methods used in previous studies for the same type of problem and cross-section (Chou et al., 2023).

5.2.2 Validation

The numerical model was validated with the experimental tests performed in the ANGELHY project and by Kettler et al. (2019a). Additionally, the boundary conditions described in the previous section were shown to effectively correspond to pinned, fixed or partially restrained rotational boundary conditions.

The ANGELHY tests comprised concentric and eccentric compressed angles with pinned boundary conditions. The Kettler et al. (2019a) tests contemplated members in eccentric compression connected by one and two bolts.

The numerical simulations strictly reproduced the dimensions, material properties, and amplitude of imperfections. The boundary conditions described in the test reports were also carefully replicated.

5.2.2.1 ANGELHY Project

In Table 5.2 and Figure 5.6, the specifications of the specimens tested in the ANGELHY project are given. As observed, the values of the amplitude of the initial geometric imperfections were given by the authors and implemented in the numerical model. However, as there was no measurement of residual stresses, the material imperfections were simulated according to Figure 5.4.

Table 5.2 – ANGELHY project parameters used in the numerical model validation.

Specimen	Section	L(mm)	$\overline{\lambda}_v$	f_y (MPa)	E (MPa)	Imperfection (mm)*	g (mm)	e_v (mm)**	Loading type
Sp11	L 150x18	2,607	1.31	417.2	197,317	0.4	70.5	0	concentric
Sp13		3,107	1.56	425.8	203,155	1.3	70.5	0	
Sp15		3,607	1.81	425.8	203,155	2.4	70.5	0	
Sp12		2,607	1.31	425.8	203,155	1.2	70.5	48.71	eccentric
Sp14		3,107	1.56	425.8	203,155	0.8	70.5	48.72	
Sp16		3,607	1.81	425.8	203,155	3.0	70.5	48.7	
Sp21	L 200x16	3,107	1.21	487.6	208,947	1.6	96	0	concentric
Sp23		3,607	1.41	487.6	208,947	1.7	96	0	
Sp25		4,107	1.60	487.6	208,947	1.5	96	0	
Sp22		3,107	1.23	487.6	208,947	2.7	96	66.6	eccentric
Sp24		3,607	1.41	472.6	203,797	2.8	96	66.65	
Sp26		4,107	1.62	487.6	208,947	1.8	96	66.63	

*Values measured at mid-span in the strong axis direction.
**In-plane load eccentricity.
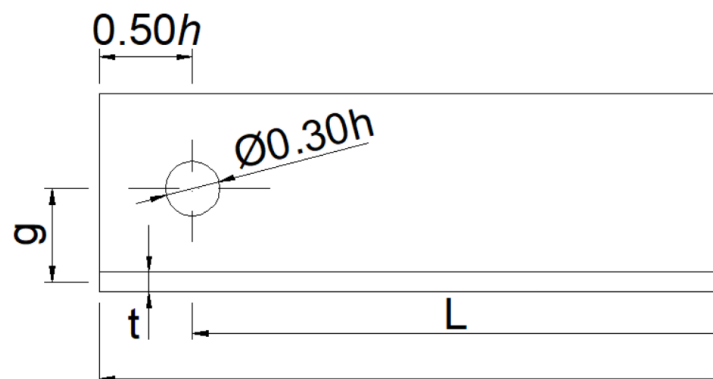
Figure 5.6 – Layout of the specimen of the ANGELHY project.

The comparison between the results from the experimental tests and the numerical model can be observed in Table 5.3. Although the numerical results showed good agreement with the

experimental ones, some results slightly deviated from the tests (6% differences), as in the case of Sp13, Sp23, and Sp26. This difference can be attributed to the residual stresses, which could not be exactly implemented according to the reality, since no measurements were done.

Table 5.3 – Comparison between ANGELHY project experimental tests and numerical model results.

Specimen	$N_{R,exp.}$ (kN)	$N_{R,num.}$ (kN)	$N_{R,num.}/N_{R,exp.}$
Sp11	1,010.6	1,005.6	1.00
Sp13	723.2	767.9	1.06
Sp15	563.9	589.1	1.04
Sp12	767.3	764.9	1.00
Sp14	628.3	624.2	0.99
Sp16	519.8	522.2	1.00
Sp21	1,661.5	1,642.6	0.99
Sp23	1,228.0	1,299.7	1.06
Sp25	1,048.1	1,034.8	0.99
Sp22	1,341.4	1,307.4	0.98
Sp24	1,092.3	1,080.3	0.99
Sp26	953.6	901.24	0.94
		Average	**1.00**
		C.O.V (%)	**3.5**

In Figure 5.7 and Figure 5.8, the comparison between the experimental and numerical load versus displacement curves are exhibited for the Sp15 (concentric compression) and Sp16 (eccentric compression, respectively. As observed, there is good agreement between numerical and experimental results, in terms of rigidity and ultimate capacity. The results from the other analyzed models presented similar accuracy, showing that the numerical model is appropriate

to predict the resistance capacity of angles under concentric and eccentric compression. Furthermore, the numerical model could also reproduce the same failure modes depicted in the experimental tests of the ANGELHY project. Minor-axis flexural buckling was observed for angles under concentric compression (see Figure 5.9-a) and torsional-flexural buckling for the ones under eccentric compression (see Figure 5.9-b).
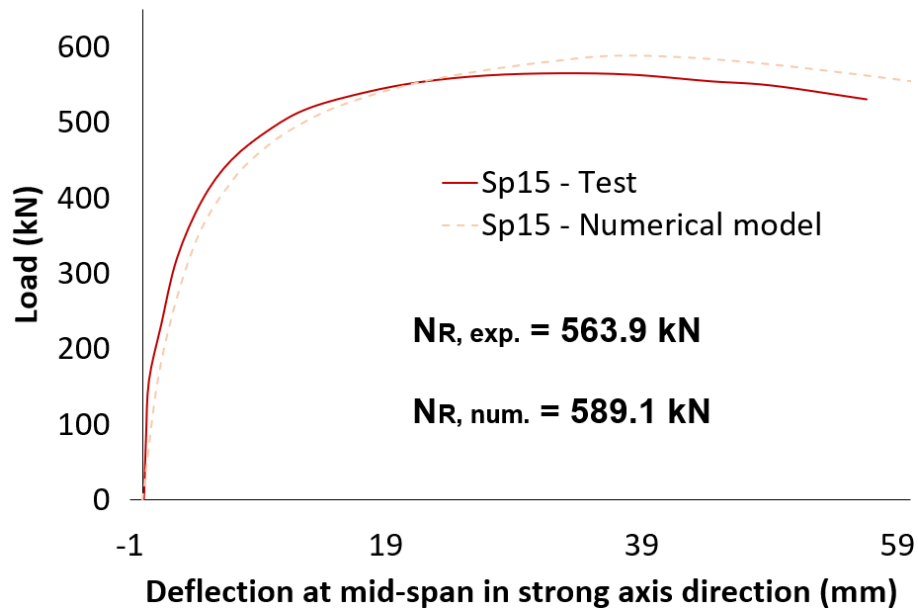
Figure 5.7 – Comparison between test and numerical model results – concentric compression (deflection at mid-span).
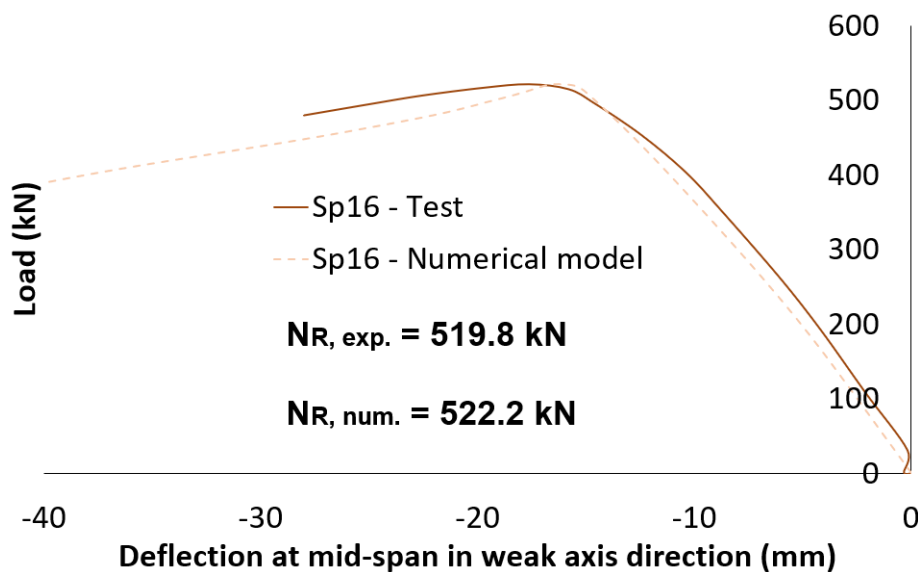
Figure 5.8 – Comparison between test and numerical model results – eccentric compression (deflection at mid-span).
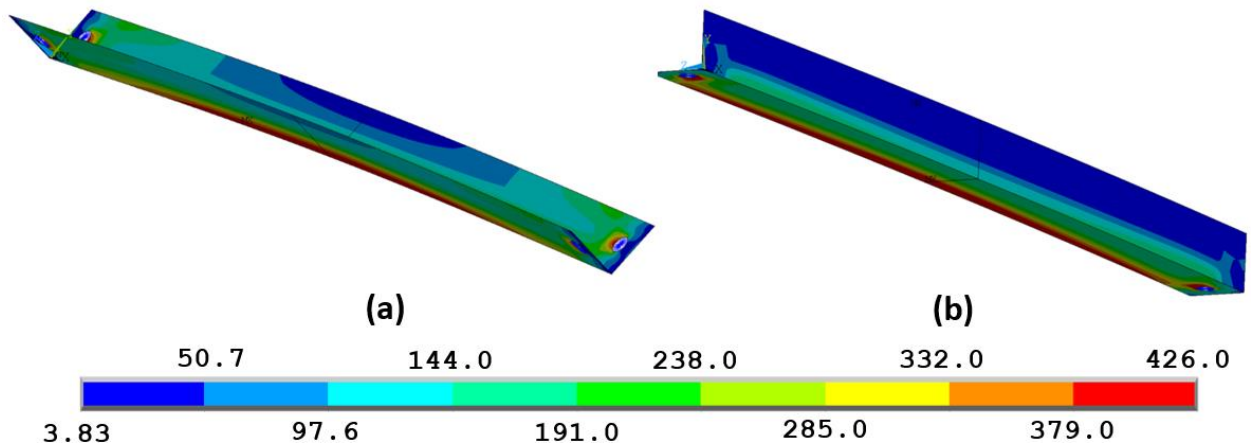
Figure 5.9 – von Mises stress distribution (in MPa) relative to the deformed shape of the angles in (a) concentric – Sp15 – and (b) eccentric – Sp16 - compression.

5.2.2.2 Kettler et al. (2019a)

The numerical model was also verified with the results from the experimental program executed by Kettler et al. (2019a). The specifications of geometry, material properties, and amplitude of imperfections are given in Table 5.4. There was no experimental measurement of residual stresses by Kettler et al. (2019a), so they were again simulated according to Figure 5.4. In Figure 5.10 and Figure 5.11, the experimental and numerical curves of load versus displacement are exhibited for specimens C1 (with one bolt) and A2 (with two bolts), respectively. There was good agreement between the experimental and numerical results for both the rigidity and ultimate capacity of the members. In Table 5.4, the numerical and experimental results of ultimate capacity are presented for all the specimens covered by Kettler et al. (2019a) and reasonable correlation can be again observed.

The average value between the capacities obtained from the numerical model and the experimental tests ($N_{R,num.}/N_{R,exp.}$) was equal to 1.00 (C.O.V of 3.5%), considering the results from the ANGELHY project, whilst it was equal to 0.96 (C.O.V of 1.3%), considering the results from Kettler et al. (2019a).

Table 5.4 – Experimental parameters from Kettler et al (2019a) used in the numerical model validation and comparison between experimental and numerical results.

Specimen	Section	Number of bolts	L (mm)	$\overline{\lambda_v}$	f_y (MPa)	E (MPa)	Imperf. (mm)*	$N_{R,exp.}$ (kN)	$N_{R,num.}$ (kN)	$\dfrac{N_{R,num.}}{N_{R,exp.}}$
B4	L 80x8	one	1,140	0.98	326.68	199,000	0.35	162.9	155.8	0.96
B5			1,820	1.55			1.15	132.1	127.2	0.96
C1			3,170	2.64	333.9	209,000	1.1	98.4	93.5	0.95
A1		two	1,140	0.89	289.9	212,000	0.4	261.1	248.9	0.95
A2			1,820	1.4			1.45	238.8	230.1	0.96
A3			2,630	2			1.6	215.4	214.2	0.99
E1	L 120x12		1,850	1.01	299.3	192,000	1.1	488.4	475.2	0.97
E2			3,170	1.72			2.85	357.2	346.2	0.97
E3			4,200	2.27			2.65	267.1	258.8	0.97
									Average	0.96
									C.O.V (%)	1.3

*Values measured at mid-span in the weak axis direction.
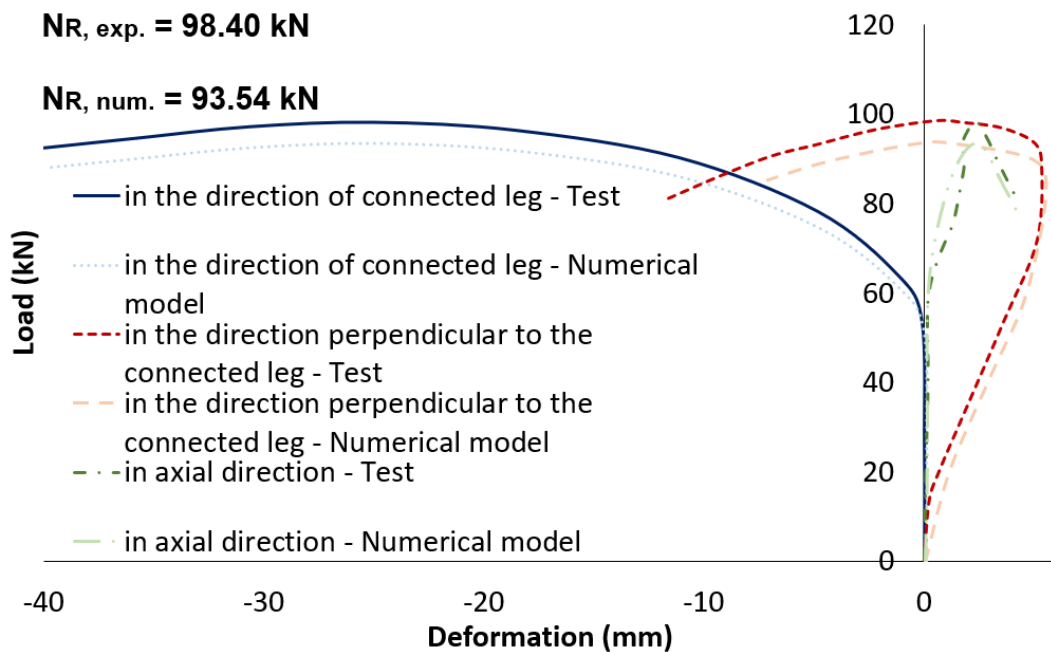
Figure 5.10 – Comparison between experimental and numerical results – specimen C1 with one bolt (deflection at mid-span).
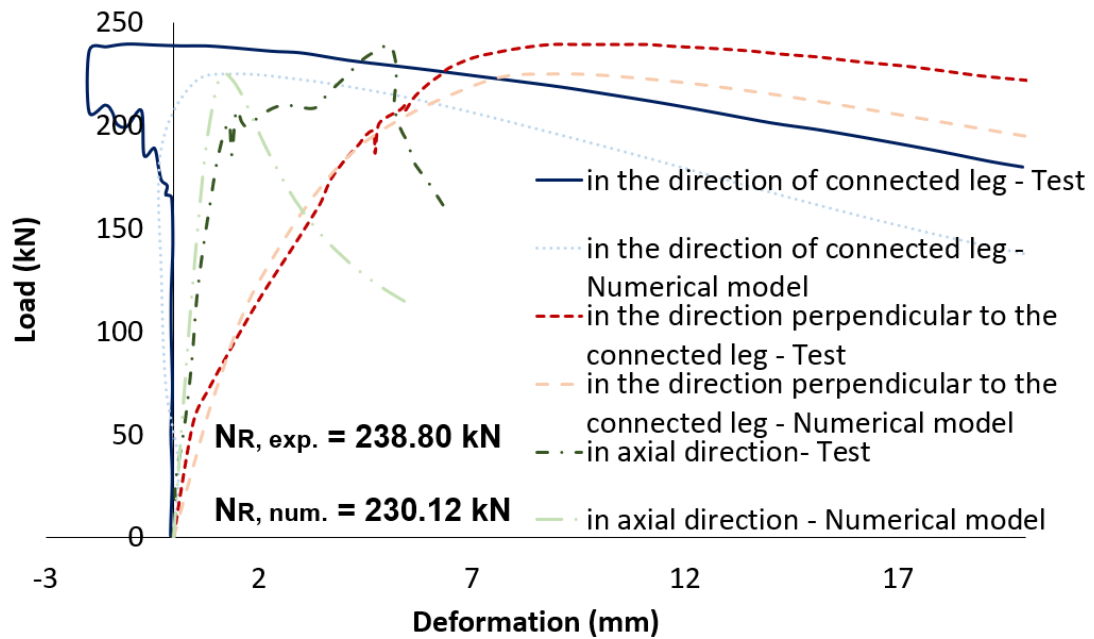
Figure 5.11 – Comparison between experimental and numerical results – specimen A2 with two bolts (deflection at mid-span).

5.2.2.3 Distinctive Boundary Conditions

The boundary conditions of the numerical models in the parametric study were implemented with the bolt holes as described in Subsection 5.2.1. It is commonly assumed that compressed angles connected through one bolt row behave like pinned members. In fact, Kettler et al. (2017), (2019a), (2021) showed that angles compressed eccentrically through one bolt tend to behave like pinned members. This is also evidenced by the results of the numerical model validation against the fully pinned experimental tests from the ANGELHY project (see Figure 5.7, Figure 5.8, and Table 5.3). This is clearly illustrated in Figure 5.12-a and -b which depicts the numerically calculated buckling modes of angles connected by one bolt that accurately match pinned members.

In the case of angles connected with two or more bolts, it is important to assess what is the degree of rotational restraint that corresponds to the numerical models. Hence, considering the standard boundary conditions of $d_0 = 0.3h$ and $p_1 = 6d_0$ in the parametric study, it was shown that the compressed angles behave like fixed members, as depicted in Figure 5.12-c and -d, with a system length corresponding to the distance between the center of the innermost holes at each end. The mean value and C.O.V of the ratio between the buckling load obtained numerically

(LBA) and that calculated by the Vlasov (1962) formulations (taking into account fixed boundary conditions as reference) were obtained for a subset of 108 numerical models, being equal to 0.96 and 4.41%, respectively, for the concentric compression case, and equal to 1.07 and 8.23%, respectively, for the eccentric compression case.

Finally, to cover cases with partially retrained boundary conditions, a model with a rotational spring at each end, equivalent to about 80% of the elastic critical buckling load of a fixed member, was implemented. It was shown that these boundary conditions are equivalent to the appropriate spacings of two bolts, with a rotational out-of-plane spring (obtained according to Kettler et al., 2021 – Equation (2.111)) applied in the innermost hole of the numerical models. Figure 5.12-e illustrates the corresponding buckling mode. Thus, in the parametric study, a set of cases with rotational springs was also considered.
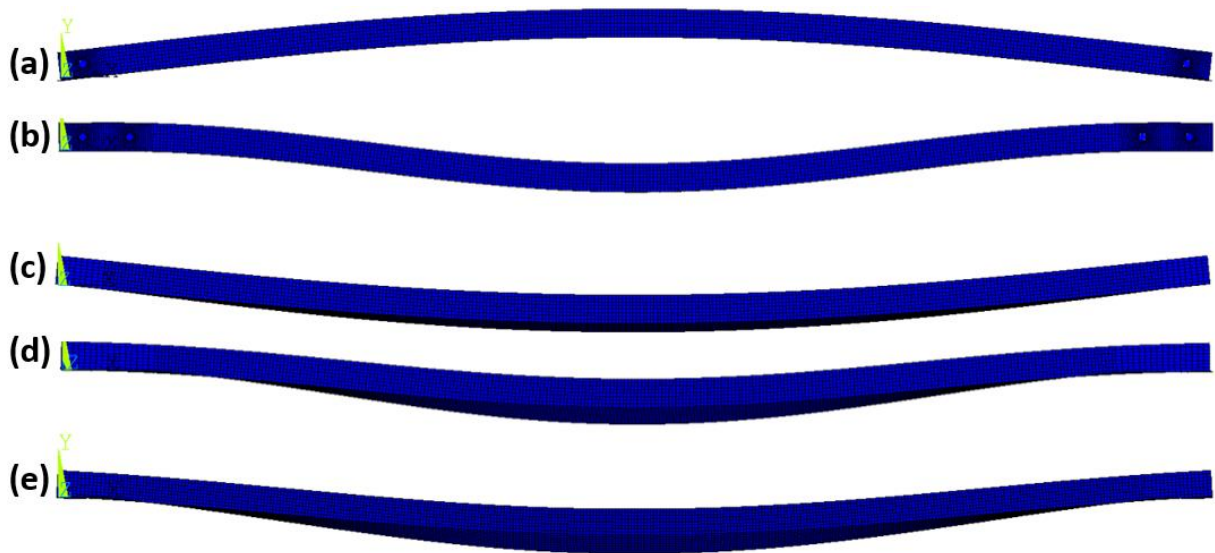
Figure 5.12 – Typical buckling modes of angles under concentric compression with (a) one and (b) two bolts, under eccentric compression with (c) one and (d) two bolts, considering $d_0 = 0.3h$ and $p_1 = 6d_0$, and (e) under eccentric compression and subjected to partially retrained boundary conditions.

5.3 Assessment of Design Procedures

In the following subsections, the ultimate load capacity of angle members in compression obtained by the numerical model ($N_{R,num.}$) are compared to the analytical values ($N_{R,anal.}$) obtained for each design procedure presented in Table 2.9 (Subsection 2.5.3 - Chapter 2). The

results are displayed in terms of r_N for the different slenderness $\bar{\lambda}_v$ covered in this work, where r_N is the ratio given by:

$$r_N = N_{R,num.}/N_{R,anal.} \tag{5.2}$$

and assessed by analyzing the mean values and the coefficient of variation (C.O.V) of r_N for appropriate sub-sets.

The study covers concentric compression and eccentric compression about the major axis of the equal leg angle cross-section. Additionally, pinned and fixed boundary conditions are considered, as well as a smaller sample of partially restrained angles. Firstly, the parametric study is defined in a comprehensive way, followed by the individual assessment of the various design proposals and a discussion of the observed physical behaviour.

5.3.1 Parametric Study

Table 5.5 shows the adopted parametric study that comprised different cross-sections; relative slenderness about the weak axis ($\bar{\lambda}_v$) ranging from 0.5 to 3.0; and pinned, fixed, and partially restrained boundary conditions. Steel grades S235, S355, and S460 were adopted in the numerical models with a modulus of elasticity (E) equal to 210,000 MPa. The main aim was to cover the most used sections in steel structures (mainly in transmission towers) with a comprehensive range of variables, totaling 1,188 numerical models generated, largely expanding the database of numerical studies existing in the literature (Kettler et al., 2017; ANGELHY project).

Concentrically compressed angles were materialized considering that both legs were bolted to the support, with the load application points coinciding with the bolt/hole axes, as shown in Figure 5.13-a. In the case of eccentric compression, the angles are only connected in one leg, as shown in Figure 5.13-b. In the numerical simulations, the holes to reproduce the connections were positioned along the weak axis, as shown in Figure 5.13, so in eccentric compression, there is only eccentricity around the strong axis (that is, $e_u = 0$).

The boundary conditions were chosen to reflect the range of practical situations, as follows:

- Pinned angle members (one bolt in each leg for concentric compression and one bolt in one leg only for eccentric compression);

- Fixed angle members (two or more bolts in each leg for concentric compression and two or more bolts in one leg only for eccentric compression);
- Partially restrained angle members, materialized by one bolt hole at each end combined with a rotational spring. This subset comprises only sections with $h > 80$ mm and S355 steel grade. The stiffness of the rotational spring is equivalent to about 80% of the elastic critical buckling load of a fixed member.

For all numerical models it is adopted: $e_1 = 3d_0$.

Table 5.5 – Proposed parametric study.

Boundary conditions	$\bar{\lambda}_v$	Steel grade	Section	h/t	L/h	Loading type
pinned fixed partially restrained	0.5 1.0 1.5 2.0 2.5 3.0	S235 S355[*] S460	L 45 x 3 L 45 x 7 L 60 x 6 L 60 x 10 L 80 x 5 L 80 x 10 L 120 x 7[*] L 120 x 16[*] L 160 x 12[*] L 160 x 20[*] L 200 x 13[*] L 200 x 25[*] L 250 x 17[*] L 250 x 25[*] L 300 x 25[*]	5 to 17	6 to 112	concentric eccentric

*Subset for partially restrained boundary conditions.
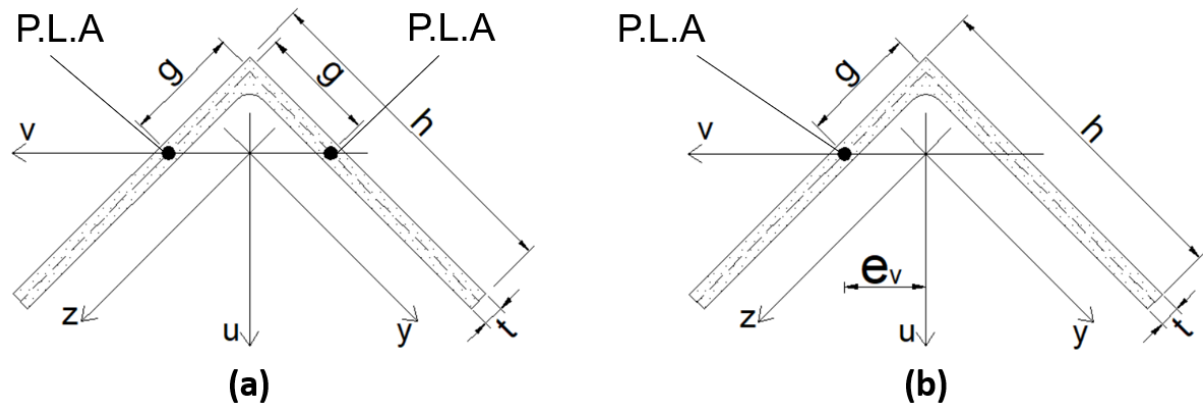
Figure 5.13 – Layout of the numerical models under (a) concentric and (b) eccentric compression. P.L.A = Point Load Application.

5.3.2 Concentric Compression (Pinned)

Figure 5.14 and Table 5.6 present the mean and C.O.V for the relevant design proposals (EN 1993-1-1, FprEN 1993-1-1, ANGELHY/prEN 1993-3, AISC and Behzadi-Sofiani et al., 2021), split according to steel grade and slenderness. Except for AISC, all proposals present design values that are lower than the "experimental" resistance. Globally, all proposals present increasing values of r_N as steel grade increases due to the favourable effect of the residual stresses. This is corrected in FprEN 1993-1-1 and ANGELHY/prEN 1993-3 for S460 by proposing the change of buckling curve *b* to *a*.

EN 1993-1-1 presents decreasing values of r_N as the normalized slenderness increases. Since compressed angles with low slenderness (0.5) are mainly affected by yielding and the code uses the torsional-flexural elastic buckling load to calculate the normalized slenderness ratio, this is the main reason for the conservative estimates of the resistance. EN 1993-1-1 presents an additional increase of r_N with steel grade because most angles made by higher grades are class 4 and the code considers local buckling and flexural-torsional buckling as two coincident modes of instability for angles, thereby negatively impacting the buckling resistance. FprEN 1993-1-1 leads to similar results except for S460 because it specifies curve a for this steel grade.

AISC presents results that are generally in good agreement with the numerical results except for the intermediate slenderness range which is clearly unconservative. This is explained because AISC considers the torsional-flexural elastic buckling load to compute the normalized

slenderness ratio of such elements, which have the design governed by plasticity rather than buckling.

The ANGELHY/prEN 1993-3 presents a very good agreement and the lowest scatter when compared to the numerical results. This results from the following recommendations: (i) torsional-flexural buckling load is no longer considered to calculate the normalized slenderness ratio; (ii) new cross-section classification limits are proposed (see Table 2.6); and (iii) the interaction between local and global buckling modes (which is guaranteed by multiplying $\bar{\lambda}_\rho$ – see Equation (2.141) – by $\sqrt{\chi_{min}}$), was improved.

Finally, the Behzadi-Sofiani et al. (2021) proposal coincides with the EN 1993-1-1 approach for high values of relative slenderness ($\bar{\lambda}_v \geq 2.0$), i.e., for slenderness range where $N_{cr,\text{TF}}/N_{cr,v} > 1.0$. For $\bar{\lambda}_v = 0.5$, the method proposed by Behzadi-Sofiani et al. (2021) is more consistent than Eurocode 3 is, since this code does not consider flexural/torsional-flexural buckling interactions in its design procedure. However, the r_N values obtained by the Behzadi-Sofiani et al. (2021) procedure are always higher than the values of ANGELHY/prEN 1993-3, because the latter adopts only flexural buckling in its design, making the method less conservative. It should also be noted that although the Behzadi-Sofiani et al. (2021) method was validated only for fixed-ended angle sections, it presented reasonable results for pinned angle members. The method presents a reasonable agreement and scatter.

Figure 5.14 – $(r_N)_{mean}$ and Standard deviation for pinned angle members compressed concentrically - (a) S235, (b) S355, and (c) S460 steel grades.

Table 5.6 – Mean values and C.O.V of r_N for all design procedures considering the entire range of slenderness – pinned angle members compressed concentrically.

Loading type	Prescription	Steel grade							
		S235		S355		S460		All	
		$(r_N)_{mean}$	C.O.V (%)	$(r_N)_{mean}$	C.O.V (%)	$(r_N)_{mean}$	C.O.V (%)	$(r_N)_{mean}$	C.O.V (%)
Concentric (pinned)	AISC 360	0.97	5.46	**1.02**	4.44	1.04	3.67	1.01	5.29
	EN 1993-1-1	1.03	4.92	1.12	7.89	1.19	9.96	1.12	9.75
	FprEN 1993-1-1	1.03	4.92	1.12	7.89	1.11	8.46	1.09	7.87
	ANGELHY	**1.01**	**1.08**	1.05	**2.87**	**1.01**	**1.14**	1.02	2.71
	Behzadi-Sofiani et al. (2021)	1.02	1.16	1.10	5.47	1.15	6.52	1.09	7.13

5.3.3 Concentric Compression (Fixed)

Figure 5.15 and Table 5.7 present the mean and C.O.V for the relevant design proposals (EN 1993-1-1, FprEN 1993-1-1, ANGELHY/prEN 1993-3, AISC and Behzadi-Sofiani et al., 2021), split according to steel grade and slenderness. For fixed-angle members, greater rigidity in the connections is observed, leading to increased resistance, and allowing the use of clamped boundary conditions in the calculation of the elastic critical load N_{cr}. The results are similar to the previous case of pinned members but with slightly smaller r_N ratios for all proposals. Although AISC presents the best overall ratio (1.00), it exhibits significant unsafe results for the intermediate slenderness range. ANGELHY/prEN 1993-3 presents the best agreement and lowest scatter when compared to the numerical results but with a mean r_N ratio lower than 1 for S460 (0.98). The Behzadi-Sofiani et al. (2021) method presents values of $(r_N)_{mean}$ for fixed

angle members slightly better than for pinned members, as expected since this proposal was calibrated for fixed-ended members.
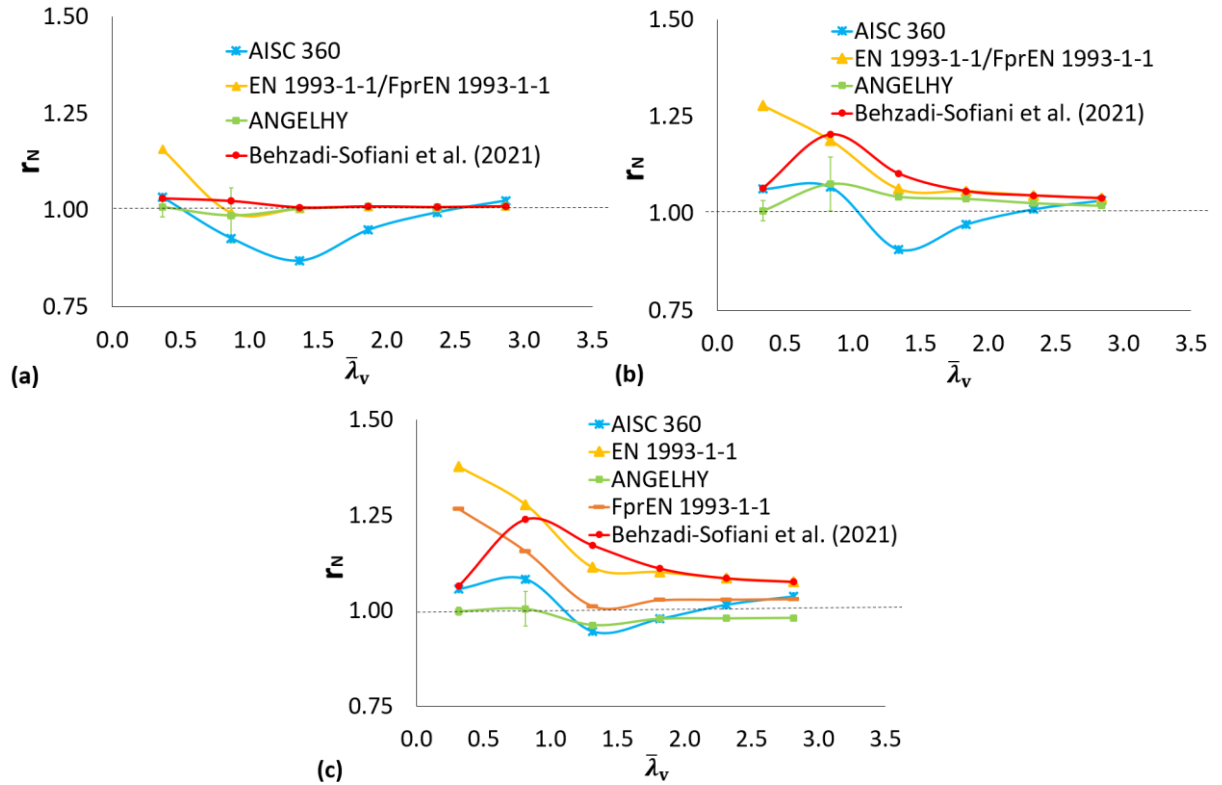
Figure 5.15 – $(r_N)_{mean}$ and Standard deviation for fixed angle members compressed concentrically - (a) S235, (b) S355, and (c) S460 steel grades.

Table 5.7 – Mean values and C.O.V of r_N for all design procedures considering the entire range of slenderness – fixed angle members compressed concentrically.

Loading type	Prescription	Steel grade							
		S235		S355		S460		All	
		$(r_N)_{mean}$	C.O.V (%)	$(r_N)_{mean}$	C.O.V (%)	$(r_N)_{mean}$	C.O.V (%)	$(r_N)_{mean}$	C.O.V (%)
Concentric (fixed)	AISC 360	0.97	6.56	**1.01**	6.11	**1.02**	4.94	1.00	6.03
	EN 1993-1-1	1.03	6.07	1.11	8.82	1.17	10.71	1.10	10.00
	FprEN 1993-1-1	1.03	6.07	1.11	8.82	1.09	9.46	1.08	8.49
	ANGELHY	**1.00**	**0.91**	1.04	**2.29**	0.98	**1.56**	1.01	2.66
	Behzadi-Sofiani et al. (2021)	1.01	0.98	1.09	5.70	1.12	6.03	1.08	6.40

5.3.4 Eccentric Compression (Pinned)

Figure 5.16 and Table 5.8 present the mean and C.O.V for the relevant design proposals (EN 1993-3-1, ANGELHY/prEN 1993-3, Kettler et al. (2021) and ANGELHY_MOD), split according to steel grade and slenderness. Globally, all proposals present a significant variation of the mean value of r_N with slenderness range, whereas the variation with steel grade is not significant. The C.O.V is significantly higher than for the previous case of concentric compression for all cases.

In EN 1993-3-1, minor-axis flexural buckling is determinant for the resistance of the members with $\bar{\lambda}_v \geq 0.9$, while for $\bar{\lambda}_v$ smaller than 0.9, the flexural buckling about the axis parallel to the connected leg is more decisive. In this design method, the code presented unsafe values for members with $\bar{\lambda}_v < 1.0$, although in practice bracing members are not designed with this slenderness. Adopting buckling curve a for S460 leads to unsafe results.

ANGELHY/prEN 1993-3 presents a similar performance to EN 1993-3-1 but with better performance for the low slenderness range and more conservative results for the high slenderness range. The values of $N_{R,anal.}$ considered in the analysis are the smallest values considering Equations (2.157) and (2.158). Thus, the ultimate capacity of eccentric compression angles can be given by Equation (5.3):

$$N_{R,anal.,ANGELHY} =$$

$$min\left\{ \frac{f - \sqrt{f^2 - 4N_{cr,u}M_{u,Rk}{}^2\chi_{LT}{}^2\chi_u N_{Rk}}}{\chi_{LT}M_{u,Rk}} ; \frac{1}{\left(\frac{1}{\chi_v N_{Rk}} + \frac{k_{vu}e_v}{\chi_{LT}M_{u,Rk}}\right)} \right\} \qquad (5.3)$$

with $f = -\left(\chi_{LT}M_{u,Rk}N_{cr,u} + \chi_u N_{Rk}N_{cr,u}e_v + \chi_u N_{Rk}\chi_{LT}M_{u,Rk}\right)$.

The analytical resistance using the recommendations of Kettler et al. (2021) for eccentrically loaded compression angles was obtained from Equation (2.114). From this expression, second- and third-degree equations were obtained, in which the smallest root is the value of $N_{R,anal.}$. The results show that the method leads to values of r_N excessively insecure for short-intermediate slenderness, because Equation (2.114) is not able enough to predict the effects of torsional-flexural buckling and severe yielding is typical in members in this slenderness range. On the other hand, the proposal of Kettler et al. (2021) presents excellent agreement with the numerical results for $\bar{\lambda}_v \geq 1.5$.

ANGELHY_MOD (see Sub-section 2.5.3) presents a congruent performance with ANGELHY/prEN 1993-3 but with higher values for r_N. This occurs mainly because buckling curve b is used.
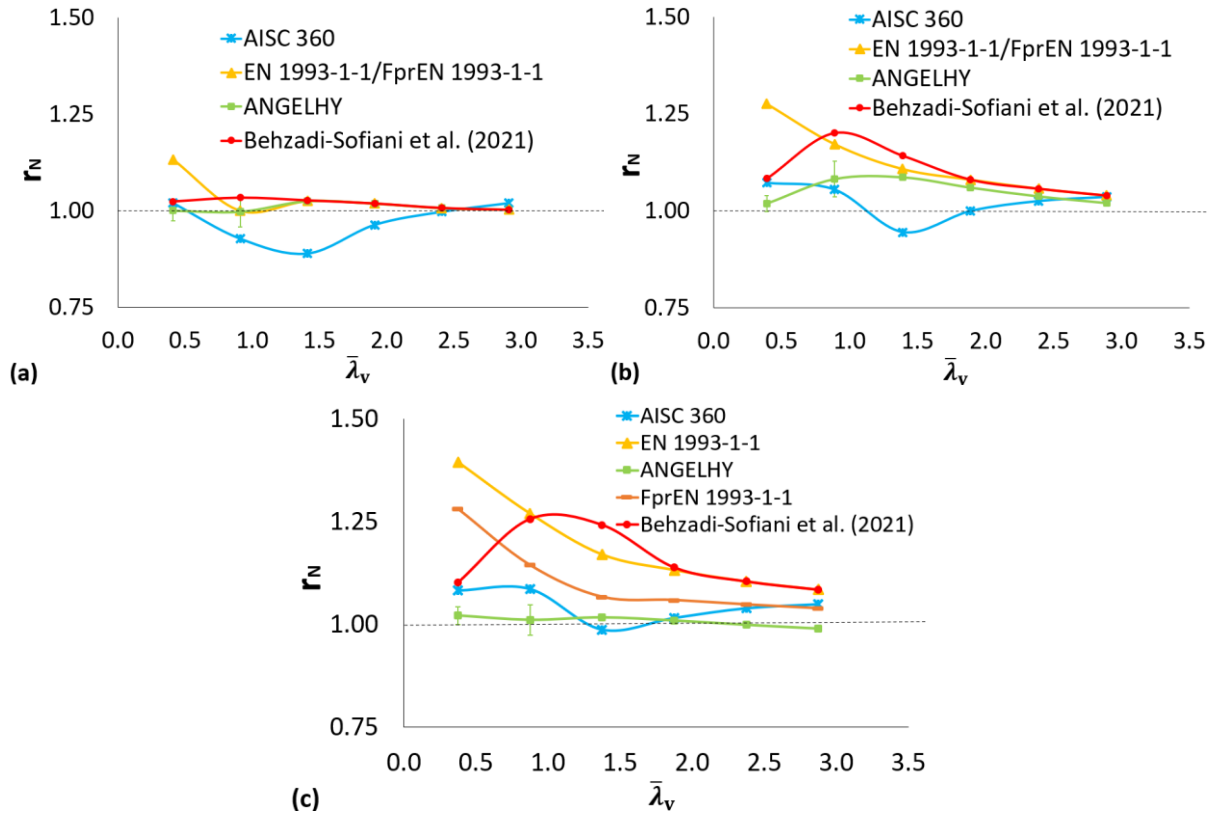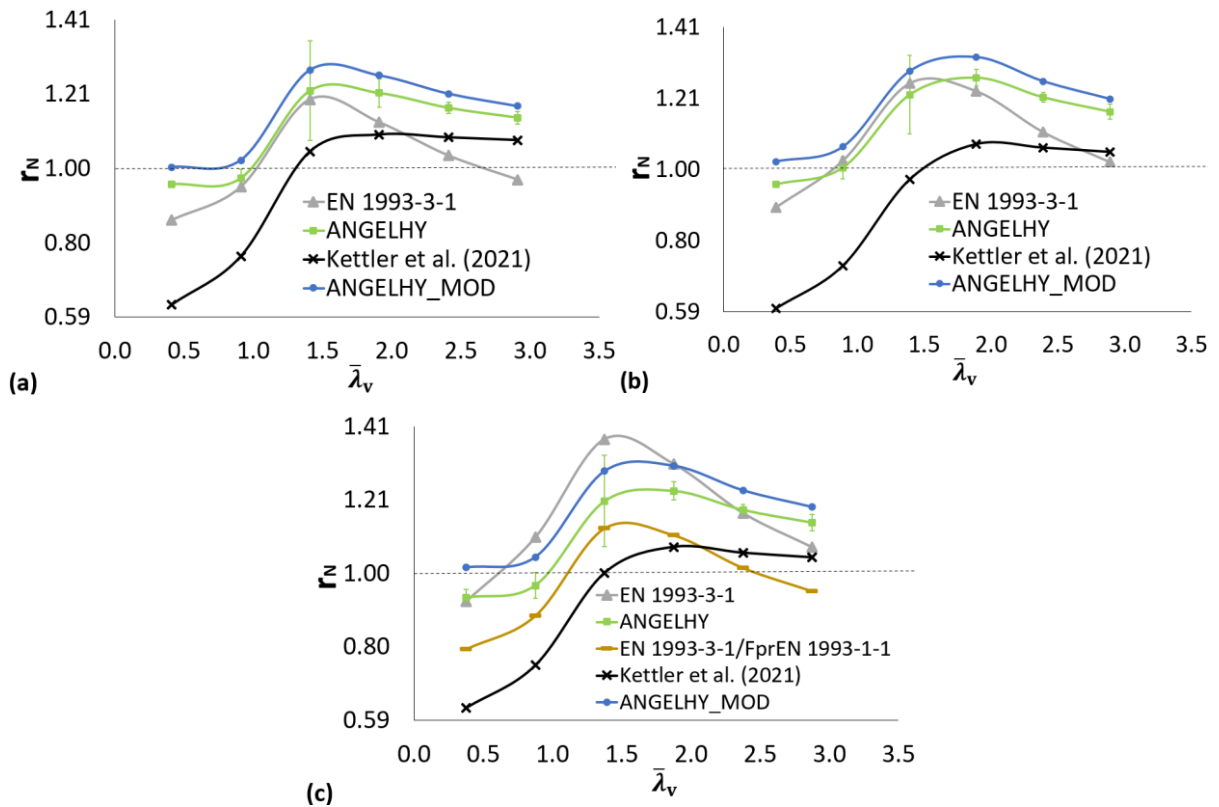
Figure 5.16 – $(r_N)_{mean}$ and Standard deviation for pinned angle members compressed eccentrically - (a) S235, (b) S355, and (c) S460 steel grades.

Table 5.8 – Mean values and C.O.V of r_N for all design procedures considering the entire range of slenderness – pinned angle members compressed eccentrically.

Loading type	Prescription	Steel grade							
		S235		S355		S460		All	
		$(r_N)_{mean}$	C.O.V (%)	$(r_N)_{mean}$	C.O.V (%)	$(r_N)_{mean}$	C.O.V (%)	$(r_N)_{mean}$	C.O.V (%)
Eccentric (pinned)	EN 1993-3-1	1.02	12.00	1.09	12.51	1.16	14.17	1.09	13.33
	ANGELHY	1.11	10.41	1.14	11.03	1.11	11.45	1.12	10.37
	ANGELHY_MOD	1.16	10.03	1.19	10.22	1.18	10.30	1.17	9.66
	Kettler et al. (2021)	0.95	21.53	0.91	22.16	0.92	20.67	0.93	20.22
	EN 1993-3-1/ FprEN 1993-1-1	1.02	12.00	1.09	12.47	0.98	13.38	1.03	12.68

5.3.5 Eccentric Compression (Fixed and Partially Restrained)

Figure 5.17 and Table 5.9 present the mean and C.O.V for the relevant design proposals (EN 1993-1-1, FprEN 1993-1-1, EN 1993-3-1, ANGELHY/prEN 1993-3, Kettler et al. (2021), AISC and ANGELHY_MOD), split according to steel grade and slenderness. EN 1993-1-1, FprEN 1993-1-1, EN 1993-3-1, and AISC exhibit a very poor agreement with the numerical results, with extremely safe-sided results ($r_N > 2$ and C.O.V $> 20\%$), with a very large variation with slenderness. The ANGELHY, Kettler et al. (2021) and ANGELHY_MOD methods exhibit reasonable results. The conclusions about the differences between ANGELHY, and ANGELHY_MOD proposals are similar to the previous case of pinned connection. Secondly, there is no significant difference when comparing the three steel grades.
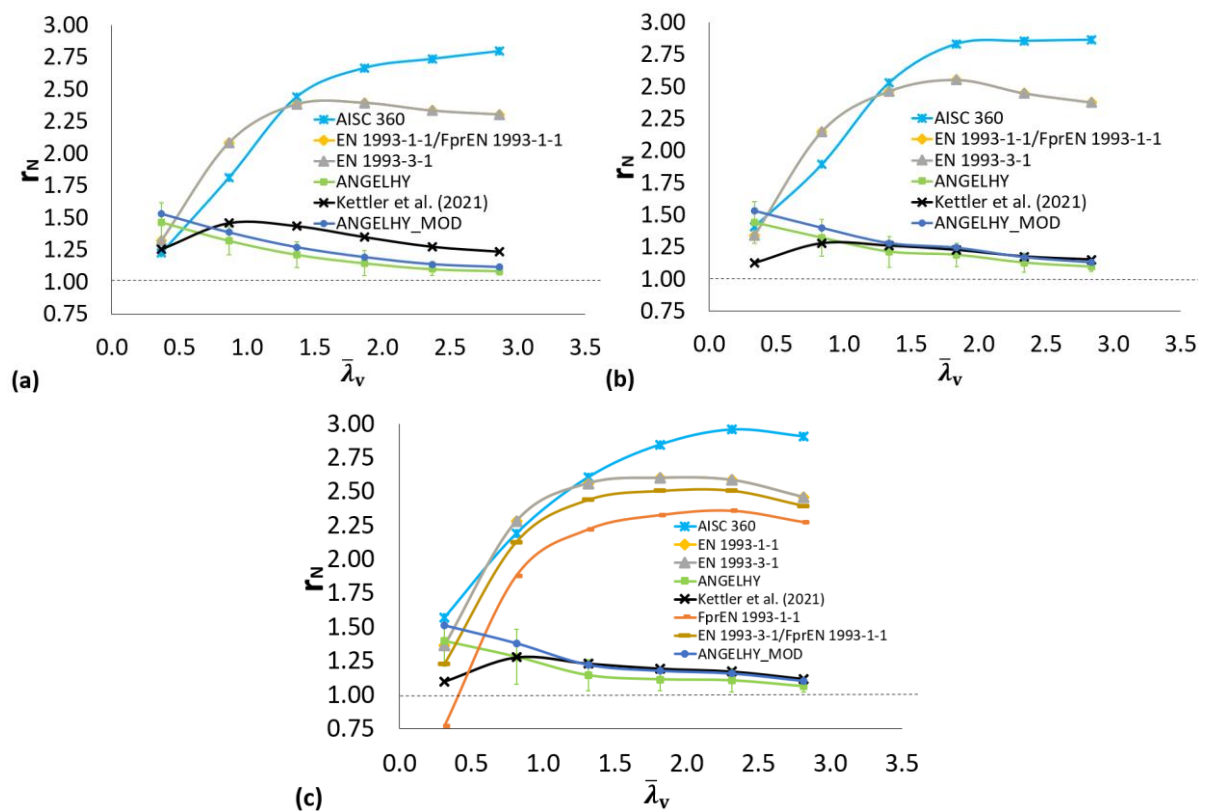
Figure 5.17 – $(r_N)_{mean}$ and Standard deviation for fixed and partially restrained angle members compressed eccentrically - (a) S235, (b) S355, and (c) S460 steel grades.

Table 5.9 – Mean values and C.O.V of r_N for all design procedures considering the entire range of slenderness – fixed and partially restrained angle members compressed eccentrically.

| Loading type | Prescription | Steel grade | | | | | | | |
| | | S235 | | S355 | | S460 | | All | |
		$(r_N)_{mean}$	C.O.V (%)	$(r_N)_{mean}$	C.O.V (%)	$(r_N)_{mean}$	C.O.V (%)	$(r_N)_{mean}$	C.O.V (%)
Eccentric (fixed and partially restrained)	AISC 360	2.28	27.63	2.40	25.48	2.51	21.60	2.40	23.70
	EN 1993-1-1	2.14	19.45	2.22	20.36	2.31	20.70	2.22	19.27
	FprEN 1993-1-1	2.14	19.45	2.22	20.36	2.02	30.37	2.11	22.90
	EN 1993-3-1	2.14	19.45	2.22	20.36	2.31	20.70	2.22	19.27
	EN 1993-3-1/ FprEN 1993-1-1	2.14	19.45	2.22	20.36	2.20	22.62	2.19	19.68
	ANGELHY	1.22	12.02	1.23	10.50	1.18	10.83	1.21	10.61
	ANGELHY_MOD	1.27	12.63	1.29	11.65	1.26	12.38	1.28	11.54
	Kettler et al. (2021)	1.33	7.12	1.24	5.83	1.18	5.75	1.25	7.92

5.3.6 Final Remarks about the Physical Behaviour of Compressed Angles

Given the assessment of the design procedures carried out in Subsections 5.3.2 to 5.3.5, this section is dedicated to the discussion of some aspects that can affect the behavior of an angle

section in compression and that, therefore, can explain problems found in the different methods analyzed in this work, serving as the basis for future improvements.

5.3.6.1 Low Slenderness Range

The deformed shape relative to the ultimate loads of members with small slenderness ratios shows that the failure of these members occurs predominantly due to the yielding of the cross-section, as expected. However, yielding occurs mostly in the connected leg and is determined by the boundary conditions at the member ends (see Figure 5.18), which is not considered by the design procedures analyzed in this work. Figure 5.18 shows that an effective area should be considered in the design of short-angle members.

As an elastic-perfectly-plastic material was used in the numerical simulations, the quad-linear material law that considers strain hardening was also used for one cross-section, showing no differences.

Finally, it is worth mentioning that situations where angle members with short lengths are subjected to high loads are rarely encountered in practice, which would explain the fact that the many codes do not strictly consider the behavior of these members in their prescriptions.
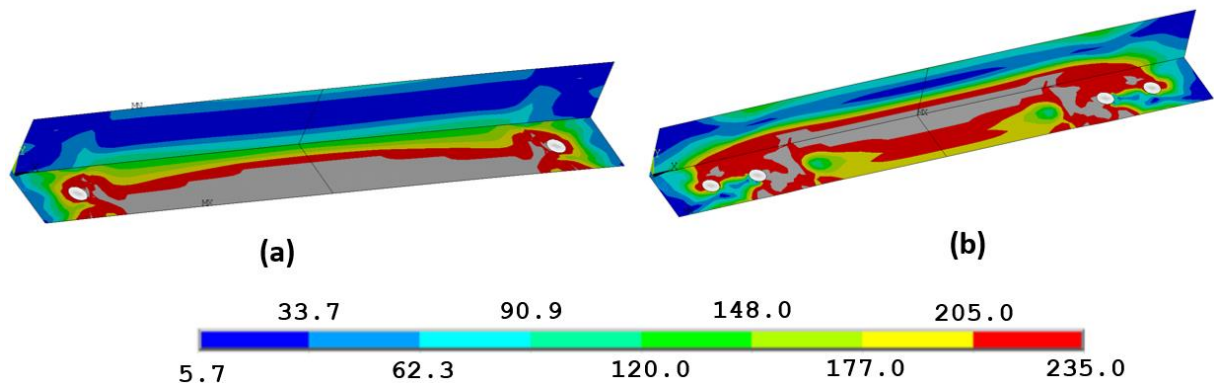
Figure 5.18 – von Mises stress distribution (in MPa) at ultimate compressive load Substep of the L 45 x 3 section (with $\bar{\lambda}_v = 0.5$) in eccentric compression, with (a) pinned and (b) fixed boundary conditions.

5.3.6.2 Influence of h/t Ratio

The most recent proposals for the design of angle members in concentric compression - ANGELHY project (Bezas et al., 2022) and Behzadi-Sofiani et al. (2021) - differ in the

considerations regarding the influence of the torsional-flexural buckling on the behaviour of the member.

Figure 5.19 shows the von Mises stress distribution and the deformed shape at the ultimate compressive load for an L 45 x t section (850 mm-member length) subject to concentric compression and with pinned boundary conditions at the ends, considering three cases: $h/t = 15$, $h/t = 45$ and $h/t = 75$. Note that for $h/t = 15$ flexural buckling about the minor axis predominates at failure, while for $h/t = 45$ and $h/t = 75$ torsional-flexural buckling is dominant. Hence, torsional effects occur mainly at shorty length members with high values of h/t ratio. It is noted that the parametric study of the ANGELHY project (Bezas et al., 2022) covers angles sections with h/t ratios lower than 15, while in the parametric study of Behzadi-Sofiani et al. (2021), h/t ratios varied between 5 to 100.
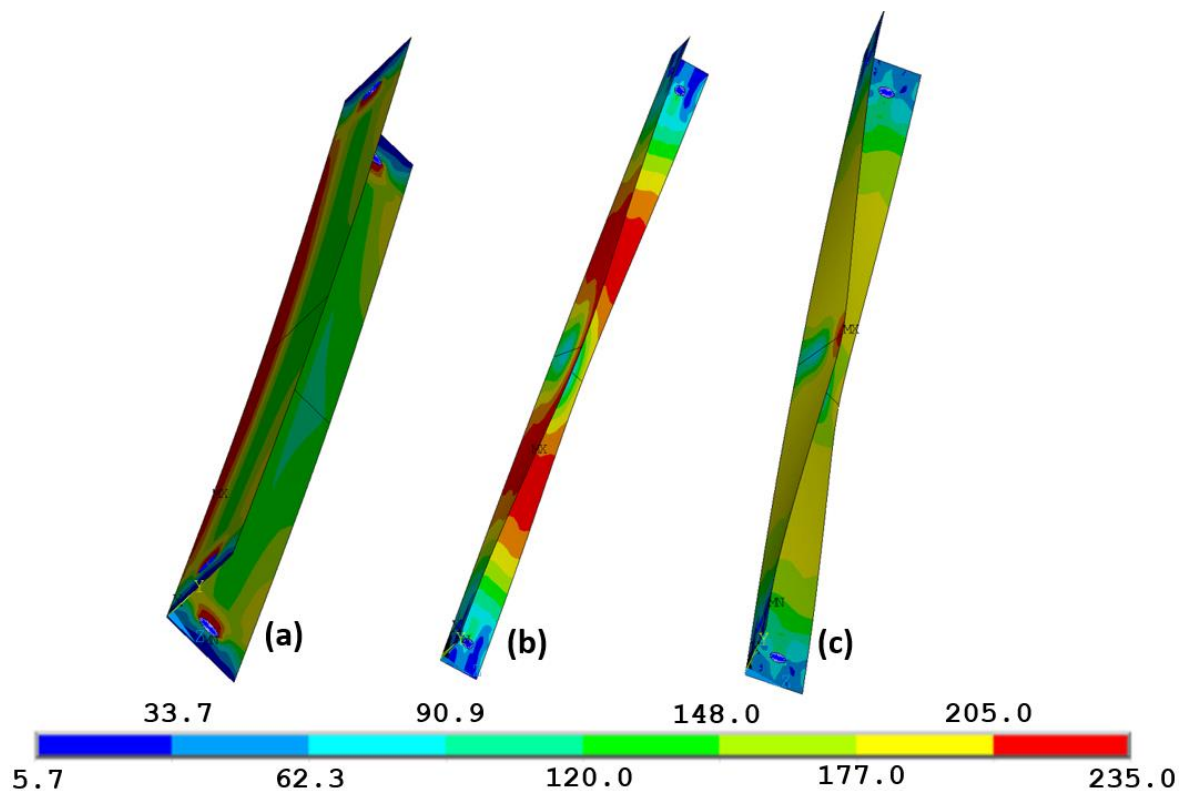
Figure 5.19 – von Mises stress distribution (in MPa) at ultimate compressive load Substep of the L 45 x t section in concentric compression and with pinned boundary conditions at the ends - (a) $h/t = 15$, (b) $h/t = 45$, (c) $h/t = 75$.

5.3.7 Summary of Results

Table 5.10 summarizes the global results for the four cases. The ANGELHY/prEN 1993-3 proposal is the only one that achieves closer results to the numerical resistance, with the lowest scatter across steel grades and slenderness.

Table 5.10 – Mean values, C.O.V, and Coefficient of Determination (R^2) of r_N for all design procedures considering the entire range of steel grades.

Prescription	Concentric (one bolt = pinned)			Concentric (two bolts = fixed)			Eccentric (one bolt = pinned)			Eccentric (two bolts = fixed and partially restrained)		
	$(r_N)_{mean}$	C.O.V (%)	R^2 (%)	$(r_N)_{mean}$	C.O.V (%)	R^2 (%)	$(r_N)_{mean}$	C.O.V (%)	R^2 (%)	$(r_N)_{mean}$	C.O.V (%)	R^2 (%)
AISC 360	1.01	5.29	98.77	1.00	6.03	98.66	N.A.	N.A.	N.A.	2.40	23.70	-7.33
EN 1993-1-1	1.12	9.75	88.48	1.10	10.00	88.49	N.A.	N.A.	N.A.	2.22	19.27	-9.26
FprEN 1993-1-1	1.09	7.87	92.41	1.08	8.49	89.51	N.A.	N.A.	N.A.	2.11	22.90	33.25
EN 1993-3-1**	N.A.	N.A.	N.A.	N.A.	N.A.	N.A.	1.09	13.33	91.71	2.22	19.27	-9.26
EN 1993-3-1/ FprEN 1993-1-1**	N.A.	N.A.	N.A.	N.A.	N.A.	N.A.	1.03	12.68	90.52	2.19	19.68	5.06
ANGELHY	1.02	2.71	99.49	1.01	2.66	99.66	1.12	10.37	94.92	1.21	10.61	42.21
ANGELHY_ MOD	N.R.	N.R.	N.R.	N.R.	N.R.	N.R.	1.17	9.66	91.04	1.28	11.54	10.69
Kettler et al. (2021)	N.A.	N.A.	N.A.	N.A.	N.A.	N.A.	0.93	20.22	68.08	1.25	7.92	79.22
Behzadi-Sofiani et al. (2021)	1.09	7.13	96.02	1.08	6.40	96.87	N.A.	N.A.	N.A.	N.A.	N.A.	N.A.

* N.A.: Not Applicable.   N.R.: Not Relevant (equal to ANGELHY)
** Considering angle members only as bracing members.

5.4 Reliability Assessment

The final step in the establishment of new code proposals corresponds to the assessment of the required partial factors that ensure compliance with the target failure probability. In the scope of the Structural Eurocodes, this is established in general terms in Annex D of EN 1090, with specific detailed guidance for stability-related problems in steel structures, also available in Tankova et al. (2014).

In practical terms, it is required to obtain the partial factor γ_{M1}^*. This requires knowledge about the variability or scatter of the basic variables of the problem. Following the results of the SAFEBRICTILE project, informative Annex E was established in EN 1993-1-1, specifying the statistical characterization of the basic variables required for the reliability assessment of design rules in Eurocode 3 namely, yield stress, Young's modulus, and cross-section geometry.

According to the results of the assessment of the various design proposals in Subsections 5.3.2 to 5.3.5, the ANGELHY/prEN 1993-3 proposal gives the most accurate results. Hence, the reliability assessment will focus on this proposal, as it will probably provide the basis for a future amendment to Eurocode 3. Following Simões da Silva et al. (2016b), (2018), (2020), and using Tables E.1 and E.2 of Annex E of FprEN 1993-1-1, with an appropriate choice of subsets (Table 5.11) leads to a required $\gamma_{M1}^* = 1.1$.

Table 5.11 – Required γ_{M1}^* for concentric compressed angles.

	S235	S355	S460	ALL
Concentric (1 bolt - pinned)	1.076	1.036	1.121	1.078
Concentric (2 bolts - fixed)	1.091	1.061	1.142	1.098
Concentric (ALL)	-	-	-	**1.09**

6

VALIDATION OF GENERAL FORMULATION FOR NON-PRISMATIC MONO-SYMMETRIC I-SECTION STEEL BEAMS

6.1 General Aspects

In Chapter 4, the comparison between the numerical and analytical values of bending moment resistance showed some inconsistency in the prescriptions of GC and AISC.

In this chapter, the General Formulation is validated for mono-symmetric I-section steel beams. First, a parametric study is defined, comprising non-prismatic beams, which are not covered by the most of existing design codes. Next, the results of the parametric study for prismatic beams obtained in Chapter 4 (presented in Table 4.7 – Subsection 4.3.1) are used to validate the proposed General Formulation for prismatic mono-symmetric I-sections. The results of this validation are compared with the available design proposals (GC and AISC).

Finally, the GF is validated for non-prismatic mono-symmetric steel beams, and its accuracy is compared with that of AISC, the General Method (GM), and the proposal of Marques et al. (2013).

6.2 Parametric Study for Non-prismatic Mono-symmetric Beams

By using the numerical model validated in Subsection 4.2.2 (Chapter 4), a parametric study on non-prismatic mono-symmetric welded I-beams is defined and performed. The parametric study comprises S235 grade steel beams, with the largest flange in tension, $\bar{\lambda}_z = 1.30$, and is divided into two subsets as follows:

(i)   mono- and doubly symmetric web-tapered members with only the largest flange inclined (for mono-symmetric sections); subjected to distributed load (TF, BF, G and D point loading application – point loading D only for mono-symmetric sections - Figure 6.1) and constant bending moment (Figure 6.2); three additional cases were studied: member with restraint at the flange in tension, located at mid-span; and at 1/3 and 2/3 of the length; and member with restraint at the flange in compression, located at mid-span (see Figure 6.1 and Figure 6.2). The following cross-sections are studied: h x 200(200) x 8 x 16(16), h x 300(200) x 8 x 16(16), and h x 410(410) x 31 x 70(55), with maximum depth equal to 500, 500, and 1138, respectively. The ratio between the maximum and minimum depth of the tapered members is equal to 2.0 for all cases studied. Number of numerical models: 56.
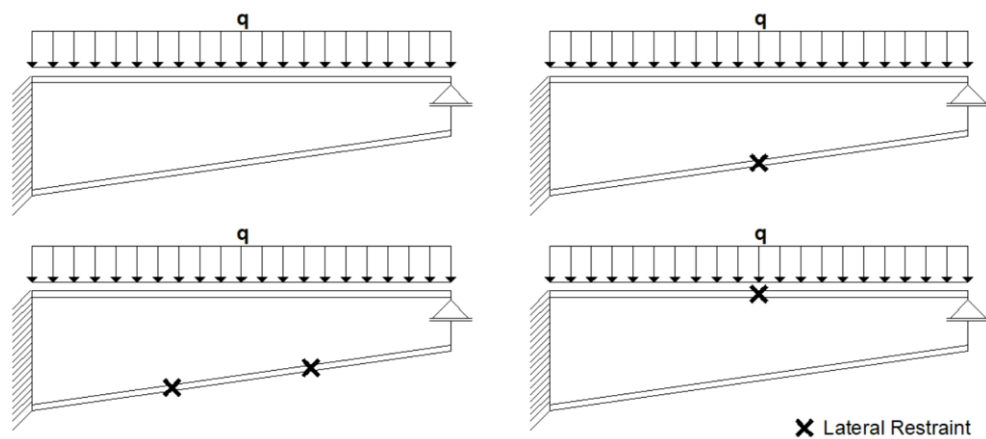
Figure 6.1 – Cases for tapered members with mono-symmetric I-sections subjected to distributed load.
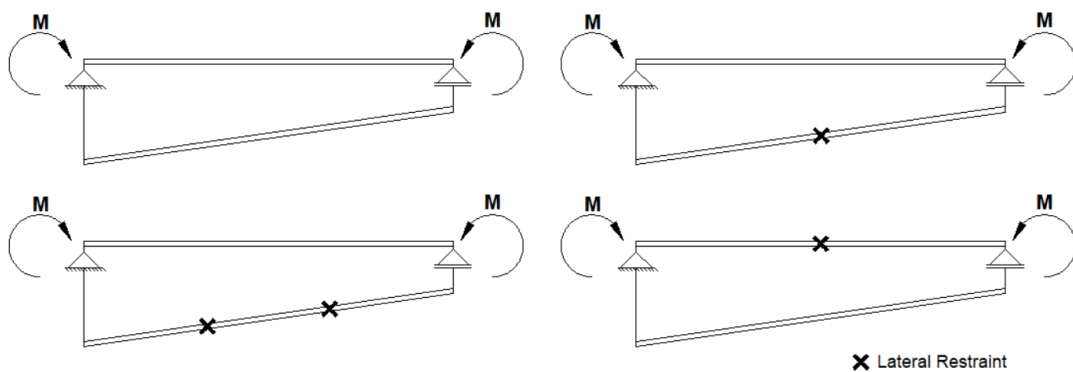
Figure 6.2 – Cases for tapered members with mono-symmetric I-sections subjected to constant bending moment.

(ii)   parabolic and anti-parabolic members with mono-symmetric cross-sections (Figure 6.3 and Figure 6.4, respectively), subjected to distributed load (TF point loading application – Figure 6.3 and Figure 6.4). Additionally, the lateral restraints cases of the subset (i) were studied in this subset (see Figure 6.3 and Figure 6.4). The considered cross-sections at the end of the members are: 500 x 200(150) x 12 x 50(30), 750 x 180(250) x 15 x 35(25), 800 x 300(200) x 18 x 35(50), and 1138 x 410(410) x 31 x 70(55), and the cross-section at mid-span has the depth incremented or subtracted by a (Figure 6.3 and Figure 6.4), considering a/L equal to 0.05. The boundary conditions at the ends of the members of this subset are equal to those of the subset exhibited in Table 4.7 (Subsection 4.3.1 – Chapter 4), except for the in-plane rotation (rotation about the y-axis – see Figure 2.6, Chapter 2), where a rotation spring equivalent to about 50% of the clamped elastic critical bending moment is applied (see Figure 6.3 and Figure 6.4). Number of numerical models: 32.
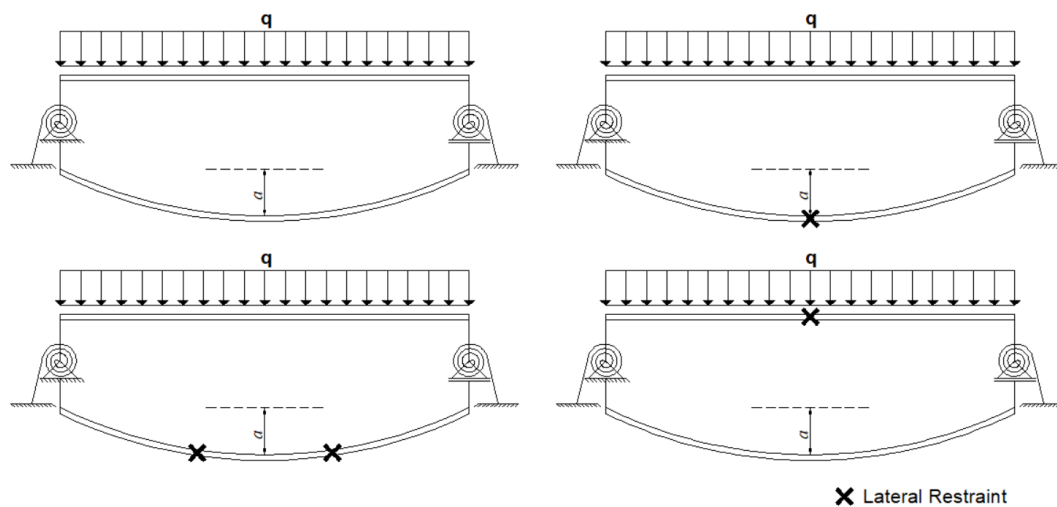
Figure 6.3 – Cases for parabolic members with mono-symmetric I-section subjected to distributed load.
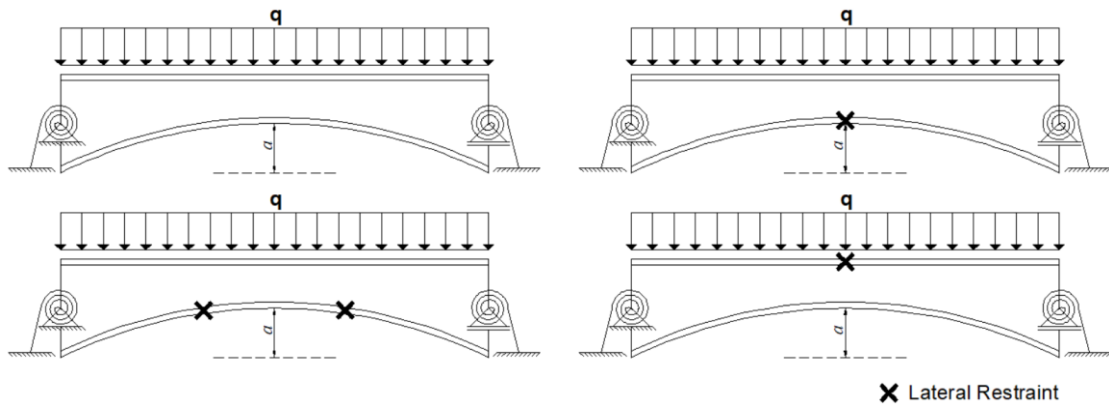
Figure 6.4 – Cases for anti-parabolic members with mono-symmetric I-section subjected to distributed load.

The two subsets (i) web-tapered and (ii) parabolic and anti-parabolic variation of the beam depth were chosen because they represent the two common practical cases. The specific choice of the cases followed a similar parametric study carried out by Tankova et al. (2018) for doubly symmetric non-prismatic beams, thereby allowing for direct comparison.

The cross-sections of the end extremities of all numerical models (subsets (i) and (ii)) of the parametric study are modeled as shown in Figure 4.3 (Subsection 4.2.1 – Chapter 4), adjusted to the appropriate loading and boundary conditions.

6.3 Comparison between LBA and GMNIA Deformed Shapes

First, as the General Formulation relies on the second derivatives of the elastic critical buckling mode shape (v''_{cr} and θ''_{cr}), it is important to verify if the deformed shape of the first eigenvalue of LBA analysis is like the GMNIA results for the ultimate compressive load substep, for the correct application of the method. Figure 6.5 compares the corresponding deformed shape of LBA and GMNIA for uniform mono-symmetric members subjected to linear bending moments.
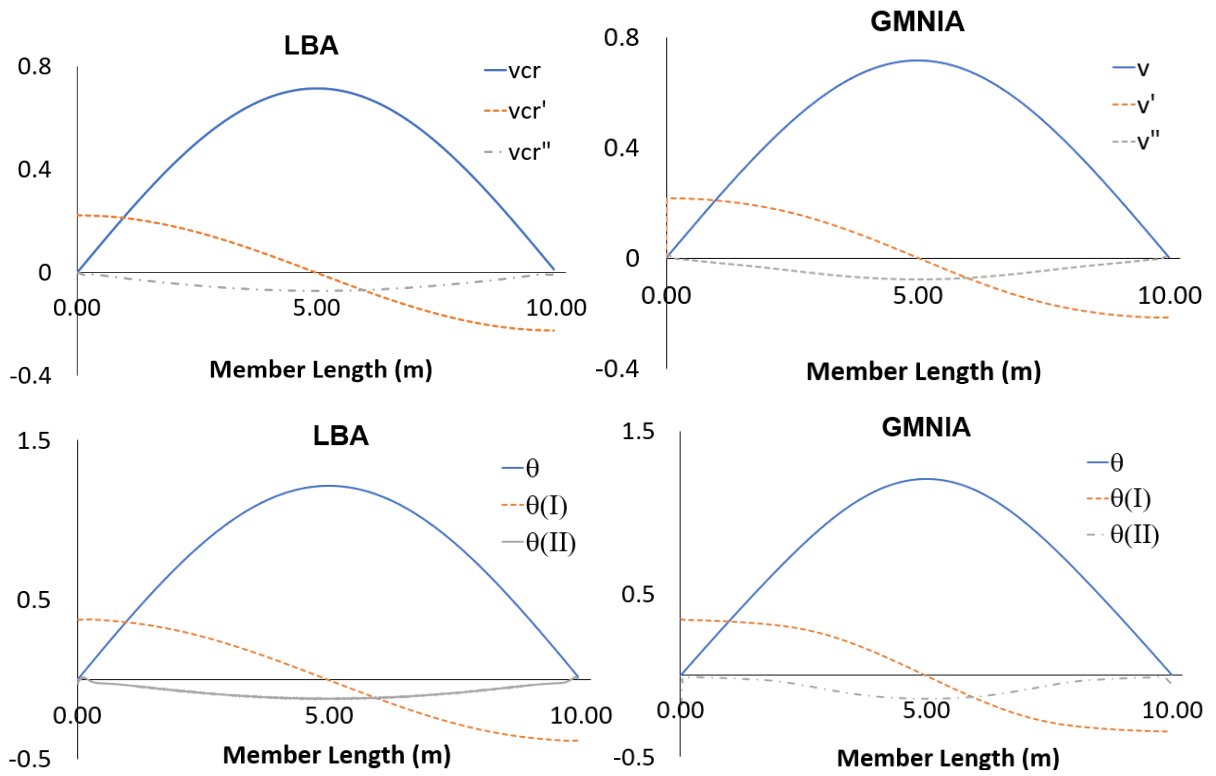
Figure 6.5 – Mode shape for uniform mono-symmetric beams subjected to linear bending moment *(ψ = 1.0)* - $\bar{\lambda}_z$ = 2.40.

Figure 6.6 compares the typical deformed shape of LBA and GMNIA for mono-symmetric tapered members subjected to distributed load.
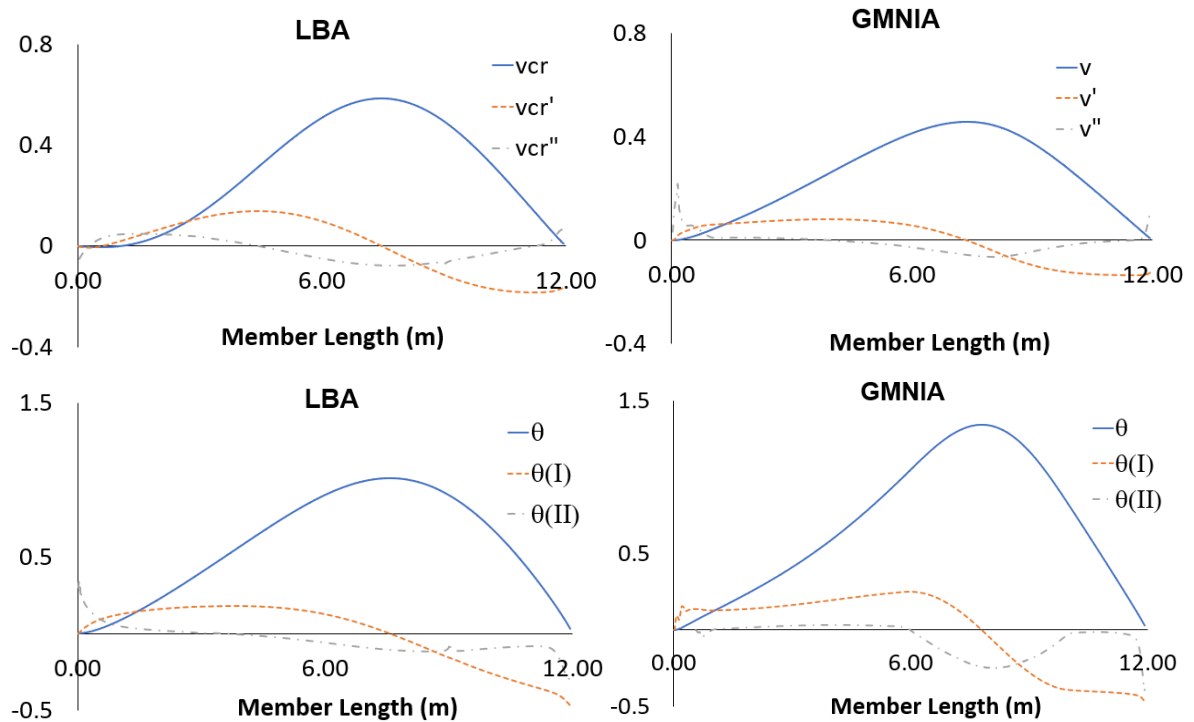
Figure 6.6 – Mode shape for tapered mono-symmetric beams subjected to distributed load (without restraints along the member) - $\bar{\lambda}_z = 1.30$.

Additional comparisons are available in APPENDIX A. In summary, the GMNIA deformed shapes are equivalent to the modal displacements and rotations (and their derivatives) obtained through the LBA analysis.

6.4 Prismatic Mono-symmetric Cross-section Results

Figure 6.7 presents the scatter plot of r_t x r_e for the different loading types for the prismatic mono- and doubly symmetric cross-section subsets (Table 4.7 – Subsection 4.3.1, Chapter 4), where r_e is the ratio between the numerical lateral-torsional buckling resistance and the plastic bending moment resistance of the cross-section, and r_t is the ratio between the analytical buckling resistance (AISC, EC3-General Case or General Formulation) and the cross-sectional plastic bending moment resistance. As already stated, AISC exhibits unsafe behaviour, while GC rules are very conservative for all cases studied. However, GF yields more accurate estimates of the lateral-torsional buckling resistance.
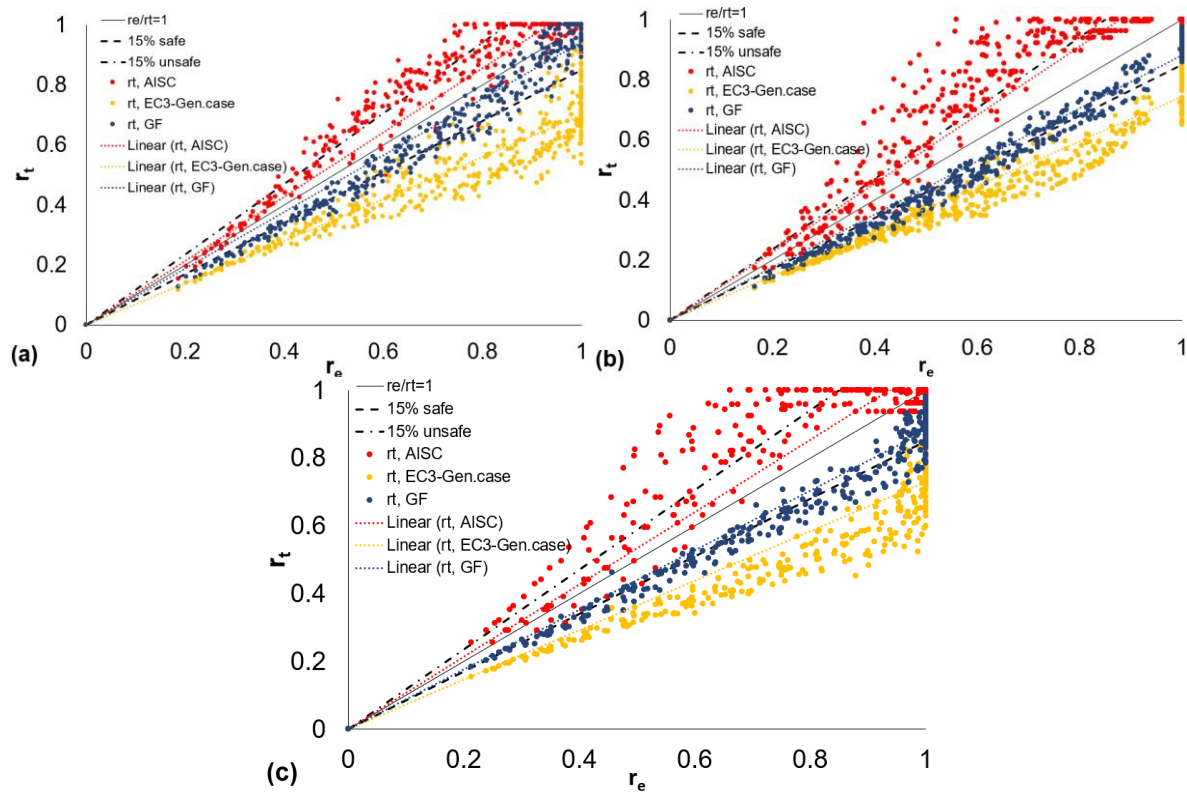
Figure 6.7 – Scatter plot: (a) linear bending moment, (b) distributed load, (c) point load.

The statistical evaluation of GF, carried out based on the ratio (r_N) between the numerical lateral-torsional buckling resistance and the analytical lateral-torsional buckling resistance, is exhibited in detail in Table 6.1 to Table 6.3. Globally, the following values were obtained for General Formulation (see Table 6.4): an average $r_N = 1.16$ and a C.O.V of 7.61%. In summary, Table 6.4 shows that the method proposed by GF is significantly more accurate than the other ones.

Comparing GC and GF, the poor performance of GC is a direct result of the lack of mechanical consistency in the derivation of this method (Tankova et al., 2022). In contrast, GF adopts the generalized imperfection factors of the mechanically consistent method developed by Taras and Greiner (2010) for prismatic double-symmetric cross-section beams and leads to similar results as this new method for doubly symmetric cross-sections.

Comparison of the results for double- and mono-symmetric cross-sections shows that the results are approximately 2% to 3% worse for mono-symmetric beams for GF (Table 6.1 to Table 6.3), while for GC this difference increases to 4% to 6% (see Table 4.10 to Table 4.12). GC only takes into account the influence of mono-symmetry in the elastic critical bending moment M_{cr} (see Equation (2.104) – Subsection 2.3.2, Chapter 2), while GF considers this effect both in the

M_{cr} determination and in the computation of the imperfection factor (see Equations (3.22) and (3.24) – Section 3.2, Chapter 3).

Table 6.1 – Statistical parameters for $r_{N,GF}$ – Linear Bending Moment.

Linear Bending Moment					
Subset	**n**	**Average**	**C.O.V(%)**	**Min**	**Max**
All	408	**1.13**	7.61	1.03	1.31
S235	136	**1.07**	6.30	1.01	1.20
S355	136	**1.14**	8.30	1.04	1.34
S460	136	**1.19**	8.49	1.04	1.39
$\psi = 1.0$	204	**1.17**	6.47	1.03	1.31
$\psi = 0.0$	132	**1.06**	1.92	1.04	1.09
$\psi = -1.0$	72	**1.02**	1.80	1.00	1.05
Stress on Fl. $> I_z =$ Ten., $\psi = 0$; $\psi = 1$	192	**1.14**	7.08	1.06	1.31
Stress on Fl. $> I_z =$ Comp., $\psi = 0$; $\psi = 1$	120	**1.12**	1.07	1.11	1.14
Mono-symmetric cross-section	348	**1.14**	7.45	1.06	1.31
Doubly symmetric cross-section	60	**1.12**	9.68	1.03	1.24

Table 6.2 – Statistical parameters for $r_{N,GF}$ – Distributed Load.

Distributed Load					
Subset	n	Average	C.O.V (%)	Min	Max
All	444	**1.19**	6.41	1.06	1.30
S235	148	**1.13**	5.66	1.04	1.23
S355	148	**1.20**	6.87	1.07	1.32
S460	148	**1.24**	7.35	1.08	1.37
Point load application = TF	120	**1.23**	7.78	1.07	1.35
Point load application = BF	120	**1.17**	5.80	1.06	1.26
Point load application = G	120	**1.18**	6.82	1.06	1.31
Point load application = D	84	**1.18**	6.92	1.06	1.29
Mono-symmetric cross-section	336	**1.20**	6.48	1.06	1.30
Doubly symmetric cross-section	108	**1.17**	7.22	1.08	1.25

Table 6.3 – Statistical parameters for $r_{N,GF}$ – Point Load.

Point Load					
Subset	n	Average	C.O.V (%)	Min	Max
All	444	**1.18**	5.83	1.05	1.26
S235	148	**1.14**	5.43	1.03	1.24
S355	148	**1.18**	6.05	1.05	1.27
S460	148	**1.21**	6.45	1.06	1.33
Point load application = TF	120	**1.19**	6.01	1.04	1.28
Point load application = BF	120	**1.16**	6.19	1.04	1.24
Point load application = G	120	**1.18**	6.23	1.04	1.29
Point load application = D	84	**1.18**	6.28	1.05	1.25
Mono-symmetric cross-section	336	**1.18**	6.24	1.05	1.26
Doubly symmetric cross-section	108	**1.16**	5.75	1.09	1.22

Table 6.4 – Statistical parameters for prismatic members.

Subset	n	$r_{N,AISC}$				$r_{N,GC}$				$r_{N,GF}$			
		Average	C.O.V (%)	Min	Max	Average	C.O.V (%)	Min	Max	Average	C.O.V (%)	Min	Max
All	1296	**0.90**	7.34	0.78	1.08	**1.42**	8.33	1.18	1.65	**1.16**	7.61	1.03	1.31
Linear bending moment	408	**0.93**	7.34	0.81	1.08	**1.41**	8.33	1.20	1.58	**1.13**	7.61	1.03	1.31
Distributed load	444	**0.87**	9.23	0.78	1.00	**1.42**	8.55	1.20	1.59	**1.19**	6.41	1.06	1.30
Concentrated load	444	**0.90**	7.89	0.82	1.01	**1.44**	10.3	1.18	1.65	**1.18**	5.83	1.05	1.26

6.5 Non-prismatic and Tapered Mono-symmetric Cross-sections Results

Figure 6.8 shows the scatter plot r_t x r_e for the mono-symmetric non-prismatic and tapered beams and Table 6.5 and Table 6.6 exhibit the comparison between the numerical lateral-torsional buckling resistance and the corresponding analytical results according to the AISC (Frame design using web-tapered members, design guide 25), the General Method (GM), the method proposed by Marques et al. (2013) and the proposed extension of the General Formulation (GF), in terms of r_N ratio, for tapered and non-prismatic beams, respectively.

For the tapered beams (see Table 6.5), AISC and GM show poor results with high scatter that are unacceptably conservative, with an average r_N = 2.14 and a C.O.V of 29.85%, and an average r_N = 1.97 and a C.O.V of 16.73%, respectively, with AISC being insecure for a few slender beams. AISC and GM methods are time-consuming procedures, where the critical location is obtained through an iterative operation. Furthermore, the definition of the imperfection factors for GM is not clearly defined and may lead to inaccurate results. In contrast, the results of Marques et al. (2013) proposal and GF are considerably closer to the numerical values, leading to an average r_N = 1.20 and a C.O.V of 11.83%, and an average r_N = 1.15 and a C.O.V of 7.52%, respectively, with GF exhibiting a similar performance when compared to the prismatic cases. The design approach of Marques et al. (2013) proposal and GF present much higher accuracy than the methods proposed by AISC and GM, because: (i) they use generalized imperfection factors based on mechanically consistent derivations; and (ii) take into account the effect of the taper. For the cases without intermediate bracings, the method

proposed by Marques et al. (2013) leads to better results because the generalized imperfection factors and the second-order critical location were specifically calibrated for web-tapered beams, by using an extensive numerical program. However, the method is not applicable to partial lateral bracings (bracing to the tension flange), as shown in Table 6.5, leading to worse results for these cases.

For the non-prismatic beams, only GM and GF are applicable (see Table 6.6). GM exhibits unsafe results for the parabolic beams and reasonable results for the anti-parabolic ones, leading to an average $r_N = 0.92$ and a C.O.V of 28.96%, and an average $r_N = 1.30$ and a C.O.V of 8.92%, respectively for both cases. AISC prescriptions do not cover non-prismatic beams. GF gives accurate results (an average $r_N = 1.23$ and a C.O.V of 7.37%, respectively, for the parabolic beams; and an average $r_N = 1.25$ and a C.O.V of 7.48%, respectively, for the anti-parabolic beams).
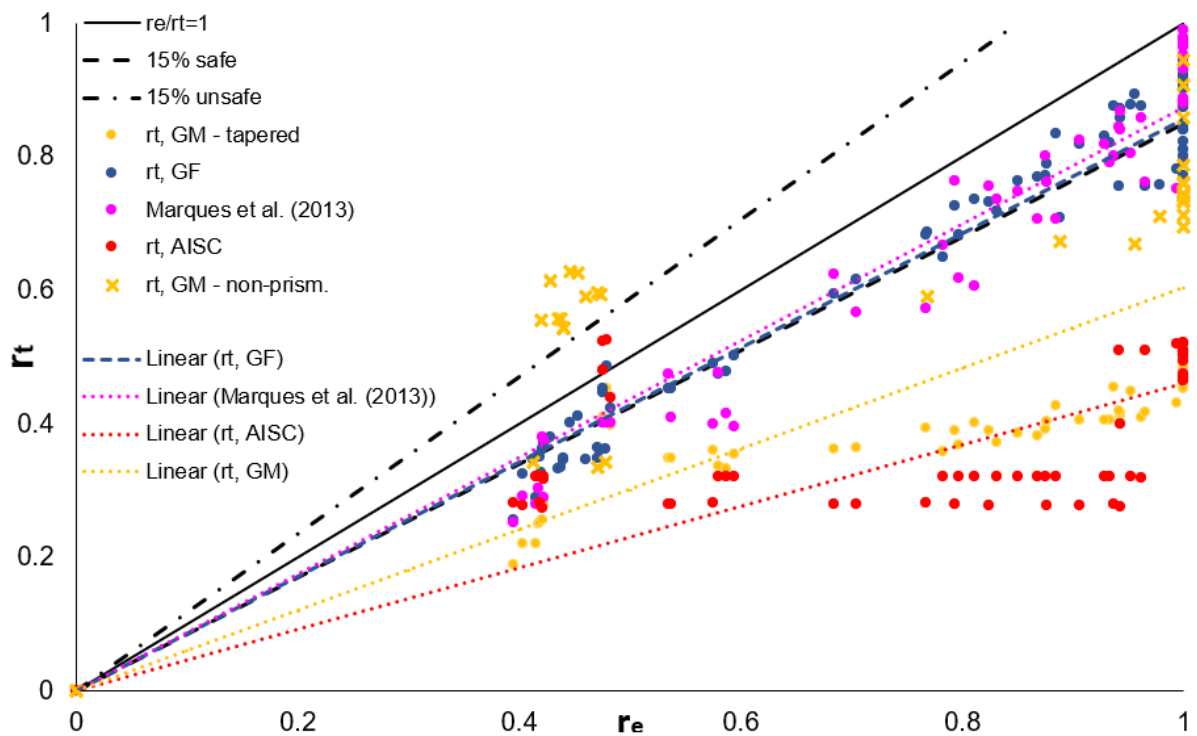
Figure 6.8 – Scatter plot for the tapered and non-prismatic members.

Table 6.5 – Statistical parameters for tapered beams.

Subset	n	$r_{N,AISC}$		$r_{N,GM}$		$r_{N,Marques\ et\ al.}$ (2013)		$r_{N,GF}$	
		Average	C.O.V (%)	Average	C.O.V (%)	Average	C.O.V (%)	Average	C.O.V (%)
All	56	**2.14**	**29.85**	**1.97**	**16.73**	**1.20**	**11.83**	**1.15**	**7.52**
Distributed load	44	2.39	20.08	2.09	10.13	1.17	10.14	1.15	4.60
Liner bending moment	12	1.25	17.66	1.53	21.28	1.31	12.52	1.19	13.36
No Restraints	14	2.01	27.95	1.98	16.06	1.17	13.65	1.21	10.89
1 restraint at flange in tension	14	2.08	29.49	1.97	17.03	1.24	8.72	1.17	4.77
2 restraints at flange in tension	14	2.12	31.79	1.86	17.66	1.28	11.77	1.12	6.17
1 restraint at flange in compression	14	2.36	30.22	2.06	16.59	1.09	4.80	1.12	2.21
Mono-symmetric cross-sections	40	2.04	28.39	1.99	17.92	1.18	10.98	1.15	6.66
Doubly symmetric cross-sections	16	2.40	30.32	1.91	13.04	1.23	13.52	1.17	9.46

Table 6.6 – Statistical parameters for the non-prismatic members.

Subset	n	$r_{N,GM}$		$r_{N,GF}$	
		Average	C.O.V (%))	Average	C.O.V (%)
Parabolic member	16	0.92	28.96	1.23	7.37
Anti-parabolic member	16	1.30	8.92	1.25	7.48

Note: AISC prescriptions do not cover non-prismatic beams.

A simplified step-by-step procedure of General Formulation, as well as a worked example summarizing the application of this proposal for non-prismatic mono-symmetric beams, are presented in APPENDIX B.

7

VALIDATION OF GENERAL FORMULATION FOR ANGLE SECTION STEEL MEMBERS IN COMPRESSION

7.1 General Aspects

In Chapter 5, it was demonstrated that EN 1993-1-1 approach and ANGELHY proposal for angle members in concentric compression (pinned and fixed members) present good accuracy for Class 1 and Class 2 cross-sections (most of them S235 steel grade). In the case of eccentric compression, EN 1993-3-1 presents a poor and scatter approach for pinned members, while the ANGELHY method shows results slightly more accurately. Considering fixed angles in eccentric compression, neither of the two methods presented good performance.

In Section 3.3 (Chapter 3), the General Formulation was further extended to angles in compression, covering all the relevant buckling modes of this member (flexural and torsional-flexural buckling. And the excellent performance of GF for mono-symmetric I-section steel beams, observed in Chapter 6, showed that the method is comprehensive and promising for other cross-sections.

Therefore, in this chapter, GF is validated for angle members in concentric and eccentric compression. The data used for this validation comprises the numerical results for the Class 1 and Class 2 cross-sections of the parametric study used in the assessment of design procedures, conducted in Chapter 5 (see Table 5.5 – Section 5.3.1). The results of this validation are compared with the accuracy of Eurocode 3 and ANGELHY proposals.

7.2 Angle Members in Concentric Compression Results

In Subsection 3.3.1 (Chapter 3), it was demonstrated that the verification of GF for angle members in concentric compression coincides analytically with the methods of the current version of Eurocode 3 for flexural and torsional-flexural buckling. In this section, both methods are compared with numerical results of pinned and fixed members in concentric compression. ANGELHY method is not addressed in this section because its prescriptions consider buckling modes different from those of General Formulation.

Figure 7.1, Figure 7.2, Table 7.1, and Table 7.2 present the mean and C.O.V of r_N (see Equation (5.2)) for EN 1993-1-1 and General Formulation, split according to steel grade, slenderness, and boundary conditions (pinned - Figure 7.1, Table 7.1 - or fixed - Figure 7.2, Table 7.2 - members). It should be emphasized that torsional-flexural buckling occurs commonly at angle members with $\bar{\lambda}_v = 0.5$. For the other slenderness ranges, flexural buckling about the minor axis predominates.

In summary, the results of the comparison between numerical and analytical results confirm that EN 1993-1-1 and GF methods are completely coincident for both cases: flexural and torsional-flexural buckling. Furthermore, the proposals present excellent agreement with the numerical results, showing also very low scattering: a global average $r_N = 1.05$ and a C.O.V of 3.87% for pinned members, and a global average $r_N = 1.04$ and a C.O.V of 3.55% for fixed members.

Figure 7.1 – $(r_N)_{mean}$ for pinned angle members compressed concentrically - (a) S235, (b) S355, and (c) S460 steel grades – Class 1 and Class 2 cross-sections.

Table 7.1 – Mean values and C.O.V of r_N for EN 1993-1-1 and GF approaches considering the entire range of slenderness – Concentric (pinned).

Loading type	Prescription	Steel grade							
		S235		S355		S460		All	
		$(r_N)_{mean}$	C.O.V (%)	$(r_N)_{mean}$	C.O.V (%)	$(r_N)_{mean}$	C.O.V (%)	$(r_N)_{mean}$	C.O.V (%)
Concentric (pinned)	EN 1993-1-1	1.01	1.48	1.06	2.74	1.08	3.34	1.05	3.87
	GF	1.01	1.48	1.06	2.74	1.08	3.34	1.05	3.87

Figure 7.2 – $(r_N)_{mean}$ for fixed angle members compressed concentrically - (a) S235, (b) S355, and (c) S460 steel grades – Class 1 and Class 2 cross-sections.

Table 7.2 – Mean values and C.O.V of r_N for EN 1993-1-1 and GF approaches considering the entire range of slenderness – Concentric (fixed).

Loading type	Prescription	Steel grade							
		S235		S355		S460		All	
		$(r_N)_{mean}$	C.O.V (%)	$(r_N)_{mean}$	C.O.V (%)	$(r_N)_{mean}$	C.O.V (%)	$(r_N)_{mean}$	C.O.V (%)
Concentric (fixed)	EN 1993-1-1	1.01	2.72	1.05	3.31	1.06	3.05	1.04	3.55
	GF	1.01	2.72	1.05	3.31	1.06	3.05	1.04	3.55

7.3 Angle Members in Eccentric Compression Results

In Section 5.3 (Chapter 5), it was evidenced that ANGELHY, in general, provides the best approach between the proposals assessed for angle members in eccentric compression, although

this method is not so accurate. Therefore, in this section, the values of r_N for GF are compared with those of ANGELHY.

Figure 7.3, Figure 7.4, Table 7.3, and Table 7.4 present the mean and C.O.V of r_N for ANGELHY and General Formulation, split according to steel grade, slenderness, and boundary conditions. Considering pinned angle members in eccentric compression (see Figure 7.3 and Table 7.3), GF (see Equation (3.75) – Section 3.3.2, Chapter 3) presents excellent performance with the numerical results (global average $r_N = 1.04$ and a C.O.V of 4.74%), providing much more accurate and less scattering values of compressive strength than those of the ANGELHY method (see Equations (2.157) and (2.158) – Section 2.5.3, Chapter 2) - global average $r_N = 1.11$ and a C.O.V of 10.35%. For the case of fixed angle members in eccentric compression (see Figure 7.4 and Table 7.4), GF gives results values for ultimate load resistance slightly more accurate than those obtained from ANGELHY prescriptions: a global average $r_N = 1.21$ and a C.O.V of 17.94% for GF, a global average $r_N = 1.25$ and a C.O.V of 12.26% for ANGELHY.

Finally, the difference between both methods is related to the fact that GF adopts specifically a buckling load for angle member in eccentric compression (Equation (2.68) or LBA), where the boundary conditions are automatically included. On the other hand, ANGELHY proposal uses the flexural buckling loads about the principal axes of inertia (buckling loads typically observed in concentrically compressed members) and does not specify any effective length factor to be used in cases with boundary conditions different from fork boundary conditions. In short, this leads GF to provide more accurate results than ANGELHY.
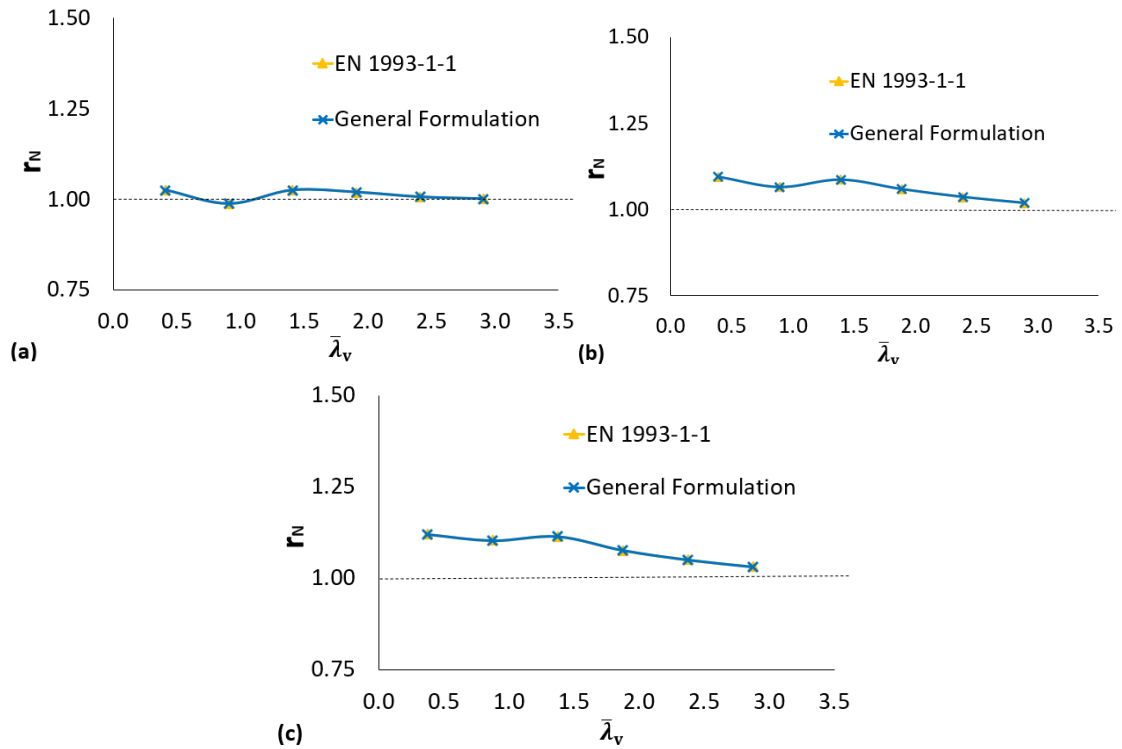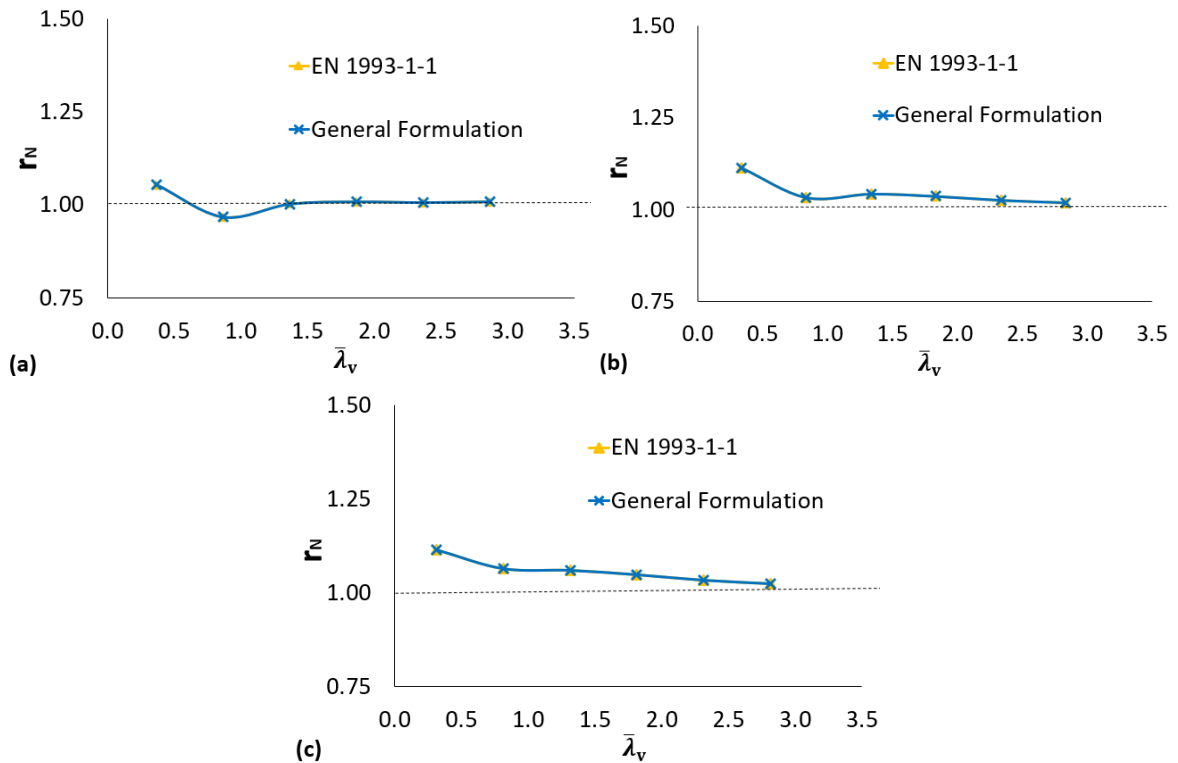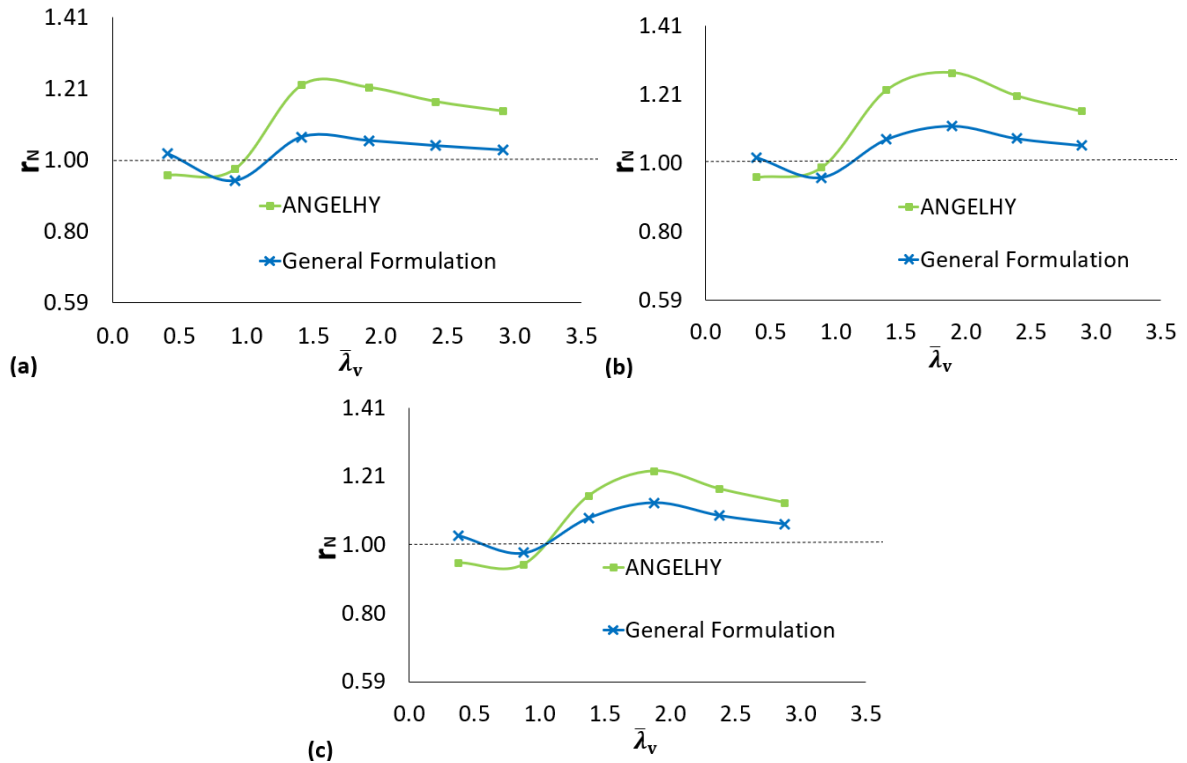
Figure 7.3 – $(r_N)_{mean}$ for pinned angle members compressed eccentrically - (a) S235, (b) S355, and (c) S460 steel grades – Class 1 and Class 2 cross-sections.

Table 7.3 – Mean values, C.O.V, and Coefficient of Determination (R^2) of r_N for ANGELHY and GF approaches considering the entire range of slenderness – Eccentric (pinned).

Loading type	Prescription	Steel grade								
		S235		S355		S460		All		
		$(r_N)_{mean}$	C.O.V (%)	$(r_N)_{mean}$	C.O.V (%)	$(r_N)_{mean}$	C.O.V (%)	$(r_N)_{mean}$	C.O.V (%)	R^2 (%)
Eccentric (pinned)	ANGELHY	1.11	10.41	1.13	11.38	1.09	10.87	1.11	10.35	95.03
	GF	1.03	4.33	1.05	5.15	1.06	4.91	1.04	4.74	98.56
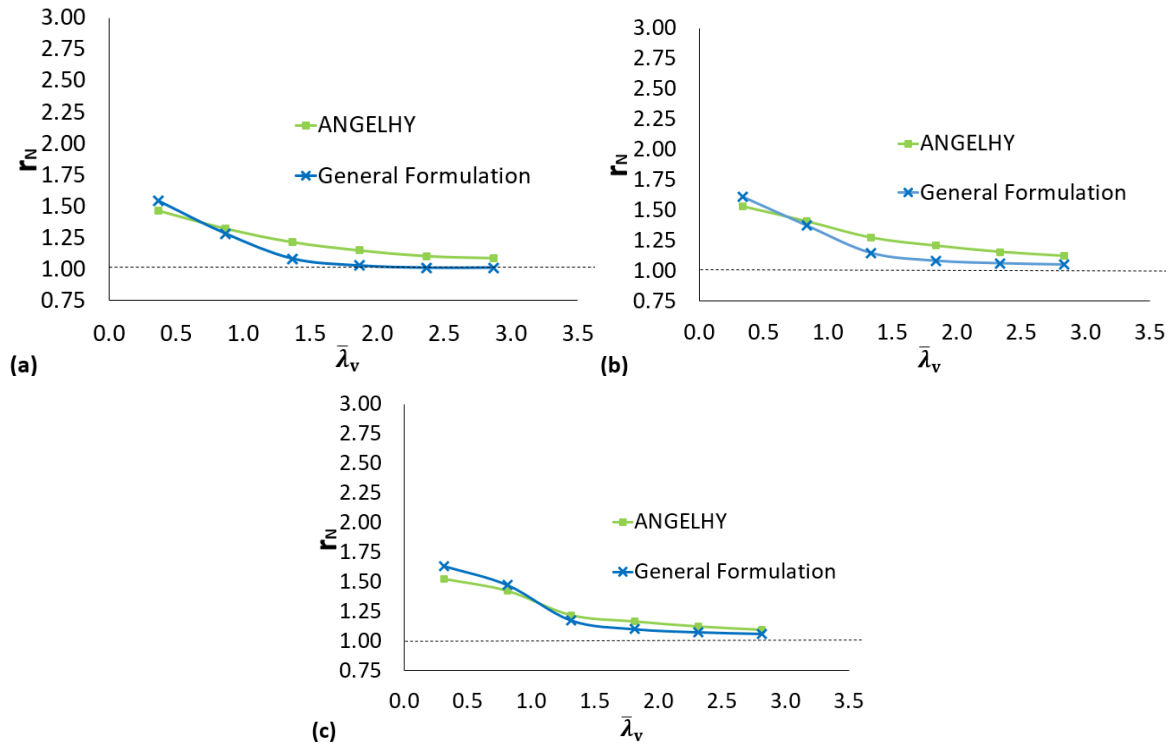
Figure 7.4 – $(r_N)_{mean}$ for fixed angle members compressed eccentrically - (a) S235, (b) S355, and (c) S460 steel grades – Class 1 and Class 2 cross-sections.

Table 7.4 – Mean values, C.O.V, and Coefficient of Determination (R^2) of r_N for ANGELHY and GF approaches considering the entire range of slenderness – Eccentric (fixed).

		Steel grade								
		S235		S355		S460		All		
Loading type	Prescription	$(r_N)_{mean}$	C.O.V (%)	$(r_N)_{mean}$	C.O.V (%)	$(r_N)_{mean}$	C.O.V (%)	$(r_N)_{mean}$	C.O.V (%)	R^2 (%)
Eccentric (fixed)	ANGELHY	1.22	12.02	1.28	12.42	1.26	14.08	1.25	12.26	25.12
	GF	1.16	18.39	1.21	18.49	1.25	19.30	1.21	17.94	4.41

7.4 Summary of Results

Table 7.5 summarizes the global results, split according to the buckling mode. The proposal of General Formulation is the method that best achieves closer to the numerical resistance.

Table 7.5 – Mean values and C.O.V of r_N for procedures of EN 1993-1-1, ANGELHY, and GF considering the buckling modes of an angle member in compression.

Buckling mode	EN 1993-1-1		ANGELHY		General Formulation	
	$(r_N)_{mean}$	C.O.V (%)	$(r_N)_{mean}$	C.O.V (%)	$(r_N)_{mean}$	C.O.V (%)
FB v-v (concentric compression)	1.04	3.19	-	-	1.04	3.19
TFB (concentric compression)	1.09	3.60	-	-	1.09	3.60
TFB (eccentric compression)	-	-	1.18	12.86	1.13	15.66

8

FINAL REMARKS

8.1 Conclusions

In this thesis, it was conducted an extensive and comprehensive study about the buckling behaviour of mono-symmetric I-section beams and angle sections in concentric and eccentric compression.

The General Formulation proposed by Tankova et al. (2018) was extended for mono-symmetric beams with variable geometry and boundary conditions, subject to arbitrary loading. A calibrated advanced FEM numerical model was used to carry out a large parametric study on uniform, tapered, and non-prismatic beams. The parametric study contains mono- and doubly symmetric welded I-sections – steel grade S235, S355, and S460 (Class 1 and 2) - subjected to different bending moment diagrams and boundary condition types. It can be concluded that:

- the AISC approach overestimates the buckling resistance of uniform mono-symmetric beams; however, considering the design value with the application of $\phi = 0.9$, the average ratio becomes close to 1.0. For tapered double-symmetric and mono-symmetric beams, AISC yields very conservative results (> 2.0);

- the application of the General Case and the General Method as specified in EC3-1-1 leads to very conservative results for most cases, the latter exhibiting unsafe results for some cases of the non-prismatic beams subset, as was already concluded in Simões da Silva et al. (2010);

- the proposal of Marques et al. (2013) leads to accurate and secure results for web-tapered beams;

- the extended General Formulation leads to good and consistent results for all cases studied. For tapered beams, the accuracy is like Marques et al. (2013); for non-prismatic beams with complex bracing conditions and supports, the General Formulation

maintains the good consistency with the prismatic cases. The results of the General Method are very poor.

Concerning angle sections, a numerical model was developed and validated against recent experimental results from the literature. An evaluation considering a wide variability of parameters, such as geometry, slenderness, steel grade, load configuration, and connection was carried out to assess the various design rules available in the structural eurocodes and AISC standards, including also recent new proposals from ANGELHY project (Bezas et al., 2022), Kettler et al. (2021), and Behzadi-Sofiani et al. (2021), (2022b). It can be concluded that:

- for angles under concentric compression, EN 1993-1-1 and FprEN 1993-1-1 show poor agreement for the low slenderness range; the recommendations from AISC 360 exhibit unsafe results for the intermediate slenderness range; Behzadi-Sofiani et al. (2021) proposal show good agreement for shorty-members, but it has basically the same approach than EN 1993-1-1 for the others slenderness range; the ANGELHY proposals present a good agreement and the lowest scatter;

- for compression angles eccentrically loaded and with pinned boundary conditions at the end, the Kettler et al. (2021) proposal is unsafe for the short-intermediate slenderness range. The EN 1993-3-1, the ANGELHY_MOD, and the ANGELHY/prEN 1993-3 proposals present similar performance, the latter being slightly more accurate;

- none of the procedures analyzed achieved results close to the numerical ones for the case of angles eccentrically loaded and with fixed or partially restrained boundary conditions; In addition, most of the proposals lead to very conservative results, reaching ratios r_N (numerical versus analytical resistances) more than 2. Kettler et al (2021) show good agreement for the low slenderness range and reasonable results for the other ranges. The ANGELHY_MOD and the ANGELHY proposals yield better agreement with the numerical results, with the latter providing even more accurate results;

- the reliability assessment for the ANGELHY design proposals for concentric compression shows that the required value of the partial factor is 1.1. This means that, for consistency with part 1-1 of Eurocode 3, a knock-down factor needs to be included in the design formulation;

To sum up, the ANGELHY proposals improve on the currently existing design rules, showing that they may efficiently replace the current design rules in the Eurocodes. For concentric

compression, it is recommended to adopt the buckling curve c instead of b (for steel grades lower than S460) and the buckling curve b instead of a (for steel grade S460).

The General Formulation was also adapted to angle section geometry and its buckling modes. The results of this method for concentrically compressed members are the same as obtained by the EN 1993-1-1 prescriptions, giving excellent results for Class 1 and Class 2 cross-sections. Concerning angle sections in eccentric compression, GF provides values of compressive strength even more accurately than ANGELHY.

In summary, the General Formulation is easily incorporated into structural design software because its practical implementation consists of a sequence of cross-sectional checks.

8.2 Future Research

General Formulation was validated for non-prismatic mono-symmetric I-section beams and steel angles in compression. However, aiming to incorporate this proposal in the future version of the existing rules, it is highly recommended to extend the scope of the validation of the method, according to the suggestions for future research summarized in the following paragraph:

- extend the validation to the case of mono-symmetric web-tapered columns and beam-columns, correctly taking into account the in-plane and out-of-plane buckling modes, with the appropriate choice of interaction or generalized slenderness;

- apply and verify the proposed methodology to the case of Class 3 and Class 4 mono- and doubly I-sections (columns, beams, and beam-columns), considering accurately the local effects. Probably, an additional verification shall be conducted due to obtaining a failure location occasioned by the local effects in which the cross-section is reduced by the effective resistance;

- check the cases covered by the General Method that still need to be verified by the General Formulation. They comprise the lateral and lateral-torsional buckling of (i) built-up members with variable geometry, boundary conditions, and loading, and (ii) plane flames composed of members in compression and/or bending in the plane, without rotative plastic hinges. For this objective, a comprehensive experimental program shall be conducted, followed by an extensive parametric study, thus covering all proposed cases;

- extend the formulation to Class 3 and Class 4 angle sections in compression, adopting appropriate values of section moduli and considering the additional bending moment about the weak axis for Class 4 cross-sections due to the shift of the centroidal axis when the cross-section is subjected to concentric compression. Furthermore, in the case of eccentric compression, the parametric study shall comprise eccentricity about the minor axis isolated and both axes simultaneously;

- extend the proposal to different types of cross-sections, subjected to bi-axial bending.

The work conducted in this thesis raised other possibilities for future research outside the scope of the General Formulation, as follows:

- calibrate a generalized imperfection factor to be used exclusively for prismatic mono-symmetric I-section beams and incorporated into the future versions of prescriptions concerning prismatic beams in Eurocode 3 (like the methods for doubly symmetric beams already included in FprEN 1993-1-1). This generalized imperfection factor is already present in the General Formulation (see Equation (3.22) – Section 3.2, Chapter 3), based mainly on the buckling modes. However, it must be adapted to a more direct format to be introduced into Equation (2.106);

- Extend the parametric studies to angle sections with unequal legs, with variable boundary conditions along the length (like those cases that occur commonly in transmission towers), and with welded connections at the extremities of the member. The new data set shall be used to assess the existing design methods and, if necessary, propose modifications that lead to more accurate results.

REFERENCES

ABDELRAHMAN, A.H.A.; DU, Z.L.; LIU, Y.P.; CHAN, S.L., Stability design of single angle member using effective stress-strain method. *Structures*, v. 20, p. 298-308, 2019.

ABDELRAHMAN, A.H.A.; LOTFY, S.; LIU, S.W., Generalized line-element formulations for geometrically nonlinear analysis of nonsymmetric tapered steel members with warping and Wagner effects. *Engineering Structures*, v. 273, p. 115052, 2022.

ADLURI, S. M. R.; MADUGULA, M. K. S., Development of column curve for steel angles. *Journal of Structural Engineering*, v. 127, n. 3, p. 318-325, 1996a.

ADLURI, S. M. R.; MADUGULA, M. K. S., Eccentrically loaded steel angle struts. *Engineering Journal*, American Institute of Steel Construction, v. 31, n. 2, p.59-66, 1992.

ADLURI, S. M. R.; MADUGULA, M. K. S., Flexural buckling of steel angles: Experimental investigation- *Journal of Structural Engineering*, v. 122, n. 3, p.309-317, 1996b.

AL-SAYED, S.H.; BJORHOVDE, R. Inelastic Behavior of Single Angle Columns, *Journal of Constructional Steel Research*, v. 12, n. 2, p. 103–118, 1989.

AMERICAN INSTITUTE OF STEEL CONSTRUCTION – *Load and Resistance Factor Design of Single Angle Members* – 3ª Edition, AISC-LRFD, 1993.

AMERICAN INSTITUTE OF STEEL CONSTRUCTION – *Manual of steel construction, load and resistance factor design* – 1ª Edition, AISC-LRFD, 1986.

AMERICAN INSTITUTE OF STEEL CONSTRUCTION – *Manual of steel construction, allowable stress design* – 9ª Edition, AISC-ASD, 1989.

AMERICAN INSTITUTE OF STEEL CONSTRUCTION – *Specification for Structural Steel Buildings* – ANSI/AISC 360, 2016.

AMERICAN SOCIETY OF CIVIL ENGINEERS - ASCE. *Guide for design of steel transmission towers*, Manuals and Reports on Engineering Practice No. 52, New York, 1971.

ANANTHI, G.B.G.; DEEPAK, M.S.; ROY, K.; LIM, J.B.P., Influence of intermediate stiffeners on the axial capacity of cold-formed steel back-to-back built-up unequal angle sections. *Structures*, v. 32, p. 827-848, 2021.

ANDERSON, J.M.; TRAHAIR, N.S., Stability of monosymmetric beams and cantilevers. *Proceedings ASCE: J Struct Div*, v. 98, p. 269-286, 1972.

ANDRADE, A.; CAMOTIM, D., Lateral-torsional buckling of singly symmetric tapered beams: theory and applications. *J Eng Mech*, v. 131, p. 586-597, 2005.

ANDRADE, A.; CAMOTIM, D.; DINIS, P.B., Lateral-torsional buckling of singly symmetric web-tapered thin-walled I-beams: 1D model vs. shell FEA. *Comp and Struct*, v. 85, p. 1343-1359, 2007.

ANDRADE, A.; CAMOTIM, D.; PROVIDÊNCIA E COSTA, P., On the evaluation of elastic critical moments in doubly and singly symmetric I-section cantilevers. *Journal of Constructional Steel Research*, v. 63, p. 894-908, 2007.

ANSYS 22.0. Release – *Documentation for ANSYS: guide to the ANSYS documentation*. ANSYS. Inc., Ltd., Canonsburg, USA, 2021.

AYRTON, W.E.; PERRY, J. On struts. *The Engineer*, 1886.

BALLIO, G.; MAZZOLANI, F. M., *Theory and Design of Steel Structures*. Chapman and Hall, London, 1983.

BASHAR, I., *Ultimate Capacity of Steel Angles Subjected to Eccentric Compressive Load*. Master Dissertation, Bangladesh University Of Engineering And Technology, Dhaka, Bangladesh, 2012.

BATHON, L., MUELLER III, W. H., KEMPNER JR., L. Ultimate Load Capacity of Single Steel Angles. *Journal of Structural Engineering*, v. 119, n. 1, p. 279-300, 1993.

BEHZADI-SOFIANI, B.; GARDNER, L.; WADEE, M. A., Testing, numerical analysis and design of stainless steel equal-leg angle section beams. *Structures*, v. 37, p. 977-1001, 2022a.

BEHZADI-SOFIANI, B.; GARDNER, L.; WADEE, M. A., Testing, simulation and design of steel equal-leg angle section beams. *Thin-Walled Structures*, v. 171, p. 108698, 2022b.

BEHZADI-SOFIANI, B.; GARDNER, L.; WADEE, M. A.; DINIS, P. D.; CAMOTIM, D., Behaviour and design of fixed-ended steel equal-leg angle section columns. *Journal of Constructional Steel Research*, v. 182, p. 106649, 2021.

BEHZADI-SOFIANI, B.; WADEE, M. A.; GARDNER, L., Testing, FE modelling and design of pin-ended stainless steel equal-leg angle section columns and beam-columns. *Journal of Constructional Steel Research*, v. 208, p. 107973, 2023.

BEZAS, M.Z., DEMONCEAU, J.F., VAYAS, I., JASPART, J.P., Design rules for equal-leg angle members subjected to compression and bending, *J. Constr. Steel Res.*, v. 189, p. 107092, 2022.

BEZAS, M.Z., *Design of Lattice Towers from Hot-Rolled Equal Leg Steel Angles*. PhD thesis, Jointly supervised between University of Liège and National Technical University of Athens, Athens, Greece, 2021.

BEZAS, M.Z., JASPART, J.P., DEMONCEAU, J.F., LABEYE, N., *Report about the Compression Tests on Large Angle Columns in High Strength Steel*, Research Report-ANGELHY Project, University of Liège, 2020.

BEZAS, M.Z.; DEMONCEAU, J.F.; VAYAS, I.; JASPART, J.P., Classification and cross-section resistance of equal-leg rolled angle profiles. *Journal Of Constructional Steel Research*, v. 185, p. 106842, 2021.

BJORHOVDE, R., *Deterministic and probabilistic approaches to the strength of steel columns*. PhD Dissertation, Lehigh University, PA, 1972.

BLEICH, F. *Buckling Strength of Metal Structures*. McGraw-Hill Book. 508p. New York, 1952.

BRADFORD, M.A.; CUK, P.E., Elastic buckling of tapered monosymmetric I-beams. *J Struct Eng*, v. 114, p. 977-996, 1988.

C.I.G.R.E. Study Committee No. 22, Test report, *Buckling Tests on Crossed Diagonals in Lattice Towers*, Electra Cigré/No. 38, 1974.

CAMOTIM, D.; ANDRADE, A.; BASAGLIA, C., Some thoughts on a surprising result concerning the lateral-torsional buckling of monosymmetric I-section beams. *Thin-Walled Structures*, v. 60, p. 216-221, 2012.

CANADIAN STANDARDS ASSOCIATION – CSA S37. *CSA S37-18, Antena, towers, and antenna supporting structures*. Rexdale, Ontario, Canada, 2018.

CHEN, F.; ASTUTA, F., *Theory of Beam-Columns Vol. 2: Space behaviour and design*. McGraw-Hill, 1977.

CHENG, R.; XU, L.; JIN, S.; SHI, Y., Compressive Behavior of Gusset Plates Connected with Single-Angle Members. *Journal of Structural Engineering*, v. 142, n. 3, 2016.

CHOU, A. P.; SHI, G.; LIU, C.; ZHOU, L., Residual stress and compression buckling of large welded equal-leg steel angles, *Journal of Constructional Steel Research*, v. 201, p. 107756, 2023.

CLARK, J.W.; HILL, H.N., Lateral Buckling of Beams. *Proceedings ASCE: J Struct Div*, v. 68, n. ST7, 1960.

COCKALINGAM, S.N.; PANDURANGAN, V.; NITHYADHARAN, M., Timoshenko beam formulation for in-plane behavior of tapered monosymmetric I-beams: Analytical solution and exact stiffness matrix. *Thin-Walled Structures*, v. 162, p. 107604, 2021.

CONSIDÈRE, A., Résistance à la compression du béton armé et du béton fretté. *Le Gènie Civil*, 1890 (in French).

ECCS - European Convention For Constructional Steelwork. *Manual on Stability of Steel Structures,* 2. Ed. Liège, Belgium, 1976.

ECCS - European Convention For Constructional Steelwork. *Recommendations for Angles in Lattice Transmission Towers*. Liège, Belgium, 1985.

ELGAALY, M., DAGHER, H., DAVIDS, H. Behavior of single-angle-compression members. *Journal of Structural Engineering*, v. 117, n. 12, p. 3720-3741, 1991.

ENGESSER, F., Über die Knickfestigkeit Gerader Stäbe, *Zeitschirift für Architektur und Ingenieurwesen*, v.35, 1899 (in German).

ENGESSER, F., Über Statisch Unbestimmte Träger bei Beliebigem Formänderungs-Gesetze und über den Satz von der Kleinsten Ergänzungsarbeit. *Zeitschrift des Architekten und Ingenierur-Vereins zu Hannover*, v. 35, p. 733-744, Hannover, 1889 (in German).

EULER, L., *Methodus Inveniendi Lineas Curvas Maxime Minimive Propriatate Gaudentes*. Lausanne et Genève: M. M. Bousquet et Soc. Euler, OO, Series I, 24, 1759 (in Latin).

EUROPEAN COMMITTEE FOR STANDARDIZATION - *EN 1990. Eurocode: Basis of Structural Design*. Brussels, 2003.

EUROPEAN COMMITTEE FOR STANDARDIZATION - *EN 1993-1-1. Eurocode 3: Design of steel structures. Part 1-1: General rules and rules for buildings*. Brussels, 2005.

EUROPEAN COMMITTEE FOR STANDARDIZATION - *EN 1993-1-5. Eurocode 3: Design of steel structures - Part 1-5: Plate Structural Elements*. Brussels, 2006.

EUROPEAN COMMITTEE FOR STANDARDIZATION - *EN 1993-3-1. Eurocode 3: Design of steel structures - Part 3-1: Towers, masts and chimneys - Towers and masts*. Brussels, 2006.

EUROPEAN COMMITTEE FOR STANDARDIZATION – *ENV 1993-1-1. Eurocode 3: Design of steel structures. Part 1-1: General rules and rules for buildings*. Brussels, 1992.

EUROPEAN COMMITTEE FOR STANDARDIZATION - *FprEN 1993-1-1. Eurocode 3: Design of steel structures. Part 1-1: General rules and rules for buildings*. Brussels, 2022.

EUROPEAN COMMITTEE FOR STANDARDIZATION – *prEN 1993-1-14. Eurocode 3: Design of steel structures. Part 1-14: Design assisted by finite element analysis*. Brussels, 2023.

EUROPEAN COMMITTEE FOR STANDARDIZATION - pr*EN 1993-3. Eurocode 3: Design of steel structures - Part 3-1: Towers, masts and chimneys*. Brussels, 2021.

FERREIRA FILHO, J.O.; TANKOVA, T.; CARVALHO, H.; MARTINS, C.S.; SIMÕES DA SILVA, L., Experimental and numerical flexural buckling resistance of high strength steel columns and beam-columns. *Engineering Structures*, v. 265, p. 114414, 2022.

GALÉA, Y., LTBeam – Lateral-torsional buckling of beams. Centre Technique Industrial de la Construction Métallique (CTICM). At: https://www.cticm.com/ (version 1.0.10) 2010.

GOMES JR, J.O.; CARVALHO, H.; SIMÕES DA SILVA, L.; FERREIRA FILHO, J.O.; LAVALL, A., Assessment of design procedures for the buckling resistance of hot-rolled steel equal leg angles under concentric and eccentric compression. *Structures*, v. 57, p. 105308, 2023.

GOODIER, J.N., Flexural-torsional Buckling of Bars of Open Section Under Bending, Eccentric Thrust or Torsional Loads, *Cornell University Engineering Expt. Station Bulletin*, Ithaca, New York, n. 28, 1942.

HAIDAR, R., *Compressive strength of steel single angles loaded through two-bolts in one leg*. Master Dissertation, University of Windsor, Windsor, Canada, 1997.

HUSSAIN, A.; LIU, Y.P.; CHAN, S.L., Finite Element Modeling and Design of Single Angle Member Under Bi-axial Bending. *Structures*, v. 16, p. 373-389, 2018.

JASINSKY F. S., Zu den Knickfragen, *Schw. Bauzeiztung*, v. 25, n. 10, p. 63-64, 1895 (in German).

JIANG, J.; YE, M.; CHEN, L.Y.; ZHU, Z.W.; WU, M., Study on static strength of Q690 built-up K-joints under axial loads. *Structures*, v. 51, p. 760-775, 2023.

KAEHLER, R.C.; WHITE, D.W.; KIM, Y.D., *Frame Design Using Web-tapered Members, Steel Design Guide 25*. Metal Building Manufacturers Association and AISC, Chicago, USA, 2011.

KANG, S.B.; YANG, B.; ZHANG, Y.; ELCHALAKANI, M.; XIONG, G., Global buckling of laterally unrestrained Q460GJ beams with singly symmetric I-sections. *Journal of Constructional Steel Research*, v. 145, p. 341-351, 2018.

KAPPUS, R., Drillknicken Zentrisch Gedrückter Stäbe mit Offenem Profile im Elastischen Bereich, *Luftfahrt-Forschung*, v. 14, n. 9, p. 444-57; English translation, Twisting Failure of Centrally Loaded Open-Sections Columns in the Elastic Range, *NACA Tech. Mem.*, n. 851, 1937.

KENNEDY, J.B., MADUGULA, M.K.S. Buckling of steel angle and tee struts. *J. Struct. Div.* v. 98, n. 11, 2507–2522, 1972.

KETTLER, M.; LICHTL, G.; UNTERWEGER, H., Experimental tests on bolted steel angles in compression with varying end supports. *Journal of Constructional Steel Research*, v. 155, p.301-315, 2019a.

KETTLER, M.; TARAS, A.; UNTERWEGER, H., Member capacity of bolted steel angles in compression – Influence of realistic end supports. *Journal of Constructional Steel Research*, v. 130, p.22-35, 2017.

KETTLER, M.; UNTERWEGER, H.; HARRINGER, T., Appropriate spring stiffness models for the end supports of bolted angle compression members. *Steel Construction*, v. 12, n. 4, p. 291-298, 2019b.

KETTLER, M.; UNTERWEGER, H.; ZAUCHNER, P., Design model for bolted angle members in compression including joint stiffness. *Journal Of Constructional Steel Research*, v. 184, p. 106778, 2021.

KETTLER, M.; UNTERWEGER, H.; ZAUCHNER, P., Design model for the compressive strength of angle members including welded end-joints. *Thin-Walled Structures*, v. 175, p. 109250, 2022.

KITIPONRCHAI, S.; AL-BERMANI, F. G. A.; CHAN, S. L., Elasto-Plastic Finite Element Models for Angle Steel Frames. *Journal Of Structural Engineering*, v. 116, n. 10, p. 2567-2581, 1990.

KITIPORNCHAI, S., Torsional—Flexural buckling of angles: a parametric study: A parametric study. *Journal Of Constructional Steel Research*, v. 3, n. 3, p. 27-31, 1983.

KITIPORNCHAI, S.; TRAHAIR, N.S., Buckling Properties of Monosymmetric I-Beams. *Proceedings ASCE: J Struct Div*, v. 106, n. 5, 1980.

LEBASTARD, M., *Stability of welded I-section steel members*. PhD Thesis, INSA Rennes, Rennes, France, 2022.

LIU, Y.; HUI, L. Finite element study of steel single angle beam–columns. *Engineering Structures*, v. 32, n. 8, p.2087-2095, 2010.

LUNDQUIST, E.E.; FLIGG, C.M., A Theory for Primary Failure of Straight Centrally Loaded Columns, *NACA Research Report*, n. 582, 1937.

MAQUOI, R.; RONDAL, J., Formulations d' Airton-Perry pour flambement de barres métalliques. *Construction Métallique*, n. 4, Paris, 1979 (in French).

MAQUOI, R.; RONDAL, J., Mise en equation des novellas courbes européennes de flambement. *Construction Métallique*, n. 1, Paris, 1978 (in French).

MARQUES, L.; SIMÕES DA SILVA, L.; GREINER, R.; REBELO, C.; TARAS, A., Development of a consistent design procedure for lateral–torsional buckling of tapered beams. *Journal Of Constructional Steel Research*, v. 89, p. 213-235, 2013.

MARTINS J.P.; CORREA, J.N.; LJUBINKOVIC, F.; SIMÕES DA SILVA, L., Cost optimization of steel I-girder cross-section using genetic algorithms. *Structures*, v. 55, p. 379-388, 2023.

MICHEL, A.G.M., Elastic Stability of Long Beams under Transverse Forces. *Philosophical magazine*, n. 48, p. 289-309, 1899.

MOHRI, F.; DAMIL, N.; POTIER-FERRY, M., Linear and non-linear stability analyses of thin-walled beams with monosymmetric I-sections. *Thin-Walled Structures*, v. 48, p. 299-315, 2010.

MORI, D.D., *Flexo-Torção: Barras com Section Transversal Aberta e Paredes Delgadas – Notas de aula*. São Carlos School of Engineering – University of São Paulo, São Carlos, Brazil, 2003 (in Portuguese).

MOZE, P.; CAJOT, L.G.; SINUR, F.; REJEC, K.; BEG, D., Residual stress distribution of large steel equal leg angles. *Eng. Struct*, v. 71, p. 35–47, 2014.

NETHERCOT, D.A., Inelastic buckling of monosymmetric I-beams. *Proceedings ASCE: J Struct Div*, v. 99, n. ST7, p. 1696-1701, 1973.

OSTENFELD, A., Politecknisk Laereanstalts Laboratorium for Bygningsstatik, *Meddelelse*, Copenhagen, n. 5, 1931 (in Danish).

PRANDTL, L., *Kipperscheinnungen*. Doctoral dissertation. Universität München, Germany, 1899 (in German).

RACHID, M., *Instabilidade de Barras de Secção Delgada*. PhD Thesis, University of São Paulo, São Carlos, Brazil, 1975 (in Portuguese).

ROBERTS, T.M., Second-order strains and instability of thin-walled bars of open cross-section. *Int J Mech Sci*, v. 23, p. 297-306, 1981.

ROBERTS, T.M.; AZIZIAN, Z.G., Influence of pre-buckling displacements on the elastic critical loads of thin-walled bars of open cross-section. *Int J Mech Sci*, v. 25, p. 93-104, 1983.

ROBERTS, T.M.; BURT, C.A., Instability of Monossymetric I-Beams and Cantilevers. *Int J Mech Sci*, v. 27, n. 5, p. 313-324, 1985.

ROBERTSON, A., The strength of struts. *ICE Selected Engineering Papers*, The Institution of Civil Engineers, Paper 28, London, 1925.

SAINT-VENANT, B., Memoite sur la Torsion des Prismes. *Memoires des Savants Etrangers*, XIV, p. 233-560, 1855 (in French).

SHANI, M.A., *Compressive strength of eccentrically loaded steel angles*. Master Dissertation, University of Windsor, Windsor, Canada, 1998.

SHANLEY, F.R., Inelastic Column Theory, *J. Aero. Sci.*, v. 14, n. 5, p. 261-267, 1947.

SIMÕES DA SILVA, L.; MARQUES, L.; REBELO, C., Numerical validation of the general method in EC3-1-1: lateral, lateral-torsional and bending and axial force interaction of uniform members. *Journal of Constructional Steel Research*, v. 66, p. 575-590, 2010.

SIMÕES DA SILVA, L.; SIMÕES, R.; GERVÁSIO, H., *Design of Steel Structures*, ECCS Eurocode Design Manuals, 2nd edition, ECCS Press and Wiley, 2016a.

SIMÕES DA SILVA, L.; TANKOVA, T.; MARQUES, L.; REBELO, C., Safety assessment of EC3 stability design rules for the flexural buckling of columns. *Advanced Steel Construction*, v. 12, n. 3, p. 328-358, 2016b.

SIMÕES DA SILVA, L.; TANKOVA, T.; MARQUES, L.; REBELO, C.; TARAS, A., Safety assessment of EC3 stability design rules for the lateral-torsional buckling of prismatic beams. *Advanced Steel Construction*, v.14, n. 4, p. 668-693, 2018.

SIMÕES DA SILVA, L.; TANKOVA, T.; REBELO, C., Safety Assessment of Eurocode 3 Stability Design Rules for Prismatic Members in Bending and Compression. *Int J Steel Struct.*, v. 20, p. 343-354, 2020.

SIRQUEIRA, A. S.; LIMA, L. R. O.; VELLASCO, P. C. G. S.; SARQUIS, F. R.; SILVA, A. T., Experimental and numerical assessments of hot-rolled carbon steel fixed-ended angles in compression. *Thin-Walled Structures*, v. 157, p. 107018, 2020.

SNIJDER, H.H.; VAN DER AA, R.P.; HOFMEYER, H.; VAN HOVE, B.W.E.M., Lateral-torsional buckling design imperfections for use in non-linear FEA. *Steel Constr*, v. 11, p. 49-56, 2018.

SSRC Guide. *Guide to stability design criteria for metal structures.* In: Structural stability research council. 5th ed. New York: John Wiley & Sons, Inc.; 1998.

STANG, A. H.; STRICKENBERG, L. R., *Results of Some Compression Tests of Structural Steel Angles*, Technologic Paper of the United States Bureau of Standards No. 218, Government Printing Office, Washington, D. C., 1922.

SURLA, A.S.; KANG, S.Y.; PARK, J.S., Inelastic buckling assessment of monosymmetric I-beams having stepped and non-compact flange sections. *Journal of Constructional Steel Research*, v. 114, p. 325-337, 2015.

SZALAI, J., Complete generalization of the Ayrton-Perry formula for beam-column buckling problems. *Engineering Structures*, v. 153, p. 205-223, 2017.

TANKOVA, T.; RODRIGUES, F.; LEITÃO, C.; MARTINS, C.; SIMÕES DA SILVA, L., Lateral-torsional buckling of high strength steel beams: Experimental resistance. *Thin-Walled Structures*, v. 164, p. 107913, 2021.

TANKOVA, T.; SIMÕES DA SILVA, L.; MARQUES, L. Buckling resistance of non-uniform steel members based on stress utilization: General formulation. *Journal Of Constructional Steel Research*, v. 149, p. 239-256, 2018.

TANKOVA, T.; SIMÕES DA SILVA, L.; MARQUES, L.; REBELO, C.; TARAS, A., Towards a standardized procedure for the safety assessment of stability design rules. *Journal of Constructional Steel Research*, v. 103, p. 290-302, 2014.

TANKOVA, T.; SIMÕES DA SILVA, L.; RODRIGUES, F., Buckling curve selection for HSS welded I-section member. *Thin-Walled Structures*, v. 177, p. 109430, 2022.

TARAS, A., *Contribution to the development of consistent stability design rules for steel members.* PhD Thesis, Technical University of Graz, Graz, Austria, 2010.

TARAS, A.; DEHAN, V.; SIMÕES DA SILVA, L.; MARQUES, L.; TANKOVA, T., *Guideline for the Safety Assessment of Design Rules for Steel Structures in Line with EN 1990*, Deliverable D1.1, SAFEBRICTILE RFSR-CT-2013-00023, 2017.

TARAS, A.; GREINER, R., New design curves for lateral–torsional buckling—Proposal based on a consistent derivation. *Journal Of Constructional Steel Research*, v. 66, n. 5, p. 648-663, 2010.

TEMPLE, M. C.; SAKLA, S. S. S. Considerations for the design of single-angle compression members attached by one leg. *Can. J. Civ. Eng*, Windsor, v. 23, p.287-294, 1996.

TEMPLE, M. C.; SAKLA, S. S. S. Single-angle compression members welded by one leg to a gusset plate. I. Experimental study. *Can. J. Civ. Eng*, Windsor, v. 25, p.569-584, 1998.

TIMOSHENKO, S.P. *On the Stability of In Plane Bending of an I-Beam*, Izvestiya St. Petersburg Politekhnicheskoqo Instituta, IV-V, 1905.

TIMOSHENKO, S.P., GERE, J.M. *Theory of elastic stability*. 2 ed. McGraw W-Hill Kogakusha, LTD,541 p, 1961.

TRAHAIR, N., Lateral buckling of tapered members. *Engineering Structures*, v. 151, p. 518-526, 2017.

TRAHAIR, N.S., Bending and buckling of tapered steel beam structures. *Engineering Structures*, v. 59, p. 229-237, 2014.

TRAHAIR, N.S., Inelastic buckling design of monosymmetric I-beams. *Engineering Structures*, v. 34, p. 564-571, 2012.

TRAHAIR, N.S.; ANSOURIAN, P., In-plane behaviour of mono-symmetric tapered beams. *Engineering Structures*, v. 108, p. 53-58, 2016.

USAMI, T.; GALAMBOS, T. V. *Eccentrically Loaded Single Angle Columns*, Pub. IABSE, Vol. 31-V, pp. 153-184, 1971.

VLASOV, V.Z. *Pieces Longues en Voiles Minces*. 10. ed. Trad. de G. Smirnoff. Paris, Eyrolles, 1962 (in French).

VON KARMAN, T. *Untersuchungen uber Knickfestigkeit*. Forschungsarbeiten, n. 81, Berlim, 1910 (in German).

WAGNER, H., Torsion and Buckling of Open Sections, *NACA Tech. Mem.*, n. 807, 1936.

WAGNER, H.; PRETSHNER, W. Torsion and Buckling of Open Sections, *NACA Tech. Mem.*, n. 784, 1936.

WAKABAYASHI, M.; NONAKA, T. On the buckling strength of angles in transmission towers. *Bulletin of the Disaster Prevention Research Institute*, v. 15, part 2, n. 91, 1965.

WANG, C.M.; KITIPORNCHAI, S., On stability of monosymmetric cantilevers. *Eng Struct*, v. 8, n. 3, p. 169-180, 1986.

WANG, C.M.; KITIPORNCHAI, S.; THEVENDRAN, V., Buckling of braced monosymmetric cantilevers. *Int J Mech Sci*, v. 29, n. 5, p. 321-337, 1987.

WOOLCOCK, S.T.; KITIPORNCHAI, S. Design of single angle web struts in trusses. *Journal of Structural Engineering*, v. 112, n. 6, p. 1327-1345, 1986.

YANG, B.; KANG, S.B.; XIONG, G.; NIE, S.; HU, Y.; WANG, S., Experimental and numerical study on lateral-torsional buckling of singly symmetric Q460GJ steel I-shaped beams. *Thin-Walled Structures*, v. 113, p. 205-216, 2017.

YOUNG, T. *A Course of Lectures on Natural Philosophy and the Mechanical Arts*. vol. 2, London, 1807.

YUN, X.; GARDNER, L.; Stress-strain curves for hot-rolled steels. *Journal of Constructional Steel Research*, v. 133, p. 36-46, 2017.

ZHANG, L.; JASPART, J.P., *Stability of Members in Compression Made of Large Hot- Rolled and Welded Angles*, Research Report, University of Liège, 2013.

ZHAO, J.; LI, J.; SUN, Y., Experimental and numerical study on overall buckling behavior of Q460 high-strength steel continuous beams with welded singly symmetric I-section. *Engineering Structures*, v. 280, p. 115678, 2023.

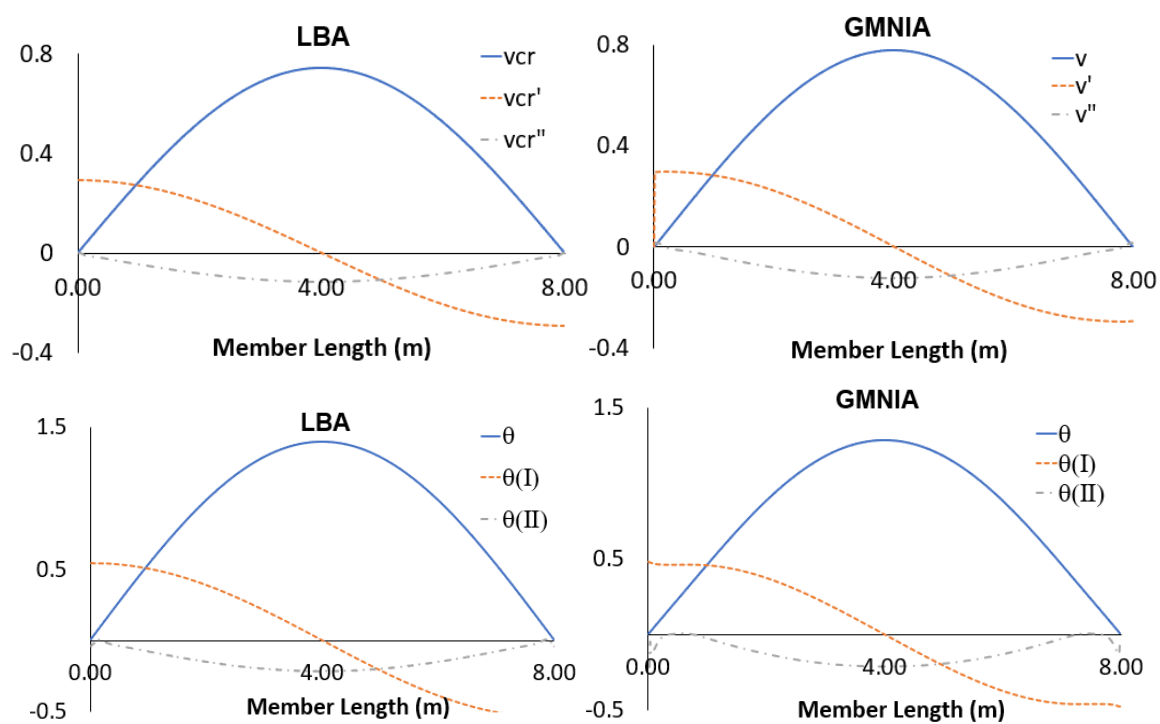# APPENDIX A – COMPARISON BETWEEN LBA AND GMNIA DEFORMED SHAPES

Figure A.1 - Mode shape for uniform doubly symmetric beams subjected to linear bending moment (ψ = 1.0) - $\bar{\lambda}_z$ = 1.90.
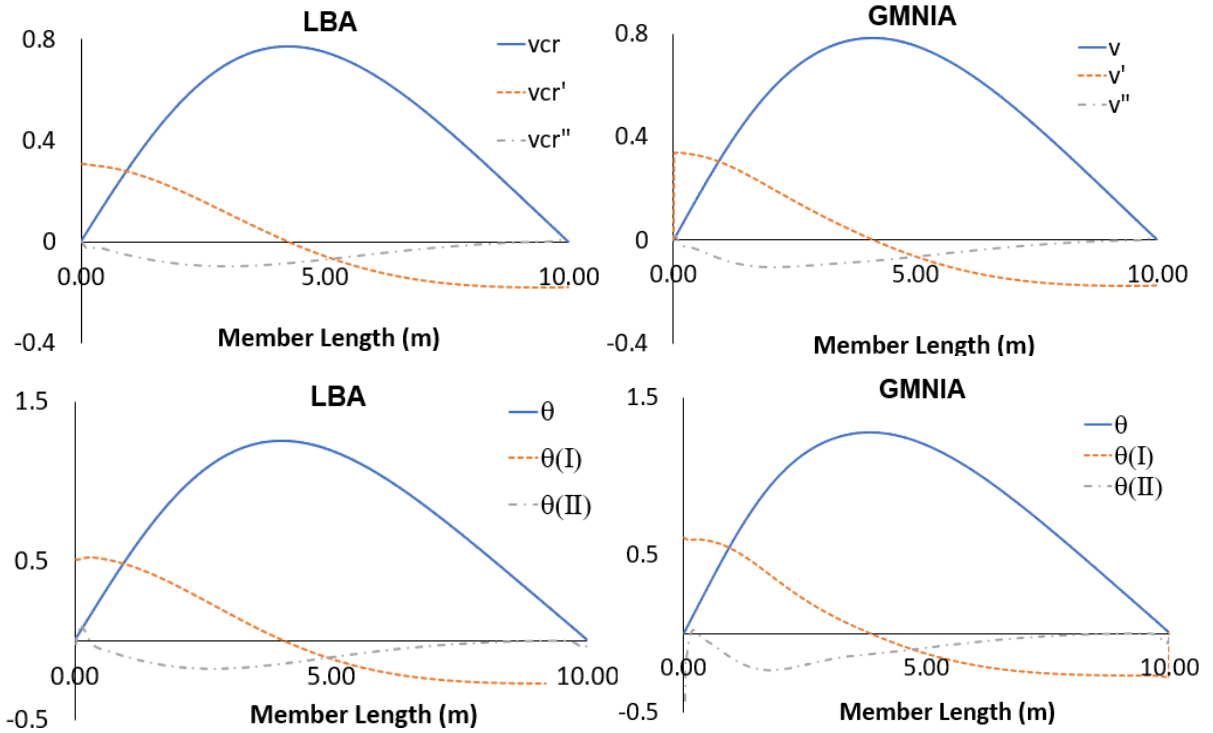
Figure A.2 - Mode shape for uniform doubly symmetric beams subjected to linear bending moment ($\psi = 0.0$) - $\bar{\lambda}_z = 2.40$.
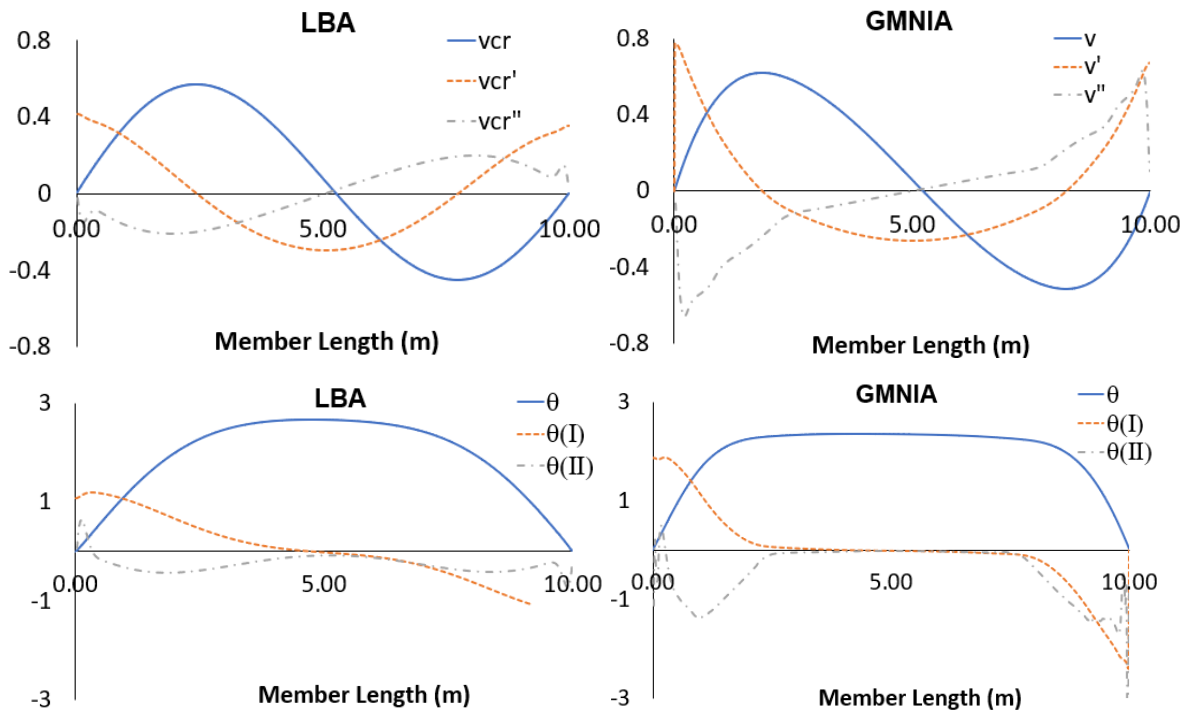

Figure A.3 - Mode shape for uniform doubly symmetric beams subjected to linear bending moment ($\psi = -1.0$) - $\bar{\lambda}_z = 2.40$.

Figure A.4 - Mode shape for uniform mono-symmetric beams subjected to linear bending moment ($\psi = 0.0$) - $\bar{\lambda}_z$ = 2.40.
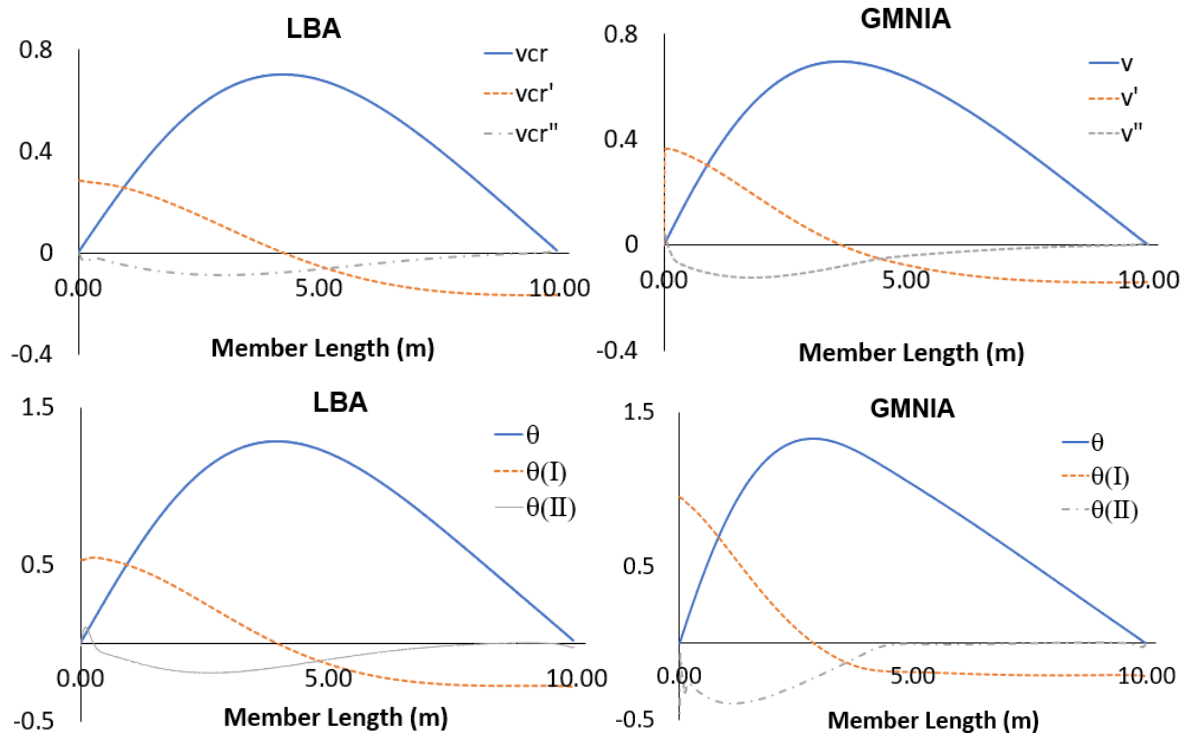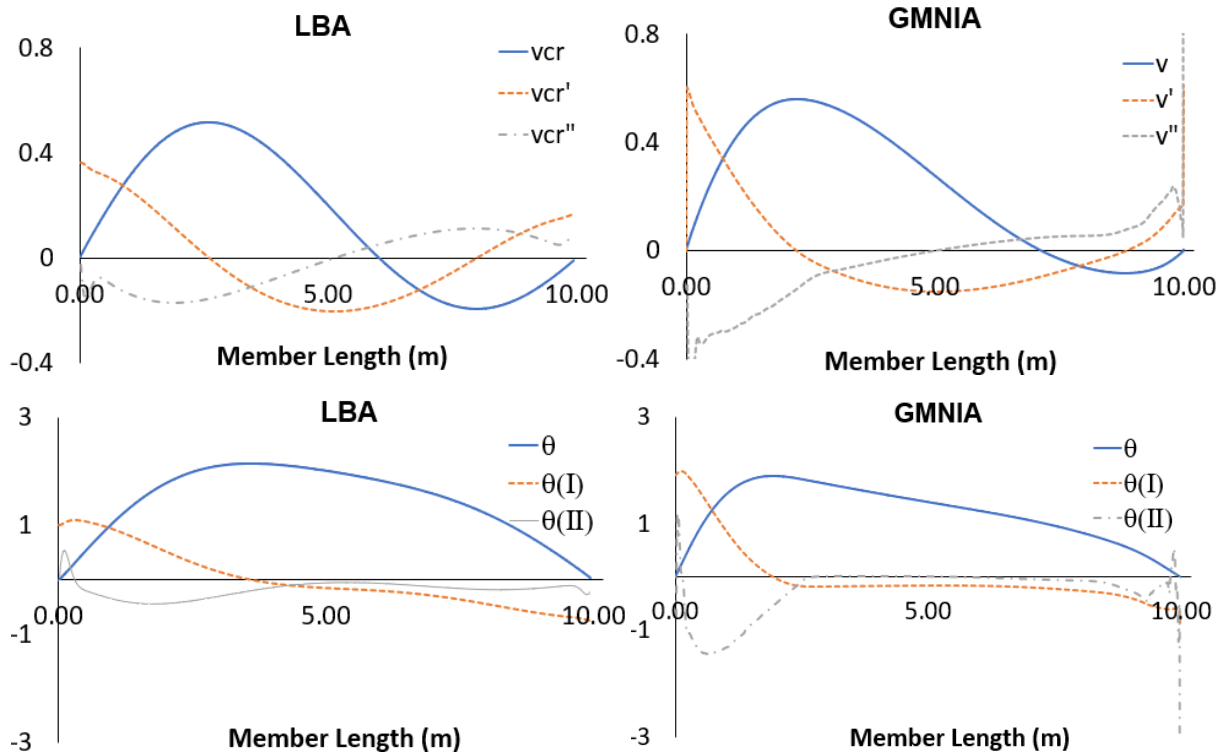

Figure A.5 - Mode shape for uniform mono-symmetric beams subjected to linear bending moment ($\psi = -1.0$) - $\bar{\lambda}_z$ = 2.40.
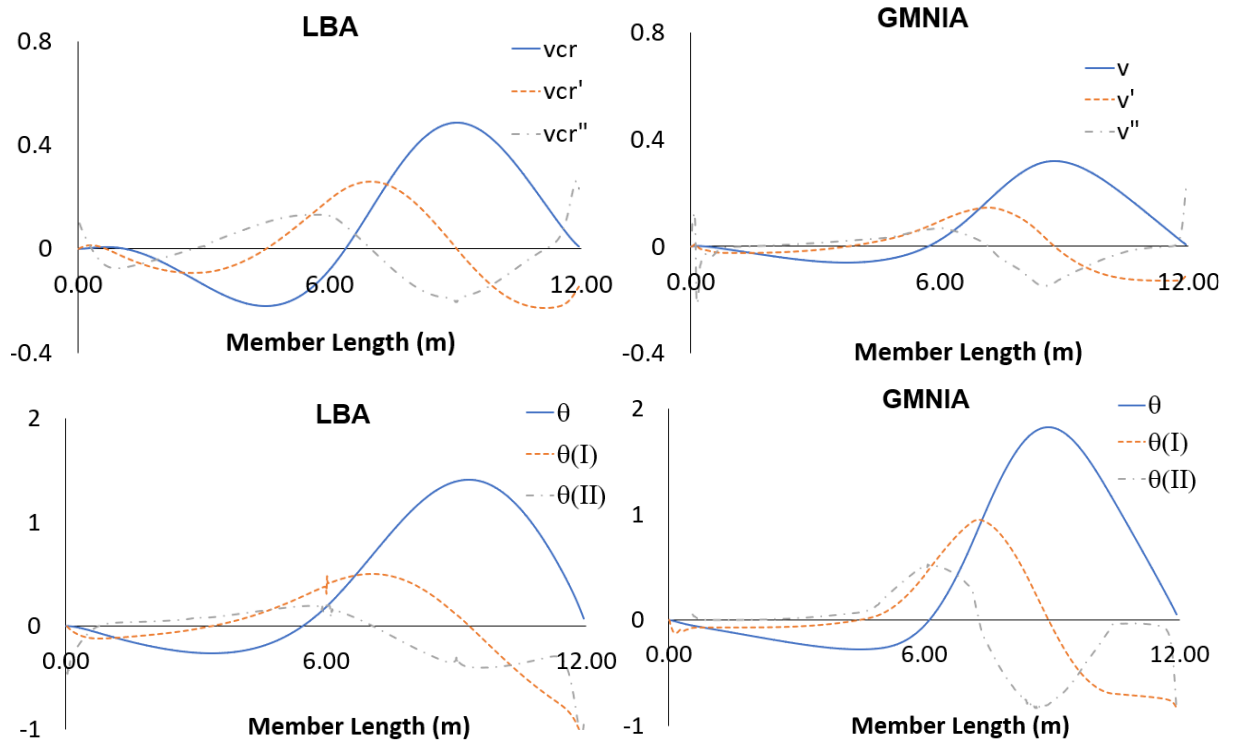
Figure A.6 - Mode shape for tapered mono-symmetric beams subjected to distributed load (with lateral restraint at compression flange) - $\bar{\lambda}_z = 1.30$.

APPENDIX B – WORKED EXAMPLE ON THE APPLICATION OF GENERAL FORMULATION FOR NON-PRISMATIC MONO-SYMMETRIC BEAMS

The following example aims to demonstrate the step-by-step application of the General Formulation to mono-symmetric beams. Consider the beam shown in Figure B.1 in steel grade S235. The depth of the beam exhibits a parabolic variation with a mono-symmetric cross-section, subjected to a distributed load (135 kN/m) applied at the top face of the cross-section. The cross-section at the member ends is 500 x 200(150) x 12 x 50(30), with maximum section depth at mid-span equal to 800 mm. The member ends exhibit simply supported conditions boundary conditions except for the in-plane rotation (rotation about the y-axis) for the left end, which is restrained by a rotational spring with a stiffness equal to 3.5 x 10^5 kN.m/rad. Additionally, the tensioned flange is braced at mid-span.
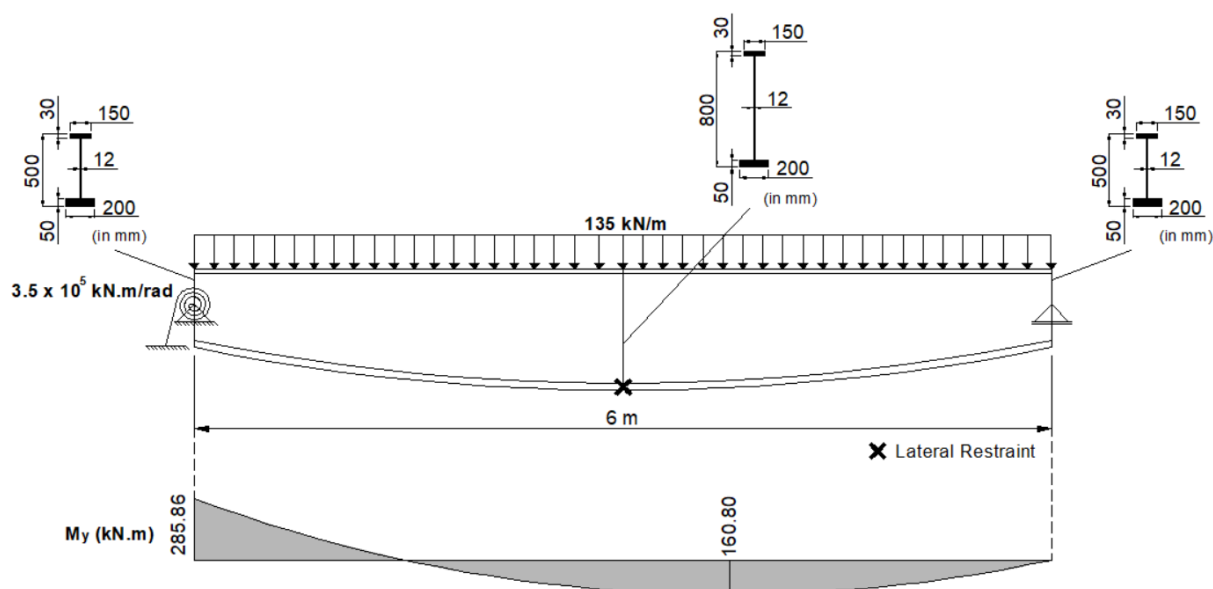

Figure B.1 – Worked example: geometry and internal first-order bending moment diagram.

The application of the General Formulation is summarized in the flowchart shown in Figure B.2 for the design of a beam potentially failing by lateral-torsional buckling. Firstly, the user must determine the eigenmode and its corresponding load multiplier, α_{cr}, by using a Linear

Buckling Analysis. For the example shown in Figure B.1, the following can be retrieved: $\alpha_{cr} = 1.35183$; Figure B.3 presents separately the mode shape, in terms of lateral displacement (v_{cr}) and twist rotation (θ_{cr}), and their first and second derivatives.
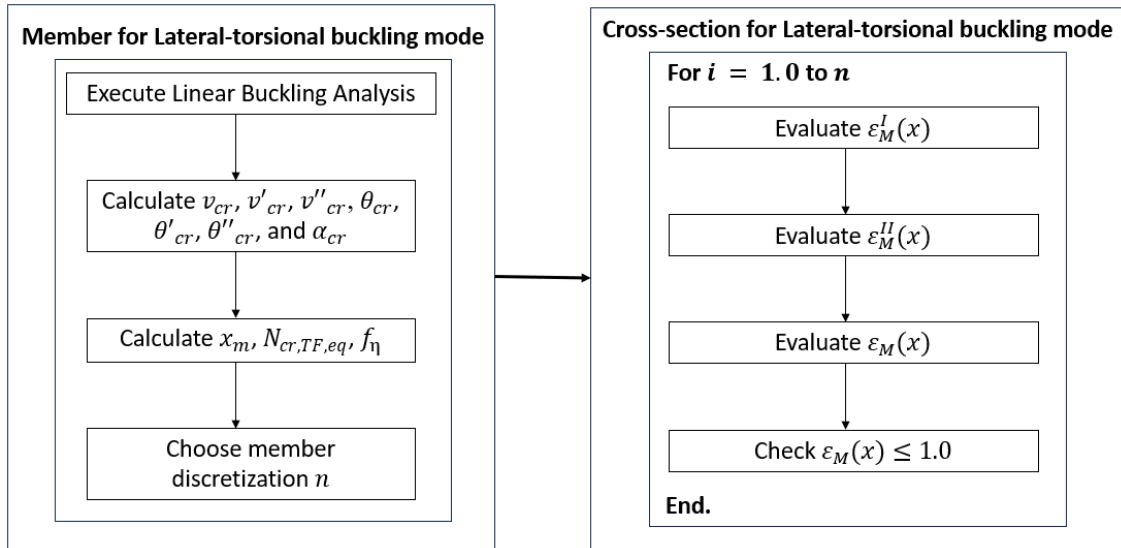
Figure B.2 – Application of the method for the lateral-torsional buckling mode.
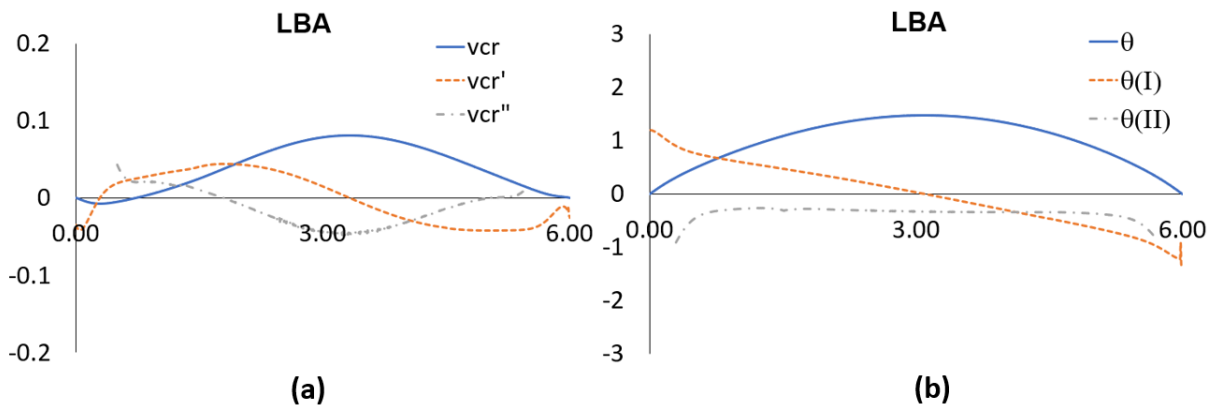
Figure B.3 – Mode shape for the parabolic member in terms of $v_{cr}(x)$ and $\theta_{cr}(x)$, and their derivatives.

Secondly, it is necessary to calculate the cross-section that corresponds to the critical location, x_m. This is taken as the location where v''_{cr} is maximum. This position occurs in this case at 3.27 meters from the left end of the beam. Hence, using Equation (3.24), the equivalent elastic critical force is:

$$N_{cr,TF,eq} = \frac{EI_z(x_m)|v''_{cr}(x_m)|}{|v_{cr}(x_m)+z_0\theta_{cr}(x_m)|} = \frac{21000\text{x}10^4\text{x}4187.42\text{x}10^{-8}\text{x}|-0.0484|}{|0.0812+0.13749\text{x}1.4760|} = 1497.19 \; kN \qquad \text{(B.1)}$$

and, using Equation (3.19) the factor f_η becomes:

$$f_\eta = \frac{N_{cr,TF}}{EI_z(x_m)\left[v''_{cr}(x_m)+\frac{W_z(x_m)\,C_w(x_m)}{W_w(x_m)\,I_z(x_m)}\left(\theta''_{cr}(x_m)+\frac{W_w(x_m)\,I_z(x_m)}{W_z(x_m)\,C_w(x_m)}\theta'_{cr}(x_m)h'\right)\right]} = 0.5749 \qquad \text{(B.2)}$$

Following the flowchart shown in Figure B.2, the utilization ratio is verified at multiple locations along the member. Thus, the member was discretized in 10 elements, 0.6 m long, as shown in Figure B.4.
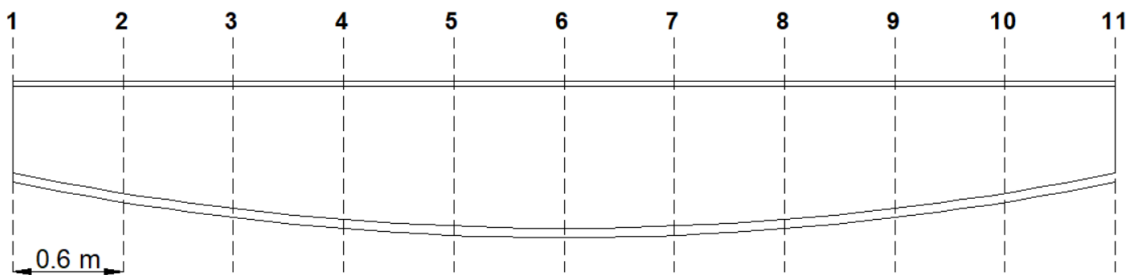

Figure B.4 – Member discretization.

Table B.1 summarizes the geometric properties of each cross-section in Figure B.4, as well as the associated internal first order bending moments.

Table B.1 – Geometric properties and internal first-order bending moment.

n	x (m)	A (cm^2)	W_y (cm^3)	W_z (cm^3)	I_z (cm^4)	C_w (cm^6)	W_w (cm^4)	$M_{y,Ed}$ ($kN.m$)
1	0	195.40	3265.64	683.87	4183.13	1424738.15	4971.84	-285.86
2	0.6	208.39	4354.23	687.77	4184.69	2174179.63	6188.10	-154.50
3	1.2	218.50	5253.25	690.80	4185.90	2866576.03	7134.94	-45.81
4	1.8	225.68	5917.93	692.95	4186.77	3416639.08	7807.84	40.00
5	2.4	229.97	6325.02	694.24	4187.28	3768053.38	8209.63	102.89
6	3.0	231.40	6462.49	694.67	4187.45	3889077.31	8343.64	142.93
x_m	**3.27**	**231.11**	**6434.84**	**694.58**	**4187.42**	**3864640.42**	**8316.75**	**153.44**
7	3.6	229.97	6325.02	694.24	4187.28	3768053.38	8209.63	160.08
8	4.2	225.68	5917.93	692.95	4186.77	3416639.08	7807.84	154.37
9	4.8	218.50	5253.25	690.80	4185.90	2866576.03	7134.94	125.78
10	5.4	208.39	4354.23	687.77	4184.69	2174179.63	6188.10	74.32
11	6.0	195.40	3265.64	683.87	4183.13	1424738.15	4971.84	0

Table B.2 summarizes the mode shape for the lateral torsional buckling mode, its derivatives and the general displacement given by Equation (3.20), for each discretized cross-section.

Table B.2 – Mode shape and its derivatives for lateral-torsional buckling, considering each cross-section discretized along the member.

n	x (m)	h (mm)	h' (−)	v_{cr} (−)	v''_{cr} (m^{-2})	θ_{cr} (−)	θ'_{cr} (m^{-2})	θ''_{cr} (m^{-2})	$\delta^{fl}(x)$ (−)
1	0	500	0	0	0	0	0	0	0
2	0.6	608.25	0.1607	-0.0032	0.0268	0.5554	0.7287	-0.3721	0.2570
3	1.2	692.49	0.1204	0.0140	0.0166	0.9366	0.5527	-0.2569	0.5157
4	1.8	752.34	0.0796	0.0379	0.0009	1.2201	0.3917	-0.2734	0.7498
5	2.4	788.08	0.0399	0.0629	-0.0251	1.4038	0.2195	-0.3011	0.9220
6	3.0	800	0.0002	0.0788	-0.0435	1.4793	0.0320	-0.3229	0.9982
x_m	3.27	797.61	-0.0176	0.0812	**-0.0484**	1.4760	-0.0553	-0.3190	0.9956
7	3.6	788.08	-0.0395	0.0795	-0.0422	1.4392	-0.1647	-0.3348	0.9603
8	4.2	752.34	-0.0792	0.0653	-0.0253	1.2799	-0.3646	-0.3330	0.8121
9	4.8	692.49	-0.1200	0.0422	-0.0043	1.0011	-0.5629	-0.3432	0.5785
10	5.4	608.25	-0.1603	0.0169	0.0062	0.5967	-0.7921	-0.4559	0.2964
11	6.0	500	0	0	0	0	0	0	0

Finally, the global utilization ratio ($\varepsilon_M(x)$) for the lateral-torsional buckling mode is calculated using Equation (3.21). The utilization ratio due to first order forces is determined for each cross-section by using the bending moment diagram shown in Figure B.1. The generalized imperfection (η) is calculated using Equation (3.22):

$$\eta(x) = \alpha_{LT}(x)\left(\bar{\lambda}(x) - 0.2\right)f_\eta\left|\delta^{fl}(x)\right| = 0.5749\alpha_{LT}(x)\left(\bar{\lambda}(x) - 0.2\right)\left|\delta^{fl}(x)\right| \qquad \text{(B.3)}$$

with the imperfection factor, $\alpha_{LT}(x)$, calculated according to the FprEN 1993-1-1 rules for the lateral-torsional buckling of doubly symmetric I-section welded prismatic members.

Table B.3 summarizes the application of Equation (3.21), showing a maximum utilization ratio of 0.96, and Figure B.5 illustrates the variation of the utilization ratio along the beam.

Table B.3 – Lateral-torsional buckling verification.

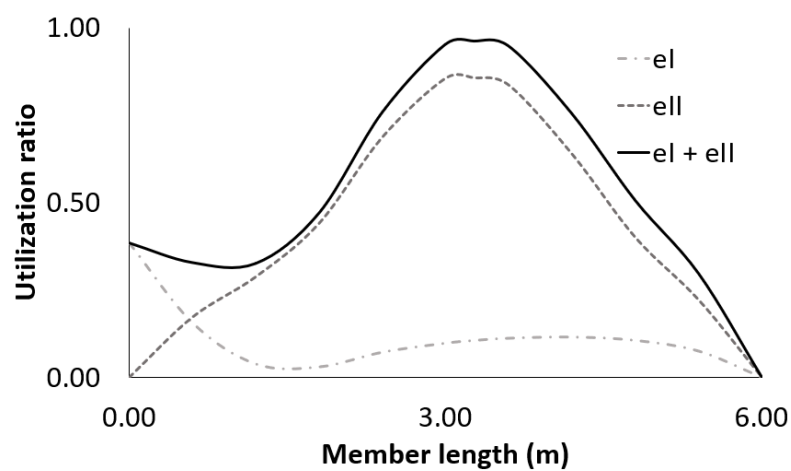| n	x (m)	$\bar{\lambda}$	α_{LT}	$M_{y,Ed}$ (kN.m)	$\varepsilon_M^I(x)$	$\varepsilon_M^{II}(x)$	$\varepsilon_M(x)$
1	0	1.70	0.51	-285.86	0.38	0.00	0.38
2	0.6	1.76	0.58	-154.50	0.16	0.17	0.33
3	1.2	1.81	0.64	-45.81	0.04	0.29	0.33
4	1.8	1.84	0.64	40.00	0.03	0.44	0.47
5	2.4	1.86	0.64	102.89	0.07	0.69	0.76
6	3.0	1.86	0.64	142.93	0.10	0.86	0.95
x_m	3.27	1.86	0.64	153.44	0.11	0.86	**0.96**
7	3.6	1.86	0.64	160.08	0.11	0.84	0.95
8	4.2	1.84	0.64	154.37	0.12	0.64	0.75
9	4.8	1.81	0.64	125.78	0.11	0.40	0.51
10	5.4	1.76	0.58	74.32	0.08	0.22	0.30
11	6.0	1.70	0.51	0	0.00	0.00	0.00

Figure B.5 – Utilization ratio for lateral-torsional buckling.